UILU-ENG-78-2010

CIVIL ENGINEERING STUDIES
STRUCTURAL RESEARCH SERIES NO. 449

APPROXIMATE MODAL ANALYSIS OF BILINEAR MDF SYSTEMS SUBJECTED TO EARTHQUAKE MOTIONS

By
V. TANSIRIKONGKOL
D. A. PECKNOLD

Technical Report of Research
Supported by the
NATIONAL SCIENCE FOUNDATION (RANN)
under Grants
ENV 75-08456
ENV 77-07190

DEPARTMENT OF CIVIL ENGINEERING
UNIVERSITY OF ILLINOIS
at URBANA-CHAMPAIGN
URBANA, ILLINOIS
AUGUST 1978

BIBLIOGRAPHIC DATA SHEET	1. Report No. UILU-ENG-78-2010	2.	3. Recipient's Accession No. PB286569
4. Title and Subtitle: Approximate Modal Analysis of Bilinear MDF Systems Subjected to Earthquake Motions			5. Report Date: August 1978 6.
7. Author(s): V. Tansirikongkol and D. A. Pecknold			8. Performing Organization Rept. No. SRS 449
9. Performing Organization Name and Address: University of Illinois at Urbana-Champaign, Urbana, Illinois 61801			10. Project/Task/Work Unit No. 11. Contract/Grant No. ENV75-08456, ENV77-07190
12. Sponsoring Organization Name and Address: National Science Foundation (RANN), Washington, D.C. 20550			13. Type of Report & Period Covered 14.

15. Supplementary Notes

16. Abstracts: The study investigated two approximate methods of modal analysis for hysteretic multi-degree-of-freedom lumped mass structural models subjected to earthquakes. The methods were (1) approximate modal analysis using elastic response spectra, and (2) approximate modal analysis using inelastic response spectra. Both modal analysis procedures were iterative and used a perturbation method to successively modify the original elastic mode shapes at each iterative step to reflect yielding in the system. The procedures were developed and evaluated only for shear beam structural systems consisting of members with bilinear hysteresis. Extensive comparisons of exact and approximate responses were made for various 1-, 3- and 10-degree-of-freedom systems. Four existing earthquakes were used, and several structural stiffness and strength parameters were varied. Maximum story displacements were generally predicted within about 5-40 percent accuracy. The equivalent nonlinear approach using inelastic response spectra appeared to give generally better accuracy than the equivalent linear approach using elastic response spectra.

17. Key Words and Document Analysis. 17a. Descriptors

Earthquake engineering, Nonlinear dynamic analysis, Response spectrum, Modal Analysis, Hysteretic multi-degree-of-freedom structures

17b. Identifiers/Open-Ended Terms

17c. COSATI Field/Group

i

18. Availability Statement	19. Security Class (This Report)	21. No. of Pages
Release Unlimited	UNCLASSIFIED	221
	20. Security Class (This Page) UNCLASSIFIED	22. Price A10-A01

ABSTRACT

The study investigated two approximate methods of modal analysis for hysteretic multi-degree-of-freedom lumped mass structural models subjected to earthquakes. The methods were (1) approximate modal analysis using elastic response spectra, and (2) approximate modal analysis using inelastic response spectra. Both modal analysis procedures were iterative and used a perturbation method to successively modify the original elastic mode shapes at each iterative step to reflect yielding in the system. The procedures were developed and evaluated only for shear beam structural systems consisting of members with bilinear hysteresis. Extensive comparisons of exact and approximate responses were made for various 1-, 3- and 10-degree-of-freedom systems. Four existing earthquakes were used, and several structural stiffness and strength parameters were varied. Maximum story displacements were generally predicted within about 5-40 percent accuracy. The equivalent nonlinear approach using inelastic response spectra appeared to give generally better accuracy than the equivalent linear approach using elastic response spectra.

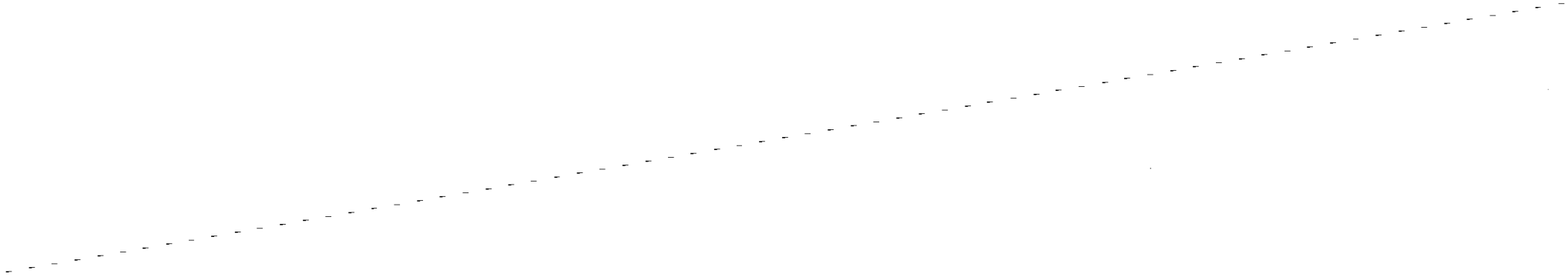

ACKNOWLEDGMENT

This report was prepared as a doctoral dissertation by Visit Tansirikongkol, under the direction of Professor David A. Pecknold.

The authors wish to express their appreciation to Professors W. J. Hall, University of Illinois at Urbana-Champaign, and C. J. Montgomery, University of Alberta at Edmonton, for the use of computer programs developed by them.

The study was supported by the National Science Foundation (RANN) under Grants ENV75-08456 and ENV77-07190. Extensive computer services support was received from the Research Board of the Graduate College of the University of Illinois at Urbana-Champaign. The above-noted support is gratefully acknowledged.

Any opinions, findings, and conclusions or recommendations expressed in this report are those of the authors and do not necessarily reflect the views of the National Science Foundation.

TABLE OF CONTENTS

Page

LIST OF TABLES

LIST OF FIGURES

Figure Page

Figure Page

Figure Page

Figure Page

CHAPTER 1

INTRODUCTION

1.1 Background

The design of structures to resist severe earthquake motions is an area of structural engineering which has received a great deal of attention in recent years. Requirements of economical design demand that most structures be designed to respond in the inelastic range under the most severe ground motions. Thus design procedures recognize, either implicitly or explicitly, that inelastic response will occur. It is desirable that the inelastic deformation capacities required of the structural members be explicitly recognized by the designer, rather than be implied by a set of reduced design forces.

In order to explicitly consider inelastic behavior in design procedures, simple methods of analysis are needed. Current capabilities in analytical modeling of structural components and their hysteretic behavior make it possible, in principle, to carry out step-by-step numerical computations of structural response to selected earthquake acceleration records. However, because of uncertainties in such structural and material property modeling, variabilities in possible earthquake motions, and the high cost of inelastic response history calculations for large structures, such methods are not suitable for preliminary design. Approximate methods of analysis are needed which are relatively inexpensive, allow assessment of the effects of design changes, and facilitate understanding of structural behavior.

It appears that the only viable approach is a modal analysis-response spectrum approach. Such methods are becoming more widely used for elastic response calculations. Modifications of this general approach to recognize inelastic behavior have been proposed although modal analysis is strictly applicable only to linear systems. Shibata and Sozen [32] developed a design method for reinforced-concrete frames in which a softer and more highly damped "substitute structure" is analyzed by elastic modal analysis. Newmark and Hall [27] proposed the use of inelastic response spectra combined with elastic modal analysis. A reduced design spectrum is used which is essentially determined from inelastic single-degree-of-freedom response calculations. Several recent studies [1, 23] have examined this concept, and have concluded that the method appears unable to accurately predict localized yielding and that the level of inelastic deformation implied in the response spectrum does not closely correspond to the levels of inelastic deformations in the structural members.

1.2 Object and Scope of Study

The objective of this study was to investigate and evaluate two approximate methods of modal analysis for hysteretic multi-degree-of-freedom lumped mass structural models.

The methods are: (1) Approximate modal analysis using elastic response spectra. This type of approximation uses the well-known method of "equivalent linearization" for nonlinear structures regarding which an extensive body of literature exists. The "Substitute Structure Method" of Shibata and Sozen [32] is of this type. (2) Approximate modal analysis using inelastic response spectra. The procedure developed in this study

recognizes changes in "mode shapes" as a function of inelastic behavior and defines in terms of member ductilities a "modal ductility" with which to enter the inelastic response spectrum.

The procedures are developed and evaluated only for shear beam structural systems consisting of members with bilinear hysteresis. Extensive comparisons of exact and approximate responses were made for various 1-, 3-, and 10-degree-of-freedom systems subjected to four different earthquake acceleration inputs.

In Chapter 2, the approximate steady state solutions for nonlinear single degree-of-freedom (SDF) and multi degree-of-freedom (MDF) systems subjected to harmonic base excitation are derived by the method of equivalent linearization. The development is from a slightly different viewpoint than taken by Iwan [15] who has considered the MDF problem previously. This leads naturally to the use of the mode shapes of the equivalent linear system for the modal decomposition, for both methods of approximate analysis. The solutions for harmonic excitation provide insight into the behavior of the nonlinear systems and are used later as basic components of the approximate solution methods for earthquake excitation. The use of the simple excitation also allows a logical definition of modal ductility to be obtained.

In Chapter 3 a pseudo-steady state harmonic response is found which gives the same frequency shift and damping as the transient response of a SDF bilinear system. This pseudo-steady state harmonic response is related to the maximum earthquake response by means of a correlation factor. The correlation factor is obtained from available analog computer

results for bilinear SDF systems subjected to stationary Gaussian white noise excitation and to bursts of white noise. For comparative purposes, earthquake and pulse-like excitation responses are examined in the frequency domain using Fourier analysis.

In Chapter 4, the approximate modal analysis procedures are summarized in a step-by-step format and numerical examples are given. A perturbation method is used for modifying the original elastic mode shapes depending on the level of inelastic response.

In Chapter 5, extensive numerical comparisons are made between maximum responses calculated by "exact" numerical step-by-step integration and maximum responses predicted by the two approximate modal analysis procedures. A large number of 1, 3 and 10 story bilinear shear beam systems subjected to four different earthquakes are studied. Additional results for SDF systems are contained in Appendix E.

1.3 Previous Work

Relevant previous work is briefly noted here, and is discussed later in the text where appropriate.

A large body of literature exists which deals with the response of nonlinear SDF systems. An excellent overview of nonlinear analysis techniques is given by Iwan [16].

The steady state harmonic response of hysteretic SDF systems has been investigated by Caughey [7], Jennings [18] and Iwan [13], by approximate analytical methods including equivalent linearization. Jennings [19] summarized various ways of modeling resonant frequency shift and equivalent viscous damping for steady state harmonic response.

The random vibration of hysteretic SDF systems subjected to white noise excitation has also been extensively investigated by Caughey [5, 6] using extensions of the same approximate analytical techniques. A considerable amount of empirical response data, obtain via analog computer, has been compiled by Brown [4], Iwan and Lutes [17], Lutes [20], and Chokshi and Lutes [8].

Many studies of earthquake response of nonlinear SDF systems have been carried out. Veletsos, Newmark and Chelapati [34] presented simple approximate rules for the construction of deformation spectra for undamped and lightly damped systems from consideration of the gross characteristics of the displacement, velocity and acceleration diagrams of the ground motion. The spectra for the inelastic systems were related to those applicable to elastic systems. Veletsos and Vann [35] presented results for 1, 2 and 3 degree-of-freedom elastoplastic systems subjected to simple pulse and earthquake motions.

Results of general applicability for MDF systems are much less extensive than for SDF systems.

The steady state harmonic response of a class of hysteretic MDF systems has been treated by Iwan [15], using decomposition of response into elastic mode shapes.

Random vibration response of hysteretic MDF systems to stationary white noise excitation has been considered by several authors [2, 10].

Procedures for step-by-step numerical integration of the equations of motion for hysteretic MDF systems subjected to earthquake excitation have been described in many papers which are too numerous to cite individually.

These procedures are described in standard texts [28]. Design-oriented approximate procedures have been investigated by Shibata and Sozen [32], Montgomery and Hall [23], Agnastopoulous, et al. [1], and Guerra and Esteva [11].

CHAPTER 2

STEADY STATE RESPONSE OF A NONLINEAR HYSTERETIC SYSTEM TO HARMONIC EXCITATION

2.1 Introduction

The steady state response of linear systems to harmonic input can be expressed in terms of a transfer function which depends on the system properties but not on the excitation. Transient response to a general input can be found by superposition in the frequency domain. For a nonlinear hysteretic system, a transfer function does not, strictly speaking, exist since superposition does not apply. However, given a specific input, one can still define the ratio of output to input at each frequency as a "nonlinear transfer function". Although this nonlinear transfer function depends strongly on the input, it is still useful since the shift of effective frequency and increase in effective damping as a function of response nonlinearity can be easily observed.

In this chapter, results for linear systems are first briefly reviewed for completeness and to introduce notation. The approximate steady state solutions for nonlinear SDF and MDF systems subjected to harmonic base excitation are then obtained by the method of equivalent linearization [6]. These solutions provide some insight into the behavior of the nonlinear systems and are used later as basic components of the approximate solution methods for earthquake excitation.

2.2 Linear Systems

Steady state response of linear SDF and MDF systems subjected to harmonic excitation is treated in many texts. Only a brief review of

these results is presented herein. Details may be found in Ref. [33].

2.2.1 Single Degree-of-Freedom System -- Consider a SDF system subjected to harmonic base excitation as shown in Fig. 2.1. The equation of motion of the system is

$$m\ddot{x} + c\dot{x} + k_0 x = mR \cos \omega t \tag{2.1}$$

where m, c and k_0 are the system mass, damping and stiffness, respectively; mR cos ωt is harmonic excitation with circular frequency ω; and x, $\dot{x}$ and $\ddot{x}$ are respectively the spring displacement, velocity, and acceleration relative to the base.

The steady state displacement response, x, is at the same frequency as the input with a phase shift, ϕ.

$$x = A \cos (\omega t + \phi) \tag{2.2}$$

where

$$\frac{A}{R} = \frac{1}{m[(\omega_0^2 - \omega^2)^2 + (-2\xi\, \omega_0 \omega)^2]^{1/2}} \tag{2.3a}$$

$$\tan \phi = \frac{-2\xi\, \omega_0 \omega}{\omega_0^2 - \omega^2} \tag{2.3b}$$

in which ξ is the fraction of the critical damping and ω_0 is the natural circular frequency.

The plots of Eqs. (2.3a) and (2.3b) for a system with $\xi = 0.02$ are shown in Fig. 2.2.

2.2.2 Multi Degree-of-Freedom System -- Consider a discrete, lumped-mass system with N degrees-of-freedom subjected to harmonic base excitation. The equation of motion of the system is

$$[M]\{\ddot{u}\} + [C]\{\dot{u}\} + [K]\{u\} = [M]\{r\}\, R \cos \omega t \tag{2.4}$$

where [M], [K] and [C] are mass, stiffness, and damping matrices of order (N x N). $\{u\}$, $\{\dot{u}\}$ and $\{\ddot{u}\}$ are, respectively, (NX1) displacement, velocity, and acceleration vectors relative to the base. $\{r\}$ is a vector of order (NX1) which represents the displacements resulting from a unit base displacement.

Free vibration mode shape vectors of order (NX1), $\{\Phi_n\}$ of the system satisfy

$$[K]\{\Phi_n\} = \omega_n^2\, [M]\{\Phi_n\} \tag{2.5}$$

and the orthogonality conditions

$$\{\Phi_m\}^T[M]\{\Phi_n\} = 0 \qquad m \neq n \tag{2.6a}$$

$$\{\Phi_m\}^T[K]\{\Phi_n\} = 0 \qquad m \neq n \tag{2.6b}$$

By applying modal decomposition, the displacement vector, $\{u\}$, becomes

$$\{u\} = \sum_{n=1}^{N} \{\Phi_n\}\, \eta_n \tag{2.7}$$

where n denotes the mode n, and η_n is the normal mode displacement.

Equation (2.4), in view of Eqs. (2.6a), (2.6b) and (2.7) and the assumption that the corresponding orthogonality condition applying to [M] and [K] also applies to [C], becomes

$$m_n\ddot{\eta}_n + 2\xi_n m_n \omega_n \dot{\eta}_n + k_n \eta_n = \Gamma_n\, R \cos \omega t \tag{2.8}$$

$$\text{for } n = 1, 2, \ldots, N$$

in which

$$m_n = \{\Phi_n\}^T [M]\{\Phi_n\} \tag{2.9a}$$

$$k_n = \{\Phi_n\}^T [K]\{\Phi_n\} = m_n\omega_n^2 \tag{2.9b}$$

$$2\xi_n m_n \omega_n = \{\Phi_n\}^T [C]\{\Phi_n\} \tag{2.9c}$$

$$\Gamma_n = \{\Phi_n\}^T [M]\{r\} \tag{2.9d}$$

where m_n, ξ_n and k_n are modal mass, damping and stiffness, respectively, ω_n is the modal natural circular frequency, and Γ_n is the modal participation factor.

The modal stiffness, k_n, can be directly related to the element stiffness properties as follows.

$$\begin{aligned} k_n &= \{\Phi_n\}^T [K]\{\Phi_n\} \\ &= \{\Phi_n\}^T \left[\sum_e [L]_e^T [K]_e [L]_e \right] \{\Phi_n\} \end{aligned} \tag{2.10a}$$

in which

$$\{u\}_e = [L]_e \{u\} \tag{2.10b}$$

where the subscript e denotes element, $\{u\}_e$ is the element displacement vector of order (MX1), $[L]_e$ is the localizing matrix of order (MXN), $[K]_e$ is the element stiffness matrix of order (MXM), and M is the number of degrees of freedom in element e.

The element stiffness may be expressed, for a constant strain element, as

$$[K]_e = [B]_e^T [\tilde{K}]_e [B]_e \tag{2.11a}$$

in which

$$\{\varepsilon\}_e = [B]_e \{u\}_e \tag{2.11b}$$

$$\{\sigma\}_e = [\tilde{K}]_e \{\varepsilon\}_e \tag{2.11c}$$

where $\{\varepsilon\}_e$ is the element strain vector of order (SX1), $[B]_e$ is the element strain-displacement relation matrix of order (SXM), $\{\sigma\}_e$ is the element stress vector of order (SX1) and $[\tilde{K}]_e$ is the element stress-strain matrix of order (SXS), and S is the number of strain components in the element e.

From this point on, it is assumed that each element has only a single strain component. For example, in a shear-beam model of a frame, the strain component is the relative story displacement.

Equation (2.10a), in view of Eq. (2.11a), becomes

$$k_n = \sum_e \varepsilon_{en}^2 \tilde{K}_e \tag{2.12a}$$

in which

$$\varepsilon_{en} = [B]_e[L]_e\{\Phi_n\} \tag{2.12b}$$

where ε_{en} is the element strain in mode n.

The modal natural circular frequency, ω_n, could be expressed in terms of the element stiffnesses by relating Eqs. (2.9b) and (2.12a).

Under steady state conditions, the modal displacement, η_n may be expressed in the form

$$\begin{aligned} \eta_n &= A_n \cos(\omega t + \phi_n) \\ &= A_n \cos \theta_n \end{aligned} \tag{2.13}$$

where A_n is the modal displacement amplitude and ϕ_n is the modal phase angle.

Substituting Eq. (2.13) into Eq. (2.8) and equating the coefficients of $\cos \theta_n$ and $\sin \theta_n$ yields the modulus and the phase angle of the modal transfer function as follows

$$\frac{A_n}{R} = \frac{\Gamma_n}{m_n[(\omega_n^2 - \omega^2)^2 + (-2\xi_n\omega_n\omega)^2]^{\frac{1}{2}}} \tag{2.14a}$$

$$\tan \phi_n = \frac{-2\xi_n\omega_n\omega}{\omega_n^2 - \omega^2} \tag{2.14b}$$

The displacement vector, {u}, can be obtained from Eqs. (2.7) and (2.13) as

$$\{u\} = \sum_{n=1}^{N} \{\Phi_n\}A_n \cos(\omega t + \phi_n) = \sum_{n=1}^{N} \{\Phi_n\}A_n \cos \theta_n \tag{2.15}$$

By expanding the cos θ_n term and rearranging the expression, Eq. (2.15), in component form, becomes

$$u_k = U_k \cos(\omega t + \gamma_k); \qquad k=1, 2, \ldots, N \tag{2.16a}$$

in which

$$U_k^2 = \sum_{n=1}^{N} (A_n\Phi_{kn})^2 + \sum_{\substack{i=1 \\ i\neq j}}^{N} \sum_{j=1}^{N} A_iA_j\Phi_{ki}\Phi_{kj} \cos(\phi_i - \phi_j) \tag{2.16b}$$

$$\tan \gamma_k = \frac{\sum_{n=1}^{N} A_n\Phi_{kn} \sin \phi_n}{\sum_{n=1}^{N} A_n\Phi_{kn} \cos \phi_n} \tag{2.16c}$$

The element strain ε_e can also be obtained in a similar way as

$$\varepsilon_e = E_e \cos(\omega t + \psi_e) \tag{2.17a}$$

in which

$$E_e^2 = \sum_{n=1}^{N} (A_n\varepsilon_{en})^2 + \sum_{\substack{i=1 \\ i\neq j}}^{N} \sum_{j=1}^{N} \varepsilon_{ei}\varepsilon_{ej}A_iA_j \cos(\phi_i - \phi_j) \tag{2.17b}$$

$$\tan \psi_e = \frac{\sum_{n=1}^{N} A_n \varepsilon_{en} \sin \phi_n}{\sum_{n=1}^{N} A_n \varepsilon_{en} \cos \phi_n} \tag{2.17c}$$

and

$$\varepsilon_{en} = [B]_e[L]_e\{\Phi_n\} \tag{2.18}$$

Figure 2.3 shows the plots of Eqs. (2.14a), (2.14b), (2.16b), and (2.17b), respectively, for the 2DF simple shear beam system in Fig. 2.1.

2.3 Nonlinear Single Degree-of-Freedom System

The approximate solution derived by the method of equivalent linearization is summarized here. The method is well-known and has been applied by many authors to the study of response of nonlinear systems [6, 17]. In this method, an optimum linear equation of motion is substituted for the actual nonlinear equation of motion by the method of mean square error minimization.

Consider a SDF system with softening hysteresis subjected to harmonic base excitation. The equation of motion is

$$m\ddot{x}_{ex} + c\dot{x}_{ex} + F(x_{ex}, \dot{x}_{ex}) = mR \cos \omega t \tag{2.19}$$

where x_{ex} is the relative displacement, and $F(x_{ex}, \dot{x}_{ex})$ is the hysteretic restoring force.

A linear equation of motion

$$m\ddot{x} + c_{eq}\dot{x} + k_{eq}x = mR \cos \omega t \tag{2.20a}$$

is substituted for Eq. (2.19). The equation deficiency or error is

given by

$$\varepsilon = c^*\dot{x} + k_{eq}x - F \; ; \quad c^* = c_{eq} - c \tag{2.20b}$$

and x is the solution of the substitute or equivalent linear system.

Let the average value of a quantity over one cycle of response be denoted by

$$(\overline{\quad}) \equiv \int_0^{2\pi} (\quad) d\omega t \tag{2.21}$$

To minimize the mean square error

$$\overline{\varepsilon^2} = \min \tag{2.22a}$$

it is required that

$$\overline{\varepsilon \frac{\partial \varepsilon}{\partial c^*}} = 0 \tag{2.22b}$$

$$\overline{\varepsilon \frac{\partial \varepsilon}{\partial k_{eq}}} = 0 \tag{2.22c}$$

Equations (2.22b) and (2.22c) in view of Eq. (2.20b) become, respectively,

$$\overline{x^2}\, k_{eq} + \overline{x\dot{x}}\, c^* = \overline{Fx} \tag{2.23a}$$

$$\overline{x\dot{x}}\, k_{eq} + \overline{\dot{x}^2}\, c^* = \overline{F\dot{x}} \tag{2.23b}$$

For the steady state solution, $\overline{x\dot{x}}$ vanishes and Eqs. (2.23a) and (2.23b) become, respectively,

$$k_{eq} = \overline{Fx} / \overline{x^2} \tag{2.24a}$$

$$c^* = \overline{F\dot{x}} / \overline{\dot{x}^2} \tag{2.24b}$$

in which

$$\overline{Fx} = \pi A^2 \overline{C}(A) \tag{2.24c}$$

$$\overline{F\dot{x}} = -\omega\pi A^2 \overline{S}(A) \tag{2.24d}$$

$$\overline{C}(A) = \frac{1}{\pi A} \int_0^{2\pi} F \cos\theta d\theta \tag{2.24e}$$

$$\overline{S}(A) = \frac{1}{\pi A} \int_0^{2\pi} F \sin\theta d\theta \tag{2.24f}$$

Equations (2.24a) and (2.24b) in view of Eqs. (2.2) and (2.24c) to (2.24f) become, respectively,

$$k_{eq} = m\omega_{eq}^2 = \overline{C}(A) \tag{2.25}$$

$$\beta_{eq} = \frac{c_{eq}}{2m\omega_{eq}} = \xi \frac{\omega_0}{\omega_{eq}} - \frac{\overline{S}(A)}{2m\omega_{eq}\omega} \tag{2.26}$$

For a bilinear hysteretic system, Caughey [1] derived the expressions

$$\overline{C}(A) = \frac{k_0}{\pi}[(1-\alpha)\,\theta^* + \alpha\pi - \frac{1-\alpha}{2}\sin 2\theta^*]; \quad \mu > 1.0$$
$$= k_0 \qquad ; \quad \mu \leq 1.0 \tag{2.27a}$$

$$\overline{S}(A) = \frac{-(1-\alpha)\,k_0}{\pi}\sin^2\theta^* \qquad ; \quad \mu > 1.0$$
$$= 0 \qquad ; \quad \mu \leq 1.0 \tag{2.27b}$$

$$\theta^* = \cos^{-1}\left(1 - \frac{2}{\mu}\right) \qquad ; \quad \mu > 1.0$$
$$= \pi \qquad ; \quad \mu \leq 1.0 \tag{2.27c}$$

where α is the bilinear hardening coefficient, and μ is the ductility factor defined as the ratio of maximum displacement A to yield displacement x_y, as shown in Fig. 2.1.

The modulus $\frac{A}{R}$ and the phase angle ϕ of the nonlinear transfer function can be expressed in terms of ω_{eq} and β_{eq} by using Eqs. (2.3a) and (2.3b) as follows.

$$\frac{A}{R} = \frac{1}{m[(\omega_{eq}^2 - \omega^2)^2 + (-2\beta_{eq}\omega_{eq}\omega)^2]^{\frac{1}{2}}} \tag{2.28a}$$

$$\tan \phi = \frac{-2\beta_{eq}\omega_{eq}\omega}{\omega_{eq}^2 - \omega^2} \tag{2.28b}$$

Figure 2.4 shows plots of Eqs. (2.28a) and (2.28b) for different ductility factors. It was shown by Iwan [14] that the solutions are very accurate for moderately nonlinear systems and reasonably accurate for nearly-elastoplastic systems. It is evident that the effective frequency of the system decreases with increasing level of response nonlinearity. As the ductility factor increases to large values, the effective frequency approaches $\sqrt{\alpha}\,\omega_0$, which corresponds to a system with stiffness αk_0.

It may be noted that the equivalent linear damping obtained from Eq. (2.26) is frequency dependent. For response calculations in the time domain, a constant equivalent damping is needed. For this purpose, Eq. (2.26) may be approximated as

$$\beta_{eq} = \xi \frac{\omega_0}{\omega_{eq}} - \frac{\bar{S}(A)}{2\bar{C}(A)} \tag{2.29}$$

Use of the equivalent linear damping given by Eq. (2.29) instead of Eq. (2.26) distorts the transfer function in Eqs. (2.28a) and (2.28b). The results are shown in Fig. 2.4.

The equivalent linear frequency and damping in Eqs. (2.25) and (2.29), respectively, as shown in Fig. 2.5, yield the same results as the Dynamic Stiffness method discussed by Jennings [19]. Several other approaches to the equivalent linearization of an elastoplastic system were summarized in Ref. [19]. One of the simplest approaches is the use of the secant stiffness of the equivalent linear system [31, 32]. Equivalent linear frequency and damping as a function of ductility factor, based on this approach are compared in Fig. 2.5 with those of Eqs. (2.25) and (2.29).

2.4 Nonlinear Multi Degree-of-Freedom System

The approximate solution is derived by the same technique which was used for the nonlinear SDF system in Section 2.3.

Consider a MDF system with softening hysteresis subjected to harmonic base motion. The equation of motion is

$$[M]\{\ddot{u}\}_{ex} + [C]\{\dot{u}\}_{ex} + \{F(\{u\}_{ex}, \{\dot{u}\}_{ex})\} = [M]\{r\}\, R \cos \omega t \qquad (2.30)$$

where $\{u\}_{ex}$ is the vector of displacements relative to ground, and $\{F(\{u\}_{ex}, \{u\}_{ex})\}$ is the hysteretic restoring force vector.

The nonlinear system is replaced by an equivalent linear system

$$[M]\{\ddot{u}\} + [C]_{eq}\, \{\dot{u}\} + [K]_{eq}\, \{u\} = [M]\{r\}\, R \cos \omega t \qquad (2.31)$$

where $\{u\}$ is the displacement vector of the linear system.

Equation (2.31) is uncoupled using the mode shapes $[\Phi]$ of the equivalent linear system. Equation (2.31) then becomes

$$m_n \ddot{\eta}_n + 2\beta_{neq} m_n \omega_{neq} \dot{\eta}_n + k_{neq} \eta_n = \Gamma_{neq}\, R \cos \omega t \qquad (2.32)$$

The damping matrix of the equivalent linear system will be constructed so that it can be uncoupled by the equivalent linear mode shapes.

The displacement vector, $\{u\}$, of the equivalent linear system is substituted into Eq. (2.30). Decomposing using the equivalent linear mode shapes yields

$$m_n\ddot{\eta}_n + 2\xi_n m_n \omega_n \dot{\eta}_n + f_n + \varepsilon_n = \Gamma_{neq} R \cos \omega t \tag{2.33a}$$

in which

$$f_n = \{\Phi_n\}^T \{F\} \tag{2.33b}$$

and f_n is the modal force which is nonlinear. ε_n is the equation deficiency of mode n and is given by

$$\varepsilon_n = c_n^* \dot{\eta}_n + k_{neq} \eta_n - f_n \quad ; \quad c_n^* = c_{neq} - c_n \tag{2.33c}$$

Minimizing the modal mean square error over one cycle of response as in Section 2.3 yields

$$k_{neq} = \overline{f_n \eta_n} \,/\, \overline{\eta_n^2} \tag{2.34a}$$

$$c_n^* = \overline{f_n \dot{\eta}_n} \,/\, \overline{\dot{\eta}_n^2} \tag{2.34b}$$

The hysteretic restoring force may be put in the form

$$\{F\} = \sum_e [L]_e^T \{F\}_e \tag{2.35}$$

where $\{F\}_e$ is the element hysteretic restoring force vector of order (MX1).

Equation (2.33b) in view of Eqs. (2.10b), (2.11b), (2.11c) and (2.13) becomes

$$f_n = \sum_e \varepsilon_{en} \sigma_e \tag{2.36}$$

where ε_{en} is the element strain for mode n which may be expressed in the form of Eq. (2.17a) as

$$\varepsilon_{en} = E_{en} \cos (\omega t + \psi_n) \tag{2.37}$$

The numerators in Eqs. (2.34a) and (2.34b) may be rearranged as

$$\overline{f_n r_n} = \pi \sum_e A_n \varepsilon_{en} E_e [\bar{C}_e \cos (\phi_n - \psi_e) - \bar{S}_e \sin (\phi_n - \psi_e)] \tag{2.38a}$$

$$\overline{f_n \dot{r}_n} = -\pi \sum_e \omega A_n \varepsilon_{en} E_e [\bar{C}_e \sin (\phi_n - \psi_e) + \bar{S}_e \cos (\phi_n - \psi_e)] \tag{2.38b}$$

in which

$$\bar{C}_e = \frac{1}{\pi E_e} \int_0^{2\pi} \sigma_e \cos \theta_e \, d\theta_e \tag{2.38c}$$

$$\bar{S}_e = \frac{1}{\pi E_e} \int_0^{2\pi} \sigma_e \sin \theta_e \, d\theta_e \tag{2.38d}$$

Equations (2.34a) and (2.34b) become, respectively,

$$k_{neq} = \sum_e \frac{\varepsilon_{en}}{A_n} \left[\bar{C}_e \sum_{j=1}^{N} \varepsilon_{ej} A_j \cos (\phi_n - \phi_j) - \bar{S}_e \sum_{j=1}^{N} \varepsilon_{ej} A_j \sin (\phi_n - \phi_j) \right] \tag{2.39}$$

$$c_{neq} = c_n - \frac{1}{\omega} \sum_e \frac{\varepsilon_{en}}{A_n} \left[\bar{S}_e \sum_{j=1}^{N} \varepsilon_{ej} A_j \cos (\phi_n - \phi_j) + \bar{C}_e \sum_{j=1}^{N} \varepsilon_{ej} A_j \sin (\phi_n - \phi_j) \right] \tag{2.40}$$

For a bilinear hysteretic system, Eqs. (2.38c) and (2.38d) become, respectively,

$$\begin{aligned} \bar{S}_e &= \frac{-(1 - \alpha_e) k_e}{\pi} \sin^2 \theta_e^* && ; \mu_e > 1.0 \\ &= 0 && ; \mu_e \leq 1.0 \end{aligned} \tag{2.41a}$$

$$\bar{C}_e = \frac{k_e}{\pi}\left[(1-\alpha_e)\,\theta_e^* + \alpha_e\pi - \frac{1-\alpha_e}{2}\sin 2\theta_e^*\right] \quad ; \mu_e > 1.0$$
$$= k_e \quad ; \mu_e \leq 1.0 \tag{2.41b}$$

$$\theta_e^* = \cos^{-1}\left(1 - \frac{2}{\mu_e}\right) \quad ; \mu_e > 1.0$$
$$= \pi \quad ; \mu_e \leq 1.0 \tag{2.41c}$$

where α_e is the bilinear hardening coefficient and μ_e is the element ductility factor defined as the ratio of maximum element relative displacement to yield displacement. These expressions are identical to those given in Eqs. (2.27) for the SDF system.

Equations (2.39) and (2.40) give the equivalent linear stiffness and damping in terms of the element properties. If these element equivalent linear stiffnesses are used to calculate a set of mode shapes $[\Phi]$, then the orthogonality conditions yield

$$\sum_e \varepsilon_{en}\,\bar{C}_e\,\varepsilon_{ej} = 0 \qquad n \neq j \tag{2.42a}$$

$$\sum_e \varepsilon_{en}\,\bar{S}_e\,\varepsilon_{ej} = 0 \qquad n \neq j \tag{2.42b}$$

The damping matrix $[C]_{eq}$ can be constructed from the $\bar{S}_e$ values in such a way that Eq. (2.42b) is satisfied, if the original viscous damping matrix $[C]$ can be uncoupled by the equivalent linear mode shapes.

Equations (2.39) and (2.40) in view of Eqs. (2.42a) and (2.42b) become, respectively,

$$k_{neq} = \sum_e \varepsilon_{en}^2\,\bar{C}_e$$
$$= m_n\,\omega_{neq}^2 \tag{2.43}$$

$$\beta_{neq} = \frac{c_{neq}}{2m_n \omega_{neq}}$$

$$= \xi_n \frac{\omega_n}{\omega_{neq}} - \frac{\sum_e \varepsilon_{en}^2 \bar{S}_e}{2m_n \omega_{neq} \omega} \tag{2.44}$$

Iwan [15] derived the steady state solution for a hysteretic system using the original elastic mode shapes as a basis. If this approach is taken, a significant amount of coupling between the modal responses can occur. Use of the equivalent linear mode shapes eliminates this coupling (to the degree of accuracy inherent in the approximate solution).

As in the SDF case, the equivalent modal damping in Eq. (2.44) is frequency dependent. Similarly to Eq. (2.29), Eq. (2.44) may be approximated as

$$\beta_{neq} = \xi_n \frac{\omega_n}{\omega_{neq}} - \frac{\sum_e \varepsilon_{en}^2 \bar{S}_e}{2 \sum_e \varepsilon_{en}^2 \bar{C}_e} \tag{2.45}$$

The equivalent linear modal damping β_{neq} in Eq. (2.45) is the relative strain energy weighted average of the equivalent linear damping associated with each strain element [30, 32].

The approximate nonlinear modal transfer function may be obtained by inserting Eqs. (2.43) and (2.44) in Eqs. (2.14).

The steady state response of the 2DF bilinear system shown in Fig. 2.1 was found by iteration. The yielding was permitted to occur only at the base story. The input frequency, ω, was varied for a constant excitation intensity, R. The linear solutions were used in the first iteration.

The element ductility factors were estimated using Eq. (2.17b). The element ductility factors were then used to modify the mode shapes in Eq. (C.18). The equivalent frequency and damping in Eqs. (2.43) and (2.44) and the modal transfer function in Eqs. (2.14a) and (2.14b) were consecutively obtained. New estimates of the element ductility factors were then used to iterate the process until a preset 2% convergence criterion on the element ductility factors was met. Figure 2.6 shows plots of Eqs. (2.14a), (2.14b), (2.16b) and (2.17b), respectively, of the converged systems for different levels of constant excitation intensity, R. The plots show the four different curves labeled 1, 2, 3 and 4. Each curve corresponds to a constant excitation level with mR/F_{y1} equal to 0, 0.13, 0.195 and 0.25, respectively. The response ductility varies along each curve. The maximum ductilities of the base story at resonance are approximately equal to 1, 3, 10 and 30, respectively. A few cycles of iteration were normally sufficient. More cycles of iteration were needed at frequencies close to resonance. It is noted that the frequency shift of the first mode response is quite consistent with that of the SDF system shown in Fig. 2.4. It is also interesting to note that as the response ductility increases, the amplitude of the second mode response decreases and its frequency shift is insignificant. This implies that for this particular 2DF system with yielding at the base story, the first mode participation increases while the second mode participation decreases. The system displacements, u_1 and u_2, and the element strains, ε_1 and ε_2, consist of increasing amounts of first mode and decreasing amounts of second mode response as the ductility increases.

Computed element strains of the 2DF bilinear system for $mR/F_{y1} = 0.195$ are compared with the approximate results in Fig. 2.6. These were calculated by step-by-step numerical integration of harmonic forced vibration for a duration equal to 40 times the fundamental natural period of the system. The duration was chosen long enough to essentially eliminate transient effects due to zero initial conditions. The comparison is quite satisfactory, as shown in Fig. 2.6.

As noted previously, the original elastic mode shapes result in a coupling between modes. To investigate whether the coupling is significant, the modal transfer functions referred to the linear mode shapes were calculated.

The approximate nonlinear transfer functions may be obtained for an arbitrary set of mode shapes. The transformation from the equivalent linear mode shape basis to the arbitrary mode shape basis yields

$$\left(\frac{A_{n_0}}{R}\right)^2 = \sum_{m=1}^{N} a_{nm}^2 \left(\frac{A_m}{R}\right)^2 + \sum_{\substack{i=1 \\ l \neq j}}^{N} \sum_{j=1}^{N} a_{ni}\, a_{nj}\, \frac{A_i}{R}\, \frac{A_j}{R} \cos(\phi_i - \phi_j) \tag{2.46a}$$

$$\tan \phi_{n_0} = \frac{\sum_{m=1}^{N} a_{nm} \frac{A_m}{R} \sin \phi_m}{\sum_{m=1}^{N} a_{nm} \frac{A_m}{R} \cos \phi_m} \tag{2.46b}$$

in which

$$a_{nm} = \frac{1}{m_{n_0}} \{\Phi_{n_0}\}^T [M] \{\Phi_m\} \tag{2.47a}$$

$$m_{n_0} = \{\Phi_{n_0}\}^T [M] \{\Phi_n\} \tag{2.47b}$$

Iwan [15] derived a result similar to Eq. (2.46a).

Figure 2.7 shows the computed responses, using the original elastic mode shapes, of the same system shown in Fig. 2.6. It is obvious that the modal responses are now highly coupled.

Discussion -- In a later chapter, the use of inelastic response spectra for earthquake response will be investigated. It is convenient for this purpose to make several observations here regarding the equivalent linear system.

The equivalent linear stiffness and damping of the modal SDF system given by Eqs. (2.43) and (2.44) can be regarded as representing the equivalent linearization of a nonlinear SDF system.

Let

$$\overline{C}_n = \sum_e \varepsilon_{en}^2 \, \overline{C}_e \tag{2.48a}$$

$$\overline{S}_n = \sum_e \varepsilon_{en}^2 \, \overline{S}_e \tag{2.48b}$$

If $\overline{C}_n$ and $\overline{S}_n$ are viewed as the parameters of a nonlinear modal SDF system, the modal ductility factor and the modal hysteresis properties could be determined from Eqs. (2.48a) and (2.48b). The elastic stiffness of the nonlinear modal SDF system is taken as

$$\overline{k}_n = \sum_e \varepsilon_{en}^2 \, k_e \tag{2.49}$$

Note that the "elastic stiffnesses" of the modal bilinear SDF systems are shifted slightly from the original elastic modal stiffnesses, since the modal strains of the equivalent linear system are used in the computation.

For a bilinear MDF system, Eqs. (2.48a) and (2.48b) in view of Eqs. (2.41a) to (2.41c) and Eq. (2.49) can be put in the forms

$$(1 - \alpha_n)\, \bar{k}_n\, \bar{c}_n = \sum_e \varepsilon_{en}^2\, (1 - \alpha_e)\, k_e\, \bar{c}_e \tag{2.50a}$$

$$(1 - \alpha_n)\, \bar{k}_n\, \bar{s}_n = \sum_e \varepsilon_{en}^2\, (1 - \alpha_e)\, k_e\, \bar{s}_e \tag{2.50b}$$

in which

$$\bar{c}(\mu) = 1 - \frac{\theta^*}{\pi} + \frac{\sin 2\theta^*}{2\pi} \tag{2.50c}$$

$$\bar{s}(\mu) = \sin^2 \theta^* \tag{2.50d}$$

$$\theta^* = \cos^{-1} \left(1 - \frac{2}{\mu}\right) \tag{2.50e}$$

$$\Delta k = (1 - \alpha)\, k\, \bar{c}(\mu) = k - \bar{C} \tag{2.50f}$$

where μ_n and α_n are the modal ductility and bilinear hardening, respectively. Δk is the change in stiffness. In this form, the ductility factor and bilinear hardening can be separated by dividing Eq. (2.50a) by (2.50b) to yield a transcendental equation for μ_n.

If the equivalent linear stiffness $\bar{C}(\mu)$ is approximated by the secant stiffness, Eq. (2.50c) and Eq. (2.50d) become

$$\bar{c}(\mu) = 1 - \frac{1}{\mu} \tag{2.50g}$$

$$\bar{s}(\mu) = \frac{4(\mu-1)}{\mu^2} \tag{2.50h}$$

By dividing Eq. (2.50b) by Eq. (2.50a) in view of Eqs. (2.50f), (2.50g) and (2.50h), an explicit expression for modal ductility can be written as

$$\frac{1}{\mu_n} = \frac{\sum_e \varepsilon_{en}^2\, \Delta k_e\, \frac{1}{\mu_e}}{\sum_e \varepsilon_{en}^2\, \Delta k_e} \tag{2.51}$$

Thus modal ductility μ_n is defined as a weighted average of element ductilities μ_e. When all $\mu_e = 1$, i.e., the system is elastic, Eq. (2.51) degenerates to a 0/0 form. In this case, of course, the modal ductility $\mu_n = 1$, for all modes n.

Although Eq. (2.51) was derived using the secant stiffness approximation, it can be used with the equivalent linear stiffness expression for Δk_e.

The modal bilinear hardening can then be found using μ_n and Eq. (2.50a) or (2.50b). This removes one of the major difficulties associated with using nonlinear response spectra, i.e., the determination of a modal ductility.

CHAPTER 3

CORRELATION OF STEADY STATE AND EARTHQUAKE RESPONSES OF A BILINEAR HYSTERETIC SYSTEM

3.1 Introduction

The purpose of this study is to investigate approximate methods of solution for MDF systems subjected to earthquake excitation. It is possible to obtain an equivalent linear system for transient response by minimizing mean square error over the duration of the motion. This can be done iteratively until some convergence criterion is met. The major disadvantage of this approach is that a sequence of time histories of response must be computed. From a practical standpoint, it is necessary that the procedure can be carried out knowing only the maximum responses of the equivalent systems, i.e., using response spectra. A second alternative would be to develop a relationship between equivalent linear stiffness and maximum response, essentially using the first approach for a large number of earthquakes and then correlating the maximum response with the computed values of equivalent linear stiffness and damping. This would require a great deal of computational effort primarily because of the variability in the characteristics of recorded earthquakes. The approach which is taken here is to utilize the steady state harmonic response results of Chapter 2 for earthquake response. This is done for two reasons; first, the equivalent linear stiffness and damping are given by relatively simple closed-form expressions, and second, these expressions can be easily derived for types of hysteresis other than bilinear.

The steady state solution for harmonic input cannot be directly applied to the transient earthquake response. The most obvious reason for this is

that the harmonic steady state maximum response is reached at every cycle while the earthquake maximum response is reached only once during the motion. In addition, the earthquake response and input motion both start from rest and require some build-up time to reach "stationary" values. Therefore, the direct use of the maximum earthquake response in the steady state harmonic solution would generally overestimate the equivalent linear damping and frequency shift.

The objective of this chapter is to find a pseudo-steady state harmonic response which gives the same effective damping and frequency shift as the transient response of a SDF system. This pseudo-steady state harmonic response is related to the maximum response by means of a correlation factor. The correlation factor is obtained from available analog computer results for bilinear SDF systems subjected to stationary Gaussian white noise input and to bursts of white noise and later verified using earthquake input.

The first part of the chapter (Sec. 3.2) gives a general description of the computed results for SDF bilinear systems used later. These consist of analog computer results for Gaussian white noise input, and digital computer results for earthquake and pulse-like inputs. The earthquake and pulse-like input responses are examined in the frequency domain using Fourier analysis.

In the second part of the chapter (Sec 3.3), the analog computer data is used first to relate the stationary rms response to the pseudo-steady state maximum response. Later, an approximate relation between the expected maximum response and the stationary rms response is developed, using analog computer data and a theoretical result of Davenport [9]. This makes it

possible to directly correlate the expected maximum and the pseudo-steady state maximum responses.

In the third part (Sec. 3.4), equivalent linear frequencies and damping determined from frequency decomposition of earthquake response are compared with those for white noise input, using the relationship between maximum and stationary rms responses. Then the earthquake responses of a number of 3DF bilinear systems decomposed into both the original elastic and the equivalent linear mode shapes are compared in the frequency domain with the approximate analytical ones. The effect of modal coupling between the original elastic mode shapes is discussed.

3.2 Computed Results

In this section the computed responses of the bilinear SDF system shown in Fig. 3.1 are briefly described and discussed.

3.2.1 Analog Computer Data -- Caughey [6] applied the equivalent linearization technique to the random vibration of a bilinear SDF system subjected to stationary Gaussian white noise. It can be shown that the mean square displacement and velocity of the equivalent linear system can be expressed in the form,

$$\sigma_x^2 = \frac{S_0}{4m^2\beta_{eq}\omega_{eq}^3} \tag{3.1a}$$

$$\sigma_{\dot{x}}^2 = \frac{S_0}{4m^2\beta_{eq}\omega_{eq}} \tag{3.1b}$$

where S_0 is the power spectral density of the stationary Gaussian white noise.

The equivalent linear frequency, ω_{eq}, and the equivalent linear damping, β_{eq}, can be calculated if the rms displacement and velocity are known. Brown [4] and Lutes and Takemiya [21] calculated the equivalent linear frequency and damping using this method by measuring the rms levels of displacement and velocity of bilinear SDF systems on an analog computer. The computed equivalent linear frequency and damping are shown in Fig. 3.2 as a function of stationary rms ductility, μ_{σ_s}, for different values of damping, ξ, and bilinear hardening, α. The term ductility as used here means response normalized by the yield displacement of the system.

The equivalent linear system yields a transfer function whose modulus is a smooth single lobe function. The analog computer results [17] show a transfer function whose modulus has two lobes, one close to the linear frequency and the other close to the frequency of a system with stiffness equal to the second slope of the hysteresis loop. It is interesting that the same nonlinear system under steady state harmonic excitation has a transfer function modulus resembling that of a linear system. The relative sizes of the two lobes depend on the magnitude of the response. However, an equivalent linear frequency and damping can still be determined by matching the rms displacement and velocity of the nonlinear system regardless of the dissimilarity of its transfer function to that of a linear system.

Caughey's theoretical result [6] for equivalent linear stiffness for random vibration is compared with the analog computer results in Fig. 3.8. The expression for equivalent linear stiffness is too complicated to evaluate in closed form and does not agree particularly well with the analog results for highly nonlinear systems (i.e., systems with small

values of bilinear hardening, α). The method is based on the assumption that the response is narrow frequency banded and approximately Gaussian. These assumptions are not very accurate for systems with small bilinear hardening as shown in Fig. 3.8. It was shown by Iwan and Lutes [17] that for $\alpha = 1/21$, the error of the Kryloff-Bogoliuboff method is about 25% maximum underprediction of velocity when stationary rms ductility $\mu_{\sigma_s} \simeq 5$ and approximately 50% maximum underprediction of displacement when $\mu_{\sigma_s} \simeq 1$. More accurate procedures have been developed subsequently. Lutes and Takemiya [21] developed an approximate analytical method to predict the stationary rms response. The method was based on a power balance between the exciting force and the energy dissipating elements. In view of the relative complexity of these theoretical approaches, it seems worthwhile to attempt to use the steady state results of Chapter 2, as outlined previously.

The response parameter which is of greatest interest is the maximum or extreme value of the response during the motion. Analog computer data for linear and bilinear SDF systems subjected to bursts of stationary Gaussian white noise were presented by Lutes and Chokshi [22] and Chokshi and Lutes [8]. These studies presented the relation between the "zero-start" maximum ductility, μ_z, and stationary rms ductility, μ_{σ_s} as a function of duration of excitation, T_d, and system linear natural frequency, f_o, as shown in Fig. 3.3. This relationship allows for the fact that the oscilator starts from rest.

3.2.2 Earthquake Response -- A useful advantage achieved from the study of nonlinear response in the frequency domain is that the response behavior and the change in the frequency content as a function of ductility

and nonlinearity can be clearly observed.

Two series of bilinear SDF systems with 5% of critical damping are subjected to 16 seconds of El Centro 1940-NS. The first series has linear natural frequency f_o = 1.0 cps and bilinear hardening α = 0.3. The second has f_o = 0.5 cps, α = 0.5. The El Centro input is shown in Fig. D.1. The maximum ductility ranges from 1.5 to 10. By using the digital Fast Fourier Transformation technique (FFT), the displacement response histories of these systems and the corresponding ground motions are transformed into the frequency domain. The displacement response is then normalized by the ground motion in the frequency domain yielding the so-called "nonlinear transfer functions" shown in Fig. 3.4.

The low frequency tail of each curve in Fig. 3.4 is terminated at about twice the lowest significant frequency. The lowest significant frequency depends on the time duration used in the FFT technique. It is equal to the reciprocal of the time duration used. Frequency content lower than this frequency is considered to be insignificant due to inadequate response duration in the time domain. The curves are cut at twice this value to compensate for the spreading introduced by the Hanning smoothing in the FFT technique. Details of the use of the digital FFT technique are given in Appendix B.

Systems with the bilinear hardening smaller than 0.3 are not considered in the portion of the study dealing with frequency decomposition. This is because of the large amount of low frequency content which arises in these systems for high ductilities.

As observed from Fig. 3.4, the nonlinear transfer functions do not have a close similarity to a linear transfer function. The dominant low

and high frequency lobes of the nonlinear transfer function may be approximately weighted to yield a smooth single lobe equivalent linear transfer function. A more elaborate procedure was not justified because the equivalent linear frequencies and damping which were determined in this way are not an essential part of the procedure. Extensive calculations comparing maximum responses are made later to assess accuracy. The fitting was done by approximately weighting the two lobes of the nonlinear transfer function to determine resonant frequency and amplitude at resonance. At resonance, Eq. (2.28a) becomes

$$\left(\frac{A}{R}\right)_{res} = \frac{1}{m[(\omega_{eq}^2 - \omega_{res}^2)^2 + (2\beta_{eq}\omega_{eq}\omega_{res})^2]^{1/2}} \tag{3.2}$$

in which

$$\omega_{res} = \omega_{eq}\sqrt{1 - 2\beta_{eq}^2} \tag{3.3}$$

where the subscript res denotes the resonance.

The equivalent linear frequency, ω_{eq}, and damping, β_{eq}, are found from Eqs. (3.2) and (3.3) using the resonant frequency and amplitude. The equivalent linear frequency and damping versus the maximum ductility, μ_z, are shown in Figs. 3.5.

3.2.3 Pulse-Like Excitation Response -- A number of bilinear SDF systems with 5% of critical damping and bilinear hardening of 0.7, 0.5 and 0.3 are subjected to the pulse-like excitation shown in Fig. D.5 with 10 seconds of zero input at the end. The maximum ductility ranges from 1.5 to 11. The computed nonlinear transfer functions are shown in Fig. 3.6.

The computed nonlinear transfer functions in Fig. 3.6 show the influence of ductility on the nonlinear response. The most significant effects are the shifting of the effective frequency and widening of the transfer function which results in an increase of the effective damping. In all cases, the amplitude of the nonlinear transfer function decreases as the ductility increases from 1.0 to about 4.0 and increases as the ductility increases from about 4.0 to higher values. This phenomenon is also observed in the nonlinear transfer function of bilinear SDF systems subjected to stationary Gaussian white noise excitation [17].

It is noted from the figures that the nonlinear transfer functions look very different from the transfer function of a linear system and also very different from the nonlinear transfer function for steady state response in Chapter 2. Furthermore, the shape of the nonlinear transfer function of a bilinear system subjected to the El Centro 1940-NS motion is quite different from that of the same system subjected to the pulse-like excitation. This is, of course, expected.

The plots of the nonlinear transfer functions show that the response of systems with high values of bilinear hardening is approximately narrow frequency banded. This is shown in Fig. 3.6a for the 1 cps system with bilinear hardening of 0.7 and 5% of critical damping subjected to the pulse-like excitation. The maximum ductility ranges from 2.2 to 9.7. As the nonlinearity increases (i.e., as the bilinear hardening decreases), the nonlinear response is not, in general, narrow frequency banded except in the case of very low ductility systems. Figs. 3.4, 3.6b and 3.6c show the responses of bilinear systems with natural frequencies of 0.5 and 1.0 cps, bilinear hardening of 0.5 and 0.3 and 5% critical damping. The maximum

ductility ranges from 1.5 to 10.8. The nonlinear transfer functions of very low ductility systems show that the responses are primarily narrow frequency banded at a frequency close to the linear natural frequency with a small amount of low frequency content close to the second slope natural frequency. The response of such systems in the time domain is close to linear response with a small amount of low frequency drifting. As the ductility increases, the low frequency content becomes larger while the high frequency content becomes smaller. The total response is no longer narrow frequency banded. The response of such systems in the time domain contains large low frequency drifting together with high frequency oscillations.

3.3 Correlation Factor

In this section, a correlation factor is obtained which relates the maximum response to a pseudo-steady state maximum. The steady state solutions of Chapter 2 for equivalent linear frequency and damping can then be applied when the system is subjected to earthquake input.

Consider a steady state response as shown schematically in Fig. 3.7. The steady state rms and maximum ductilities are related by

$$\mu_A = \sqrt{2}\, \mu_{\sigma_A} \tag{3.4}$$

where μ_A and μ_{σ_A} are the steady state maximum and rms ductilities, respectively.

Now, consider a zero-mean stationary narrow band Gaussian process as shown schematically in Fig. 3.7. The peaks have a Rayleigh probability distribution. The stationary rms ductility and the stationary rms peak

ductility are related by

$$\mu_s = \sqrt{2}\mu_{\sigma_s} \tag{3.5}$$

where μ_s and μ_{σ_s} are the stationary rms peak ductility and the stationary rms ductility, respectively.

Since the peak response varies from cycle to cycle when the input has a broad band frequency content, it might be thought that a good measure of "average peak response" would be the rms value of the peaks. The similarity of Eq. (3.4) for harmonic input and Eq. (3.5) for random input suggests that a pseudo-steady state maximum ductility might be defined as

$$\mu_A^* = \sqrt{2}\mu_{\sigma_s} \tag{3.6}$$

where * denotes the pseudo-steady state value.

The pseudo-steady state maximum ductility μ_A^* is substituted into Eqs. (2.25), (2.27) and (2.29). The equivalent linear stiffness and damping are compared in Fig. 3.8 with those obtained via the Kryloff-Bogoliuboff method [4].

It is observed from the shapes of the curves of equivalent linear damping versus the rms ductility that a single expression for all values of bilinear hardening, α, cannot give a reasonable match with the analog computer data. In order to be on the conservative side and to agree with the analog computer data in Fig. 3.2 in the range of practical interest, i.e., $\mu_{\sigma_s} \simeq$ 1-3, the equivalent linear damping in Eq. (2.29) is reduced by a factor RF which is taken as $\frac{1}{\sqrt{2}}$ for bilinear systems. The reduced equivalent linear damping for α = 1/2 and 1/21 versus the stationary rms response ductility is shown in Fig. 3.8.

For linear or slightly nonlinear systems, the pseudo-steady state maximum given by Eq. (3.6) is adequate. As the nonlinearity becomes higher (or α becomes smaller), the expression in Eq. (3.6) has to be modified. Figure 3.8 shows that different correlation factors are required for the equivalent linear frequency and damping. The correlation factor required for the equivalent linear frequency is sensitive to the degree of nonlinearity (i.e., the bilinear hardening) while the correlation factor for the equivalent linear damping is not. It is interesting that the correlation factors are quite insensitive to ductility.

The modifications to Eq. (3.6) which are necessary for low values of bilinear hardening were determined as follows. From the analog computer data in Fig. 3.2, each value of the equivalent linear frequency and damping is associated with a corresponding stationary rms ductility, μ_{σ_s}. Equations (2.25), (2.27) and (2.29) were used to determine the pseudo-steady state maximum ductility factors, $\mu^*_{A_F}$ and $\mu^*_{A_D}$, which give the same equivalent linear frequency and damping. The ratios of $\mu_{\sigma_s}/\mu^*_{A_D}$ and $\mu_{\sigma_s}/\mu^*_{A_D}$ were then plotted for each value of bilinear hardening as shown in Figs. 3.9 and 3.10. A single best-fit value of each ratio was then determined for each value of α as shown in Figs. 3.9 and 3.10. Figure 3.11 shows these values of $\mu_{\sigma_s}/\mu^*_{A_F}$ and $\mu_{\sigma_s}/\mu^*_{A_D}$ as a function of bilinear hardening, α, on a log-log scale. These relations can be expressed in the form

$$\frac{\mu_{\sigma_s}}{\mu^*_{A_F}} = \frac{1}{\sqrt{2}}\,\alpha^{0.2} \tag{3.7a}$$

$$\frac{\mu_{\sigma_s}}{\mu^*_{A_D}} = \frac{1}{\sqrt{2}} \tag{3.7b}$$

Equations (3.7a) and (3.7b) relate the stationary rms ductility and the pseudo-steady state maximum ductilities. $\mu^*_{A_F}$ is used to calculate equivalent linear frequency, and $\mu^*_{A_D}$ is used to calculate equivalent linear damping, given the stationary rms ductility.

It is now necessary to obtain a relation between stationary rms ductility and the expected maximum response so that the equivalent linear frequency and damping can be calculated from maximum response. The term "zero-start expected maximum" response is used to denote the average over a very large number of response histories of the maximum response of a system which starts from rest. The ratio of zero-start expected maximum response to the stationary rms response from the analog computer data described in Section 3.2.1 is shown in Fig. 3.3. This ratio can be quite well represented by the single expression

$$\frac{\mu_z}{\mu_{\sigma_s}} = [2 \ln (f_o T_d)]^{1/2}, \qquad \text{small } f_o T_d \tag{3.8}$$

where μ_z is the zero-start expected maximum ductility factor. The form of the relation was suggested by the theoretical result of Davenport [9]. It appears to be sufficiently accurate for all values of bilinear hardening, ductility, and viscous damping.

Equation (3.8) applies to a bilinear SDF system with short duration of excitation ($f_o T_d$ less than about 10) and is plotted in Fig. 3.3. For larger values of $f_o T_d$, Chokshi and Lutes [8] assumed that the maximum response has a Gumbel probability distribution and derived an expression for the ratio in Eq. (3.8). For $f_o T_d$ between 10 and 40, their result and Eq. (3.8) yield approximately the same value. Equation (3.8) is used in this study.

Substitution of Eq. (3.8) into Eqs. (3.7a) and (3.7b) yields

$$\mu^*_{A_F} = \frac{1}{\alpha^{0.2}\sqrt{\ln(f_o T_d)}}\,\mu_z \tag{3.9a}$$

$$\mu^*_{A_D} = \frac{1}{\sqrt{\ln(f_o T_d)}}\,\mu_z \tag{3.9b}$$

Figure 3.12 shows plots of Eqs. (3.9).

Equations (3.9a) and (3.9b) provide the means for calculating equivalent linear frequency and damping from the maximum response. Given the maximum response μ_z, the pseudo-steady state maxima $\mu^*_{A_F}$ and $\mu^*_{A_D}$ are used to calculate equivalent linear frequency and damping, respectively, from the steady-state relations.

Equations (2.25) and (2.29), in view of Eqs. (3.9a) and (3.9b) and the application of the reduction factor RF, become respectively

$$\begin{aligned} k_{eq} &= m\omega^2_{eq} \\ &= \bar{C}(\mu^*_{A_F}) \end{aligned} \tag{3.10}$$

$$\beta_{eq} = \xi\frac{\omega_0}{\omega_{eq}} - RF\left[\frac{\bar{S}(\mu^*_{A_D})}{2\bar{C}(\mu^*_{A_D})}\right] \tag{3.11}$$

Equations (2.43) and (2.45), in view of Eqs. (3.9a) and (3.9b) and the application of the reduction factor RF, become respectively

$$\begin{aligned} k_{neq} &= m_n\omega^2_{neq} \\ &= \sum_e \varepsilon^2_{en}\,\bar{C}_e(\mu^*_{Ae_F}) \end{aligned} \tag{3.12}$$

$$\beta_{neq} = \xi_n \frac{\omega_n}{\omega_{neq}} - RF \left(\frac{\sum_e \varepsilon_{en}^2 \, \overline{S}(\mu^*_{Ae_D})}{2\sum_e \varepsilon_{en}^2 \, \overline{C}(\mu^*_{Ae_D})} \right) \tag{3.13}$$

3.4 Earthquake Response in the Frequency Domain

The correlation factor developed in Section 3.3 was obtained using data for response to white noise input. In this section a comparison is first made of this data with that for SDF systems subjected to earthquake input.

A series of 3DF system responses is then examined in the frequency domain to compare computed responses with analytically "predicted" ones. The analytically "predicted" responses are obtained using (1) the maximum ductilities computed from a numerical step-by-step integration, (2) the correlation factors given in Eqs. (3.9), and (3) the procedure developed in Chapter 2 for steady state harmonic response of MDF systems. Of course, the numerically computed maximum ductilities are not normally available. In a practical situation one must begin with a linear solution, or some other initial guess, and iterate. This is dealt with in the following chapter.

3.4.1 SDF Systems -- The equivalent linear frequency and damping of the SDF systems subjected to earthquake input as described in Section 3.2.2 are compared with those of the SDF systems subjected to stationary Gaussian white noise as described in Section 3.2.1. This is done by transforming the scale of maximum response μ_z to rms ductility by using Eq. (3.8). The earthquake data, which was not used in the development of the correlation factor, agrees well with the white noise data as shown in Fig. 3.13. An extensive series of computations was done for SDF systems to evaluate

the accuracy of the approximate procedure. These comparisons are discussed in Chapter 5 and Appendix E.

3.4.2 3DF Systems -- A number of bilinear 3DF shear-beam systems with mass and stiffness arrangements defined in Tables 5.2 and 5.3 and with 2% modal damping for all modes were studied. The bilinear hardening is 0.3 for all stories, and the yield levels are arranged to give three different general ranges of story ductility factor. All the systems were subjected to El Centro 1940-NS and analyzed by step-by-step numerical integration. The displacements of the masses relative to the ground were decomposed into normal mode coordinates by using both the elastic and the equivalent linear mode shapes.

The nonlinear modal displacement transfer functions shown in Figs. 3.14a, 3.15a, 3.16a and 3.17a were obtained by performing a frequency decomposition using the FFT technique on the modal displacements and ground acceleration as described in Section 3.2.2.

Figure 3.14a shows the nonlinear modal transfer functions of the uniform systems in which yielding was permitted to occur only at the base story. The base story ductility ranged from 2 to 14 while the other stories remained elastic. The elastic mode shapes were used in the modal response decomposition. It is noted that the modal response is significantly coupled.

Figure 3.15a shows the nonlinear modal transfer functions of the same systems when the equivalent linear mode shapes were used in the modal response decomposition. The cross coupled response in this case is much reduced compared to that in Fig. 3.14a. Note that the analytically determined

equivalent linear stiffnesses are used to determine the equivalent linear mode shapes into which the numerically computed responses are decomposed.

Figure 3.16a shows the nonlinear modal transfer function of the uniform system where yielding was permitted in all stories, and was relatively uniform throughout the system. The largest ductility for any story ranged from 2 to 15. The equivalent linear mode shapes were used in the modal response decomposition. The frequency shift of the systems in Fig. 3.16a is greater than that of the systems in Fig. 3.15a. Yielding in all stories is expected to produce a greater frequency shift than the same amount of yielding in a single story.

Figure 3.17a shows the nonlinear modal transfer functions of the systems with nonuniform stiffness arrangement. Higher mode participation is greater in these systems than in the uniform systems. The equivalent linear mode shapes still uncouple the response to a satisfactory degree.

In all cases shown in Figs. 3.14a, 3.15a, 3.16a and 3.17a, the higher mode response in the frequency domain tends to be jagged. This may be partially due to numerical sensitivity in using the FFT technique. However, the overall behavior of the modal transfer functions in Figs. 3.15a, 3.16a and 3.17a is quite similar to those of SDF systems subjected to the same earthquake input and shown in Fig. 3.4a. Thus it appears that the modal transfer function of a nonlinear MDF system (in the equivalent linear normal mode coordinates) can be approximated by that of a nonlinear SDF system. This nonlinear SDF system has properties (stiffness, mass, yield level) which are determined as weighted averages of the properties of the nonlinear members making up the original MDF system, as discussed in Chapter 2.

Figures 3.14b, 3.15b, 3.16b and 3.17b also show the analytical modal transfer functions determined using the steady-state solutions in Chapter 2, together with the pseudo-steady state maximum responses described previously. Figures 3.18 to 3.21 show a more detailed comparison of the computed and analytical nonlinear modal transfer functions of the 3DF systems for several ductility levels. Despite the irregularity of the numerically computed responses, the general trends of frequency shift and spreading with increasing ductility are reasonably well predicted. The disadvantage of using the elastic mode shapes in modal response decomposition is obvious from a comparison of Figs. 3.18 and 3.19.

CHAPTER 4

APPROXIMATE MODAL ANALYSIS PROCEDURES FOR MDF SYSTEMS USING ELASTIC AND INELASTIC RESPONSE SPECTRA

4.1 Introduction

The objective of this chapter is to summarize and present numerical examples of the two procedures for approximate modal analysis of nonlinear MDF structures: (1) equivalent linear modal analysis using elastic response spectra and (2) equivalent nonlinear modal analysis using inelastic response spectra. The equivalent linear approach considers the change of mode shapes, effective frequencies, and increase in damping due to hysteresis. The equivalent nonlinear approach considers the change of mode shapes and superposes a series of modal SDF systems which are nonlinear. The modal hysteresis parameters and ductilities are found by appropriately weighting the contributions of each structural element.

The proposed procedures are iterative ones, in which the first step is the determination of elastic mode shapes and frequencies. Two or three cycles of iteration are normally sufficient. Very little computational effort beyond the initial determination of elastic mode shapes and frequencies is required.

Approximate modal analysis using design response spectra modified to account for inelastic behavior was first proposed by Newmark and Hall [27]. Several recent studies have investigated this concept [1, 23]. The general approach of these studies was to design a series of structures using elastic modal analysis and a smoothed response spectrum corresponding to a selected design ductility. The structures were then subjected to earthquake motions

approximately equivalent to the design spectrum. The responses computed by step-by-step numerical integration were compared with assumed design values. It was found that elastic modal analysis tended to smooth out patterns of yielding in the structure and was unable to adequately predict large local variations of yielding. Secondly, member response ductilities were often considerably above the ductility level implied by the inelastic spectrum.

The approximate modal analysis method using inelastic response spectra proposed in this study addresses both of these difficulties. Use of mode shapes, different from the elastic mode shapes, which reflect yielding in the structure should give better results when yielding is nonuniform. Modal ductility, defined as weighted average of member ductilities, is used for each mode of vibration. Thus, the ductilities used in the inelastic response spectrum are directly related to member ductilities.

4.2 Summary of Approximate Modal Analysis Procedures

In this section, the procedures for both the elastic and inelastic response spectrum approaches are outlined in a step-by-step format, and numerical examples of both procedures are given for a 3DF shear beam system.

Both procedures are iterative, beginning with an elastic modal analysis, and both take into account the change in mode shapes due to inelastic behavior. To avoid solving a new eigenvalue problem at each cycle of iteration, a perturbation method is used which determines first or second order changes in mode shapes as a function of stiffness changes in the structural elements.

4.2.1 Perturbation Method for Approximate Determination of Equivalent Linear Mode Shapes

A simple perturbation method is outlined in Appendix C for approximately determining the equivalent linear mode shapes from the elastic mode shapes as a function of stiffness "modification" due to inelastic behavior. These approximate mode shapes are termed "modified mode shapes" in this study to distinguish them from the equivalent linear mode shapes.

Once the modified mode shapes are determined, the equivalent linear frequencies are estimated with excellent accuracy using the Rayleigh quotient. This gives better accuracy than using the perturbation expansion of the same order as used for the modified mode shapes, and is consistent with Eq. (2.43).

Often the first order perturbation is sufficient for determining the modified mode shapes, since the shapes change very little if the yielding is fairly uniform throughout the structure.

Details of the perturbation method are given in Appendix C, which contains a series of comparisons from which the accuracy of the perturbation method can be judged.

4.2.2 MDF Equivalent Linear System - Elastic Response Spectrum

1. Determine elastic mode shapes and modal frequencies from the eigenvalue problem. At this step, the equivalent linear modal frequencies and damping and modified mode shapes are estimated as the elastic values.

2. Determine maximum modal displacements using elastic response spectra. Estimate element maximum strains (relative displacements) using

the usual RSS[1] or 1/2(RSS + ABS[2]) rules for combining the maximum modal strains. The element maximum strains are then normalized by the element yield strains to obtain element ductilities, μ_{z_e}.

3. Determine the element pseudo-steady state ductilities, $\mu^*_{Ae_F}$ and $\mu^*_{Ae_D}$, from Eqs. (3.9) or Fig. 3.12, where α_e is element bilinear hardening. The frequency f_0 is taken as the system fundamental elastic frequency in cps, and T_d is earthquake duration in seconds.

4. Determine the element equivalent linear stiffness $\bar{C}(\mu^*_{Ae_F})$ from Eqs. (2.41b) and (2.41c) or Fig. 2.5, where k_e is element elastic stiffness. $\bar{C}(\mu^*_{Ae_F})$ is then used as the element stiffness to determine the modified mode shapes from Eq. (C.18), in which ΔE_{nk} represents a strain energy change and is given by Eq. (C.17). The superscript (0) denotes the elastic values, ω_n is the modal natural circular frequency, ε_{en} is the element strain in mode n, and M is the number of modes considered in the modal analysis.

Eq. (C.18) gives the first-order expression for the modified mode shapes. If greater accuracy is required because of localized yielding in the structure, the second-order expressions given in Eq. (C.21) can be used.

The modified mode shapes obtained are then normalized with respect to the mass matrix and the participation factors are recomputed.

5. The equivalent linear modal frequencies are determined from the Rayleigh quotient expression in Eq. (2.43), in which the element modal strains ε_{en} are computed from the modified mode shapes.

$$m_n \omega^2_{neq} = \sum_e \varepsilon^2_{en} \bar{C}(\mu^*_{Ae_F})$$

---

(1) RSS denotes the square root of the squares of the modal maximum responses.

(2) ABS denotes the sum of the absolute values of modal maximum responses.

The equivalent linear modal damping is determined from Eq. (2.45).

$$\beta_{neq} = \xi_n \frac{\omega_n}{\omega_n} - RF \frac{\sum_e \varepsilon_{en}^2 \bar{S}(\mu^*_{Ae_D})}{2 \sum_e \varepsilon_{en}^2 \bar{C}(\mu^*_{Ae_D})}$$

where $\bar{C}$ and $\bar{S}$ are determined from Eqs. (2.41a) to (2.41c) or Fig. 2.8. The modal mass $m_n = 1$ if the modified mode shapes are normalized. RF is taken as $1/\sqrt{2}$ for bilinear hysteresis, and ξ_n is the modal viscous damping.

6. Repeat steps 2 to 5 using updated frequencies and damping until some preset convergence criterion on the maximum element ductilities is met.

7. Compute final values of structural responses desired.

Numerical example - A 3DF undamped bilinear system with uniform mass and stiffness distributions as shown below is subjected to 16 seconds of El Centro 1940-NS with 2 seconds of zero input at the end.

Element	DF	Mass, m_e (kip-in^2/sec)	Stiffness, k_e (kip/in)	x_{ye} (in)	α_e	Exact rel. disp. (in)
	3	1.0				
3			199.5	0.15	0.3	1.04(μ_z = 6.90)
	2	1.0				
2			199.5	0.25	0.3	1.53(μ_z = 6.10)
	1	1.0				
1			199.5	0.3	0.3	1.77(μ_z = 5.89)

Step 1 Determination of elastic mode shapes and modal frequencies.

		Mode n 1	2	3
Natural frequencies, f_n (cps)		1.0	2.803	4.051
Participation factors, Γ_n		1.656	0.474	0.182
	Element e			
Mode shape matrix, Φ_{en}	1	0.32799	0.73698	0.59101
	2	0.59101	0.32799	-0.73698
	3	0.73698	-0.59101	0.32799

Step 2 Estimation of element ductilities, μ_{z_e}.

At this first cycle of iteration, μ_{z_e} are determined from elastic element maximum strains (relative displacements).

	Element e 1	2	3
Element maximum strain (in)	4.73	3.45	2.11
Element ductilities	15.65	13.80	14.08

Step 3 Determination of element pseudo-steady state ductilities, $\mu^*_{Ae_F}$ and $\mu^*_{Ae_D}$.

	Element e 1	2	3
$\mu^*_{Ae_F}$	11.96	10.54	10.76
$\mu^*_{Ae_D}$	9.40	8.29	8.46

Step 4 Determination of modified mode shapes.

	Element e 1	2	3
$\bar{C}(\mu^*_{Ae_F})$	65.4	66.5	66.3
$k_e - \bar{C}_e(\mu^*_{Ae_F})$	134.1	133.0	133.2

		Mode n 1	2	3
$\varepsilon^{(0)}_{en}$	Element e			
	1	0.32799	0.73698	0.51901
	2	0.26302	0.40899	1.32799
	3	0.14597	0.91900	1.06497

	Mode n	Mode k 1	2	3
ΔE_{nk}	1	-26.47	-65.59	-89.99
	2	-65.59	-207.58	-261.01
	3	-89.99	-261.01	-421.75

	Element e	Mode n 1	2	3
$\Phi_{en,eff}$	1	0.3296	0.7379	0.5906
(1st-order)	2	0.5910	0.3260	-0.7373
	3	0.7363	-0.5909	0.3279
$\Gamma_{n,eff}$		1.66	0.48	0.18
$\varepsilon_{en,eff}$	1	0.3296	0.7379	0.5906
	2	0.2614	0.4119	1.3279
	3	0.1453	0.9169	1.0652

Step 5 Determination of the equivalent linear modal frequencies and damping.

	Element e 1	2	3
$\overline{C}(\mu^*_{Ae_D})$	67.8	69.3	69.1
$\overline{S}(\mu^*_{Ae_D})$	-16.9	-18.8	-18.5

Mode n

1 $m_1\omega^2_{1eq} = 13.1$, $f_{1eq} = 0.57$ cps; $\beta_{1eq} = 0 + \frac{1}{\sqrt{2}}\left[\frac{3.51}{2 \times 13.56}\right] = 0.09$

2 $m_2\omega^2_{2eq} = 102.3$, $f_{2eq} = 1.61$ cps; $\beta_{2eq} = 0 + \frac{1}{\sqrt{2}}\left[\frac{27.95}{2 \times 106.8}\right] = 0.09$

3 $m_3\omega^2_{3eq} = 215.4$, $f_{3eq} = 2.34$ cps; $\beta_{3eq} = 0 + \frac{1}{\sqrt{2}}\left[\frac{60.04}{2 \times 224.3}\right] = 0.09$

Step 6 Estimation of element ductilities, μ_{z_e}.

Maximum modal displacements

1st mode $\eta_{1max} = 4.5$ in., $\Gamma_1\eta_{1max} = 1.66 \times 4.5 = 7.5$ in.

2nd mode $\eta_{2max} = 2.5$ in., $\Gamma_2\eta_{2max} = 0.48 \times 2.5 = 1.2$ in.

3rd mode $\eta_{3max} = 0.1$ in., $\Gamma_3\eta_{3max} = 0.18 \times 0.1 = 0.2$ in.

$$x_{3max}(RSS) = \sqrt{(0.1453 \times 7.5)^2 + (0.9169 \times 1.2)^2 + (1.0652 \times 0.2)^2} = 1.6 \text{ in.}$$

$$(ABS) = (0.1453 \times 7.5) + (0.9169 \times 1.2) + (1.0652 \times 0.2) = 2.4 \text{ in.}$$

$$x_{2max}(RSS) = \sqrt{(0.2614 \times 7.5)^2 + (0.4119 \times 1.2)^2 + (1.3279 \times 0.2)^2} = 2.0 \text{ in.}$$

$$(ABS) = (0.2614 \times 7.5) + (0.4119 \times 1.2) + (1.3279 \times 0.2) = 2.7 \text{ in.}$$

$$x_{1max}(RSS) = \sqrt{(0.3296 \times 7.5)^2 + (0.7379 \times 1.2)^2 + (0.5906 \times 0.2)^2} = 2.6 \text{ in.}$$

$$(ABS) = (0.3296 \times 7.5) + (0.7379 \times 1.2) + (0.5906 \times 0.2) = 3.5 \text{ in.}$$

Element, e	Exact, in.	Linear, in.	1st cycle (RSS), in.
3	1.04 (μ = 6.90)	2.11 (μ = 14.08)	1.6 (μ = 10.7)
2	1.53 (= 6.10)	3.45 (= 13.80)	2.0 (= 8.0)
1	1.77 (= 5.89)	4.73 (= 15.65)	2.6 (= 8.7)

The undamped elastic response was used as the starting point for the iteration procedure. A much better staring point would be the elastic response with, say, 5% modal damping. Additional cycles of iteration (not shown) greatly improve the results.

In the example, yielding was so uniform that the mode shapes changed very little. Often, however, the change in mode shapes is quite significant.

4.2.3 MDF Equivalent Nonlinear System - Inelastic Response Spectrum

1. Determine elastic mode shapes and frequencies from the eigenvalue problem. At this step, the modal ductilities are unity and the modified mode shapes and natural frequencies are estimated as the linear values.

2. Determine maximum modal displacements using inelastic response spectra as shown in Fig. 4.1.[1] For the first iteration the modal ductilities are all unity, which corresponds to an elastic response spectrum. Estimate element maximum strains (relative displacements) using the RSS or 1/2(RSS+ABS) rules for combining the maximum modal strains. The element maximum strains are then normalized by the corresponding element yield strains to obtain maximum element ductilities, μ_{z_e}.

3. Determine the element pseudo-steady state ductilities, $\mu^*_{Ae_F}$ and $\mu^*_{Ae_D}$ from Eqs. (3.9) or Fig. 3.12, where α_e is element bilinear hardening. The frequency of f_0 is taken as the system fundamental elastic frequency in cps, and T_d is the earthquake duration in seconds.

4. Determine the element equivalent linear stiffness $\bar{C}(\mu^*_{Ae_F})$ from Eqs. (2.41b) and (2.41c), where k_e is element elastic stiffness.

$\bar{C}(\mu^*_{Ae_F})$ is then used as the element stiffness to determine the modified mode shapes from Eq. (C.18), in which ΔE_{nk} represents a strain energy change and is shown in Eq. (C.17), the superscript (0) denotes the elastic values, ω_n is the modal natural circular frequencies, ε_{en} is the element strain in mode n, and M is the number of modes considered

---

(1) The inelastic response spectra shown in Fig. 4.1 are a form of the deformation spectra proposed by Veletsos, Newmark and Chelapati [20]. They were constructed in the frequency range of interest for use in this study. Details may be found in Ref. [20].

in the modal analysis.

Equation (C.18) gives the first-order expression for the modified mode shapes. If greater accuracy is required because of localized yielding in the structure, the second-order expressions given in Eq. (C.21) can be used.

The modified mode shapes obtained are then normalized with respect to the mass matrix, and the participation factors are recomputed.

5. Determine the modal frequencies from Eq. (2.51).

Determine the modal ductilities, μ_{z_n}, and the modal bilinear hardening, α_n, from Eqs. (2.52a) and (2.52b).

$$(1-\alpha_n)\ \bar{k}_n\ \bar{c}(\mu^*_{An_F}) = \sum_e \varepsilon^2_{en}\ (1-\alpha_e)\ k_e\ \bar{c}(\mu^*_{Ae_F})$$

$$(1-\alpha_n)\ \bar{k}_n\ \bar{s}(\mu^*_{An_D}) = \sum_e \varepsilon^2_{en}\ (1-\alpha_e)\ k_e\ \bar{s}(\mu^*_{Ae_D})$$

in which $\bar{c}$ and $\bar{s}$ are given in Eqs. (2.50c) to (2.50e) and Fig. 2.8.

The right-hand sides of the two expressions shown above are known numerical values. Since the expression for $\mu^*_{An_F}$ contains α in Eq. (3.9b), α_n cannot be eliminated to give a single expression for μ_n.

By first assuming α_n to be an average value of α_e, $\mu^*_{An_F}$ and $\mu^*_{An_D}$ are determined from these two expressions and from Eqs. (2.50c) to (2.50e) or from Fig. 2.8. The modal ductilities, μ_{z_n}, are obtained simultaneously from Eqs. (3.9a) and (3.9b), where f_0 is taken as the modal frequency as in Eq. (2.49). The μ_{z_n} values obtained from $\mu^*_{Ae_F}$ and $\mu^*_{Ae_D}$ are usually very close for relatively uniform yielding, and the average value can normally be used. If the two values do not agree closely enough, α_n can be determined from the second of the equations using the average μ_{z_n},

and the process repeated. If the secant stiffness method is used, α_n and μ_n may be determined directly from the explicit expressions given in Eqs. (2.51) and (2.50a).

6. Use the modified modal frequencies, modal bilinear hardening, α_n, and modal ductility, μ_{z_n}, from step 5 and the effective mode shapes from step 4 to repeat the procedures from step 2 to 5 until some preset convergence criterion on the element maximum ductilities is met.

7. Compute final values of structural responses desired.

Numerical Example - Consider the 3DF undamped bilinear system in Section 4.2.2.

Step 1 Determination of elastic mode shapes and modal frequencies - same as step 1 in section 4.2.2.

Step 2 Estimation of maximum element ductilities - same as step 2 in section 4.2.2.

Step 3 Determination of element pseudo-steady state ductilities, $\mu^*_{Ae_F}$ and $\mu^*_{Ae_D}$ - same as step 3 in section 4.2.2.

Step 4 Determination of modified mode shapes - same as step 4 in section 4.2.2.

Step 5 Determination of modified modal frequencies, modal ductilities, μ_{z_n}, and the modal bilinear hardening, α_n.

Modified modal frequencies:

1st mode: $\bar{k}_1 = m_1\omega_1^2 = (0.3296)^2 \times 199.5 + (0.2614)^2 \times 199.5 + (0.1453)^2 \times 199.5$

$= 39.5$

$f_1 = 1.0$ cps

2nd mode: $\bar{k}_2 = m_2\omega_2 = (0.7379)^2 \times 199.5 + (0.4119)^2 \times 199.5 + (0.9169)^2 \times 199.5$

$= 310.2$

$f_2 = 2.8$ cps

3rd mode: $\bar{k}_3 = m_3\omega_3 = (0.5906)^2 \times 199.5 + (1.3279)^2 \times 199.5 + (1.0652)^2 \times 199.5$

$= 647.7$

$f_3 = 4.1$ cps

Modal ductilities and modal bilinear hardening:

Assuming $\alpha_1 = \alpha_2 = \alpha_3 = 0.3$

1st mode: $(1-0.3) \times 39.5\ \bar{c}(\mu^*_{An_F}) = (1-0.3) \times 37.8$

$\bar{c}(\mu^*_{An_F}) = 0.957$

$\mu^*_{An_F} = 11.3,\ \mu_{z_n} = 14.8$

$(1-0.3) \times 39.5\ \bar{s}(\mu^*_{An_D}) = (1-0.3) \times 15.76$

$\bar{s}(\mu^*_{An_D}) = 0.40$

$\mu^*_{An_D} = 8.9,\ \mu_{z_n} = 14.8$

$\therefore$ use $\alpha_1 = 0.3,\ \mu_{z_n} = 14.8$

2nd mode: $(1-0.3) \times 310.2\ \bar{c}(\mu^*_{An_F}) = (1-0.3) \times 296.5$

$\bar{c}(\mu^*_{An_F}) = 0.956$

$\mu^*_{An_F} = 11.1,\ \mu_{z_n} = 17.0$

$(1-0.3) \times 310.2\ \bar{s}(\mu^*_{An_D}) = (1-0.3) \times 125.2$

$\bar{s}(\mu^*_{An_D}) = 0.40$

$\mu^*_{An_D} = 8.9,\ \mu_{z_n} = 17.3$

$\therefore$ use $\alpha_2 = 0.3,\ \mu_{z_n} = 17.2$

3rd mode: $(1-0.3) \times 647.7\ \bar{c}(\mu^*_{An_F}) = (1-0.3) \times 617.6$

$$\bar{c}(\mu^*_{An_F}) = 0.954$$

$$\mu^*_{An_F} = 10.8,\ \mu_{z_n} = 17.4$$

$$(1-0.3) \times 647.7\ \bar{s}(\mu^*_{An_D}) = (1-0.3) \times 269.5$$

$$\bar{s}(\mu^*_{An_D}) = 0.42$$

$$\mu^*_{An_D} = 8.4\ ,\ \mu_{z_n} = 17.2$$

$\therefore$ use $\alpha_3 = 0.3,\ \mu_{z_n} = 17.3$

Step 6 Estimation of element ductilities, μ_{z_e}.

Enter the inelastic spectra in Fig. 4.1 with α_n and μ_n to determine the maximum modal displacements. Then determine and combine maximum modal strains in the usual way.

1st mode: $\alpha_1 = 0.3,\ \mu_1 = 14.8,\ \eta_{1,max} = 4.1$ in., $\Gamma_1\eta_{1,max} = 6.8$ in.

2nd mode: $\alpha_2 = 0.3,\ \mu_2 = 17.2,\ \eta_{2,max} = 2.5$ in., $\Gamma_2\eta_{2,max} = 1.2$ in.

3rd mode: $\alpha_3 = 0.3,\ \mu_3 = 17.3,\ \eta_{3,max} = 1.3$ in., $\Gamma_3\eta_{3,max} = 0.2$ in.

$$x_{3,max}(RSS) = \sqrt{(0.1453 \times 6.8)^2 + (0.9169 \times 1.2)^2 + (1.0652 \times 0.2)^2} = 1.5 \text{ in.}$$

$$(ABS) = (0.1453\ \ 6.8) + (0.9169 \times 1.2) + (1.0652 \times 0.2) = 2.3 \text{ in.}$$

$$x_{2,max}(RSS) = \sqrt{(0.2614 \times 6.8)^2 + (0.4119 \times 1.2)^2 + (1.3279 \times 0.2)^2} = 1.9 \text{ in.}$$

$$(ABS) = (0.2614 \times 6.8) + (0.4119 \times 1.2) + (1.3279 \times 0.2) = 2.5 \text{ in.}$$

$$x_{1,max}(RSS) = \sqrt{(0.3296 \times 6.8)^2 + (0.7379 \times 1.2)^2 + (1.3279 \times 0.2)^2} = 2.4 \text{ in.}$$

$$(ABS) = (0.3296 \times 6.8) + (0.7379 \times 1.2) + (1.3279 \times 0.2) = 3.4 \text{ in.}$$

Element, e	Exact, in.	Linear, in.	1st cycle (RSS), in.
3	1.04 (μ = 6.90)	2.11 (μ = 14.08)	1.5 (μ = 10.0)
2	1.58 (= 6.10)	3.45 (= 13.08)	1.9 (= 7.6)
1	1.77 (= 5.89)	4.73 (= 15.65)	2.4 (= 8.0)

CHAPTER 5

RESULTS OF ANALYTICAL STUDIES

5.1 Introduction

In this chapter, extensive comparisons are made between maximum responses calculated by "exact" numerical step-by-step integration and maximum responses predicted by the two approximate modal analysis procedures outlined in Chapter 4.

The Newmark Beta-Method [25] was used with $\beta = 1/6$ and a time step of 0.02 seconds to obtain the numerically integrated "exact" responses.

The comparisons are made for a series of 1, 3 and 10 story bilinear shear beam structures with various combinations of structural properties (stiffness, strength, viscous damping). Four different earthquakes and several levels of earthquake intensity relative to the structure strength were considered.

In addition to the comparisons of maximum responses, response histories are also shown for a few 3DF systems.

5.2 Single Degree-of-Freedom Systems

The "exact" responses of a number of bilinear SDF systems are compared with those of the corresponding equivalent linear systems. Several comparisons are made using one and three cycles of iteration beginning with the linear responses. These approximate responses are found to differ little from those computed using the best initial "guess" possible, i.e., the exact maximum displacements. To make it possible to study a wider range of parameters, the exact maximum displacement rather than the linear response is then used as the initial estimate in subsequent parameter

studies. Selected results are presented and discussed in this chapter. Appendix E contains the complete results of the study on SDF systems.

5.2.1 Earthquakes and System Parameters -- Calculations were made for SDF systems covering the frequency range from 0.25 to 11 cps. The parameters which were varied are as follows.

Earthquake Excitations -- The El Centro 1940-NS, Taft 1952-N21E, Olympia 1949-N04W and Pacoima 1971-S16E with 16 seconds duration followed by 2 seconds of zero excitation at the end were used. All earthquakes were normalized to yield 0.35 g maximum ground acceleration.

System Parameters -- The SDF systems are simple spring mass systems with viscous dashpot and bilinear hysteresis, as shown in Fig. 3.1. System parameters which were varied are

(a) Natural frequency - 33 values ranging from 0.25 to 11 cps

(b) Bilinear hardening - 4 values α = 0.01, 0.05, 0.10, 0.30

(c) Viscous damping - 2 values ξ = 0.02, 0.05

(d) Yield level - 4 series of systems were proportioned to produce four different general levels of response ductility with the ductility roughly constant for each series. The yield strengths of these systems are shown as a function of natural frequency in Fig. 5.1. The target ductilities were: level 1, $\mu \simeq$ 1-3; level 2, $\mu \simeq$ 2-5; level 3, $\mu \simeq$ 3-8; level 4, $\mu \simeq$ 5-20.

5.2.2 Results -- Selected results for SDF systems are shown in Figs. 5.2 to 5.7. In some of the figures maximum and rms values of relative displacement and velocity response are shown on logarithmic scales. Results are also shown on arithmetic scales with displacements normalized

by yield displacement x_y and with velocity normalized by $\omega_0 x_y$, where ω_0 is the elastic circular frequency. The effects of various parameters on the accuracy of response prediction using the equivalent linear system is discussed in the following paragraphs.

(a) Effect of Initial Guess and Number of Iterations -- Figs. 5.2 to 5.7 show responses for the Level 2 (target ductility range 2-5) series of bilinear systems. System parameters $\alpha = 0.10$, $\xi = 0.02$ are held constant.

Figures 5.2 to 5.4 show the responses to the El Centro excitation. In these figures, results are compared for 1 and 3 cycles of iteration beginning with linear response, and 1 cycle beginning with the exact response. Figures 5.5 to 5.7 give similar results for the Olympia excitation.

In all cases, agreement with the exact values is satisfactory. The results do not vary drastically with number of cycles of iteration, or with the initial guess.

It is interesting to compare Figs. 5.5 and 5.6 for the Olympia N04W excitation. In this particular case, 3 cycles of iteration gives less accurate responses in the 4-7 cps frequency range than 1 cycle of iteration. In view of these results, the exact response previously computed by step-by-step numerical integration is used as the initial "guess" in most of the subsequent calculations and only one cycle of iteration is carried out. This reduces the amount of computation required, since the exact value is needed for comparison in any case, and allows study of a wider range of parameters.

(b) Effect of System Relative Strength -- The effect on accuracy of the system strengths relative to that of the earthquake excitation is shown in Figs. 5.8a to 5.8c. The relative strength is measured by response ductility. The relative displacement response spectra are shown for the Level 2 (target $\mu \simeq 2\text{-}5$) and level 4 (target $\mu \simeq 5\text{-}20$) series, subjected to the El Centro NS excitation. Three combinations of bilinear hardening and viscous damping ($\alpha = 0.3$, $\xi = 0.02$), ($\alpha = 0.10$, $\xi = 0.02$), ($\alpha = 0.05$, $\xi = 0.05$) are considered.

As expected the accuracy of the equivalent linear system improves as the bilinear hardening increases, and as the response ductility increases, because in both cases the bilinear system begins to behave like a linear system. This behavior was observed in the frequency decomposition of responses discussed in Chapter 3. The greatest inaccuracy occurs in the high frequency range when the ductility is moderate, approximately 2-3.

(c) Effect of Viscous Damping -- Response spectra for the Level 2 series subjected to the El Centro NS excitation are shown in Figs. 5.9a and 5.9b. Normalized maximum displacements are shown on an arithmetic scale for 2% and 5% viscous damping.

The viscous damping consistently reduces maximum response as expected and does not appear to influence the accuracy of the response prediction by the equivalent linear system.

(d) Effect of Earthquake Excitation Characteristics -- Normalized displacement response spectra are shown in Figs. 5.10a to 5.10c for the Level 2 series subjected to four different earthquake excitations. Bilinear hardening $\alpha = 0.10$ and viscous damping $\xi = 0.02$ were held constant.

Figures 5.10a to 5.10c individually compare responses of Taft N21E, Olympia N04W and Pacoima S16E to the response of El Centro NS. All earthquake acceleration records were normalized to 0.35 g maximum acceleration.

The response of a given system is obviously highly dependent on the earthquake input. This is true even for a linear system. However, the overall agreement between equivalent linear and nonlinear exact response for each earthquake seems to be quite good, and more importantly, not dependent on the particular excitation chosen. In certain frequency intervals, however, accuracy is quite sensitive to the excitation. In general, the poorest accuracy is in the medium to high frequency region, between about 2 and 7 cps as expected.

(e) Effect of Bilinear Hardening -- Normalized displacement response spectra as shown in Figs. 5.11a to 5.11c for the Level 2 series with 5% damping subjected to the El Centro input. Results for values of bilinear hardening of 0.10, 0.05 and 0.01 are individually compared to results for $\alpha = 0.30$ in Figs. 5.11a to 5.11c.

As observed in some of the previous comparisons, the accuracy of the equivalent linear system decreases as the system approaches elastoplastic. When $\alpha = 0.01$ as shown in Fig. 5.11c, the method is quite conservative in the high frequency range, giving response ductilities 100% too high in extreme cases. This trend is expected from the study of frequency content of the responses discussed in Chapter 3. As pointed out there, for nearly elastoplastic systems and moderate ductilities, the "nonlinear transfer function" is far from that of a linear system. It has two pronounced peaks, one near the elastic natural frequency and the second

near the elastic natural frequency of a system with stiffness equal to the second slope of the hysteresis loop.

5.2.3 Summary -- The results presented for the SDF systems show several clear trends: (1) The equivalent linear system accurately predicts maximum displacement responses over a wide range of conditions. (2) The procedure is not particularly sensitive to the initial estimate, or the number of iterations performed. It appears that the linear response is an adequate initial guess. (3) The accuracy predictably deteriorates under certain circumstances. When the system approaches the elastoplastic case, or when the bilinear hardening is small and the ductility is moderate (say 2-3), maximum displacements tend to be overestimated in the high frequency region (2-7 cps) by as much as 100% in isolated cases. (4) Initial viscous damping and variability of earthquake excitation appear to have little overall influence on accuracy, although in specific frequency ranges, characteristics of the excitation can greatly influence accuracy.

5.3 Three Degree-of-Freedom Systems

The two approximate methods of modal analysis were used to calculate the maximum responses of a variety of 3DF shear beam structures. The approximate results are compared with exact responses computed by the step-by-step numerical integration. Several combinations of earthquake excitations and structural properties were used.

Two different rules are used for combining maximum modal responses: the usual Root-Sum-Square (RSS) method and an average of the Root-Sum-Square and Absolute Sum (1/2(RSS + ABS)) methods [26].

5.3.1 Earthquake and System Parameters -- The parameters which were varied in the numerical calculations are detailed in the following sections.

Earthquake inputs -- Four earthquake excitations (El Centro NS, Taft N21E, Olympia NO4W and Pacoima S16E) were used as described in Section 5.2.1.

System parameters -- Two series of 3DF systems were designed: (1) a uniform mass and stiffness arrangement, and (2) a nonuniform mass and stiffness arrangement. The fundamental frequencies of both series were fixed at 1 cps, and viscous damping was zero.

The nonuniform system was proportioned to reduce the separation of modal frequencies and increase higher mode participation factors as compared to the uniform system.

Mass and stiffness distributions and resulting frequencies and mode shapes are shown for the two series of systems in Tables 5.2 and 5.3.

For each series the system parameters which were varied are

(a) Bilinear Hardening -- three values $\alpha = 0.05, 0.10, 0.30$.

(b) Yielding Level -- three different general levels of yield displacements as listed in Tables 5.2 and 5.3. The target ductilities were Level 1, $\mu \simeq 2$; Level 2, $\mu \simeq 6$; and Level 3, $\mu \simeq 15$.

5.3.2 Results -- The results are shown in Figs. 5.12 to 5.20 for the uniform systems and Figs. 5.21 to 5.29 for the nonuniform systems.

The results are presented in the form of plots of ductility versus story number, and comparisons are made between the exact responses and

those determined using 1 cycle of the approximate methods beginning with the exact solution. In some cases, as noted on the Figures, 1 cycle of the equivalent linear method are used beginning with the linear solution.

To eliminate errors associated with interpolating values from a response spectrum, the individual modal SDF responses for the equivalent linear systems were actually determined by numerical integration. This was done to isolate the errors inherent in the approximate modal analysis procedures.

The numerical results are grouped so that a single figure shows responses of one system (bilinear hardening, yield level constant) to all four earthquake excitations, and compares the two rules for combining modal responses (RSS and 1/2(RSS + ABS)). Results for the nine possible combinations of yield level (1, 2, 3) and bilinear hardening (0.3, 0.1, 0.05) are given in separate figures in Figs. 5.12 to 5.20 for uniform systems, and Figs. 5.27 to 5.35 for nonuniform systems.

1. Uniform Systems -- Figures 5.12 to 5.20 show the results for the uniform systems. The maximum ductilities are also tabulated in Tables 5.5a to 5.5d. Generally speaking, the errors in the approximate methods are in the range of 10-35% (RSS rule). The influence of the various parameters on accuracy of the approximate methods is discussed below.

(a) Effect of System Relative Strength (Yield Level) -- The equivalent linear and equivalent nonlinear methods yield accurate predictions for low ductilities. Errors are in the range of 5-20% (RSS rule), depending on the bilinear hardening. For moderate and high ductilities, the errors (RSS rule) in the equivalent linear method tend to be somewhat greater.

Some improvement in accuracy is achieved by the equivalent nonlinear method.

The larger errors associated with the equivalent linear approach for moderate ductility systems may be explained in terms of the differences noted in Chapter 3 between the exact nonlinear modal transfer functions and the transfer function of a linear system. The equivalent nonlinear modal transfer function reduces this difference and improves the response prediction.

(b) Effect of Earthquake Excitation Characteristics -- Although the nonlinear response of a particular system is very sensitive to characteristics of earthquake excitation, the accuracy of the approximate modal analysis methods does not appear to be sensitive to excitation. Somewhat larger errors are associated with the Taft N21E excitation than the other three excitations, but the overall accuracy is satisfactory.

(c) Effect of Hardening -- The approximate response predictions are relatively good with errors about 5-20% (RSS rule) for $\alpha = 0.3$. The accuracy tends to decrease as the bilinear hardening becomes smaller with the errors increasing to about 10-30% (RSS rule) for $\alpha = 0.1$ and 0.05.

Displacement response histories were constructed for several cases by superimposing the modal response histories. Figures 5.21 to 5.26 show the response histories for the uniform system with bilinear hardening $\alpha = 0.3$, and the three different yield levels, subjected to the El Centro NS and the Taft N21E. In these figures, the exact response is compared with that of the equivalent linear system and with the response of the original system with 4% viscous damping in each mode.

The much better match of response history by the equivalent linear system than by the 4% damped linear system is evident from the figures.

These figures illustrated that the frequency shift is an important aspect of the nonlinear response, and that simply increasing the viscous damping to compensate for inelastic behavior as has been suggested for SDF systems [10] may not be satisfactory.

2. Nonuniform Systems -- Comparisons of exact and approximate responses are shown in Figs. 5.27 to 5.35 and tabulated in Tables 5.7a to 5.7d. Since the natural frequencies of the nonuniform 3DF systems are not well separated as those of the uniform systems to begin with, and yielding tends to increase modal coupling, it may be more reasonable to combine modal maxima using the 1/2(RSS + ABS) rule. The elastic natural frequencies and mode shapes of the nonuniform system are shown in Table 5.3.

The accuracy of the approximate procedures is similar to that reported for uniform systems. It is noted that the estimated responses of the light substructures in the nonuniform system are very conservative when the distribution of the story ductilities is very highly nonuniform. Despite this, the overall errors are about 5-40% (1/2(RSS + ABS)) depending on earthquake excitations and system parameters. As before, larger errors are associated with small bilinear hardening, moderate ductilities, and the Taft N21E excitation. In the results presented in this portion of the study, the equivalent linear and equivalent nonlinear responses were obtained using only one cycle of iteration starting from the exact nonlinear responses.

It is also interesting to note the equivalent linear responses using one cycle of iteration starting from the linear responses for both the uniform and nonuniform systems. The approximate responses obtained in

this fashion are acceptable for uniform systems in which the distribution of the story ductilities is relatively uniform. As the story ductilities become highly nonuniform, one cycle of iteration on the linear response is not acceptable. The differences in story strains between the exact and the approximate system are relatively large. It is recommended that more cycles of iteration be used for highly nonuniform systems.

5.3.3 Summary -- The trends shown in Figs. 5.12 to 5.20 and Figs. 5.27 to 5.35 are consistent with the results for SDF systems. The approximate methods give good results, with accuracy tending to deteriorate when the bilinear hardening is small and the ductilities are moderate. One cycle of iteration beginning with the linear solution may give adequate estimates of response when the yielding is relatively uniform. Additional cycles of iteration are required when the yielding is localized.

5.4 Ten Degree-of-Freedom Systems

Approximate and exact responses of a series of three 10DF tapered systems are presented in this section.

The masses and stiffnesses are each reduced by 5% per story to give a uniformly tapered system. The fundamental frequency was set at 1.0 cps, and viscous damping was taken as zero. The distribution of yield level with height was chosen to give reasonably uniform story ductilities in the range of 4 to 10. Mass, stiffness and yield levels are shown in Table 5.7. Elastic natural frequencies, mode shapes, and participation factors are also shown.

Two parameters were varied in the response calculations reported in this section as follows.

5.4.1 Earthquakes and System Parameters --

Earthquake Excitations -- Four normalized earthquake excitations (El Centro NS, Taft N21E, Olympia NO4W, and Pacoima S16E) were used as described in section 5.2.1.

System parameters -- Three values of bilinear hardening (0.30, 0.10, 0.05) were used. All other system properties were held constant.

5.4.2 Results -- In the computation of the approximate modal responses, only the first three modes were included, and maximum modal responses were combined using both the RSS and 1/2(RSS + ABS) rules. The comparison of the approximate responses with the exact responses are shown in Figs. 5.36 to 5.38 and tabulated in Tables 5.8a to 5.8d.

Errors in the approximate responses using the RSS rule are in the range of 10-40%, depending on the earthquake and bilinear hardening. The accuracy is consistent with that of the 3DF systems. As with the 3DF systems, the accuracy of the approximate modal analysis procedures is poorer for the Taft N21E excitation than for the other earthquakes. This is probably due to the fact that the fundamental frequency of the various 3DF and 10DF systems was set at 1.0 cps. If one examines the SDF results in Fig. 5.10, it is apparent that near a frequency of 1.0 cps, the peculiarities of the Taft N21E input are such that the equivalent linearization is the least accurate among the four earthquakes used.

5.4.3 Summary -- Dependence of accuracy on the magnitude of bilinear hardening is similar to that for SDF and 3DF systems. The equivalent nonlinear approach appears to give consistently better results than the

equivalent linear approach in the limited number of 10DF cases considered. The RSS rule for combining modal maxima is generally more accurate than the 1/2(RSS + ABS) rule. This trend may be dependent on the relatively uniform yielding patterns in the particular systems studied.

While some smoothing out of yielding patterns does occur in the approximate procedures, the predicted responses seem fairly well able to follow ductility variations from story to story. It must be pointed out that large local variations of yielding did not occur in the systems studied, and that the prediction of story ductilities, which is all that the shear beam model allows, is not a severe test of the approximate procedures. Nevertheless, it seems that the equivalent nonlinear approach which incorporates mode shape changes and a modal ductility which reflects member ductilities, holds promise for being able to adequately handle flexible girder systems.

CHAPTER 6

SUMMARY AND CONCLUSIONS

6.1 Summary

Two approximate modal analysis procedures for nonlinear MDF systems were examined and evaluated: (1) equivalent linear modal analysis using elastic response spectra, and (2) equivalent nonlinear modal analysis using inelastic response spectra.

In the first portion of the study, the approximate steady state solutions for nonlinear SDF and MDF systems subjected to harmonic base excitation were derived by the method of equivalent linearization. Bilinear SDF and MDF shear beam systems subjected to harmonic excitation have both been studied previously by other authors. However, the approximate solution for MDF systems was presented from a slightly different viewpoint in this study. This led naturally to the use of the mode shapes of the equivalent linear system for modal decomposition. Study of response to this simple excitation provided insight into the behavior of bilinear hysteretic systems, and allowed a logical development of the nonlinear modal analysis procedure, of which an essential ingredient was the definition of "modal ductility" given in Eq. (2.51).

The basic approach which was used for earthquake response was to relate the transient maximum response to a "pseudo-steady state" maximum response, and then to apply the closed form steady state expressions for frequency shift and damping. Both modal analysis procedures are iterative, and use a perturbation method to successively modify the original elastic mode shapes at each iterative step to reflect yielding in the system.

Numerical comparisons between approximate and exact responses were presented for a large number of 1-, 3- and 10-DF bilinear shear beam systems. Four earthquake inputs (El Centro 1940-NS, Taft 1952-N21E, Olympia 1949-N04W, and Pacoima 1971-S16E) were used, and several structural stiffness and strength parameters were varied.

6.2 Conclusions

It is felt that the most important contribution of this study is the introduction of the definition of modal ductility and modification of mode shapes into the conventional inelastic response spectrum-modal analysis procedure. Although further study is required before any general conclusions can be drawn, these two new features appear capable of substantially improving the accuracy of the inelastic response spectrum approach for MDF systems.

In addition, based on the numerical results for shear beam systems, the following conclusions were drawn:

1. The nonlinear transfer function (defined in the frequency domain as the ratio of output to input) of a SDF bilinear system under harmonic excitation has a single peak similar to that of a linear system. Under white noise, earthquake or pulse-like excitation, it has two peaks, with one peak close to the linear frequency, ω_0, and the other close to the frequency of a system with stiffness equal to the second slope of the hysteresis loop, $\sqrt{\alpha}\,\omega_0$ [17]. The relative magnitude of these two peaks depends on the response ductility, and the separation of the peaks depends on the bilinear hardening α. Thus the similarity of the nonlinear transfer function of a bilinear SDF system to that of a linear system depends on response ductility and bilinear hardening.

2. The equivalent linear system approach predicts maximum responses of SDF systems to earthquake excitation with good accuracy over a wide range of conditions. Accuracy tends to deteriorate in the frequency range between about 2 and 7 cps when the second slope of the bilinear hysteresis loop approaches zero and when response ductilities are in the range 2-3, approximately. These trends can be understood in relation to the behavior of the transfer function noted above. In specific small frequency intervals, accuracy of the approximate procedure is very sensitive to the earthquake input.

3. The accuracy of the approximate modal analysis procedures for MDF systems is comparable to that of the equivalent linear approach for SDF systems, with the same deterioration of accuracy for small values of bilinear hardening and moderate values of ductility in the range 5-10. Maximum story displacements are generally predicted within about 10-40% accuracy, for the 3DF and 10DF systems studied. The equivalent nonlinear approach using inelastic response spectra appears to give generally better accuracy than the equivalent linear approach using elastic response spectra.

4. The equivalent linear mode shapes uncouple the nonlinear equations of motion to a much greater degree and yield more accurate approximations than do the original elastic mode shapes. Such modified mode shapes appear capable of predicting moderate variations in yielding levels through the structure. One cycle of iteration, beginning with the linear solution and using just first order modifications of the elastic mode shapes, often gives satisfactory results. In some nonuniform systems, in which the variation of yielding patterns is substantial, additional cycles of iteration are recommended to improve accuracy.

5. The RSS rule for combining the maximum modal responses yields better response predictions for systems with well separated natural frequencies, and low nonlinearity and ductility levels while the 1/2(RSS + ABS) rule yields better response predictions for systems with closely spaced natural frequencies, and high nonlinearity levels (i.e., nearly elastoplastic) and high ductility levels.

6.3 Recommendations for Further Study

The approximate modal analysis procedures have been extensively evaluated only for bilinear shear beam systems. The shear beam structural idealization is not particularly realistic, yet its simplicity made it the logical first step, and also made it economically possible to consider a wide range of parameters within a reasonable computational cost.

It would now be useful to extend the methods to other types of hysteretic behavior and structural configurations, such as frames with flexible girders and shear walls. Such structures would provide a much more severe test of the approximate methods than the shear beam systems considered in this study.

The development of approximate modal analysis procedures beginning with harmonic excitation and paralleling the development in this study, for structures composed of structural elements with more than one component of strain may present some difficulties since the definition of an element "ductility" is no longer a straightforward matter. Despite this, efforts should be made to carefully develop such procedures from a logical basis.

REFERENCES

1. Anagnostopoulos, S. A., Haviland, R. W., and Biggs, J. M., "Use of Inelastic Response Spectra in Aseismic Design," Journal of the Structural Division, American Society of Civil Engineers, Vol. 104, No. ST1, Proceedings Paper 13487, January 1978, pp. 95-109.

2. Atalik, T. S., and Uktu, S., "Stochastic Linearization of Multi Degree-of-Freedom Nonlinear Systems," Earthquake Engineering and Structural Dynamics, Vol. 4, 1976, pp. 411-420.

3. Bendat, J. S., and Piersol, A. G., "Measurement and Analysis of Random Data," John Wiley & Sons, Inc., Second Edition, New York, 1971.

4. Brown, R. N., "Analog Simulation of a Bilinear Hysteretic System Undergoing Random Vibration," Journal of Engineering for Industry, American Society of Mechanical Engineers, Vol. 91, 1969, pp. 1051-1056.

5. Caughey, T. K., "Sinusoidal Excitation of a System with Bilinear Hysteresis," Journal of Applied Mechanics, Transactions of the American Society of Mechanical Engineers, Vol. 27, Series E, No. 4, December 1960, pp. 640-643.

6. Caughey, T. K., "Random Excitation of a System with Bilinear Hysteresis," Journal of Applied Mechanics, Transactions of the American Society of Mechanical Engineers, Vol. 27, Series E, No. 4, December 1960, pp. 649-652.

7. Caughey, T. K., "Equivalent Linearization Techniques," Journal of the Acoustical Society of America, Vol. 35, No. 11, November 1963, pp. 1706-1711.

8. Chokshi, N. C., and Lutes, L. D., "Maximum Response Statistics for Yielding Oscillator," Journal of the Engineering Mechanics Division, American Society of Civil Engineers, Vol. 102, No. EM6, Proceedings Paper 12632, December 1976, pp. 983-993.

9. Davenport, A. G., "Note on the Distribution of the Largest Value of a Random Function with Application to Gust Loading," Proceedings of the Institute of Civil Engineering, Vol. 28, 1964, pp. 187-196.

10. Foster, E. T., "Semilinear Random Vibrations in Discrete Systems," Journal of Applied Mechanics, Transactions of the American Society of Mechanical Engineers, Vol. 35, No. 3, 1968, pp. 560-564.

11. Guerra, O. R., and Esteva, L. E., "Equivalent Properties and Ductility Requirements in Seismic Analysis of Nonlinear Systems," Proceedings of the Sixth World Conference on Earthquake Engineering, New Delhi, India, Vol. 5, January 1977, pp. 263-268.

12. Hudson, D. E., "Equivalent Viscous Friction for Hysteretic Systems with Earthquake-Like Excitations," Proceedings of the Third World Conference on Earthquake Engineering, New Zealand, Vol. 2, 1965, pp. 185-201.

13. Iwan, W. D., "The Dynamic Response of Bilinear Hysteretic Systems," Ph.D. Thesis, California Institute of Technology, 1961.

14. Iwan, W. D., "The Dynamic Response of the One Degree of Freedom Hysteretic System," Proceedings of the Third World Conference on Earthquake Engineering, New Zealand, Vol. 2, 1965, pp. 783-796.

15. Iwan, W. D., "Multi Degree-of-Freedom Yielding Systems," Journal of the Engineering Mechanics Division, American Society of Civil Engineers, Vol. 94, No. EM2, Proceedings Paper 5883, April 1960, pp. 421-437.

16. Iwan, W. D., "Application of Nonlinear Analysis Techniques," Applied Mechanics in Earthquake Engineering, W. D. Iwan (Editor), Applied Mechanics Symposium Series, American Society of Mechanical Engineers, New York, AMD Vol. 8, 1974.

17. Iwan, W. D., and Lutes, L. D., "Response of the Bilinear Hysteretic System to Stationary Random Excitation," Journal of the Acoustical Society of America, Vol. 43, 1968, pp. 545-552.

18. Jennings, P. C., "Response of Simple Yielding Structures to Earthquake Excitation," Ph.D. Thesis, California Institute of Technology, 1963.

19. Jennings, P. C., "Equivalent Viscous Damping for Yielding Structures," Journal of the Engineering Mechanics Division, American Society of Civil Engineers, Vol. 94, No. EM1, Proceedings Paper 5793, February 1968, pp. 103-116.

20. Lutes, L. D., "Equivalent Linearization for Random Vibration," Journal of the Engineering Mechanics Division, American Society of Civil Engineers, Proceedings Paper 7333, Vol. 96, No. EM3, June 1970, pp. 227-242.

21. Lutes, L. D., and Takemiya, H., "Vibration of Yielding Oscillator," Journal of the Engineering Mechanics Division, American Society of Civil Engineers, Vol. 100, No. EM2, Proceedings Paper 10482, April 1974, pp. 343-358.

22. Lutes, L. D., and Chokshi, N. C., "Maximum Response Statistics for a Linear Structure," Proceedings of the Fifth World Conference on Earthquake Engineering, Rome, Vol. 2, 1974, pp. 2818-2821.

23. Montgomery, C. J., and Hall, W. J., "Studies on the Seismic Design of Low-Rise Steel Buildings," Civil Engineering Studies, Structural Research Series, No. 442, Department of Civil Engineering, University of Illinois at Urbana-Champaign, Urbana, Illinois, July 1977.

24. Morse, P. M., and Feshbach, H., "Method of Theoretical Physics," McGraw-Hill Book Company, Inc., New York, 1953.

25. Newmark, N. M., "A Method of Computation for Structural Dynamics," Journal of the Engineering Mechanics Division, Proceedings of the American Society of Civil Engineers, Vol. 85, No. EM3, Proceedings Paper 2094, July 1959, pp. 67-94.

26. Newmark, N. M., "Current Trends in the Seismic Analysis and Design of High-Rise Structures," Chapter 16 in Earthquake Engineering, R. L. Weigel, Editor, Prentice-Hall, Inc., Englewood Cliffs, New Jersey, 1970.

27. Newmark, N. M., and Hall, W. J., "Procedures and Criteria for Earthquake Resistant Design," Building Science Series, No. 46, Building Practices for Disaster Mitigation, National Bureau of Standards, February 1973, pp. 209-236.

28. Newmark, N. M., and Rosenblueth, R., "Fundamentals of Earthquake Engineering," Prentice-Hall, Inc., Englewood Cliffs, New Jersey, 1971.

29. Papoulis, A., "The Fourier Integral and Its Applications," McGraw-Hill Book Company, New York, 1962.

30. Roesset, J. M., Whitman, R. V., and Dobry, R., "Modal Analysis for Structures with Foundation Interaction," Journal of the Structural Division, American Society of Civil Engineers, Vol. 99, No. ST3, Proceedings Paper 9603, March 1973, pp. 399-416.

31. Shibata, A., and Sozen, M. A., "The Substitute-Structure Method for Seismic Design in R/C," Journal of the Structural Division, American Society of Civil Engineers, Vol. 102, No. ST1, Proceedings Paper 11824, January 1976, pp. 1-18.

32. Timoshenko, S., Young, D. E., and Weaver, W., Jr., "Vibration Problems in Engineering," Fourth Edition, John Wiley & Sons, New York, 1974.

33. Veletsos, A. S., Newmark, N. M., and Chelapati, C. V., "Deformation Spectra for Elastic and Elastoplastic Systems Subjected to Ground Shock and Earthquake Motions," Proceedings of the Third World Conference on Earthquake Engineering, New Zealand, Vol. 2, 1965, pp. 663-680.

34. Veletsos, A. S., and Vann, W. P., "Response of Ground Excited Elastoplastic Systems," Journal of the Structural Division, American Society of Civil Engineers, Vol. 97, No. ST4, Proceedings Paper 8075, April 1971, pp. 1257-1281.

TABLE 5.1 EARTHQUAKES AND SYSTEM PARAMETERS USED IN SDF SYSTEMS

1 and 3 cycles of iteration starting from the linear response

ξ \ α	0.3	0.1	0.05	0.01
0.02	-	E(1,33) O(1,33)	-	-
0.05	-	-	-	-

1 cycle of iteration starting from the exact nonlinear response

ξ \ α	0.3	0.1	0.05	0.01
0.02	E(4,33)	E(4,33), T(4,33) O(4,33), P(4,33)	-	-
0.05	E(4,33)	E(4,33)	E(4,33)	E(4,33)

$E(n_1,n_2)$: El Centro NS (16 seconds)

$T(n_1,n_2)$: Taft N21E (16 seconds)

$O(n_1,n_2)$: Olympia N04W (16 seconds)

$P(n_1,n_2)$: Pacoima S16E (16 seconds)

n_1: Number of ductility levels varied

n_2: Number of natural frequencies for each ductility level

TABLE 5.2 UNIFORM 3DF SYSTEM PARAMETERS

Story, i	m_i (kip-sec^2/in)	k_i (kips/in)	Yield displacements		
			Level 1 (in)	Level 2 (in)	Level 3 (in)
1	1.0	199.5	0.9	0.3	0.18
2	1.0	199.5	0.7	0.25	0.13
3	1.0	199.5	0.45	0.15	0.09

Mode, n	f_n (cps)	Γ_n	Mode shapes		
			Story 1	2	3
1	1.0	1.656	0.32799	0.59101	0.73698
2	2.803	0.474	0.73698	0.32799	-0.59101
3	4.051	0.182	0.59101	-0.73698	0.32799

TABLE 5.3 NONUNIFORM 3DF SYSTEM PARAMETERS

Story, i	m_i (kip-sec^2/in)	k_i (kips/in)	Yield displacements		
			Level 1 (in)	Level 2 (in)	Level 3 (in)
1	3.0	388.0	1.0	0.35	0.2
2	2.0	388.0	0.65	0.2	0.12
3	1.0	77.6	2.0	0.6	0.33

Mode, n	f_n (cps)	Γ_n	Mode shapes		
			Story 1	2	3
1	1.0	2.166	0.22017	0.37320	0.75896
2	1.749	1.074	0.33411	0.35634	-0.64112
3	3.218	0.395	0.41621	-0.48347	0.11324

TABLE 5.4 EARTHQUAKES AND SYSTEM PARAMETERS USED IN 3DF SYSTEMS (UNIFORM AND NONUNIFORM SYSTEMS)*

1 cycle of iteration starting from the exact nonlinear response

Method	ξ_n \ α_i	0.3	0.1	0.05
Eq. Linear	Undamped	E(3,1), T(3,1) O(3,1), P(3,1)	E(3,1), T(3,1) O(3,1), P(3,1)	E(3,1), T(3,1) O(3,1), P(3,1)
Eq. Nonlinear	Undamped	E(3,1)	E(3,1)	E(3,1)

1 cycle of iteration starting from the linear response

Method	ξ_n \ α_i	0.3	0.1	0.05
Eq. Linear	Undamped	E(3,1), T(3,1) O(3,1), P(3,1)	E(3,1), T(3,1) O(3,1), P(3,1)	E(3,1), T(3,1) O(3,1), P(3,1)

* See symbols in Table 5.1.

TABLE 5.5a COMPARISON OF EXACT AND APPROXIMATE DUCTILITY FACTORS

3DF UNDAMPED UNIFORM SYSTEMS
EL CENTRO NS (16 SECONDS)

STORY NO.	LINEAR (4% MODAL DAMPING)	NON LINEAR	α=0.3 ALL (APPROX/EXACT) EQ.LINEAR RSS	EQ.LINEAR ABS+RSS/2	EQ.NONLINEAR RSS	EQ.NONLINEAR ABS+RSS/2	NON LINEAR	α=0.1 ALL (APPROX/EXACT) EQ.LINEAR RSS	EQ.LINEAR ABS+RSS/2	EQ.NONLINEAR RSS	EQ.NONLINEAR ABS+RSS/2	NON LINEAR	α=0.05 ALL (APPROX/EXACT) EQ.LINEAR RSS	EQ.LINEAR ABS+RSS/2	EQ.NONLINEAR RSS	EQ.NONLINEAR ABS+RSS/2
1	3.50	2.07	1.04	1.14	1.06	1.16	2.17	.88	1.04	.96	1.07	2.23	1.01	1.20	.98	1.10
2	3.37	2.53	1.01	1.09	1.03	1.11	2.98	.81	.93	.92	1.01	3.61	.84	.98	.85	.94
3	3.08	2.66	.96	1.16	.97	1.11	2.47	1.04	1.31	.96	1.18	2.54	1.19	1.52	.98	1.21
1	10.51	5.89	1.10	1.28	.98	1.14	7.48	1.20	1.33	1.00	1.12	8.96	.79	.90	1.01	1.12
2	9.44	6.10	1.00	1.15	.90	1.04	5.48	1.45	1.64	1.19	1.36	6.22	1.02	1.20	1.29	1.44
3	9.23	6.91	1.21	1.52	1.04	1.31	7.97	1.17	1.48	1.08	1.36	6.79	1.09	1.42	1.30	1.61
1	17.51	14.32	1.02	1.19	.92	1.08	13.58	1.05	1.21	1.20	1.38	15.34	.80	.92	.90	1.02
2	18.15	16.45	.98	1.15	.88	1.02	21.19	.77	.91	.87	1.01	15.77	.86	1.02	.97	1.13
3	15.39	13.37	1.31	1.66	1.21	1.53	16.94	.95	1.24	1.09	1.41	8.72	1.45	1.88	1.59	2.04

TABLE 5.5b COMPARISON OF EXACT AND APPROXIMATE DUCTILITY FACTORS

3DF UNDAMPED UNIFORM SYSTEMS
TAFT N21E (16 SECONDS)

STORY NO.	LINEAR (4% MODAL DAMPING)	NON LINEAR	α=0.3 ALL (APPROX/EXACT) EQ.LINEAR RSS	EQ.LINEAR ABS+RSS/2	EQ.NONLINEAR RSS	EQ.NONLINEAR ABS+RSS/2	NON LINEAR	α=0.1 ALL (APPROX/EXACT) EQ.LINEAR RSS	EQ.LINEAR ABS+RSS/2	EQ.NONLINEAR RSS	EQ.NONLINEAR ABS+RSS/2	NON LINEAR	α=0.05 ALL (APPROX/EXACT) EQ.LINEAR RSS	EQ.LINEAR ABS+RSS/2	EQ.NONLINEAR RSS	EQ.NONLINEAR ABS+RSS/2
1	2.58	3.03	.86	.94	-	-	3.58	.84	.92	-	-	3.85	.65	.74	-	-
2	2.92	2.51	.95	1.04	-	-	2.44	.96	1.07	-	-	3.61	.69	.80	-	-
3	3.58	3.30	.83	1.01	-	-	2.92	.90	1.11	-	-	3.30	.77	.98	-	-
1	7.74	8.98	1.02	1.14	-	-	9.96	.65	.76	-	-	10.11	.69	.80	-	-
2	8.16	10.14	.88	.99	-	-	8.14	.73	.88	-	-	6.40	.95	1.14	-	-
3	10.73	12.15	.82	1.03	-	-	6.71	1.06	1.37	-	-	6.29	1.21	1.56	-	-
1	12.90	15.53	1.11	1.27	-	-	13.44	.86	1.00	-	-	15.91	.82	.96	-	-
2	15.70	21.12	.90	1.04	-	-	18.88	.67	.81	-	-	14.77	.96	1.15	-	-
3	17.88	22.06	.90	1.14	-	-	14.23	.99	1.29	-	-	9.73	1.54	1.99	-	-

TABLE 5.5c COMPARISON OF EXACT AND APPROXIMATE DUCTILITY FACTORS

3DF UNDAMPED UNIFORM SYSTEMS
OLYMPIA NO4W (16 SECONDS)

STORY NO.	LINEAR (4% MODAL DAMPING)	NON LINEAR	α=0.3 ALL (APPROX/EXACT) EQ.LINEAR RSS	EQ.LINEAR ABS+RSS/2	EQ.NONLINEAR RSS	EQ.NONLINEAR ABS+RSS/2	NON LINEAR	α=0.1 ALL (APPROX/EXACT) EQ.LINEAR RSS	EQ.LINEAR ABS+RSS/2	EQ.NONLINEAR RSS	EQ.NONLINEAR ABS+RSS/2	NON LINEAR	α=0.05 ALL (APPROX/EXACT) EQ.LINEAR RSS	EQ.LINEAR ABS+RSS/2	EQ.NONLINEAR RSS	EQ.NONLINEAR ABS+RSS/2
1	3.10	2.67	1.05	1.16	-	-	2.16	1.10	1.22	-	-	2.03	1.24	1.38	-	-
2	2.44	2.17	1.15	1.27	-	-	2.18	1.14	1.24	-	-	2.54	1.26	1.36	-	-
3	2.85	3.27	1.01	1.25	-	-	3.62	.95	1.18	-	-	4.32	.95	1.18	-	-
1	9.29	7.30	1.14	1.28	-	-	9.29	1.05	1.15	-	-	9.99	1.05	1.16	-	-
2	6.83	6.20	1.24	1.42	-	-	5.93	1.42	1.58	-	-	3.73	2.01	2.27	-	-
3	8.55	7.58	1.15	1.47	-	-	6.51	1.37	1.70	-	-	6.32	1.58	1.97	-	-
1	15.49	19.83	.94	1.08	-	-	20.29	.87	.99	-	-	19.00	.84	.97	-	-
2	13.13	22.27	.93	1.08	-	-	23.93	.81	.94	-	-	17.20	1.00	1.18	-	-
3	14.24	19.22	1.08	1.38	-	-	17.92	1.07	1.37	-	-	6.74	2.30	2.95	-	-

TABLE 5.5d COMPARISON OF EXACT AND APPROXIMATE DUCTILITY FACTORS

3DF UNDAMPED UNIFORM SYSTEMS
PACOIMA S16E (16 SECONDS)

STORY NO.	LINEAR (4% MODAL DAMPING)	NON LINEAR	α=0.3 ALL (APPROX/EXACT) EQ.LINEAR RSS	EQ.LINEAR ABS+RSS/2	EQ.NONLINEAR RSS	EQ.NONLINEAR ABS+RSS/2	NON LINEAR	α=0.1 ALL (APPROX/EXACT) EQ.LINEAR RSS	EQ.LINEAR ABS+RSS/2	EQ.NONLINEAR RSS	EQ.NONLINEAR ABS+RSS/2	NON LINEAR	α=0.05 ALL (APPROX/EXACT) EQ.LINEAR RSS	EQ.LINEAR ABS+RSS/2	EQ.NONLINEAR RSS	EQ.NONLINEAR ABS+RSS/2
1	2.30	2.72	.92	1.00	-	-	2.76	.93	1.00	-	-	2.75	.92	.99	-	-
2	2.25	2.76	.93	1.02	-	-	2.91	.95	1.04	-	-	2.99	.93	1.01	-	-
3	2.04	2.03	.96	1.15	-	-	2.05	.89	1.07	-	-	2.35	.89	1.06	-	-
1	6.89	8.59	.96	1.02	-	-	9.06	.78	.87	-	-	10.73	.74	.84	-	-
2	6.31	8.98	.89	.96	-	-	5.78	1.05	1.18	-	-	4.24	1.41	1.60	-	-
3	6.11	9.52	.82	.97	-	-	5.03	1.22	1.51	-	-	5.75	1.33	1.65	-	-
1	11.49	15.498	1.00	1.07	-	-	15.42	.84	.96	-	-	17.31	.76	.84	-	-
2	12.14	18.65	.94	1.01	-	-	15.75	.90	1.03	-	-	17.28	.83	.98	-	-
3	10.19	16.97	.85	1.00	-	-	11.61	1.21	1.53	-	-	8.57	1.62	2.28	-	-

TABLE 5.6a COMPARISON OF EXACT AND APPROXIMATE DUCTILITY FACTORS

3DF UNDAMPED NONUNIFORM SYSTEMS
EL CENTRO NS (16 SECONDS)

STORY NO.	LINEAR (4% MODAL DAMPING)	NON LINEAR	α=0.3 ALL (APPROX/EXACT) EQ.LINEAR RSS	EQ.LINEAR ABS+RSS/2	EQ.NONLINEAR RSS	EQ.NONLINEAR ABS+RSS/2	NON LINEAR	α=0.1 ALL (APPROX/EXACT) EQ.LINEAR RSS	EQ.LINEAR ABS+RSS/2	EQ.NONLINEAR RSS	EQ.NONLINEAR ABS+RSS/2	NON LINEAR	α=0.05 ALL (APPROX/EXACT) EQ.LINEAR RSS	EQ.LINEAR ABS+RSS/2	EQ.NONLINEAR RSS	EQ.NONLINEAR ABS+RSS/2
1	3.10	2.39	.86	1.04	.89	1.07	2.58	.82	1.00	.84	.99	3.06	.81	.97	.88	1.04
2	2.88	2.10	.86	.97	.87	989	2.13	.77	.88	.84	1.09	2.06	.88	1.04	.94	1.04
3	2.94	2.44	.89	1.09	.93	1.14	2.19	.95	1.16	.85	1.04	2.14	.90	1.12	.88	1.07
1	8.86	6.33	.86	1.20	.81	1.201	7.57	1.07	1.424	.88	1.102	8.52	.86	1.101	1.00	1.315
2	9.37	6.44	.97	1.14	.86	1.00	6.83	1.09	1.42	1.09	1.25	7.23	1.12	1.30	1.29	1.47
3	9.79	5.86	1.13	1.40	1.10	1.36	3.53	1.36	1.72	1.44	1.80	2.98	1.75	2.20	1.89	2.34
1	15.51	13.86	.93	1.16	.87	1.09	16.82	.78	1.93	.83	.99	16.53	.74	.89	.88	1.03
2	15.62	15.98	.90	1.08	.81	.98	20.70	.73	.84	.79	.92	11.73	1.10	1.26	1.34	1.51
3	17.80	16.95	1.00	1.25	.96	1.19	7.09	1.80	2.26	1.92	2.38	4.93	2.38	2.97	2.59	3.21

TABLE 5.6b COMPARISON OF EXACT AND APPROXIMATE DUCTILITY FACTORS

3DF UNDAMPED NONUNIFORM SYSTEMS
TAFT N21E (16 SECONDS)

STORY NO.	LINEAR (4% MODAL DAMPING)	NON LINEAR	α=0.3 ALL (APPROX/EXACT) EQ.LINEAR RSS	EQ.LINEAR ABS+RSS/2	EQ.NONLINEAR RSS	EQ.NONLINEAR ABS+RSS/2	NON LINEAR	α=0.1 ALL (APPROX/EXACT) EQ.LINEAR RSS	EQ.LINEAR ABS+RSS/2	EQ.NONLINEAR RSS	EQ.NONLINEAR ABS+RSS/2	NON LINEAR	α=0.05 ALL (APPROX/EXACT) EQ.LINEAR RSS	EQ.LINEAR ABS+RSS/2	EQ.NONLINEAR RSS	EQ.NONLINEAR ABS+RSS/2
1	2.03	2.65	.91	1.09	-	-	3.19	.87	1.03	-	-	3.48	.74	.88	-	-
2	2.36	2.73	.86	.96	-	-	3.08	.85	.97	-	-	3.70	.71	.82	-	-
3	2.11	2.09	1.03	1.27	-	-	2.06	.93	1.15	-	-	2.25	.80	1.00	-	-
1	5.79	8.64	.86	1.03	-	-	10.18	.67	.81	-	-	10.86	.65	.80	-	-
2	7.66	10.36	.85	.96	-	-	12.36	.64	.77	-	-	9.85	.77	.94	-	-
3	7.03	6.65	1.20	1.48	-	-	2.71	1.74	2.17	-	-	2.69	2.06	2.53	-	-
1	10.14	15.57	.92	1.10	-	-	15.92	.67	.84	-	-	16.62	.75	.93	-	-
2	12.76	18.23	.86	.99	-	-	19.87	.59	.71	-	-	14.38	.92	1.09	-	-
3	12.78	16.58	1.06	1.31	-	-	6.12	2.00	2.51	-	-	4.23	2.91	3.82	-	-

TABLE 5.6c COMPARISON OF EXACT AND APPROXIMATE DUCTILITY FACTORS

3DF UNDAMPED NONUNIFORM SYSTEMS
OLYMPIA N04W (16 SECONDS)

STORY NO.	LINEAR (4% MODAL DAMPING)	NON LINEAR	α=0.3 ALL (APPROX/EXACT) EQ.LINEAR RSS	EQ.LINEAR ABS+RSS/2	EQ.NONLINEAR RSS	EQ.NONLINEAR ABS+RSS/2	NON LINEAR	α=0.1 ALL (APPROX/EXACT) EQ.LINEAR RSS	EQ.LINEAR ABS+RSS/2	EQ.NONLINEAR RSS	EQ.NONLINEAR ABS+RSS/2	NON LINEAR	α=0.05 ALL (APPROX/EXACT) EQ.LINEAR RSS	EQ.LINEAR ABS+RSS/2	EQ.NONLINEAR RSS	EQ.NONLINEAR ABS+RSS/2
1	2.77	2.78	.98	1.16	-	-	3.09	.82	.96	-	-	3.17	.97	1.13	-	-
2	2.68	1.97	1.14	1.29	-	-	1.82	.95	1.14	-	-	1.78	1.13	1.35	-	-
3	3.22	2.18	.96	1.17	-	-	2.15	.81	1.01	-	-	2.26	.98	1.22	-	-
1	7.91	5.70	1.07	1.29	-	-	7.19	1.12	1.32	-	-	7.92	1.30	1.41	-	-
2	8.72	7.94	.99	1.15	-	-	6.96	1.30	1.46	-	-	6.04	1.57	1.78	-	-
3	10.72	5.28	1.30	1.61	-	-	5.55	1.26	1.56	-	-	3.11	2.16	2.69	-	-
1	13.85	14.81	1.00	1.21	-	-	21.86	.87	.95	-	-	21.87	.91	.96	-	-
2	14.53	17.58	.95	1.10	-	-	16.62	1.14	1.22	-	-	13.59	1.35	1.57	-	-
3	19.48	15.75	1.16	1.43	-	-	8.02	1.36	1.83	-	-	4.02	2.60	3.56	-	-

TABLE 5.6d COMPARISON OF EXACT AND APPROXIMATE DUCTILITY FACTORS

3DF UNDAMPED NONUNIFORM SYSTEMS
PACOIMA S16W (16 SECONDS)

STORY NO.	LINEAR (4% MODAL DAMPING)	NON LINEAR	α=0.3 ALL (APPROX/EXACT) EQ.LINEAR RSS	EQ.LINEAR ABS+RSS/2	EQ.NONLINEAR RSS	EQ.NONLINEAR ABS+RSS/2	NON LINEAR	α=0.1 ALL (APPROX/EXACT) EQ.LINEAR RSS	EQ.LINEAR ABS+RSS/2	EQ.NONLINEAR RSS	EQ.NONLINEAR ABS+RSS/2	NON LINEAR	α=0.05 ALL (APPROX/EXACT) EQ.LINEAR RSS	EQ.LINEAR ABS+RSS/2	EQ.NONLINEAR RSS	EQ.NONLINEAR ABS+RSS/2
1	1.89	2.79	.89	.95	-	-	3.30	.86	.91	-	-	3.53	.81	.87	-	-
2	1.94	2.60	.92	1.02	-	-	2.51	.90	.99	-	-	2.75	.85	.95	-	-
3	1.63	1.12	.93	1.10	-	-	1.03	.49	.62	-	-	1.14	.43	.52	-	-
1	5.41	7.31	.88	1.02	-	-	6.08	.99	1.19	-	-	6.79	.99	1.20	-	-
2	6.30	8.61	.89	.98	-	-	9.47	.77	.88	-	-	8.50	.91	1.05	-	-
3	5.43	6.89	1.05	1.27	-	-	3.23	1.63	2.02	-	-	3.24	1.84	2.29	-	-
1	9.47	12.84	1.01	1.20	-	-	15.08	.78	.98	-	-	18.28	.86	.97	-	-
2	10.49	15.88	.89	.99	-	-	16.21	.79	.91	-	-	12.46	1.18	1.36	-	-
3	9.87	18.06	.90	1.10	-	-	5.65	2.12	2.62	-	-	3.37	2.84	3.88	-	-

TABLE 5.7 TAPERED 10DF SYSTEM

Story, i	m_i (kip-sec^2/in)	k_i (kip/in)	Yield Displacements Level 2
1	1.0	1398.0	0.15
2	0.95	1326.2	0.14
3	0.90	1256.4	0.13
4	0.85	1186.6	0.12
5	0.80	1116.8	0.11
6	0.75	1047.0	0.10
7	0.70	977.2	0.09
8	0.65	907.4	0.08
9	0.60	837.6	0.07
10	0.55	767.8	0.06

Mode, n	f_n (cps)	Γ_n	Mode Shapes									
			Story 1	2	3	4	5	6	7	8	9	10
1	1.0	2.491	.07040	.14251	.21432	.28393	.34937	.40823	.45974	.50078	.52990	.54532
2	2.652	0.965	.18948	.34993	.44548	.45228	.36506	.19397	-.03066	-.26601	-.46367	-.57873
3	4.301	0.565	.29562	.44402	.35548	.06483	-.28001	-.49160	-.44277	-.14074	.26622	.55825
4	5.866	0.386	.37584	.38649	.00075	-.40846	-.42093	.00267	.45875	.46402	-.01401	-.52063
5	7.304	0.280	.42308	.19648	-.35562	-.37208	.20692	.49150	.00186	-.52847	-.23918	.47009
6	8.582	0.208	.43311	-.06050	-.49853	.12972	.45705	-.20915	-.45623	.30097	.44220	-.40843
7	9.669	0.153	.40515	-.29588	-.21015	.46890	-.12676	-.40465	.44385	.09392	-.55416	.33712
8	10.541	0.109	.34195	-.42915	.18034	.22561	-.47961	.37563	.02732	-.44022	.55186	-.25760
9	11.179	0.071	.24994	-.41677	.43422	-.28957	.02873	.25994	-.47661	.54413	-.43333	.17100
10	11.572	0.038	.14224	-.27506	.38404	-.45805	.49036	-.47888	.42578	-.33650	.21828	-.07832

TABLE 5.8a COMPARISON OF EXACT AND APPROXIMATE DUCTILITY FACTORS

10DF UNDAMPED TAPERED SYSTEMS
EL CENTRO NS (16 SECONDS)

STORY NO.	LINEAR (4% MODAL DAMPING)	NON LINEAR	α=0.3 ALL (APPROX/EXACT) EQ.LINEAR RSS	EQ.LINEAR ABS+RSS/2	EQ.NONLINEAR RSS	EQ.NONLINEAR ABS+RSS/2	NON LINEAR	α=0.1 ALL (APPROX/EXACT) EQ.LINEAR RSS	EQ.LINEAR ABS+RSS/2	EQ.NONLINEAR RSS	EQ.NONLINEAR ABS+RSS/2	NON LINEAR	α=0.05 ALL (APPROX/EXACT) EQ.LINEAR RSS	EQ.LINEAR ABS+RSS/2	EQ.NONLINEAR RSS	EQ.NONLINEAR ABS+RSS/2
1	7.10	3.66	1.10	1.37	.97	1.22	5.13	1.12	1.39	.94	1.17	4.73	1.17	1.44	1.13	1.38
2	7.70	3.92	1.11	1.35	.98	1.19	5.16	1.18	1.39	.98	1.17	4.72	1.22	1.46	1.20	1.40
3	8.07	4.04	1.08	1.25	.97	1.11	4.51	1.33	1.49	1.09	1.24	4.88	1.23	1.38	1.22	1.36
4	8.18	4.42	1.10	1.17	.93	1.03	5.08	1.31	1.45	1.06	1.16	5.16	1.29	1.46	1.23	1.34
5	7.92	5.65	.93	1.10	.84	1.01	4.61	1.47	1.76	1.19	1.42	6.19	1.20	1.46	1.14	1.33
6	8.62	6.58	.95	1.18	.84	1.05	5.99	1.28	1.57	1.07	1.32	7.07	1.10	1.37	1.07	1.29
7	9.15	6.71	1.08	1.30	.93	1.10	6.44	1.26	1.53	1.09	1.34	6.77	1.16	1.41	1.15	1.39
8	9.04	6.54	1.19	1.30	1.02	1.31	6.26	1.33	1.53	1.16	1.52	6.60	1.27	1.70	1.20	1.56
9	7.86	5.07	1.34	1.73	1.17	1.54	4.51	1.53	2.01	1.32	1.77	7.24	1.15	1.57	1.01	1.36
10	5.07	3.11	1.69	2.20	1.49	1.98	3.44	1.16	1.58	.98	1.32	3.58	1.00	1.36	.87	1.17

TABLE 5.8b COMPARISON OF EXACT AND APPROXIMATE DUCTILITY FACTORS

10DF UNDAMPED TAPERED SYSTEMS
TAFT N21E (16 SECONDS)

STORY NO.	LINEAR (4% MODAL DAMPING)	NON LINEAR	α=0.3 ALL (APPROX/EXACT) EQ.LINEAR RSS	EQ.LINEAR ABS+RSS/2	EQ.NONLINEAR RSS	EQ.NONLINEAR ABS+RSS/2	NON LINEAR	α=0.1 ALL (APPROX/EXACT) EQ.LINEAR RSS	EQ.LINEAR ABS+RSS/2	EQ.NONLINEAR RSS	EQ.NONLINEAR ABS+RSS/2	NON LINEAR	α=0.05 ALL (APPROX/EXACT) EQ.LINEAR RSS	EQ.LINEAR ABS+RSS/2	EQ.NONLINEAR RSS	EQ.NONLINEAR ABS+RSS/2
1	5.05	5.36	1.02	1.23	1.08	1.29	4.83	.89	1.14	1.09	1.33	5.53	.83	1.08	.88	1.12
2	5.40	6.18	.99	1.15	1.14	1.26	6.38	.76	.94	.96	1.11	7.50	.62	.78	.72	.87
3	5.81	6.85	.95	1.05	1.02	1.11	8.15	.63	.73	.83	.91	8.00	.67	.79	.71	.81
4	6.14	7.85	.89	.96	.96	.04	9.04	.61	.80	.81	.90	7.96	.66	.76	.75	.85
5	6.55	8.04	.91	1.05	.99	1.14	8.86	.67	.83	.87	1.02	6.75	.83	1.05	.92	1.12
6	7.25	8.68	.90	1.05	.96	1.15	8.32	.76	.96	.93	1.12	8.05	.78	1.00	.82	1.02
7	8.02	9.65	.85	1.01	.88	1.03	7.67	.89	1.11	1.01	1.22	8.40	.85	1.07	.84	1.05
8	8.54	9.07	.91	1.16	.93	1.19	6.00	1.16	1.54	1.23	1.62	8.23	.96	1.28	.91	1.21
9	7.98	8.92	.85	1.13	.88	1.18	5.14	1.21	1.63	1.25	1.69	4.54	1.38	1.86	1.29	1.75
10	5.38	6.32	1.09	1.47	1.14	1.55	3.63	.96	1.29	.98	1.33	3.32	.80	1.08	.75	1.02

TABLE 5.8c COMPARISON OF EXACT AND APPROXIMATE DUCTILITY FACTORS

10DF UNDAMPED TAPERED SYSTEMS
OLYMPIA N04W (16 SECONDS)

STORY NO.	LINEAR (4% MODAL DAMPING)	NON LINEAR	α=0.3 ALL (APPROX/EXACT) EQ.LINEAR RSS	EQ.LINEAR ABS+RSS 2	EQ.NONLINEAR RSS	EQ.NONLINEAR ABS+RSS 2	NON LINEAR	α=0.1 ALL (APPROX/EXACT) EQ.LINEAR RSS	EQ.LINEAR ABS+RSS 2	EQ.NONLINEAR RSS	EQ.NONLINEAR ABS+RSS 2	NON LINEAR	α=0.05 ALL (APPROX/EXACT) EQ.LINEAR RSS	EQ.LINEAR ABS+RSS 2	EQ.NONLINEAR RSS	EQ.NONLINEAR ABS+RSS 2
1	6.35	4.19	1.10	1.37	.93	1.17	7.58	.84	1.01	.72	.90	8.92	.79	.98	.60	.77
2	6.70	4.24	1.16	1.39	.97	1.18	6.45	1.01	1.15	.85	1.01	6.09	1.14	1.35	.85	1.01
3	6.79	4.28	1.18	1.33	.99	1.12	5.31	1.21	1.433	1.00	1.13	5.13	1.33	1.49	.98	1.12
4	6.63	5.59	1.04	1.16	.86	.97	5.47	1.25	1.37	1.04	1.16	4.69	1.48	1.61	1.10	1.23
5	6.47	6.82	.95	1.13	.79	.95	5.06	1.38	1.63	1.16	1.42	4.85	1.40	1.76	1.15	1.42
6	7.68	7.74	.91	1.12	.77	.96	6.19	1.22	1.47	1.05	1.31	5.99	1.38	1.69	1.05	1.32
7	9.13	8.53	.92	1.08	.76	.98	5.29	1.38	1.66	1.23	1.52	5.16	1.23	1.79	1.28	1.56
8	9.83	7.98	.98	1.28	.86	1.12	5.00	1.43	1.87	1.34	1.78	5.58	1.55	2.02	1.26	1.68
9	9.07	5.73	1.21	1.64	1.07	1.44	4.92	1.32	1.79	1.28	1.74	5.77	1.40	1.88	1.18	1.60
10	6.07	3.20	1.69	2.30	1.49	2.02	4.02	1.00	1.36	.97	1.32	4.89	.90	1.22	.77	1.05

TABLE 5.8d COMPARISON OF EXACT AND APPROXIMATE DUCTILITY FACTORS

10DF UNDAMPED TAPERED SYSTEMS
PACOIMA S16E (16 SECONDS)

STORY NO.	LINEAR (4% MODAL DAMPING)	NON LINEAR	α=0.3 ALL (APPROX/EXACT) EQ.LINEAR RSS	EQ.LINEAR ABS+RSS 2	EQ.NONLINEAR RSS	EQ.NONLINEAR ABS+RSS 2	NON LINEAR	α=0.1 ALL (APPROX/EXACT) EQ.LINEAR RSS	EQ.LINEAR ABS+RSS 2	EQ.NONLINEAR RSS	EQ.NONLINEAR ABS+RSS 2	NON LINEAR	α=0.05 ALL (APPROX/EXACT) EQ.LINEAR RSS	EQ.LINEAR ABS+RSS 2	EQ.NONLINEAR RSS	EQ.NONLINEAR ABS+RSS 2
1	4.47	5.17	.93	1.06	1.01	1.14	4.85	.86	1.04	.90	1.07	5.97	.85	1.04	.84	.99
2	4.94	5.55	.96	1.06	1.04	1.14	4.98	.89	1.04	.94	1.07	6.18	.87	1.01	.87	.98
3	5.20	6.27	.94	1.00	1.02	1.08	6.03	.82	.91	.87	.95	6.17	.85	.98	.92	1.00
4	5.39	6.92	.92	.98	1.01	1.06	6.19	.84	.91	.90	.98	6.02	.94	1.02	.99	1.00
5	5.55	7.24	.92	1.02	.99	1.10	5.54	.95	1.12	1.02	1.18	4.02	1.32	1.59	1.33	1.54
6	5.43	7.30	.92	1.04	.99	1.11	5.94	.95	1.13	.98	1.15	3.29	1.52	1.90	1.46	1.70
7	5.38	7.31	.89	1.01	1.10	1.15	5.40	1.05	1.29	1.05	1.26	4.21	1.43	1.77	1.29	1.54
8	5.80	6.74	.91	1.11	.97	1.18	4.43	1.19	1.55	1.16	1.50	4.37	1.43	1.86	1.23	1.59
9	5.33	5.87	.88	1.14	.94	1.20	4.33	1.05	1.40	1.02	1.36	5.62	1.09	1.44	.91	1.21
10	3.55	3.22	1.20	1.59	1.25	1.64	2.01	.69	.90	.67	.87	2.21	.72	.92	.60	.76

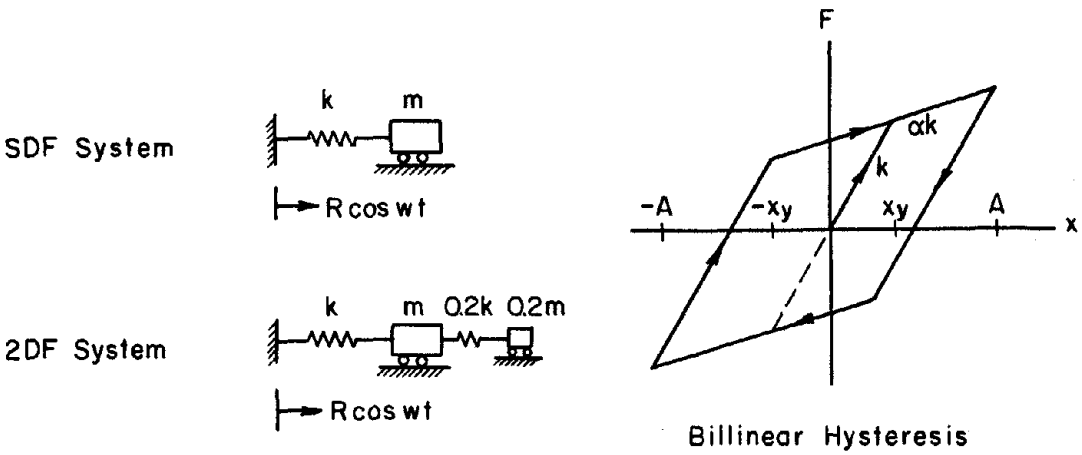

$w_2/w_1 = 1.57$

$\{\Phi_1\}^T = [0.2796 \quad 0.7805] \quad \Gamma_1 = 2.178$

$\{\Phi_2\}^T = [0.3490 \quad -0.6252] \quad \Gamma_2 = 1.120$

FIGURE 2.1 BILINEAR SHEAR BEAM SYSTEMS

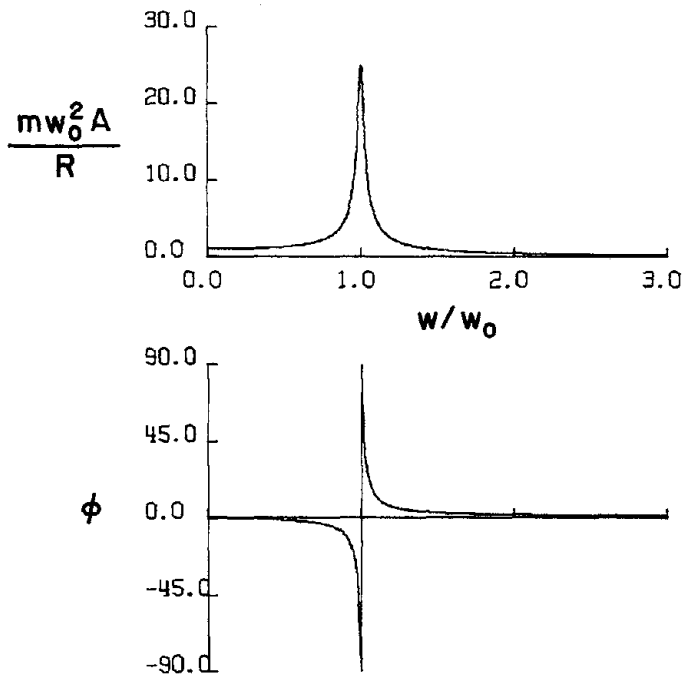

FIGURE 2.2 LINEAR DISPLACEMENT TRANSFER FUNCTION
(SDF SYSTEM, ξ = 0.02, HARMONIC EXCITATION)

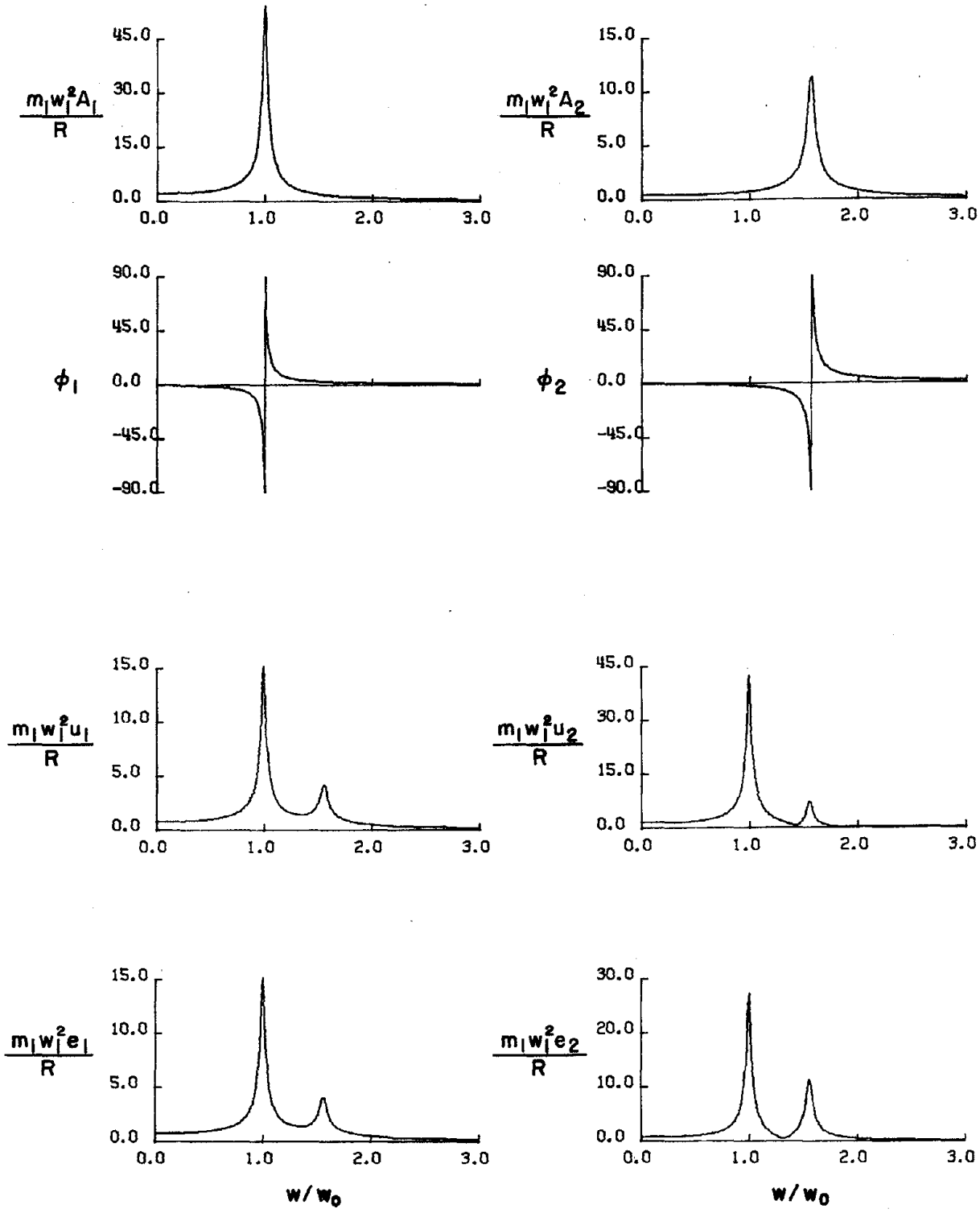

FIGURE 2.3 LINEAR TRANSFER FUNCTIONS FOR MODAL DISPLACEMENTS, JOINT DISPLACEMENTS AND ELEMENT STRAINS (2DF SYSTEM, $\xi_1 = \xi_2 = 0.02$, HARMONIC EXCITATION)

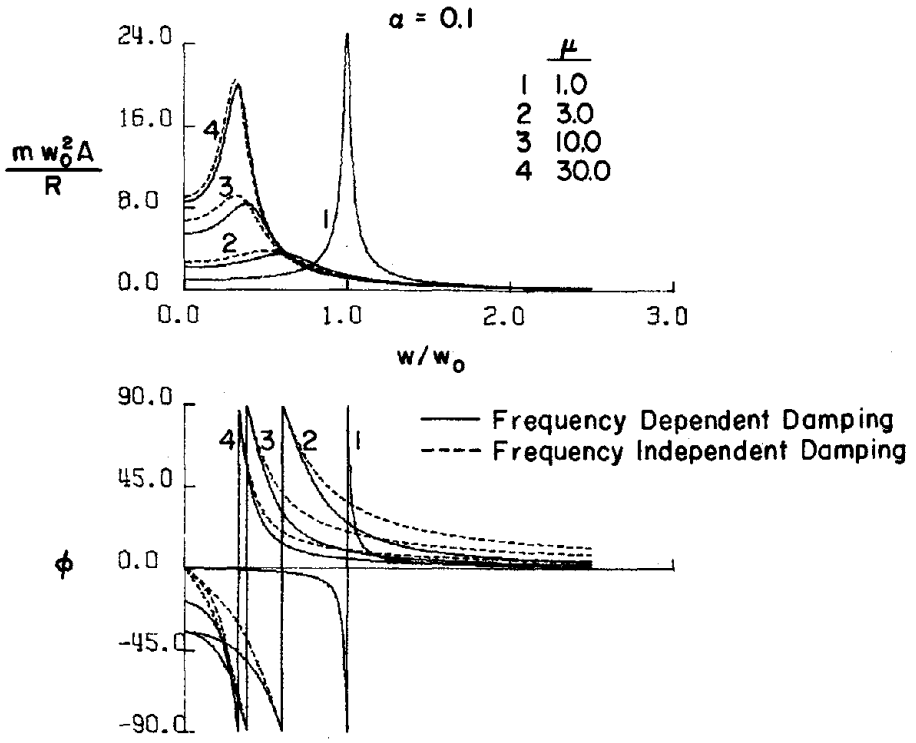

FIGURE 2.4 EQUIVALENT LINEAR DISPLACEMENT TRANSFER FUNCTION (BILINEAR SDF SYSTEM, ξ = 0.02, HARMONIC EXCITATION)

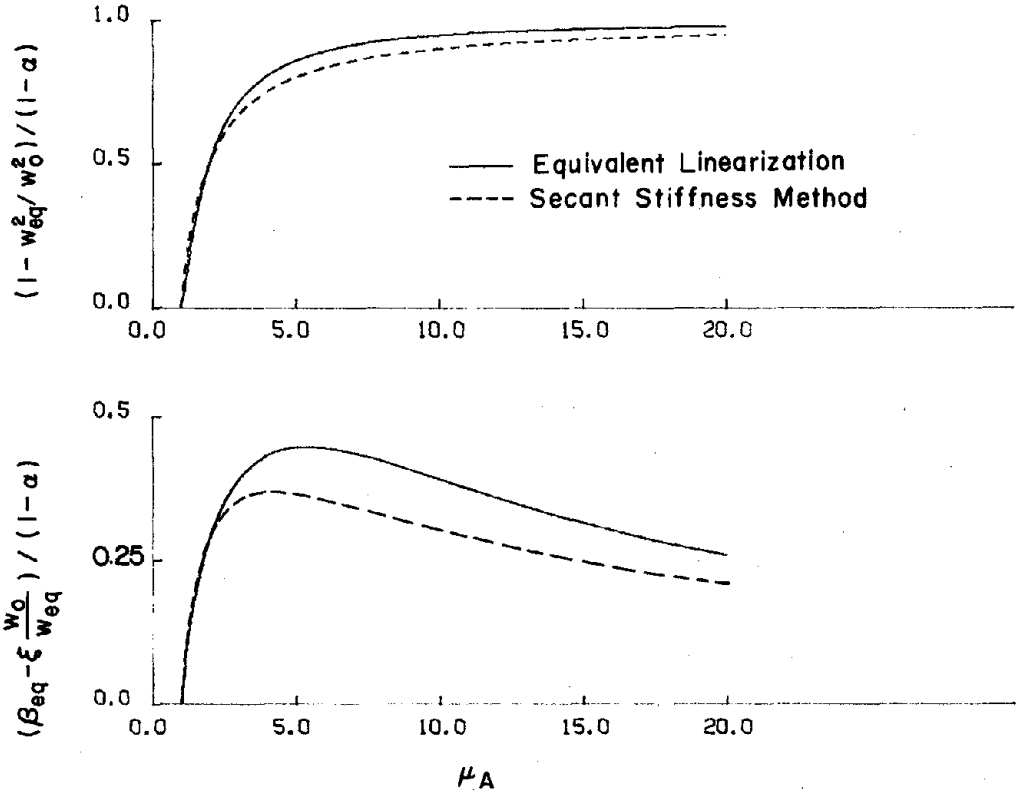

FIGURE 2.5 EQUIVALENT LINEAR FREQUENCY AND DAMPING (BILINEAR SDF SYSTEM, HARMONIC EXCITATION)

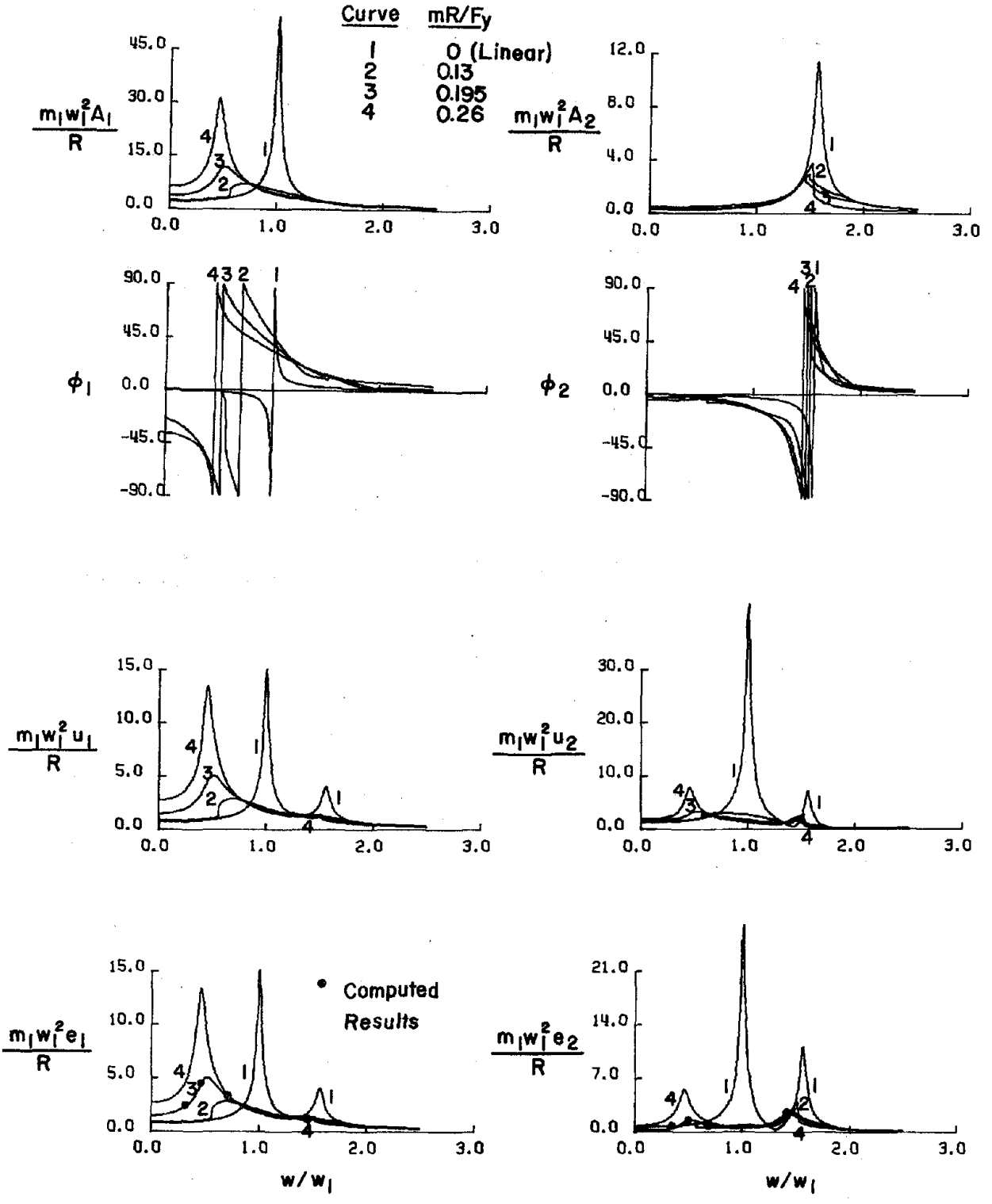

FIGURE 2.6 EQUIVALENT LINEAR TRANSFER FUNCTIONS FOR MODAL DISPLACEMENTS, JOINT DISPLACEMENTS AND ELEMENT STRAINS (BILINEAR 2DF SYSTEMS, $\xi_1=\xi_2=0.1$, $\alpha_1=\alpha_2=0.02$, HARMONIC EXCITATION, EQUIVALENT LINEAR MODE SHAPES)

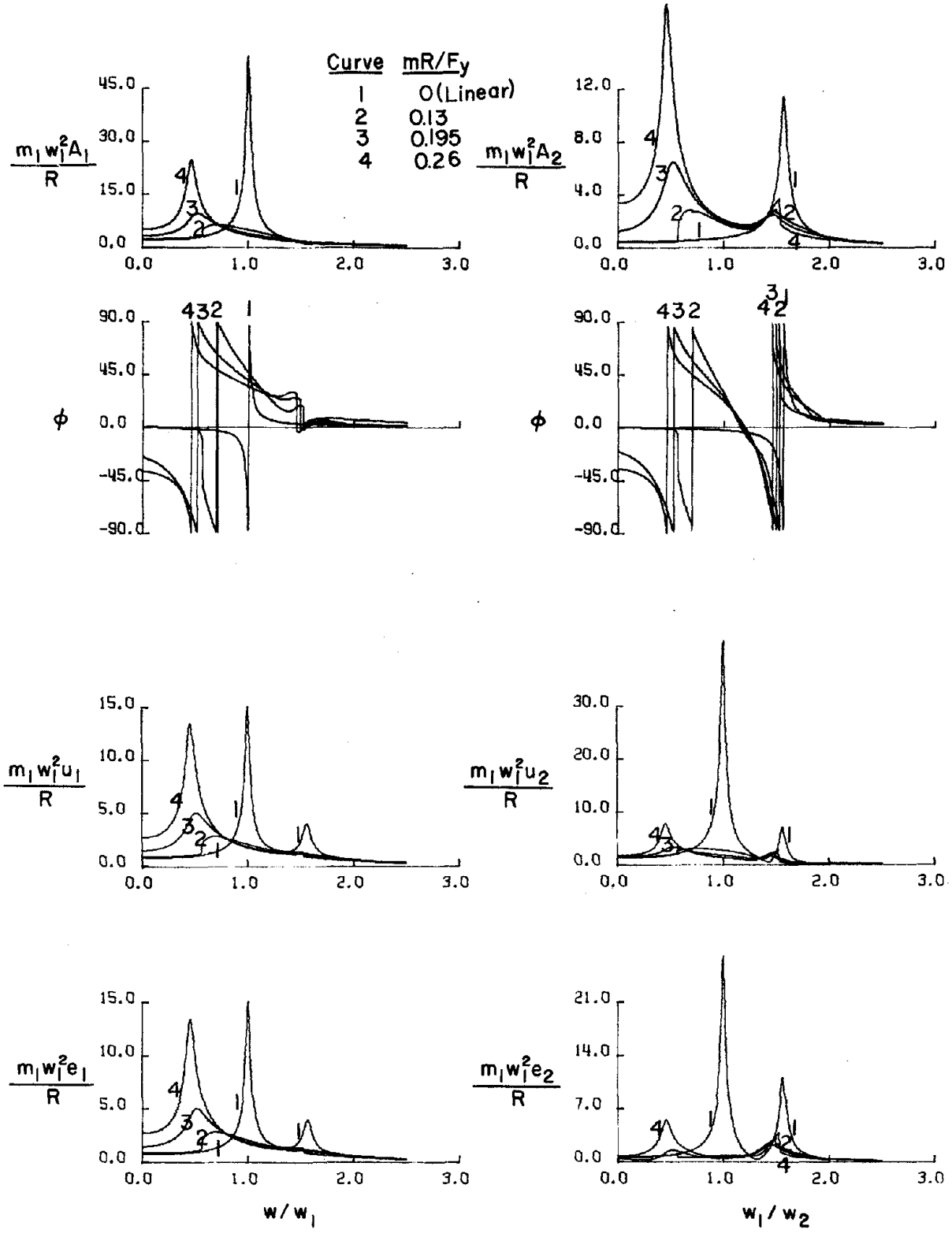

FIGURE 2.7 EQUIVALENT LINEAR TRANSFER FUNCTIONS FOR MODAL DISPLACEMENTS, JOINT DISPLACEMENTS AND ELEMENT STRAINS (BILINEAR 2DF SYSTEMS, $\xi_1=\xi_2=0.1$, $\alpha_1=\alpha_2=0.02$, HARMONIC EXCITATION, LINEAR MODE SHAPES)

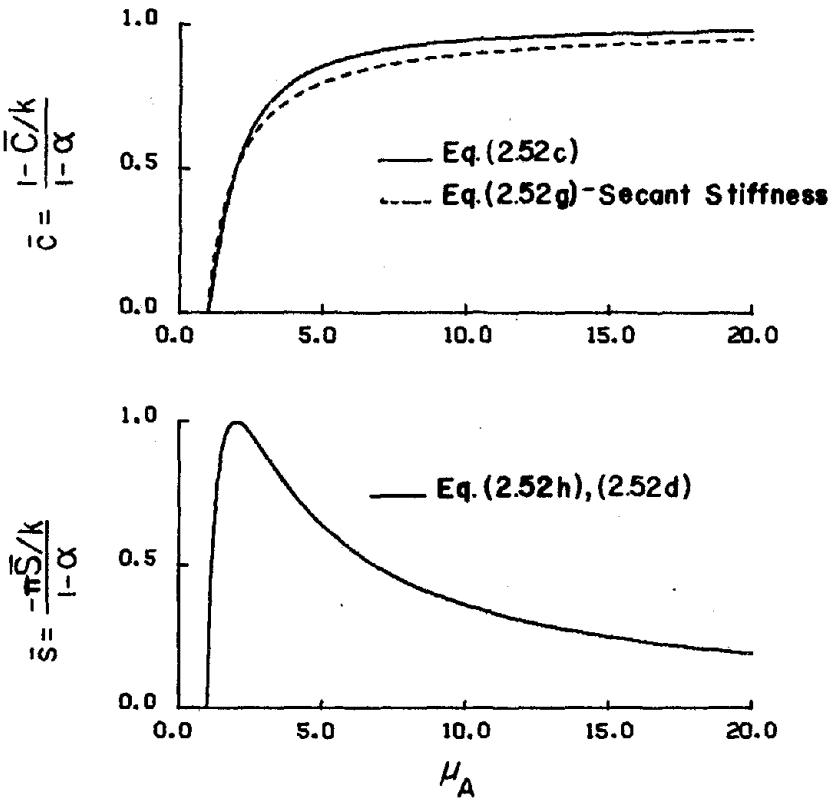

FIGURE 2.8 BILINEAR HYSTERESIS PARAMETERS

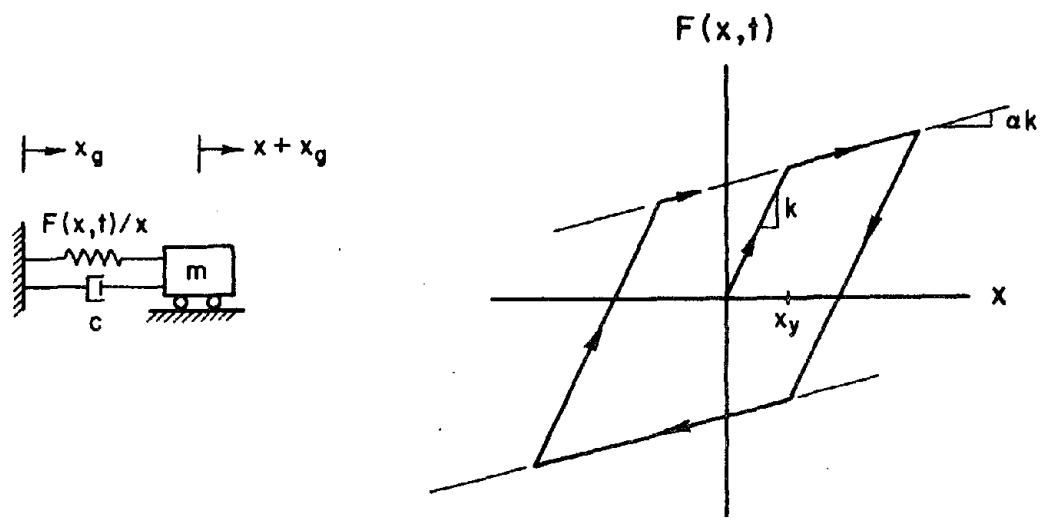

FIGURE 3.1 SINGLE DEGREE-OF-FREEDOM BILINEAR SYSTEM

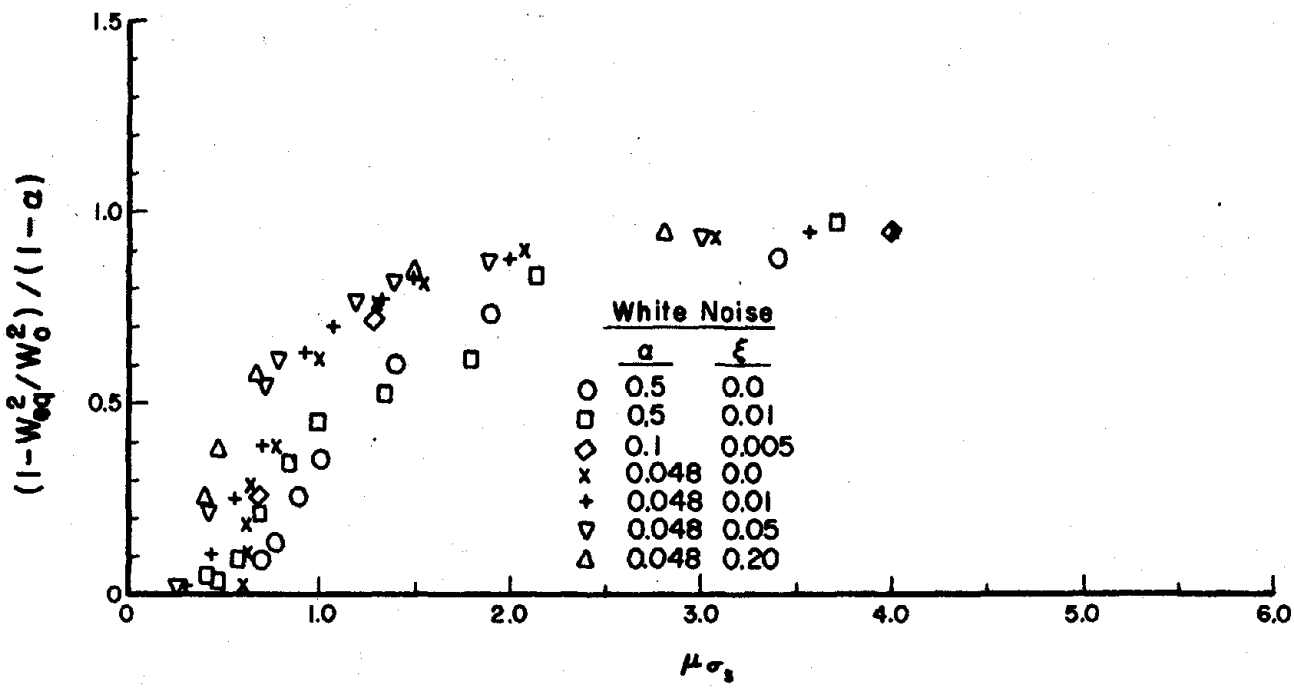

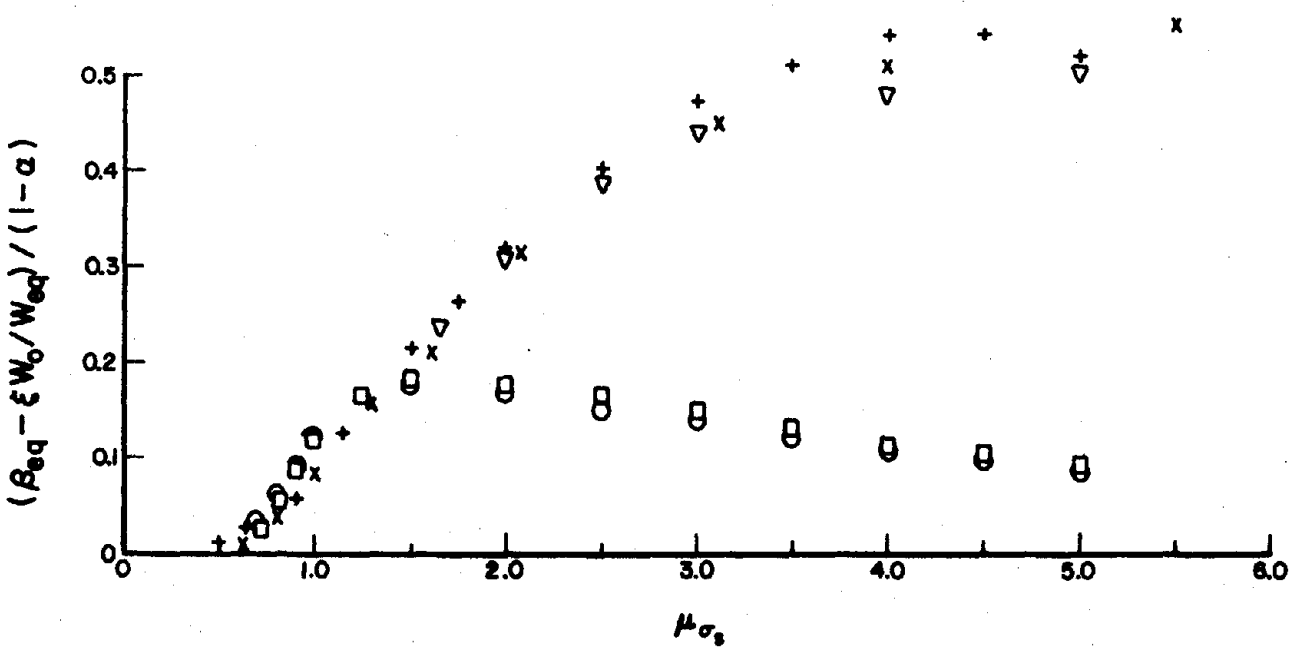

FIGURE 3.2 EQUIVALENT LINEAR FREQUENCY AND DAMPING (WHITE NOISE EXCITATION; AFTER LUTES, L.D., AND TAKEMIYA, H.)

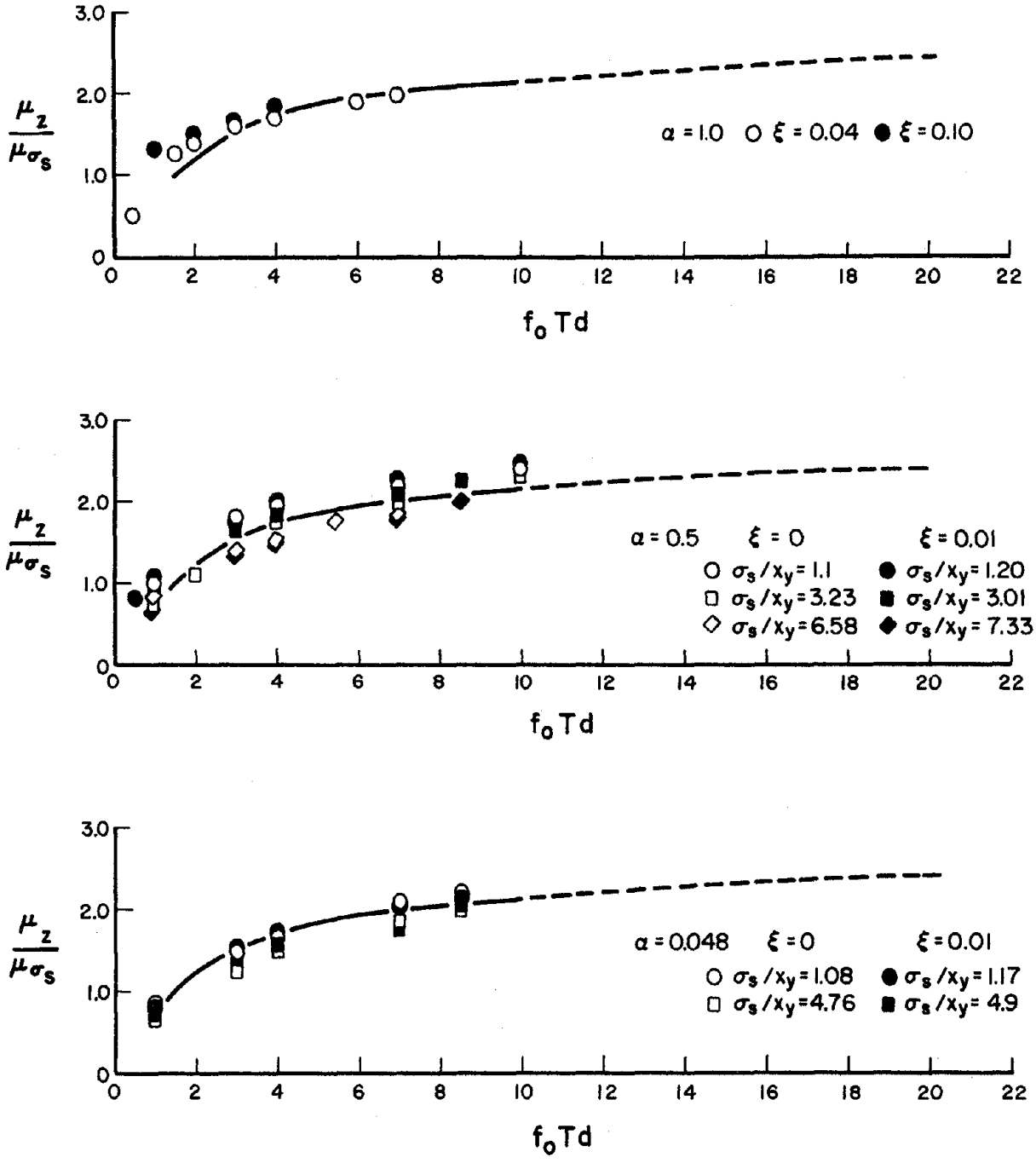

FIGURE 3.3 EXPECTED MAXIMUM DUCTILITY, ZERO-START
(WHITE NOISE EXCITATION; AFTER CHOKSHI, N.C., AND LUTES, L.D.)

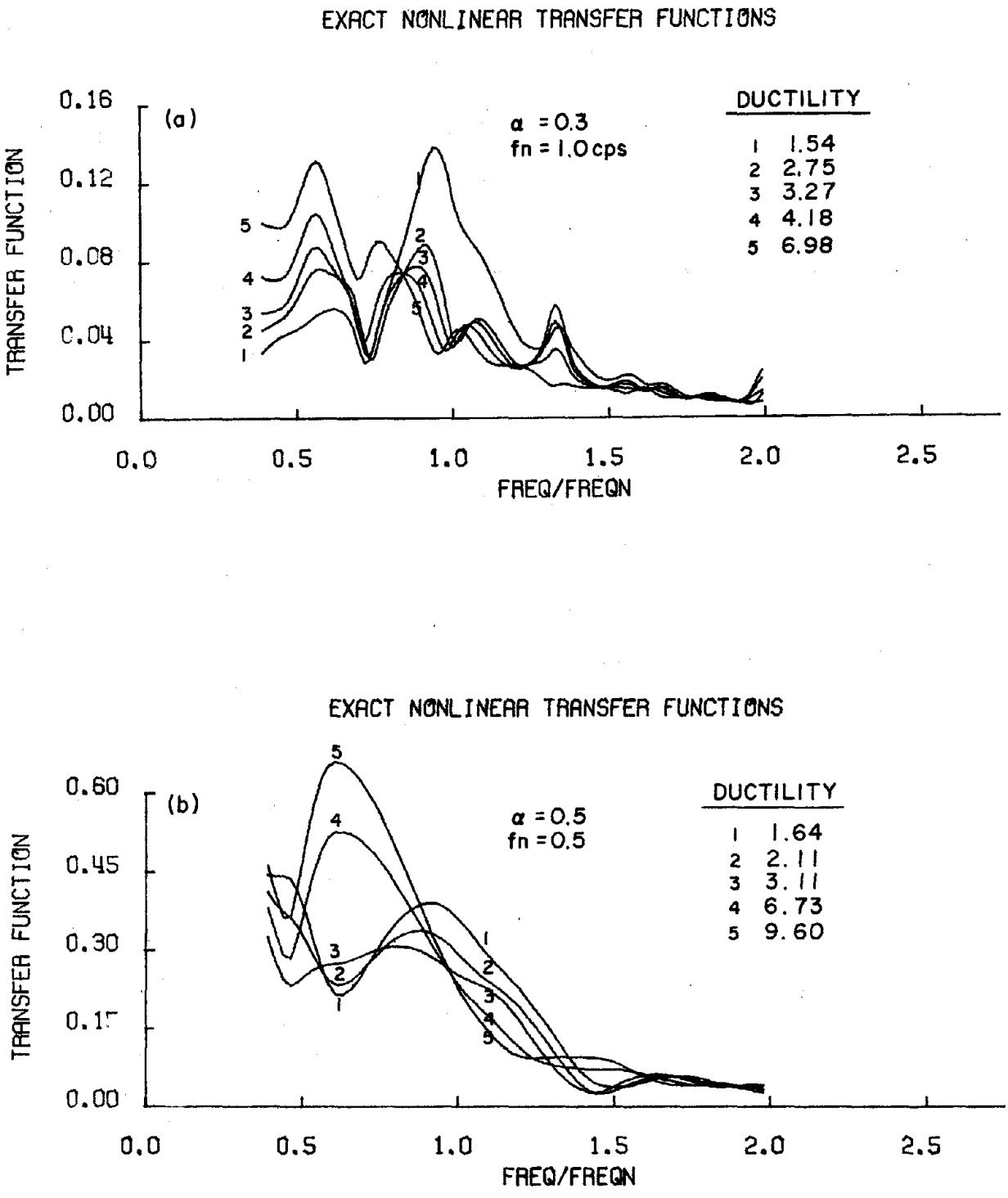

FIGURE 3.4 NONLINEAR DISPLACEMENT TRANSFER FUNCTIONS - UNIT = IN-SEC^2/IN (BILINEAR SDF SYSTEMS, ξ = 0.05, EL CENTRO 1940-NS)

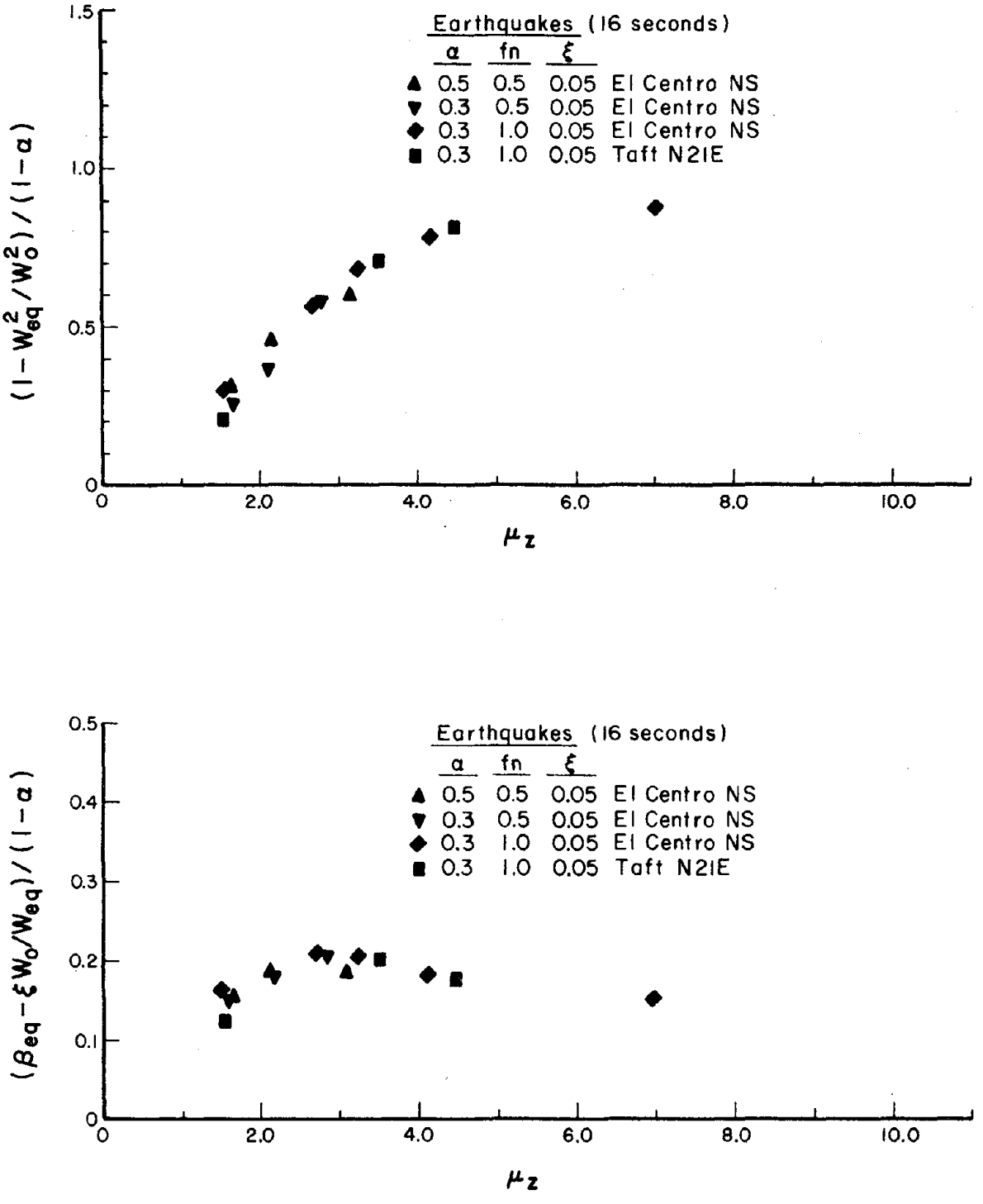

FIGURE 3.5 EQUIVALENT LINEAR FREQUENCY AND DAMPING (EARTHQUAKE EXCITATIONS)

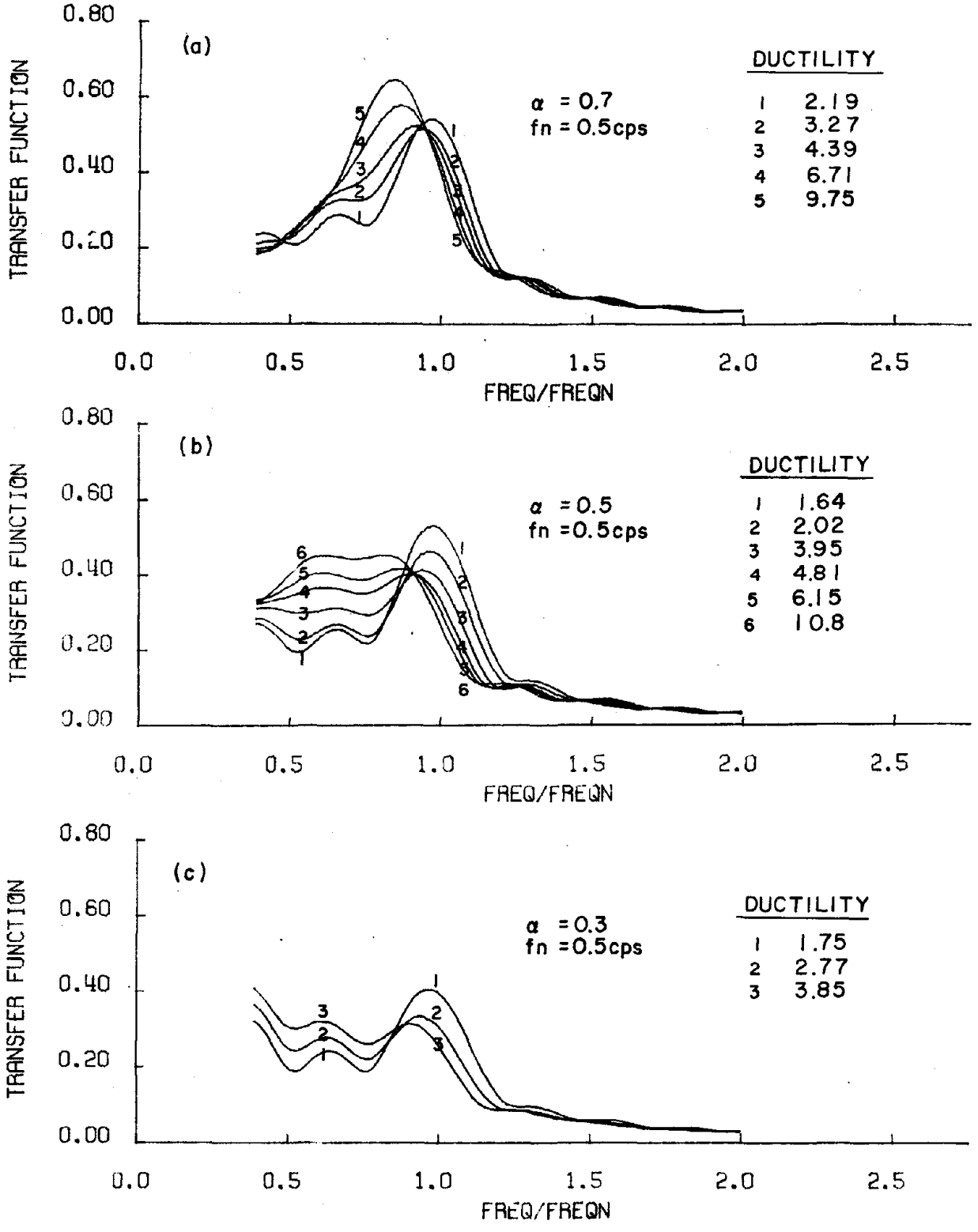

FIGURE 3.6 NONLINEAR DISPLACEMENT TRANSFER FUNCTIONS - UNIT = IN-SEC^2/IN
(BILINEAR SDF SYSTEMS, ξ = 0.05, PULSE-LIKE EXCITATION)

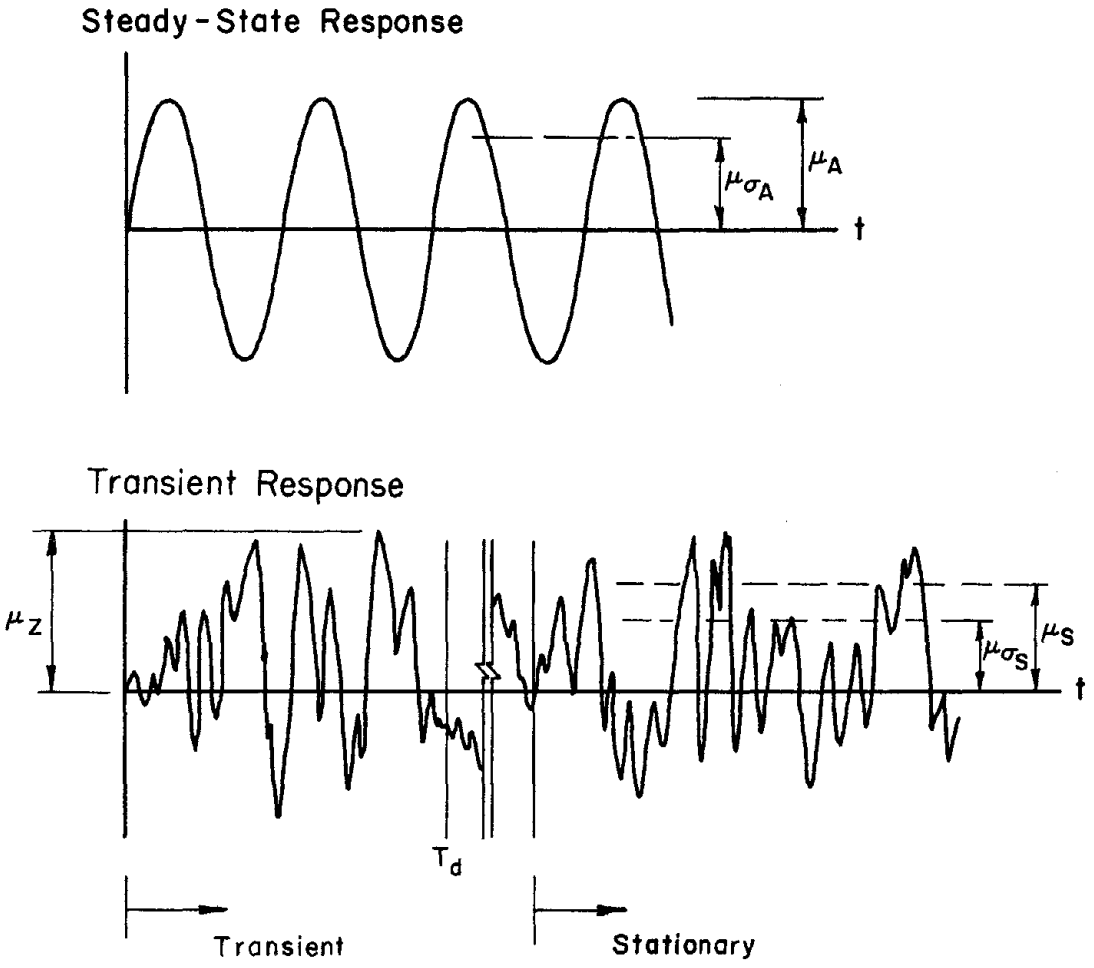

FIGURE 3.7 TRANSIENT, STATIONARY AND STEADY-STATE RESPONSES

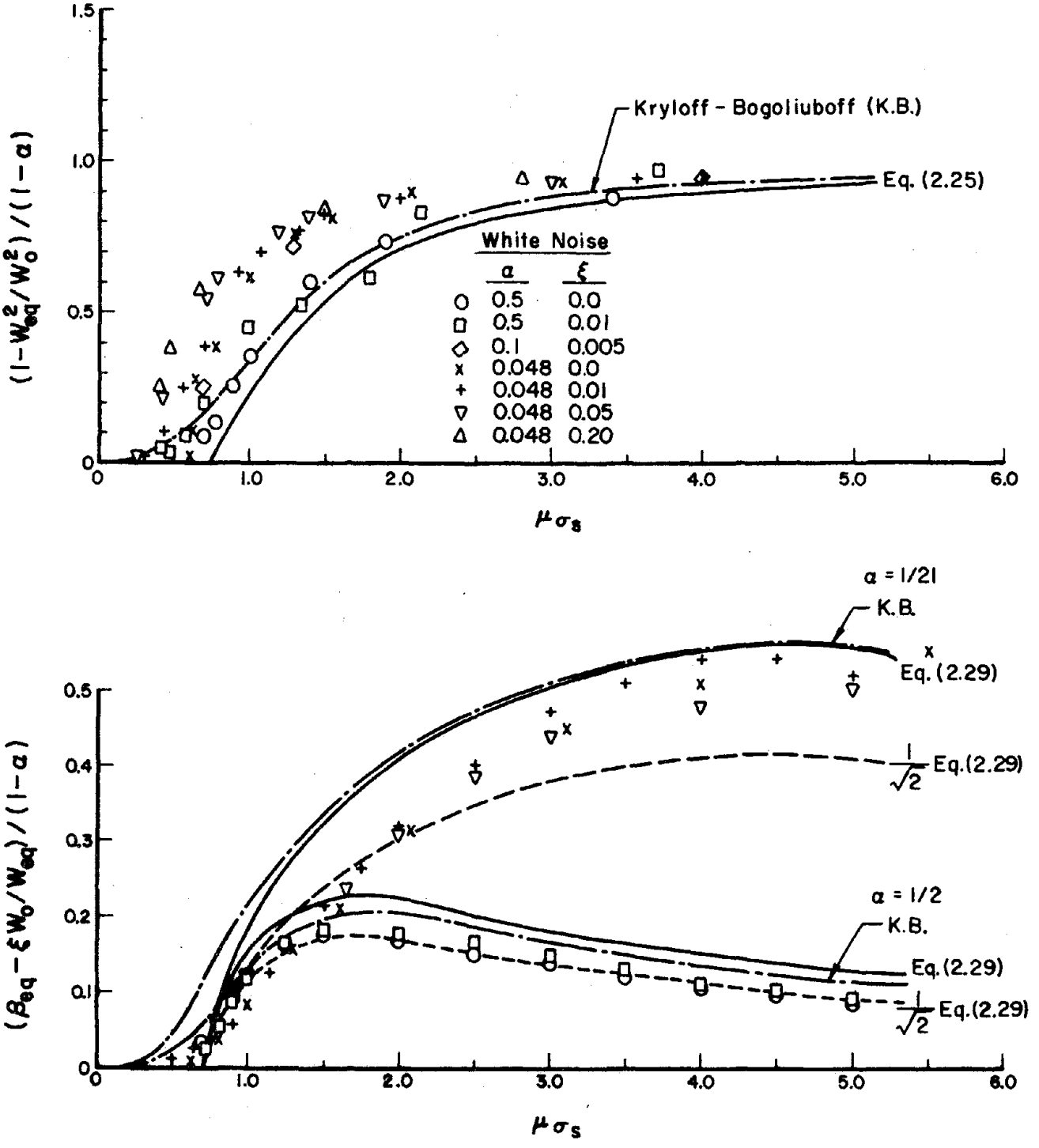

FIGURE 3.8 EQUIVALENT LINEAR FREQUENCY AND DAMPING

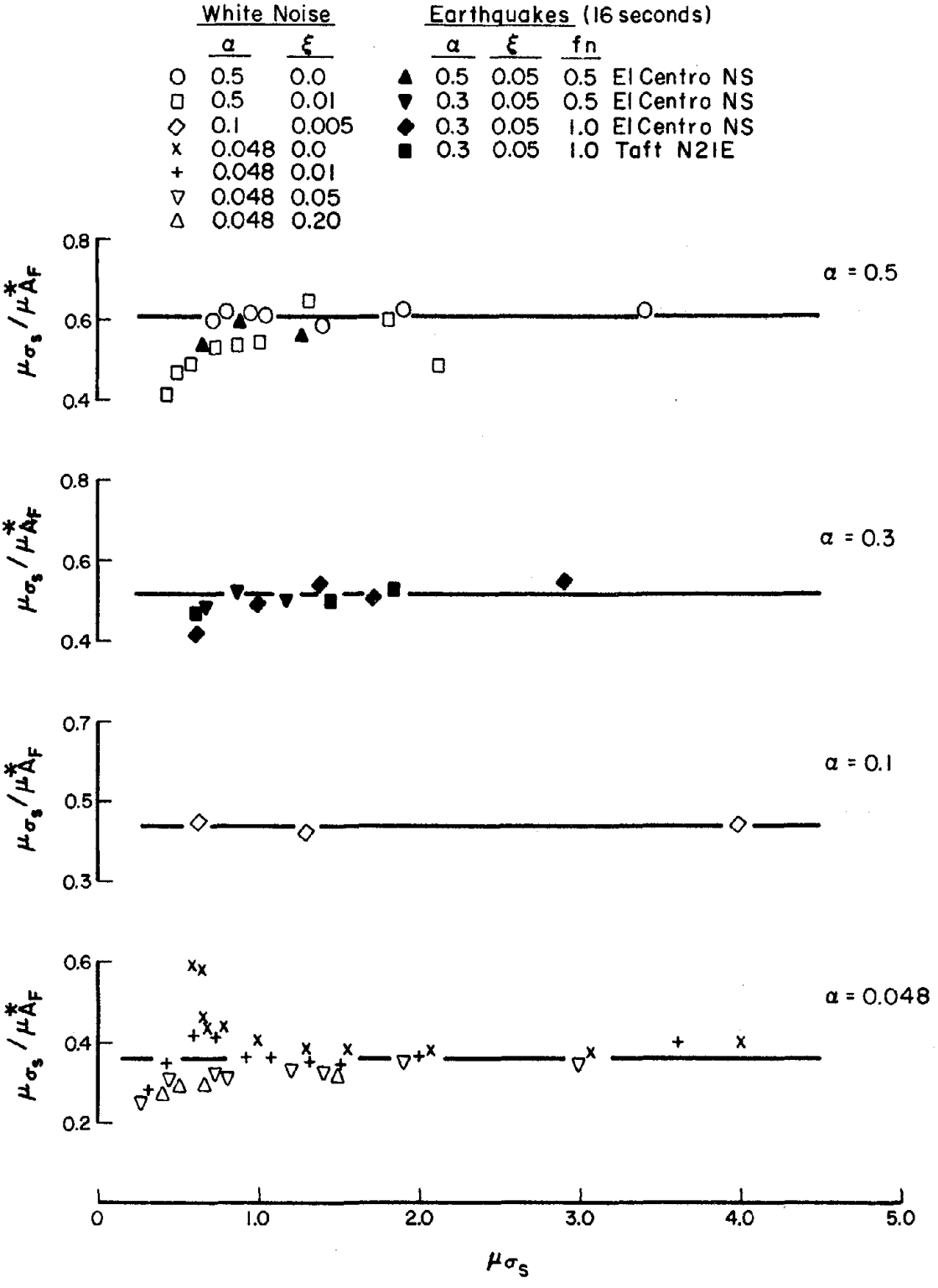

FIGURE 3.9 PSEUDO STEADY-STATE AND STATIONARY RMS DUCTILITY RELATION (FOR EQUIVALENT LINEAR FREQUENCY)

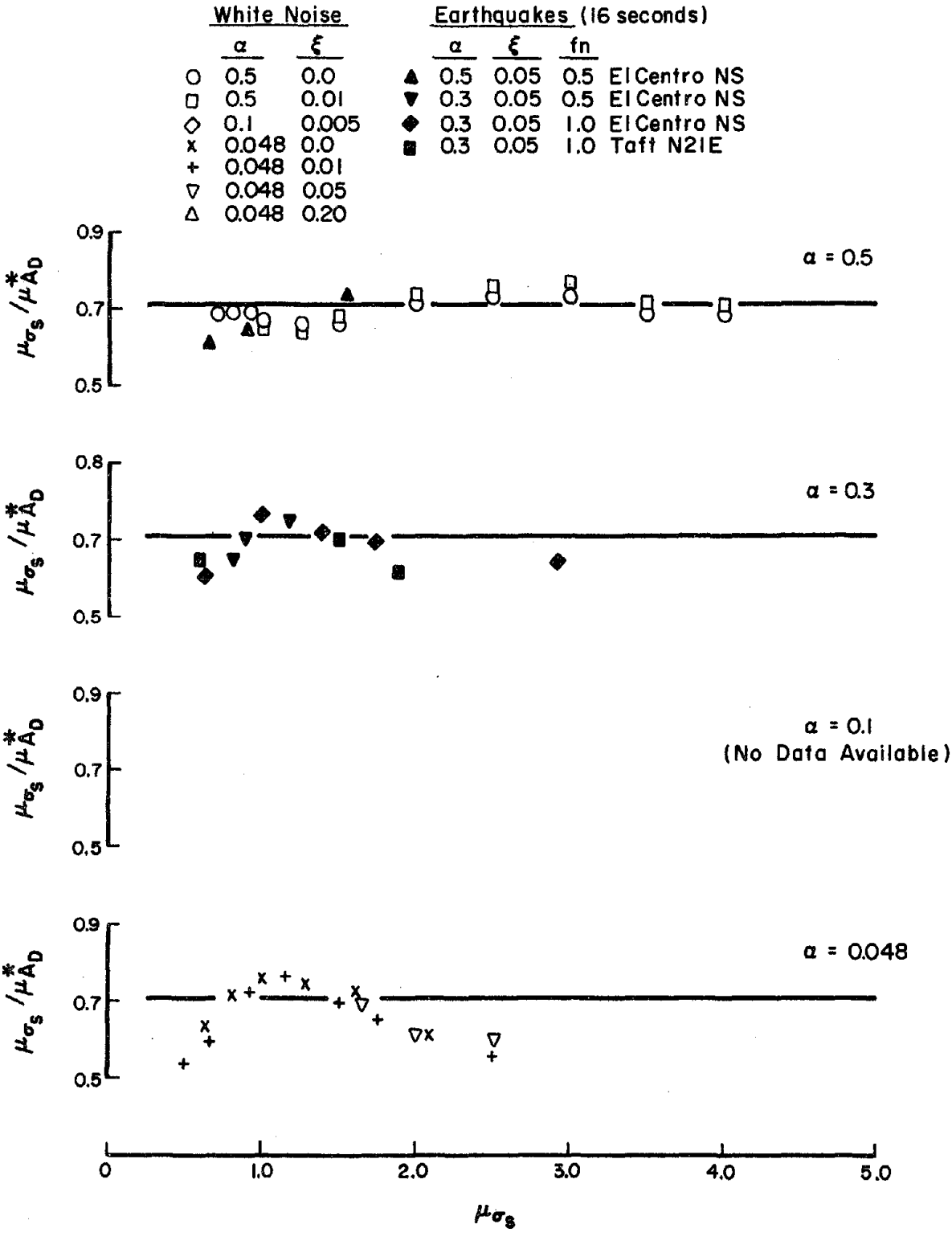

FIGURE 3.10 PSEUDO STEADY-STATE AND STATIONARY RMS DUCTILITY RELATION (FOR EQUIVALENT LINEAR DAMPING)

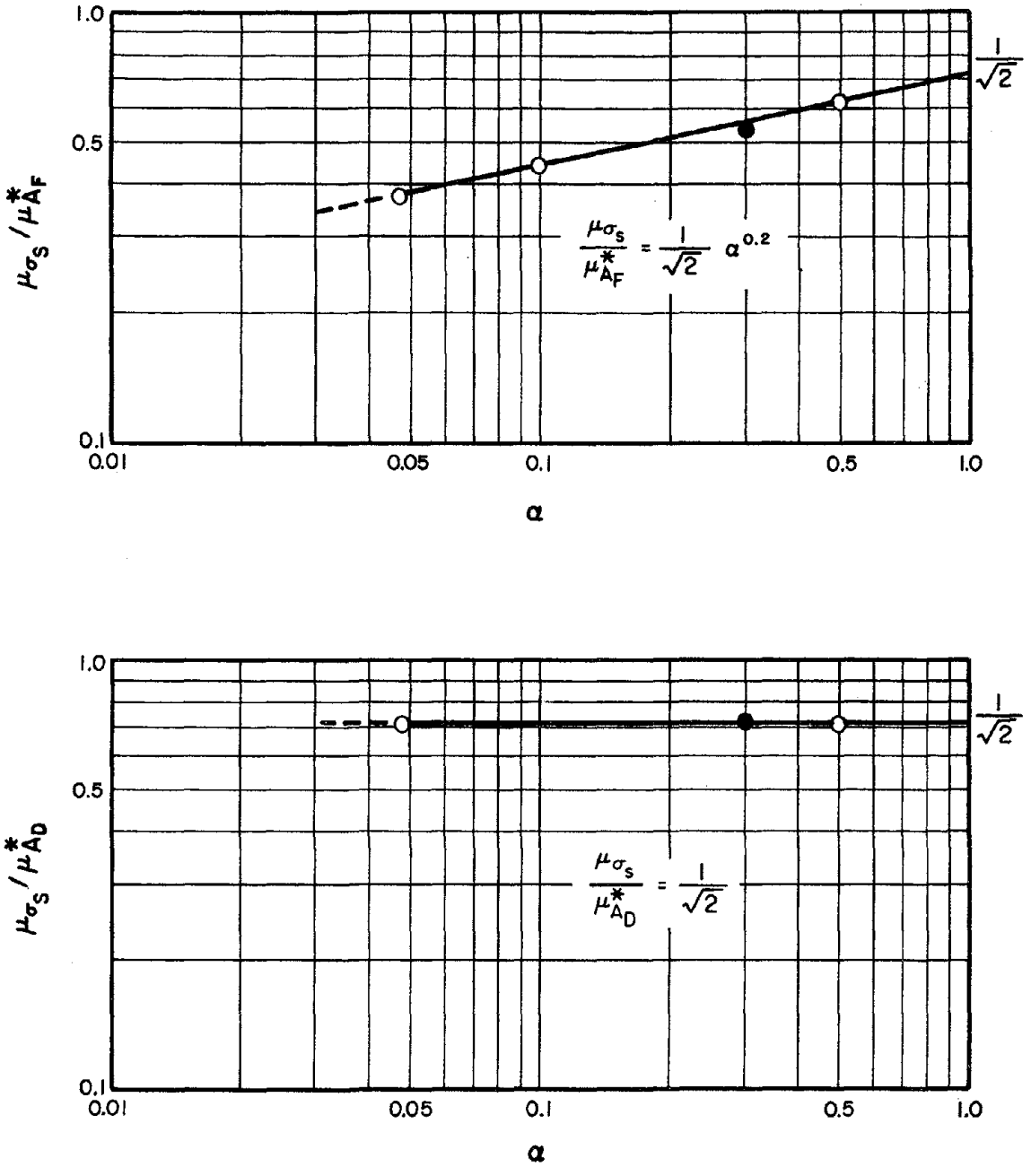

FIGURE 3.11 PSEUDO STEADY-STATE AND STATIONARY RMS DUCTILITY CORRELATION FACTORS

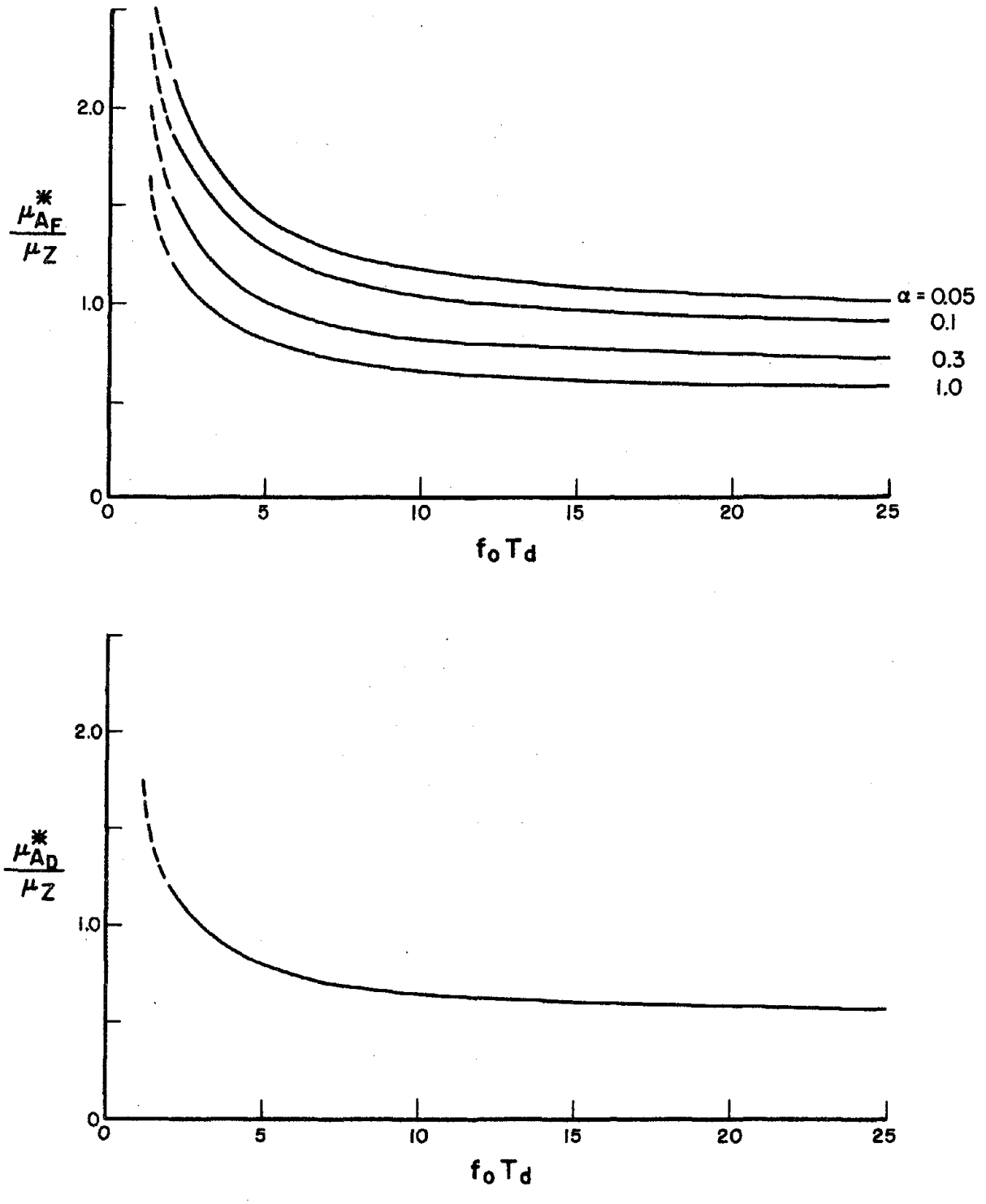

FIGURE 3.12 ZERO-START AND PSEUDO STEADY-STATE MAXIMUM DUCTILITY RELATION

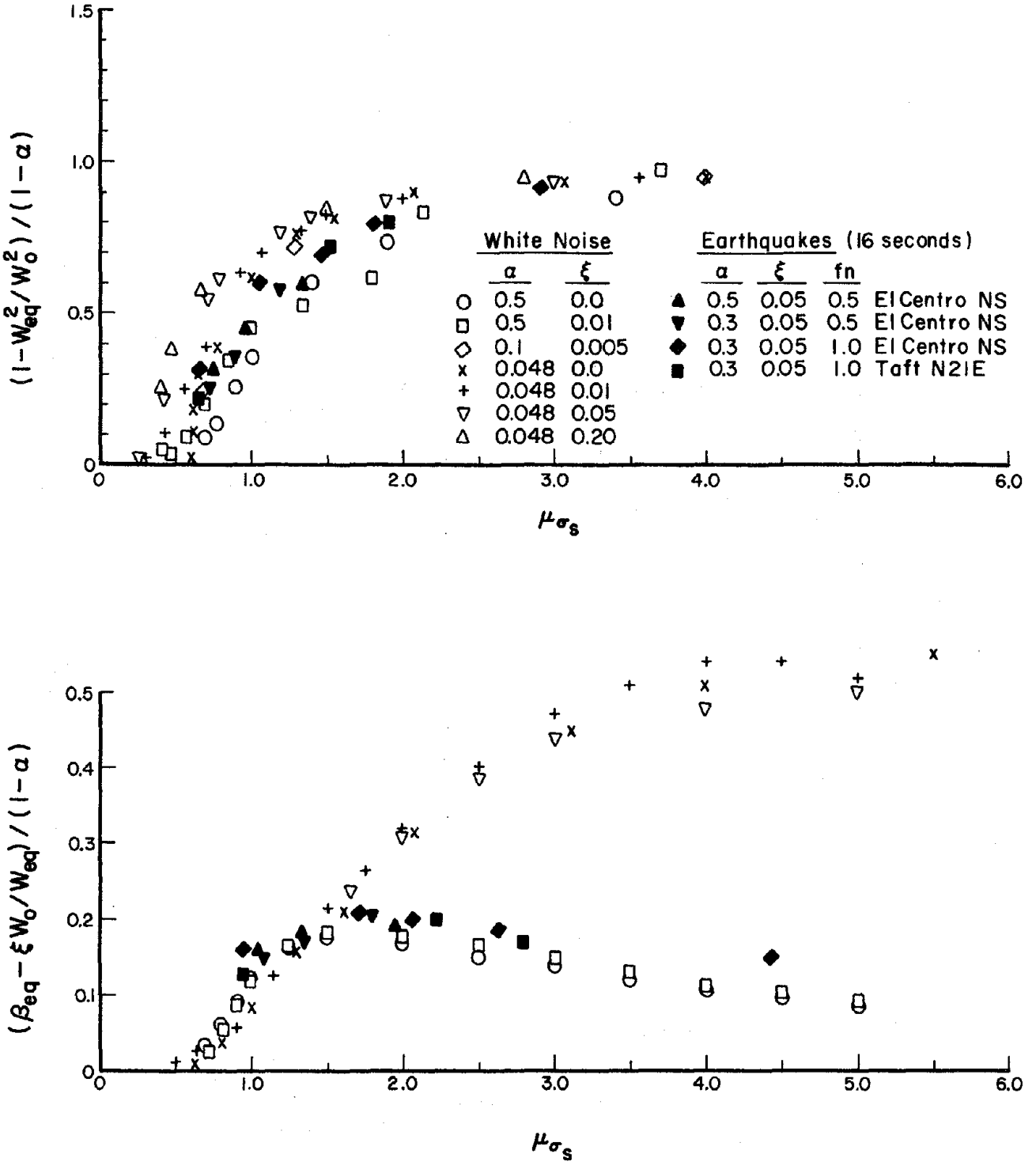

FIGURE 3.13 EQUIVALENT LINEAR FREQUENCY AND DAMPING (WHITE NOISE AND EARTHQUAKE EXCITATIONS)

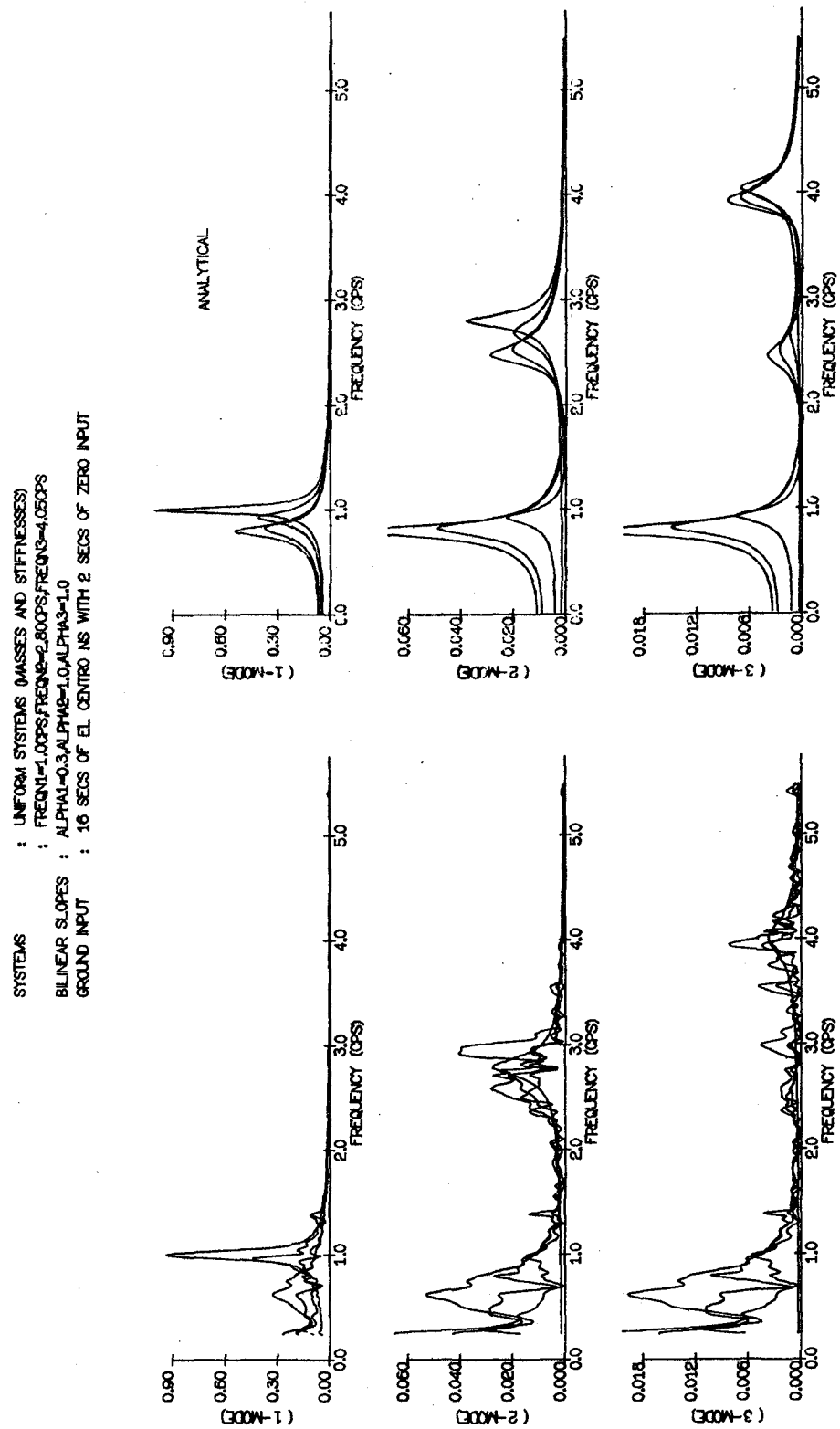

FIGURE 3.14 NONLINEAR MODAL DISPLACEMENT TRANSFER FUNCTIONS - UNIT = IN-SEC^2/IN
(BILINEAR 3DF UNIFORM SYSTEMS, YIELDING AT FIRST STORY,
LINEAR MODE SHAPES)

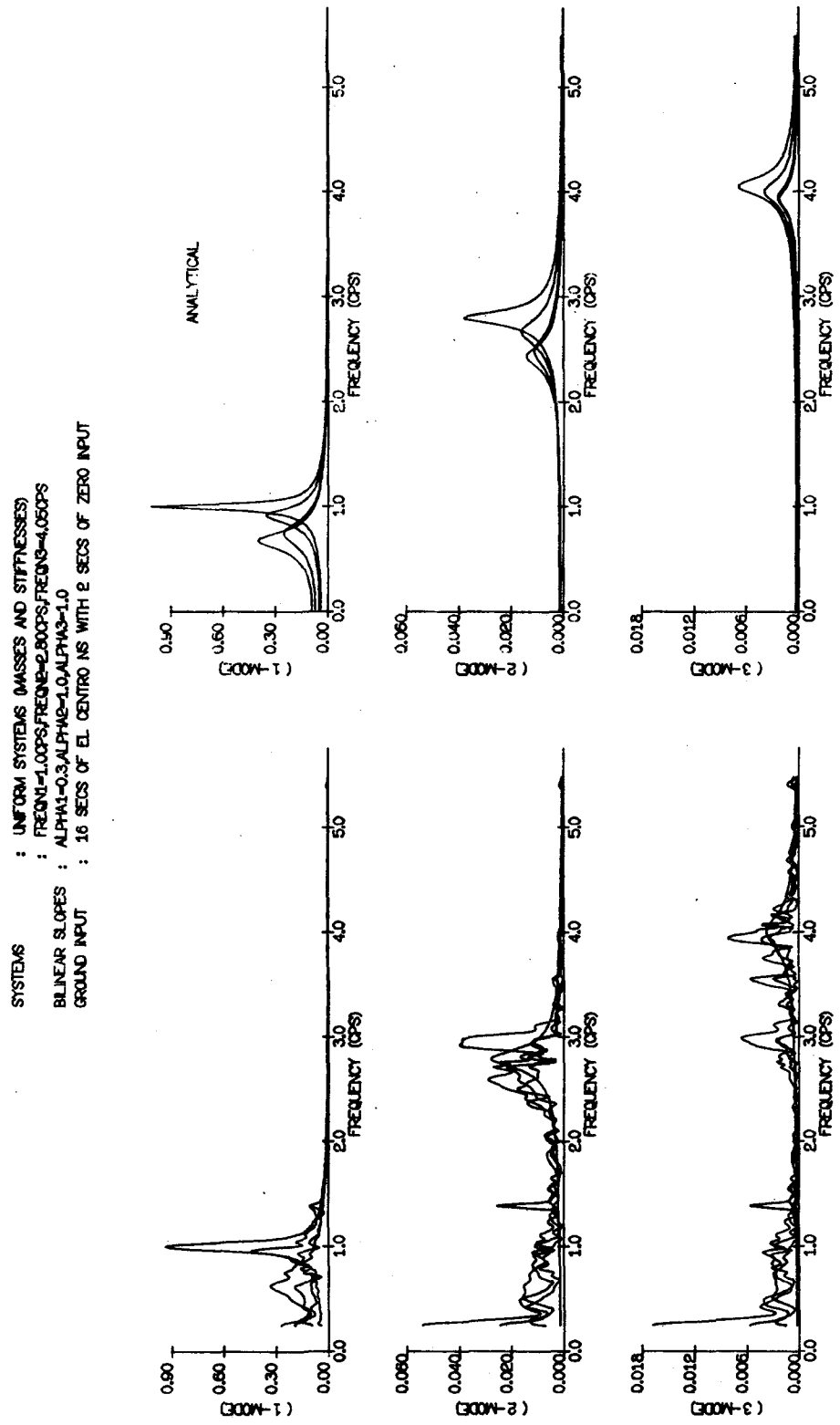

FIGURE 3.15 NONLINEAR MODAL DISPLACEMENT TRANSFER FUNCTIONS - UNIT = IN-SEC^2/IN
(BILINEAR 3DF UNIFORM SYSTEMS, YIELDING AT FIRST STORY,
EQUIVALENT LINEAR MODE SHAPES)

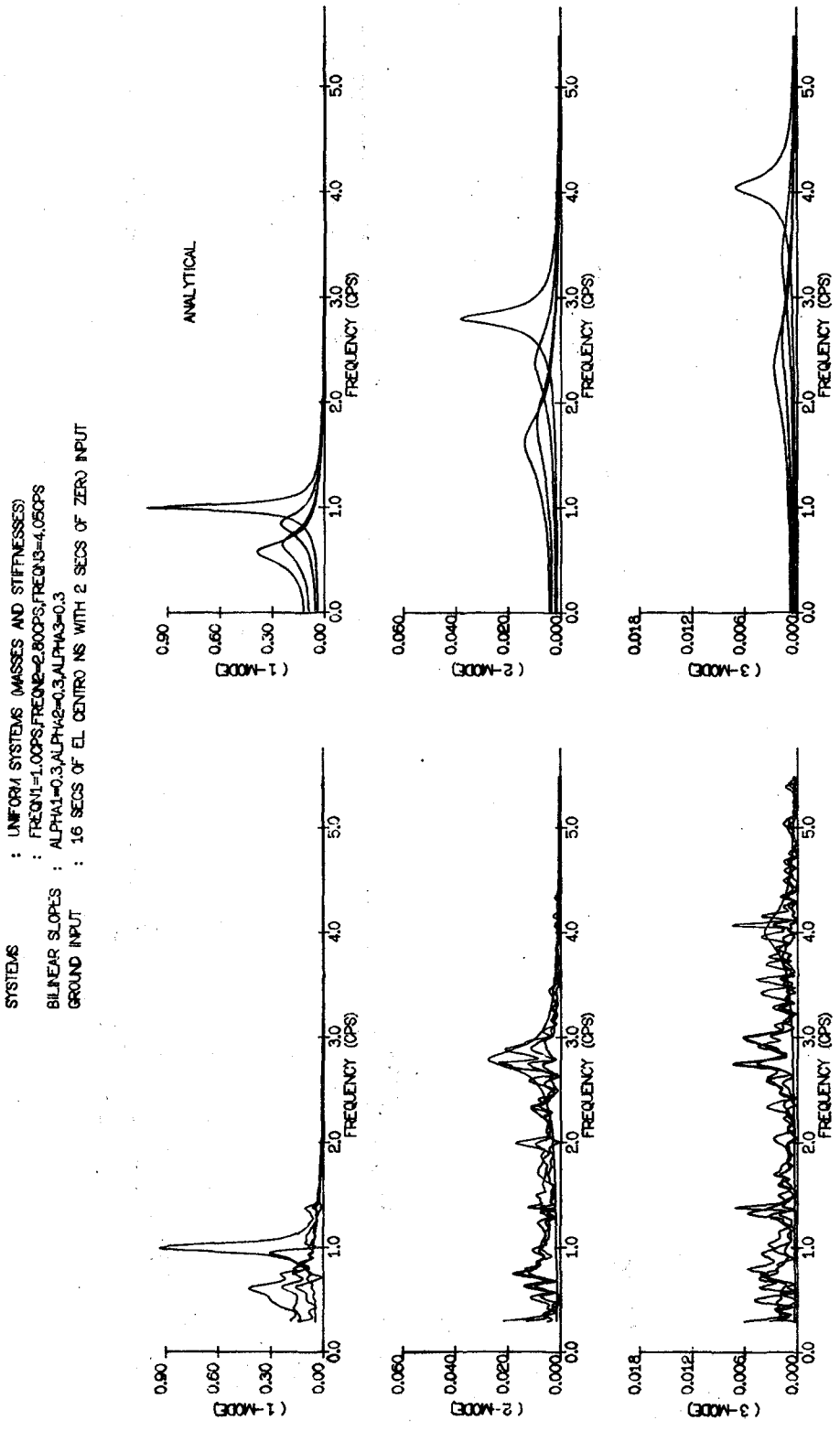

FIGURE 3.16 NONLINEAR MODAL DISPLACEMENT TRANSFER FUNCTIONS - UNIT = IN-SEC^2/IN
(BILINEAR 3DF UNIFORM SYSTEMS, YIELDING AT ALL STORIES,
EQUIVALENT LINEAR MODE SHAPES)

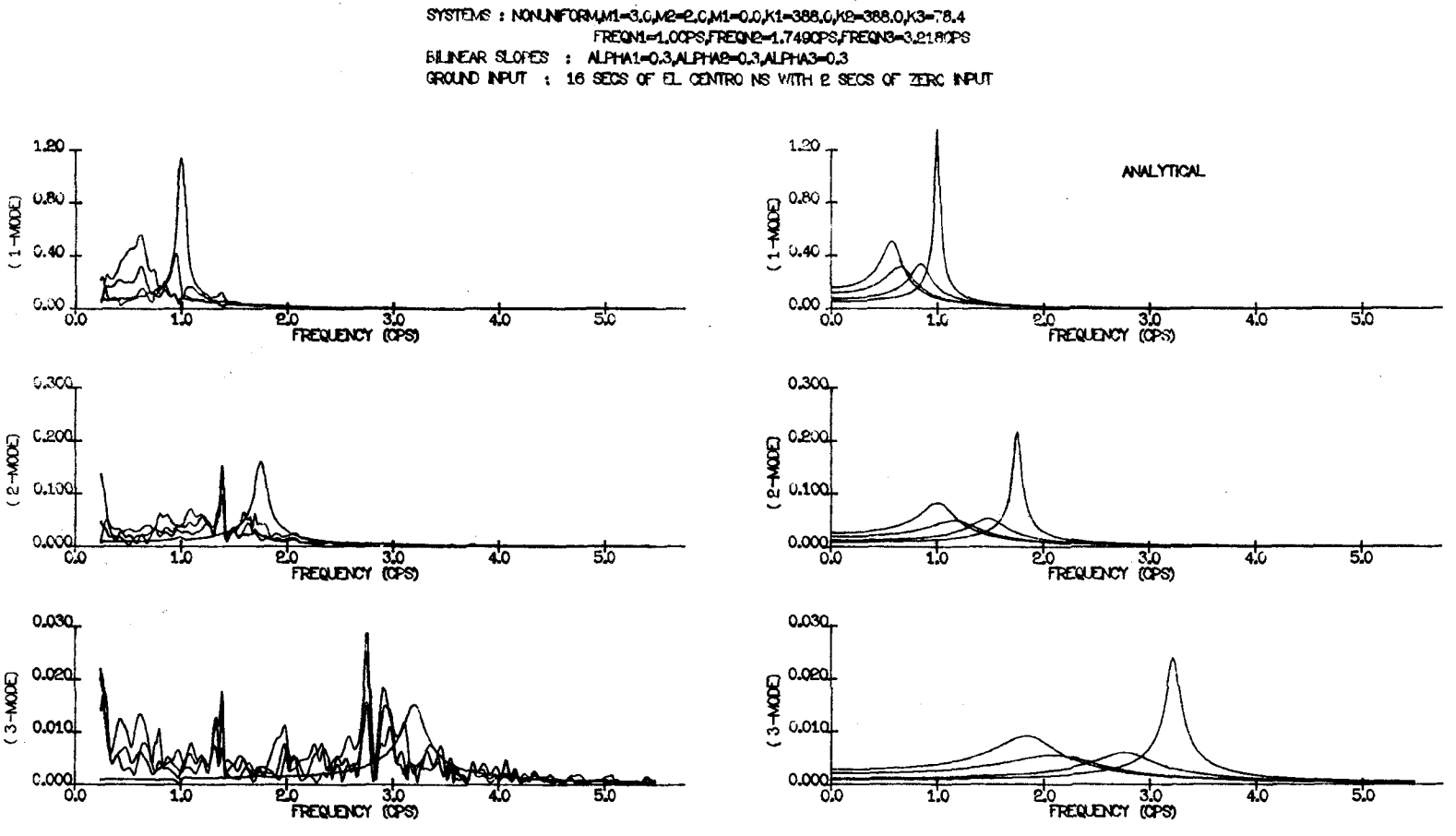

FIGURE 3.17 NONLINEAR MODAL DISPLACEMENT TRANSFER FUNCTIONS - UNIT = IN-SEC^2/IN
(BILINEAR 3DF NONUNIFORM SYSTEMS, YIELDING AT ALL STORIES,
EQUIVALENT LINEAR MODE SHAPES)

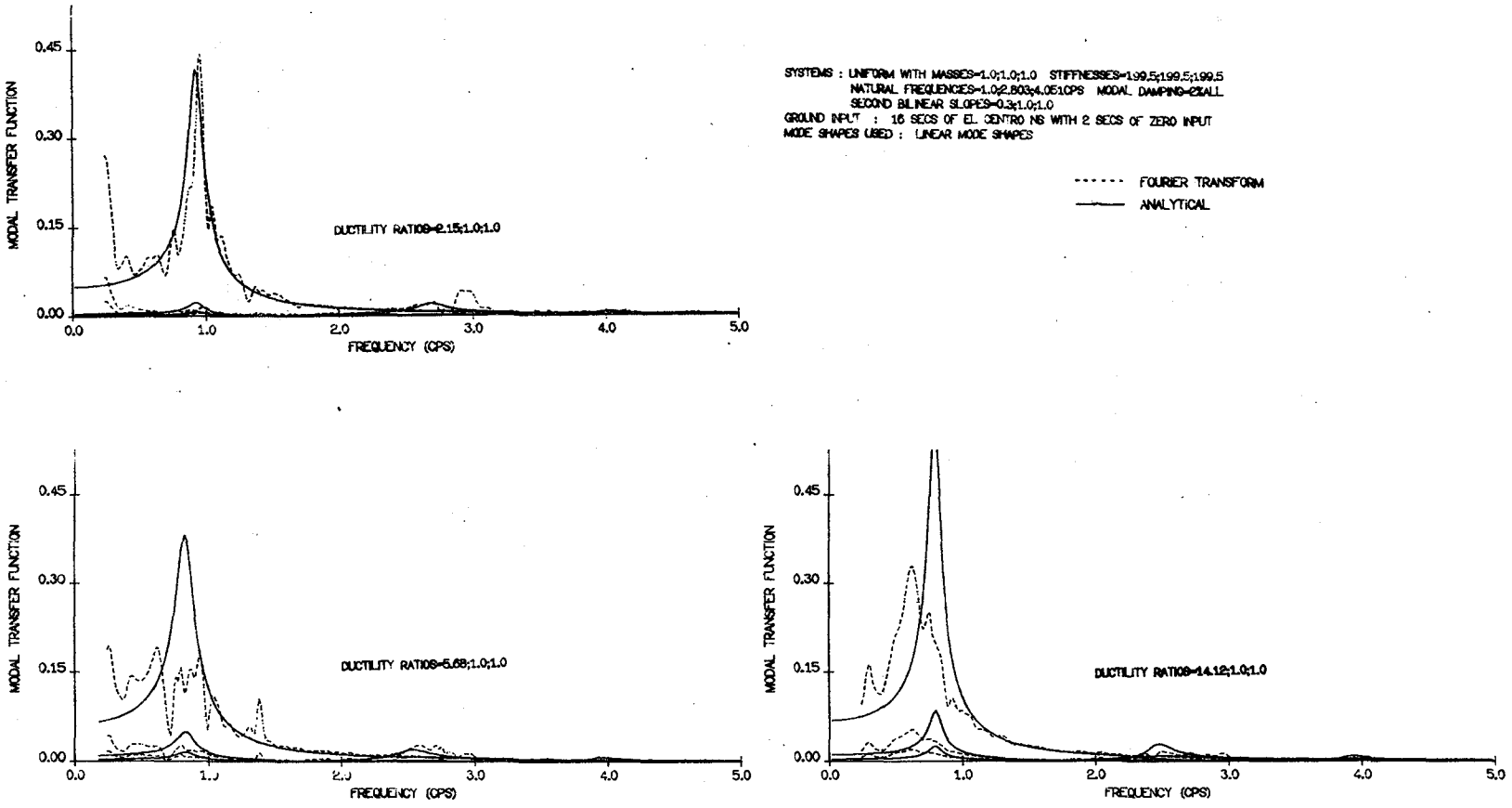

FIGURE 3.18 COMPARISON OF NONLINEAR MODAL DISPLACEMENT TRANSFER FUNCTIONS - UNIT = IN-SEC^2/IN (BILINEAR 3DF UNIFORM SYSTEMS, YIELDING AT FIRST STORY, LINEAR MODE SHAPES)

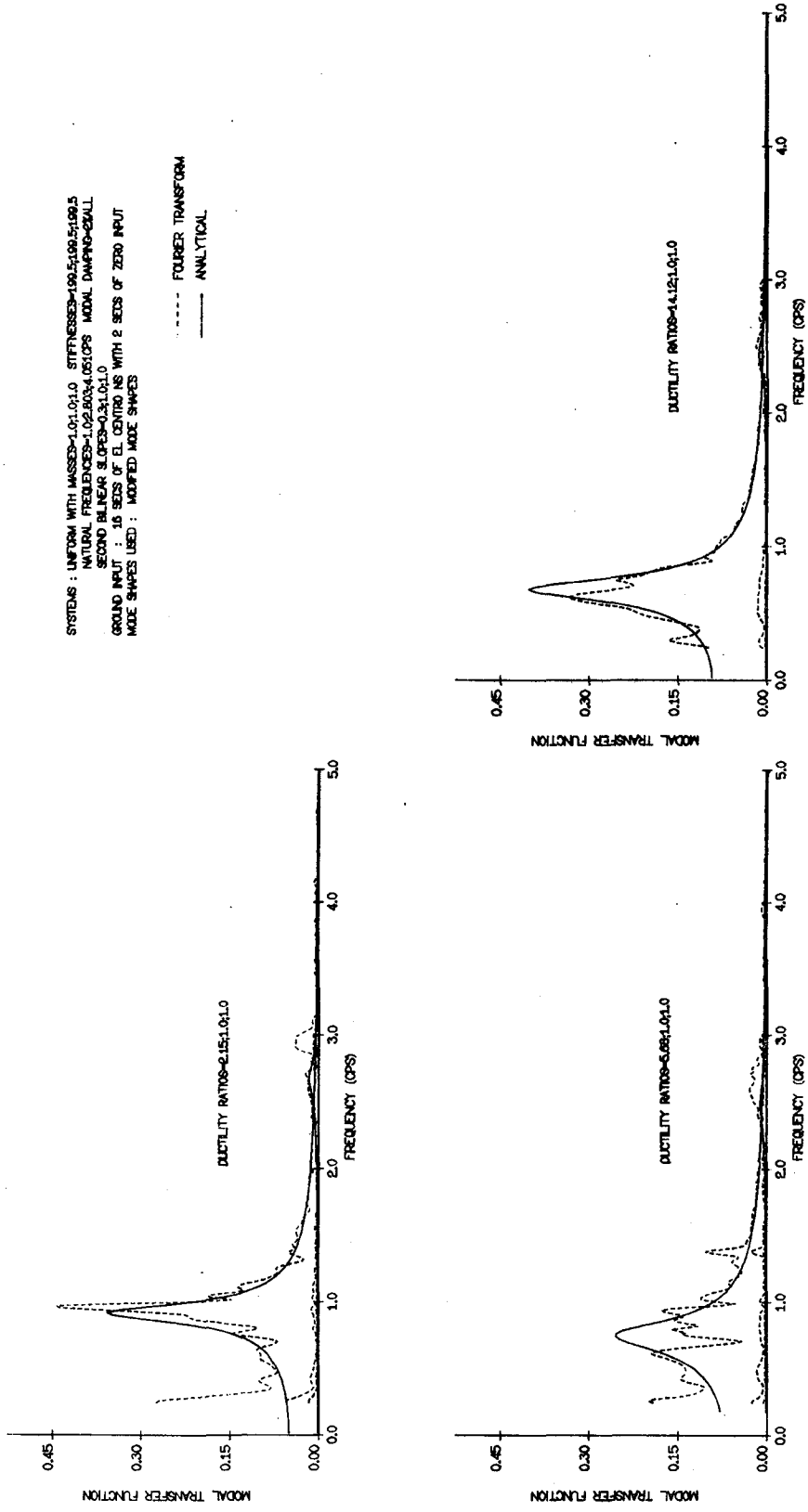

FIGURE 3.19 COMPARISON OF NONLINEAR MODAL DISPLACEMENT TRANSFER FUNCTIONS - UNIT = IN-SEC^2/IN (BILINEAR 3DF UNIFORM SYSTEMS, YIELDING AT FIRST STORY, EQUIVALENT LINEAR MODE SHAPES)

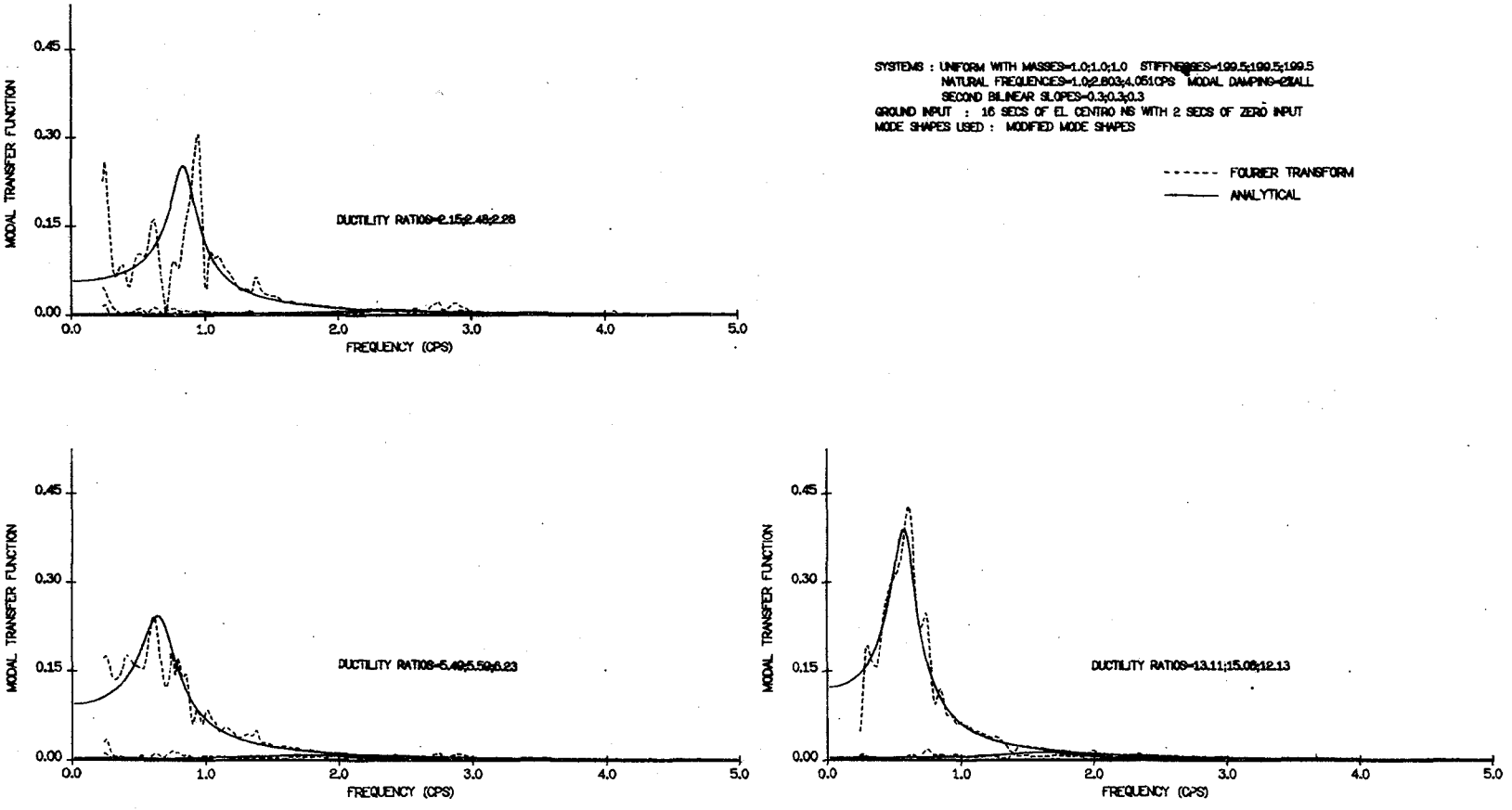

FIGURE 3.20 COMPARISON OF NONLINEAR MODAL DISPLACEMENT TRANSFER FUNCTIONS - UNIT = IN-SEC^2/IN (BILINEAR 3DF UNIFORM SYSTEMS, YIELDING AT ALL STORIES, EQUIVALENT LINEAR MODE SHAPES)

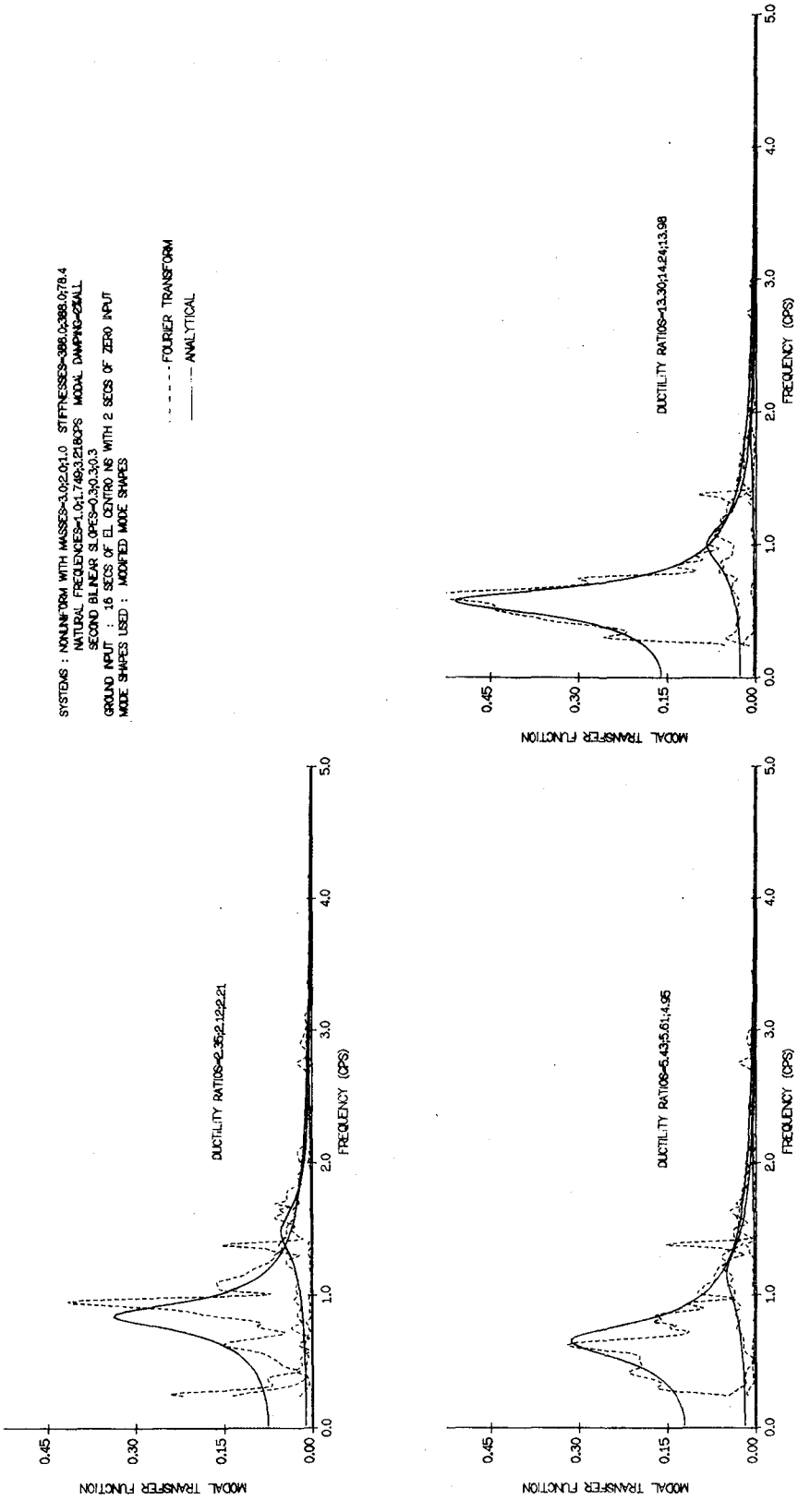

FIGURE 3.21 COMPARISON OF NONLINEAR MODAL DISPLACEMENT TRANSFER FUNCTIONS - UNIT = IN-SEC^2/IN (BILINEAR 3DF NONUNIFORM SYSTEMS, YIELDING AT ALL STORIES, EQUIVALENT LINEAR MODE SHAPES)

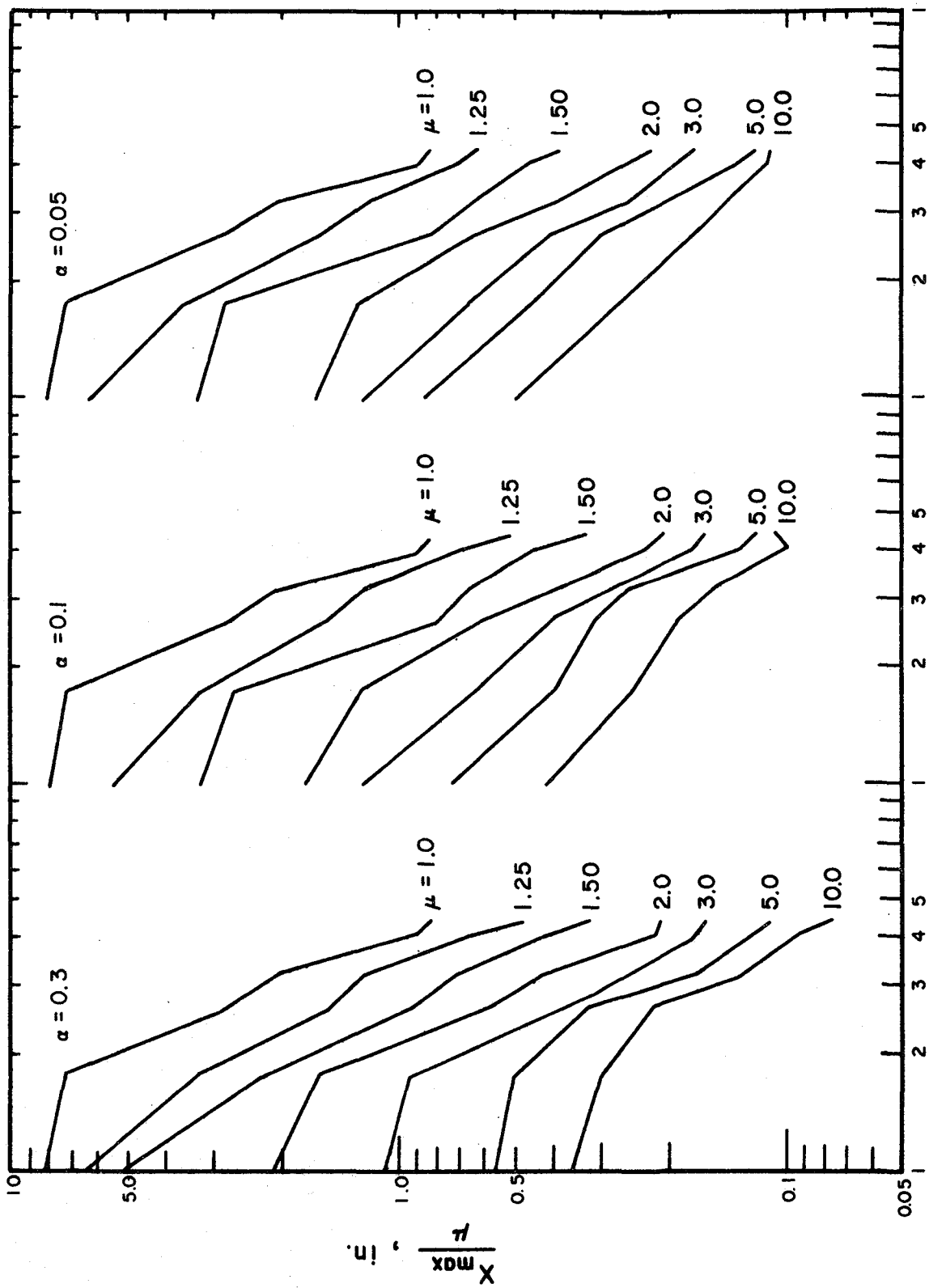

FIGURE 4.1 RESPONSE SPECTRA FOR UNDAMPED BILINEAR SYSTEMS (EL CENTRO 1940-NS)

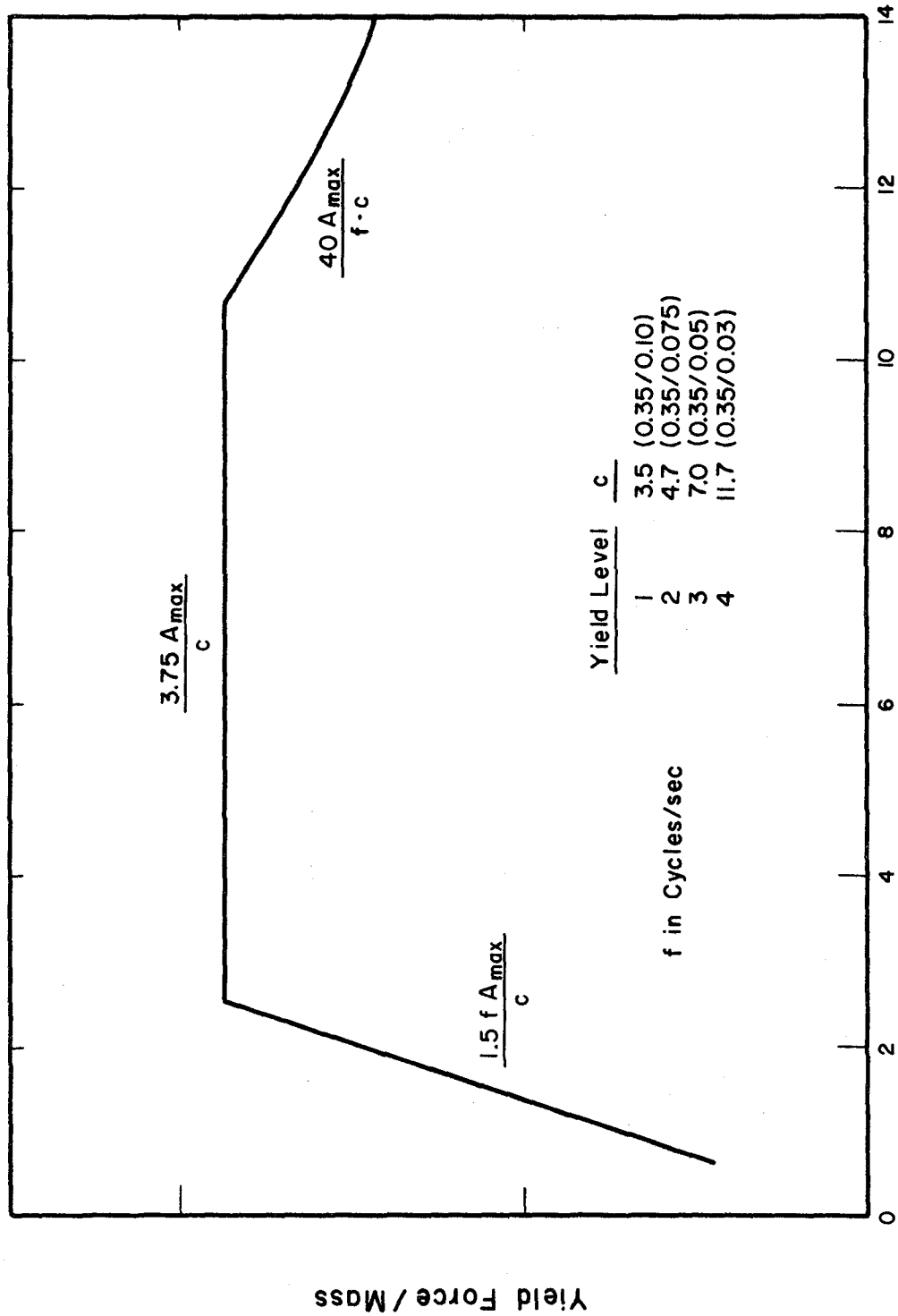

FIGURE 5.1 DESIGN YIELD STRENGTH SPECTRA FOR SDF SYSTEMS
(ADAPTED FROM SHIBATA, A., AND SOZEN, M.A.)

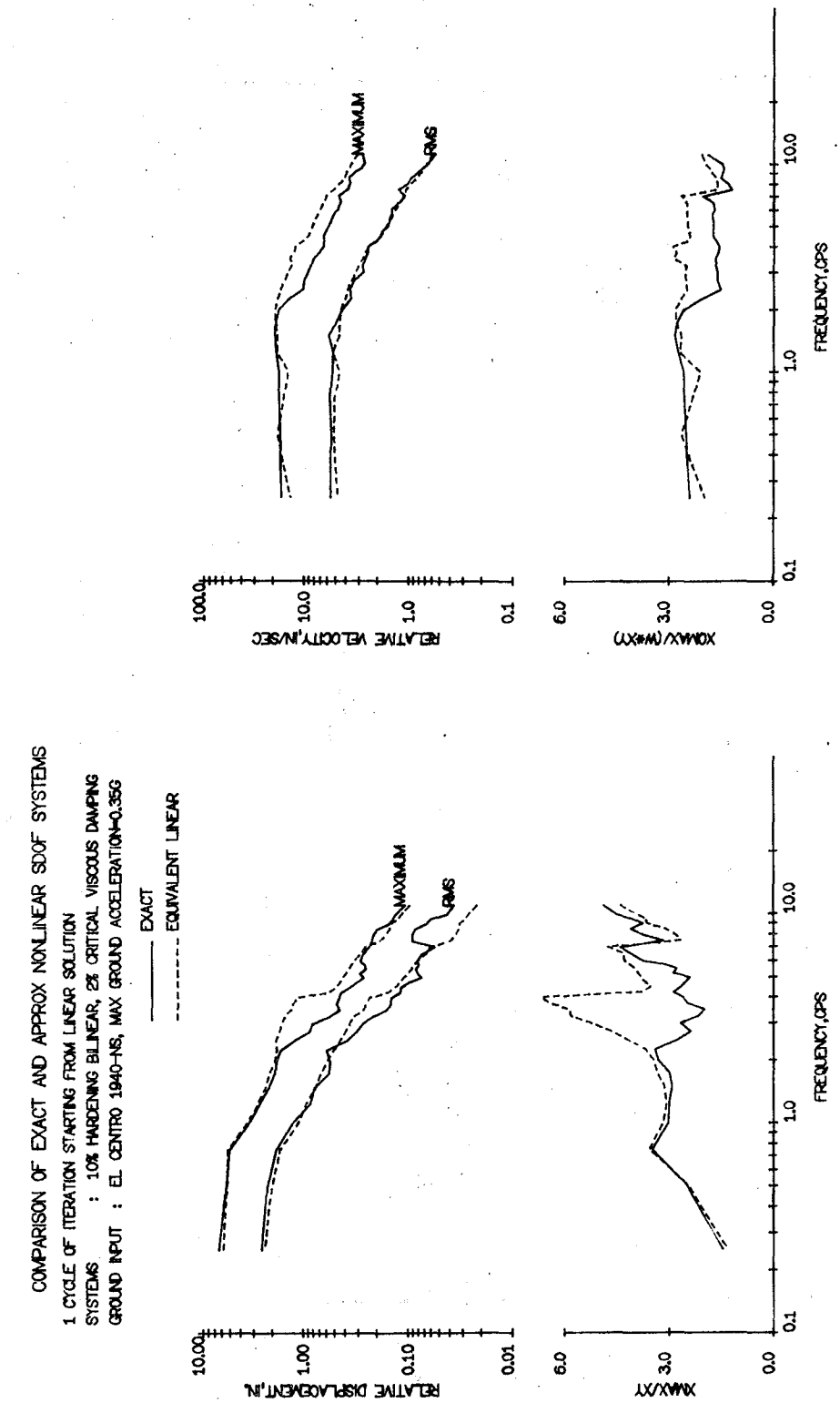

FIGURE 5.2 COMPARISON OF EXACT AND EQUIVALENT LINEAR RESPONSES (BILINEAR SDF SYSTEMS, $\alpha = 0.10$, $\xi = 0.02$, EL CENTRO 1940-NS, 1 CYCLE OF ITERATION STARTING FROM LINEAR SOLUTIONS)

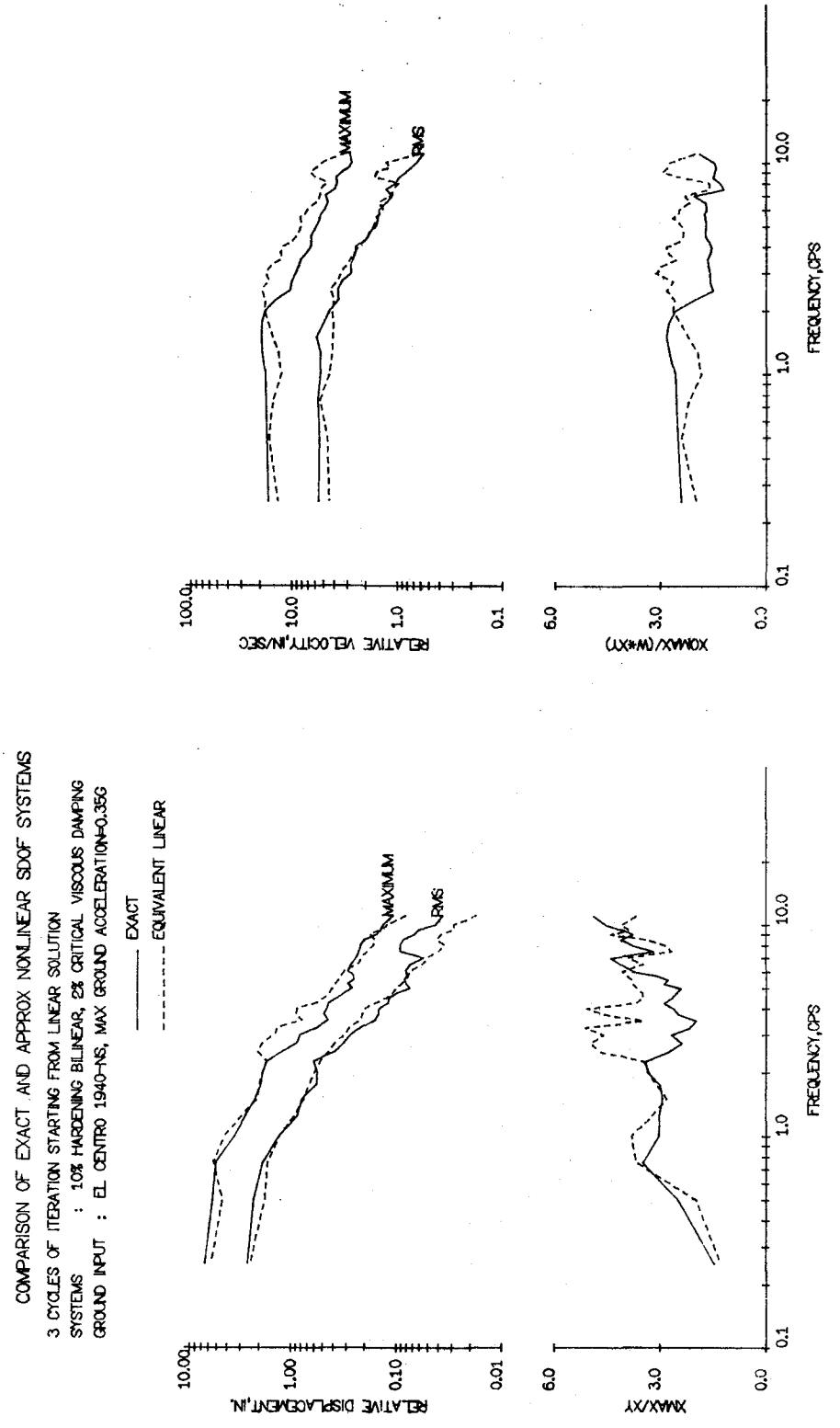

FIGURE 5.3 COMPARISON OF EXACT AND EQUIVALENT LINEAR RESPONSES (BILINEAR SDF SYSTEMS, $\alpha = 0.10$, $\xi = 0.02$, EL CENTRO 1940-NS, 3 CYCLES OF ITERATION STARTING FROM LINEAR SOLUTIONS)

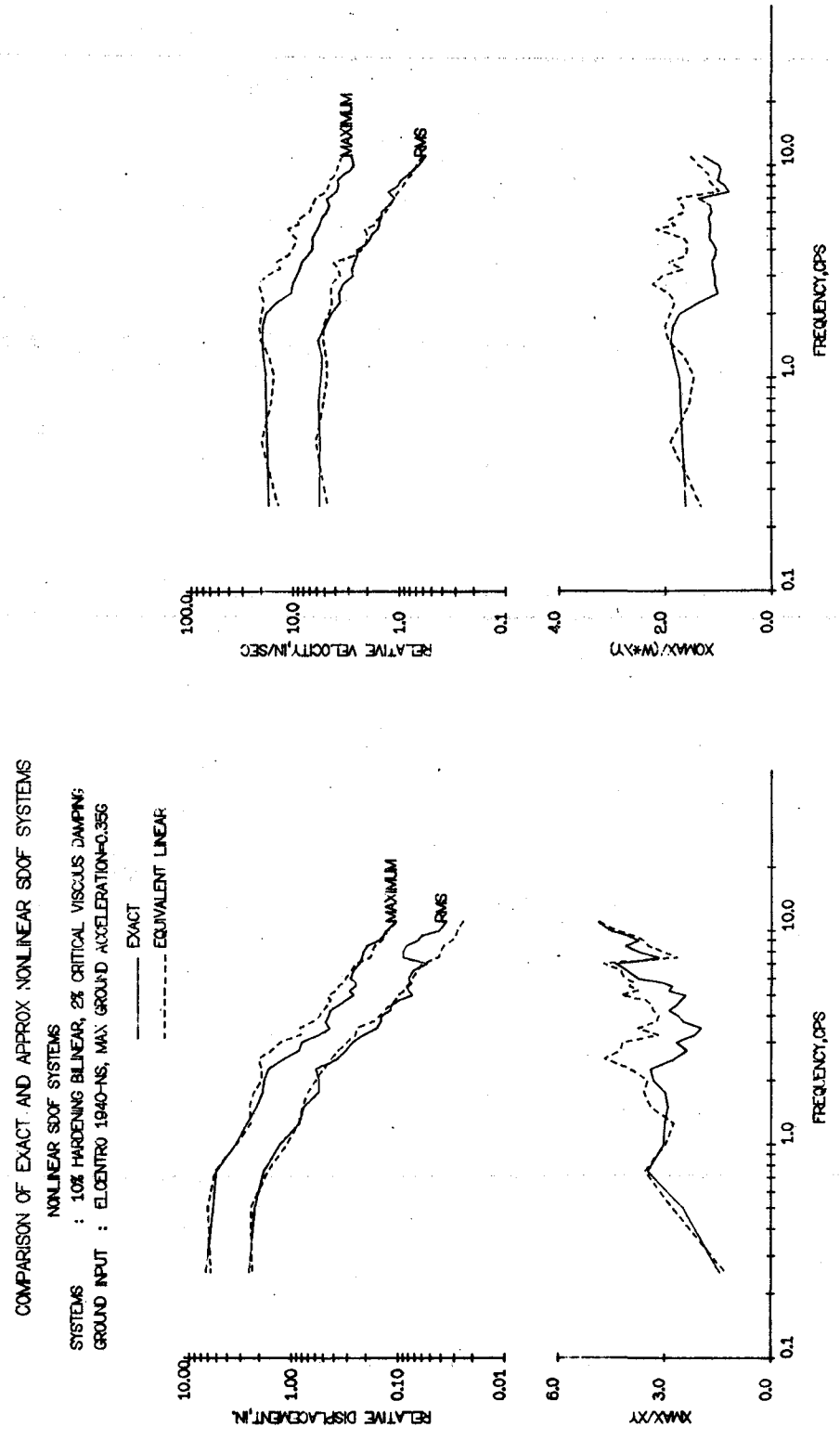

FIGURE 5.4 COMPARISON OF EXACT AND EQUIVALENT LINEAR RESPONSES
(BILINEAR SDF SYSTEMS, α = 0.10, ξ = 0.02, EL CENTRO 1940-NS,
1 CYCLE OF ITERATION STARTING FROM EXACT NONLINEAR SOLUTIONS)

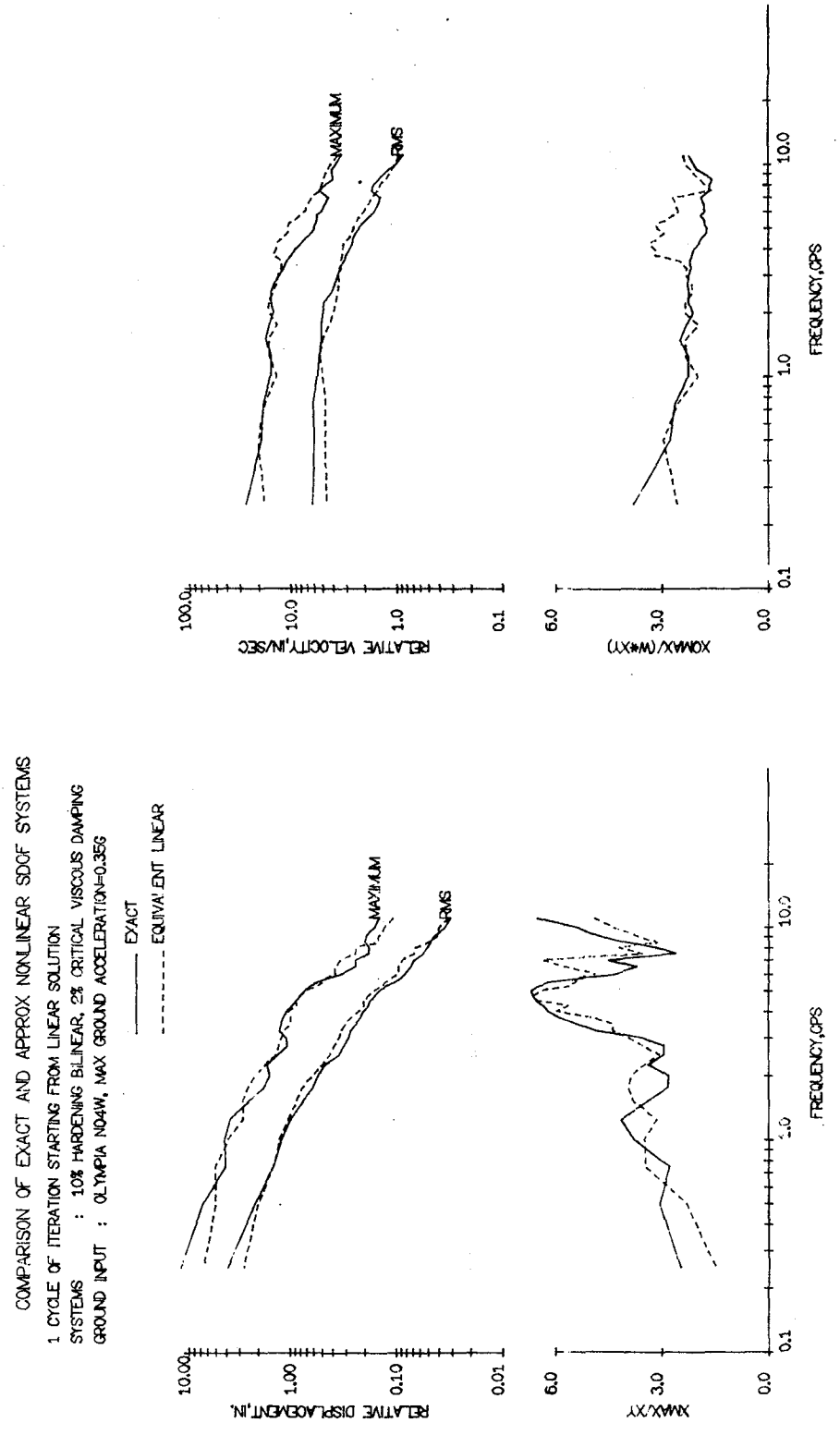

FIGURE 5.5 COMPARISON OF EXACT AND EQUIVALENT LINEAR RESPONSES (BILINEAR SDF SYSTEMS, $\alpha = 0.10$, $\xi = 0.02$, OLYMPIA 1949-N04W, 1 CYCLE OF ITERATION STARTING FROM LINEAR SOLUTIONS)

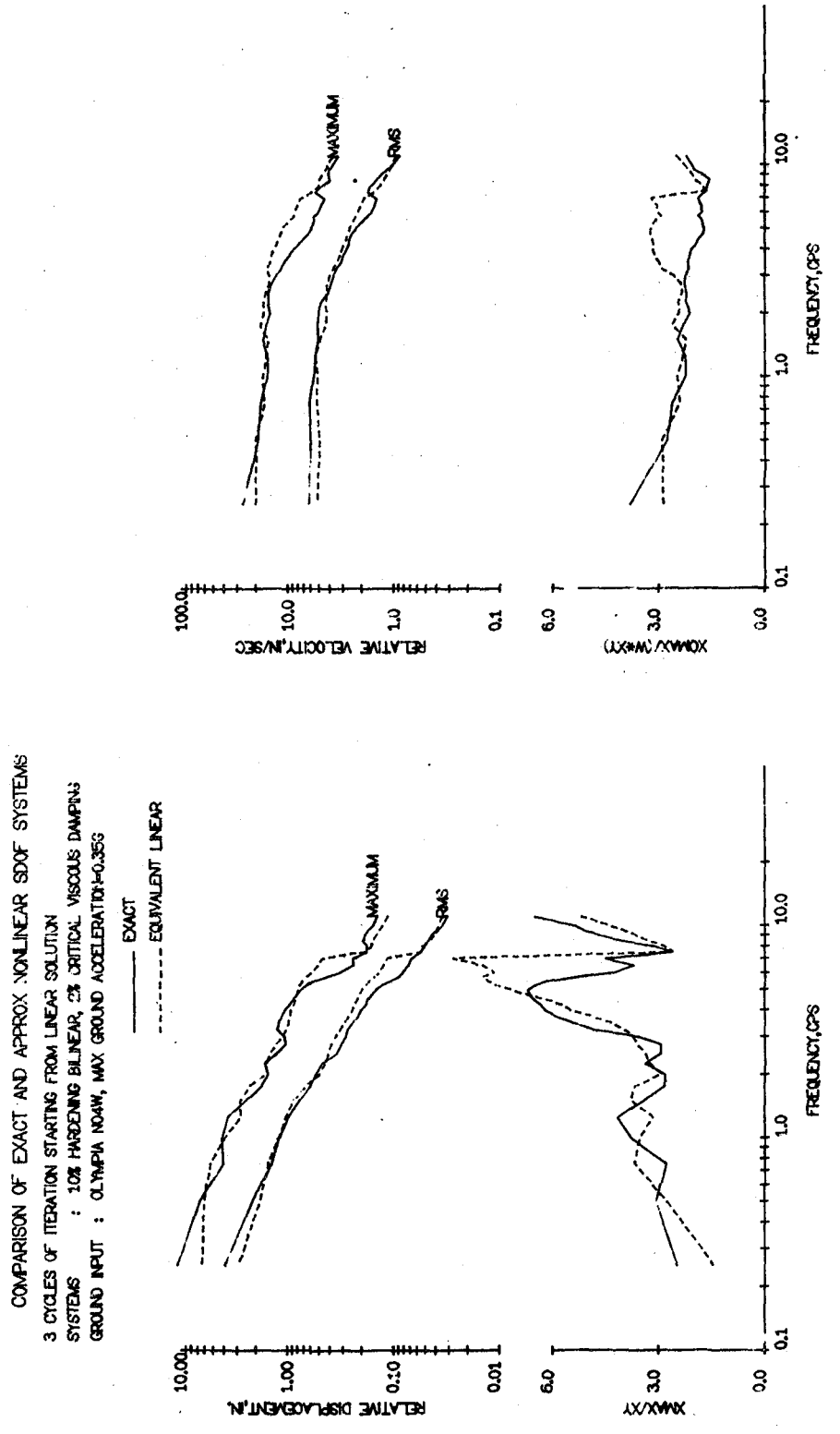

FIGURE 5.6 COMPARISON OF EXACT AND EQUIVALENT LINEAR RESPONSES (BILINEAR SDF SYSTEMS, $\alpha = 0.10$, $\xi = 0.02$, OLYMPIA 1949-NO4W, 3 CYCLES OF ITERATION STARTING FROM LINEAR SOLUTIONS)

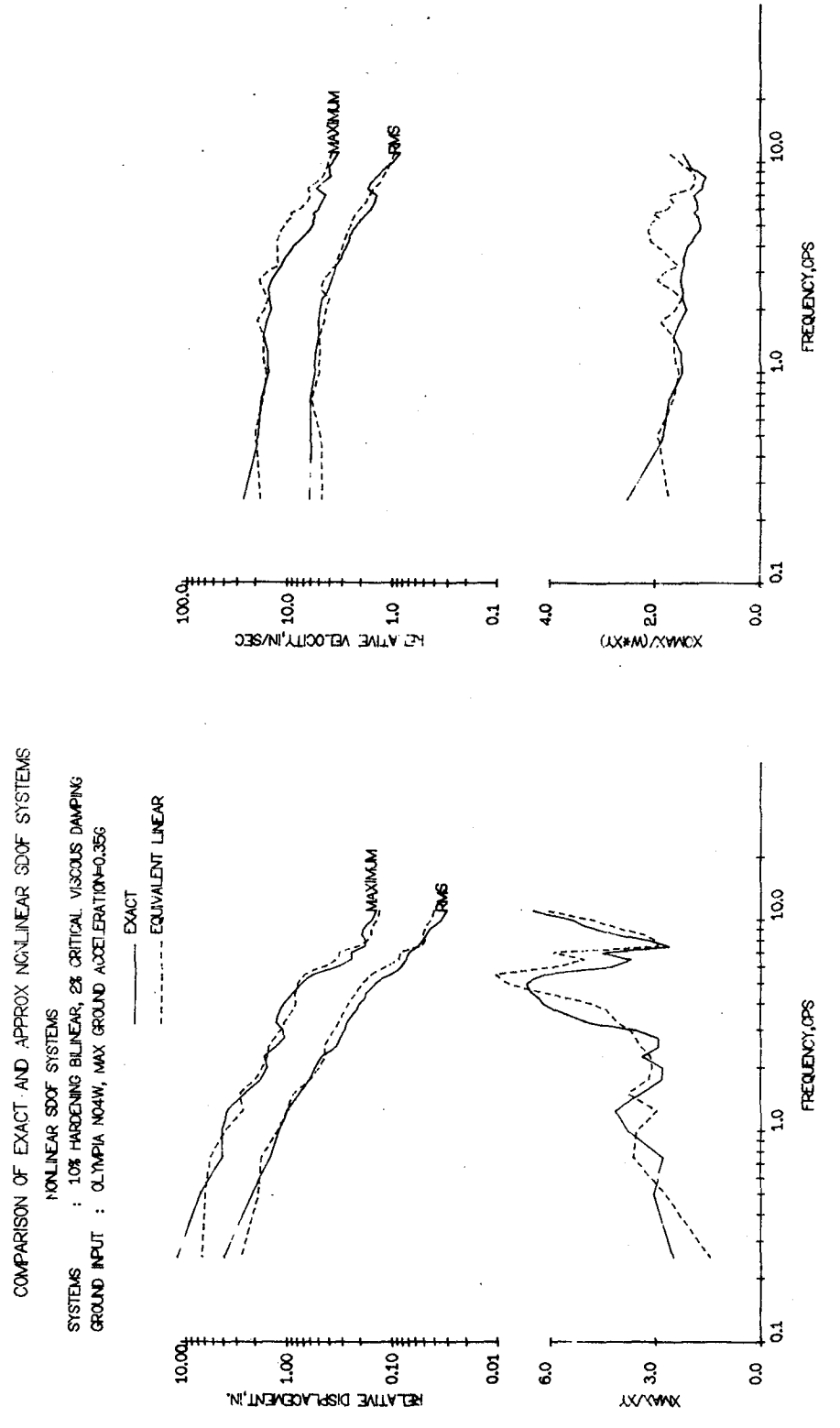

FIGURE 5.7 COMPARISON OF EXACT AND EQUIVALENT LINEAR RESPONSES (BILINEAR SDF SYSTEMS, $\alpha = 0.10$, $\xi = 0.02$, OLYMPIA 1949-N04W, 1 CYCLE OF ITERATION STARTING FROM EXACT NONLINEAR SOLUTIONS)

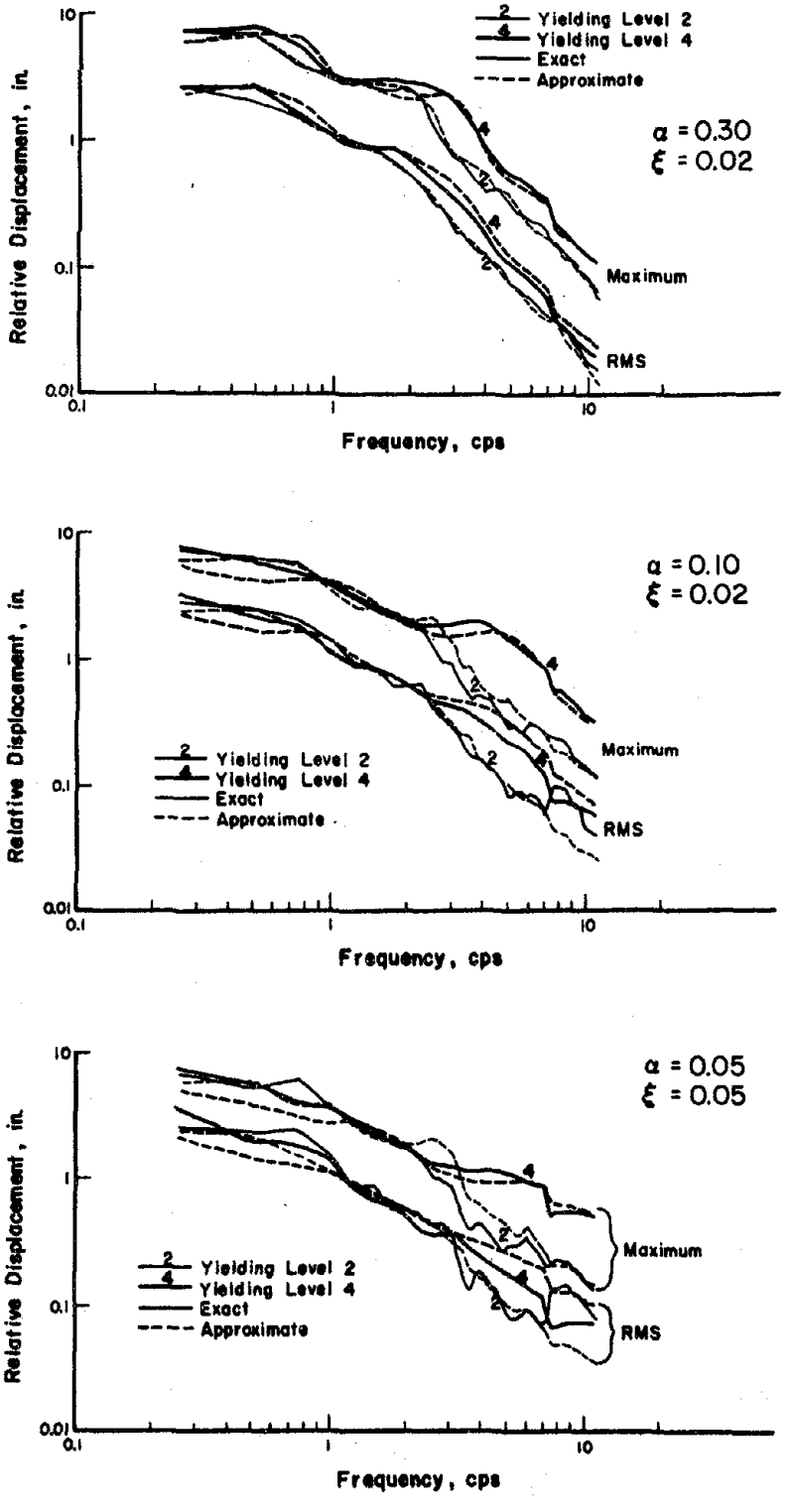

FIGURE 5.8 EFFECT OF DUCTILITY ON ACCURACY OF EQUIVALENT LINEAR METHOD (BILINEAR SDF SYSTEMS, EL CENTRO 1940-NS)

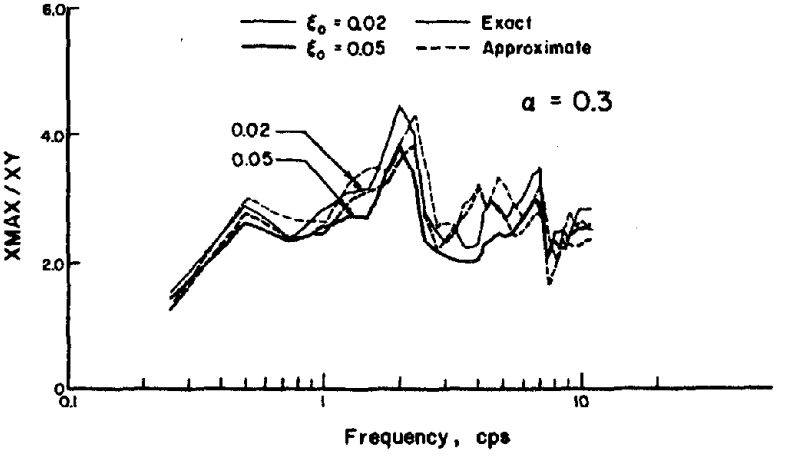

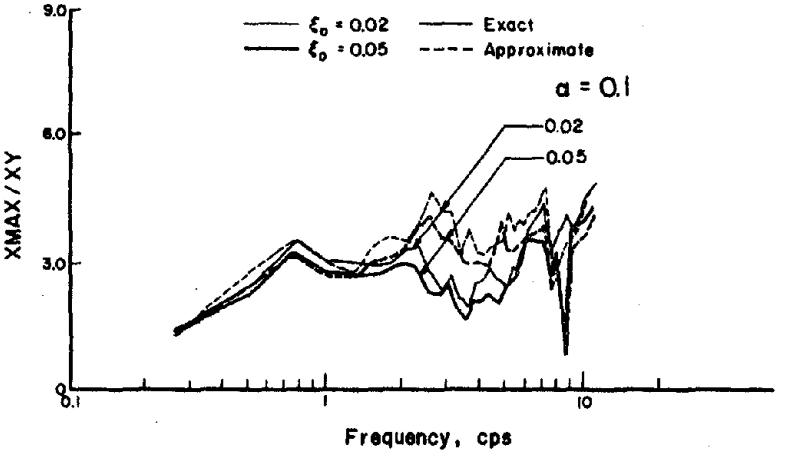

FIGURE 5.9 EFFECT OF VISCOUS DAMPING ON ACCURACY OF EQUIVALENT LINEAR METHOD (BILINEAR SDF SYSTEMS, EL CENTRO 1940-NS, YIELD LEVEL 2)

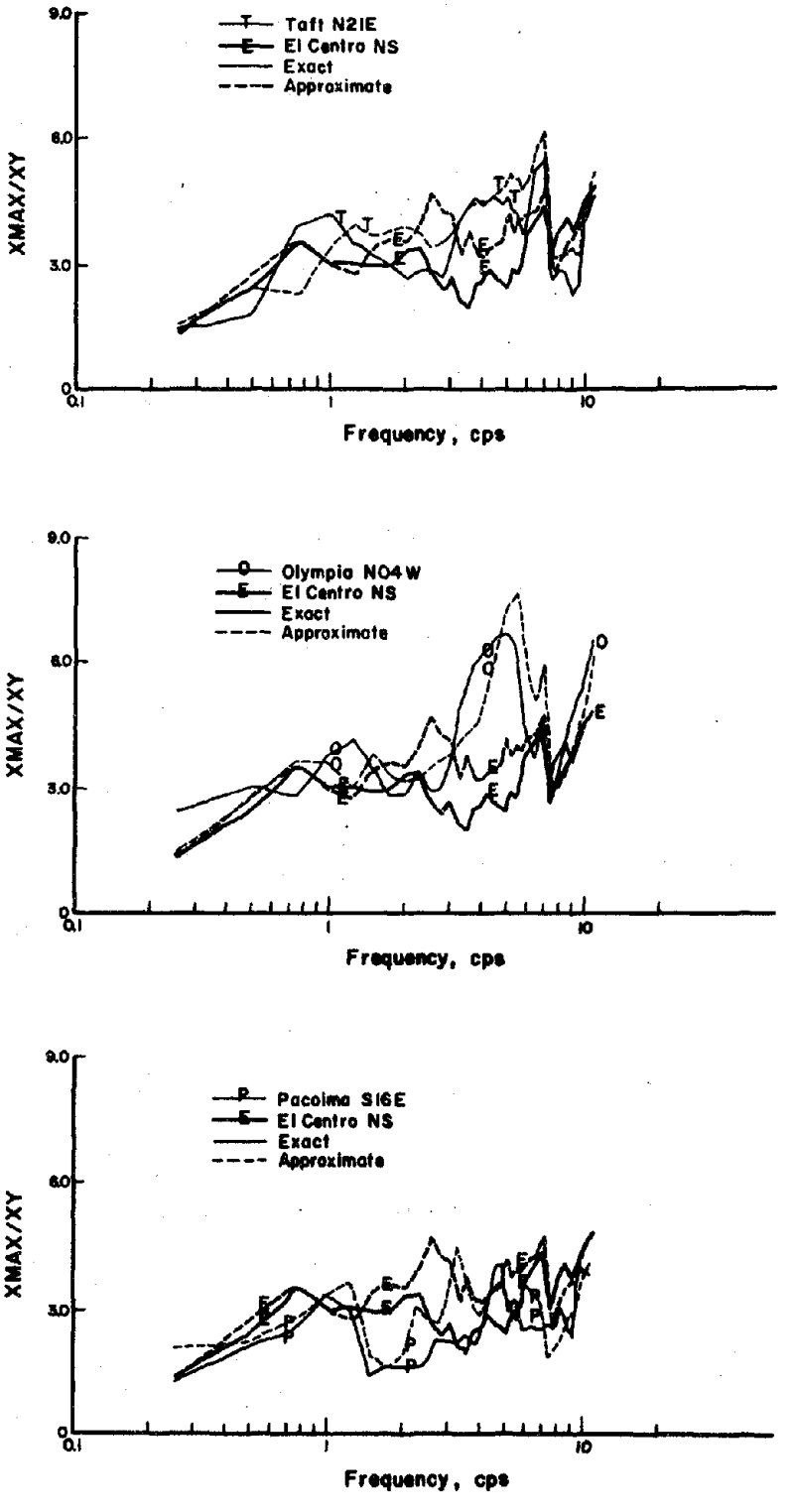

FIGURE 5.10 EFFECT OF EARTHQUAKE EXCITATIONS ON ACCURACY OF EQUIVALENT LINEAR METHOD (SDF SYSTEMS, $\alpha = 0.1$, $\xi = 0.02$, YIELD LEVEL 2)

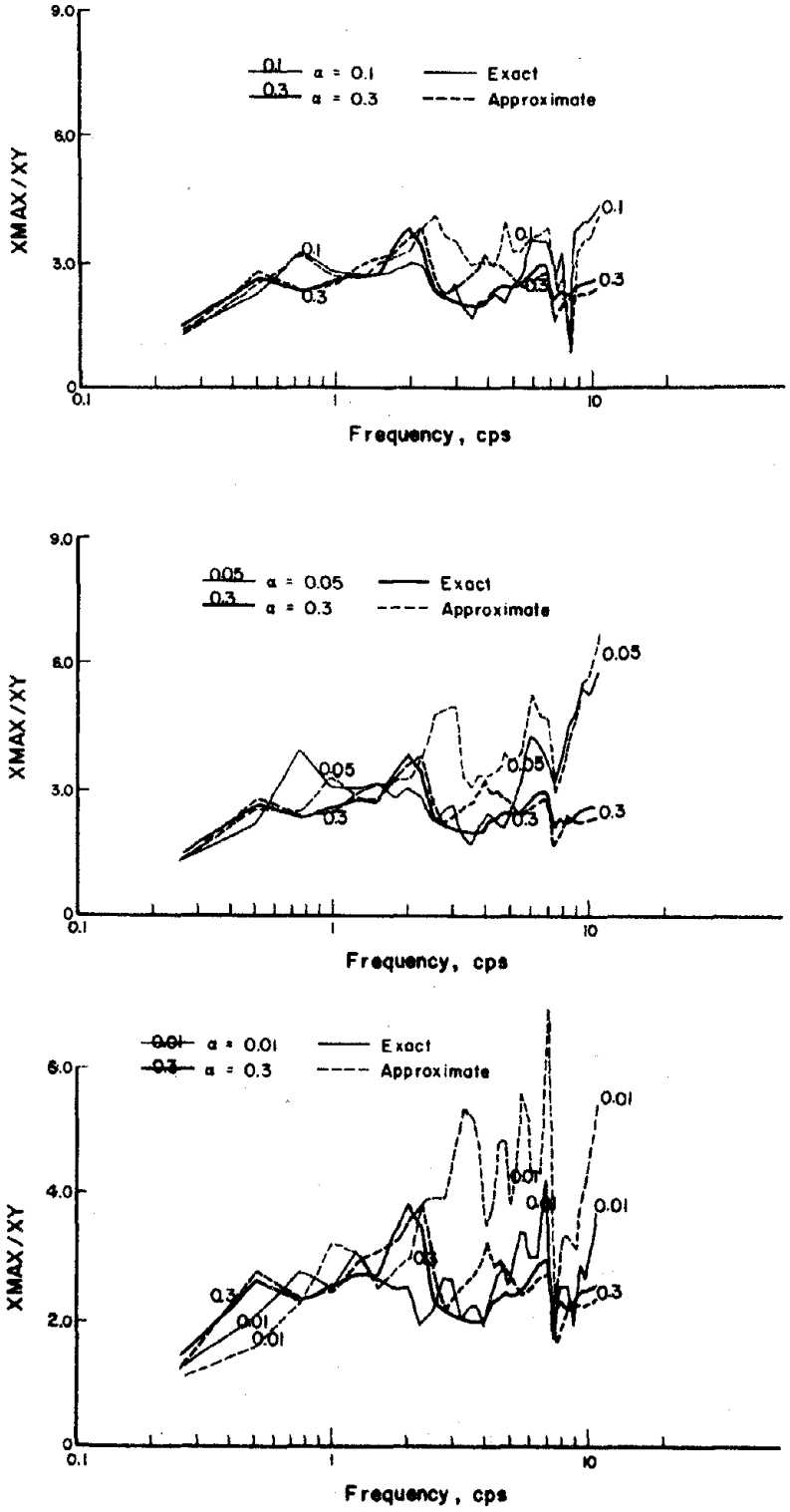

FIGURE 5.11 EFFECT OF BILINEAR HARDENING ON ACCURACY OF EQUIVALENT LINEAR METHOD (BILINEAR SDF SYSTEMS, ξ = 0.05, EL CENTRO 1940-NS, YIELD LEVEL 2)

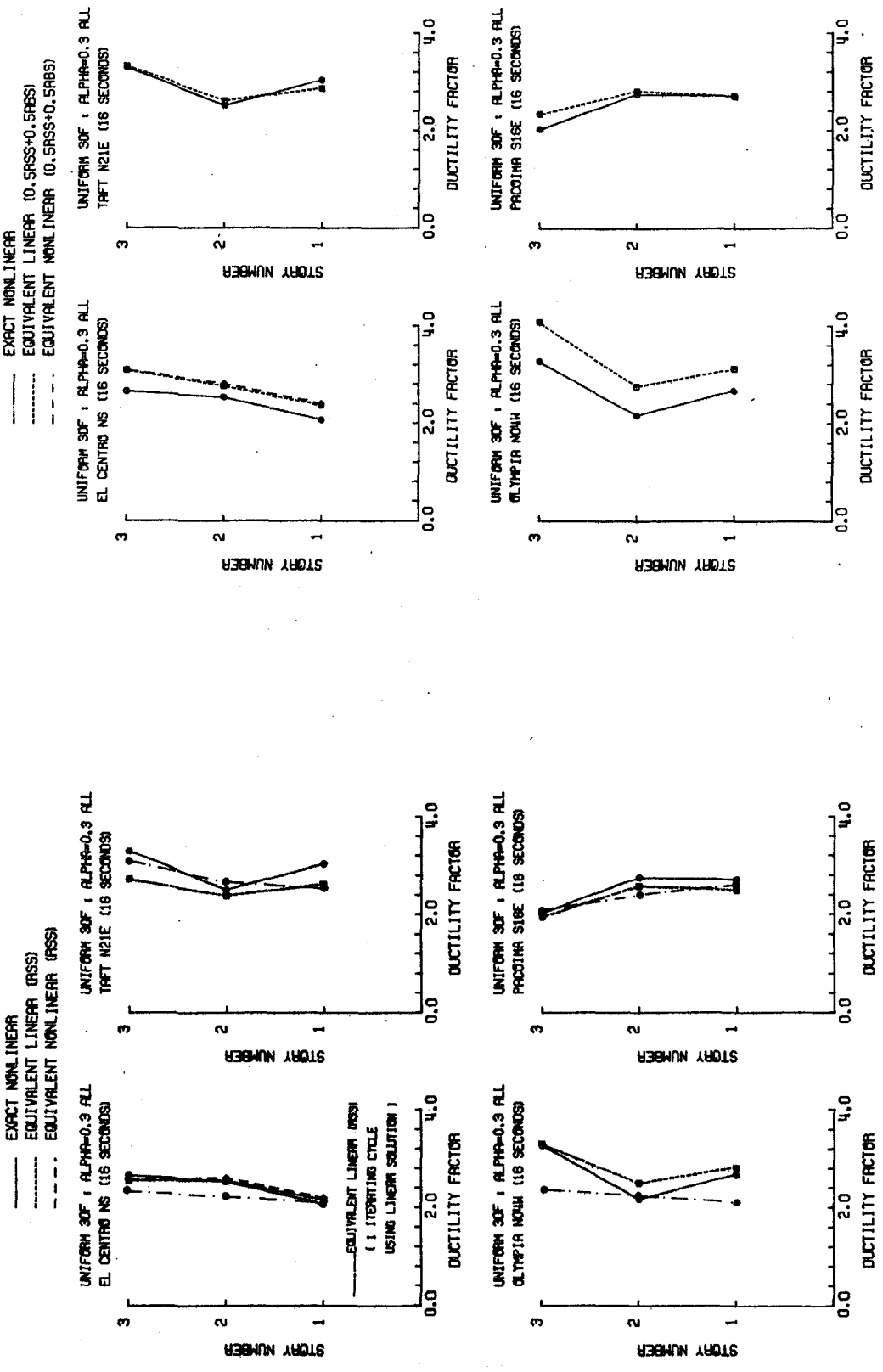

FIGURE 5.12 COMPARISON OF EXACT AND APPROXIMATED STORY DUCTILITIES (UNDAMPED UNIFORM BILINEAR 3DF SYSTEMS, α_e = 0.3, YIELD LEVEL 1)

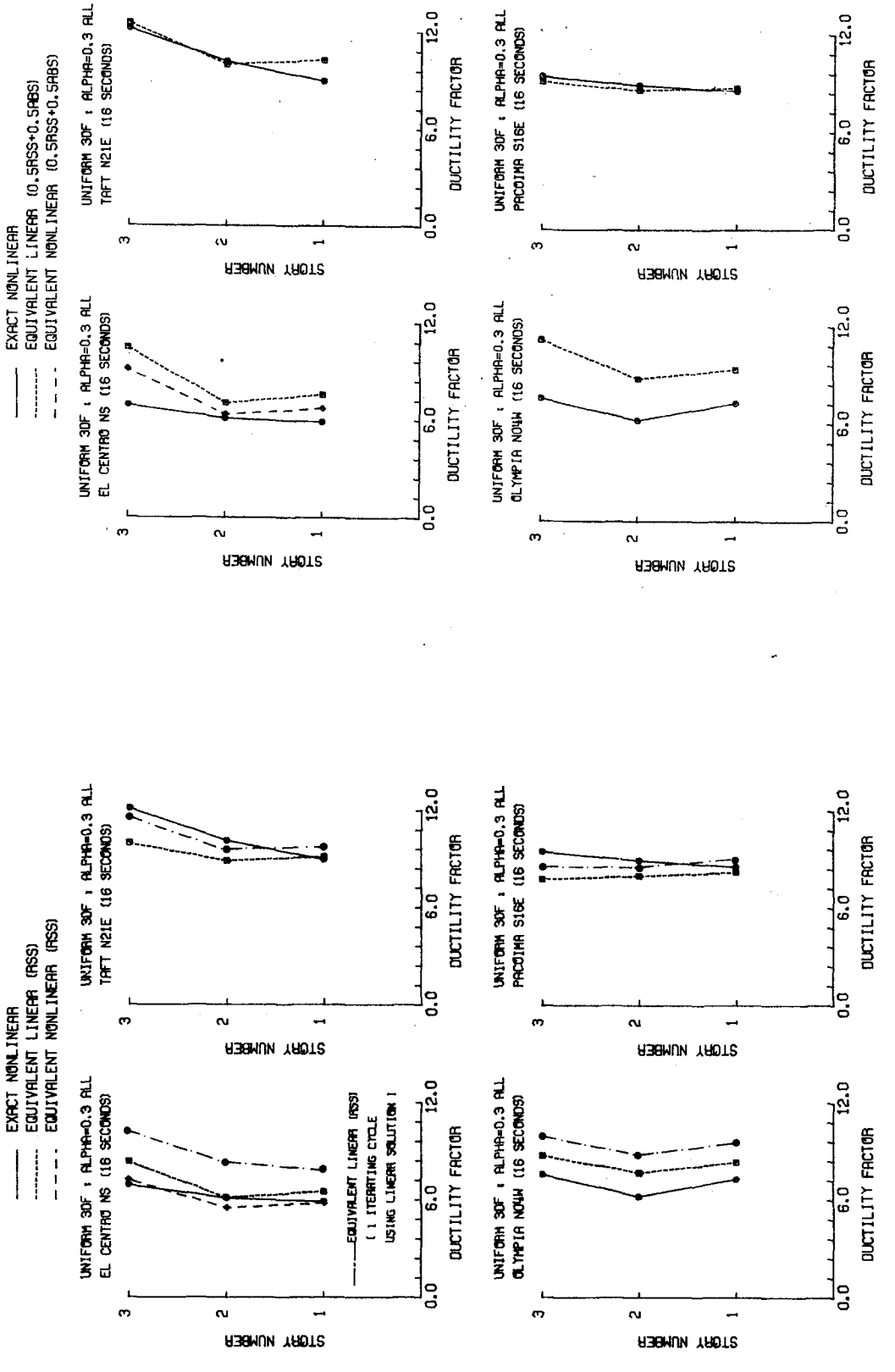

FIGURE 5.13 COMPARISON OF EXACT AND APPROXIMATE STORY DUCTILITIES (UNDAMPED UNIFORM BILINEAR 3DF SYSTEMS, α_e = 0.3, YIELD LEVEL 2)

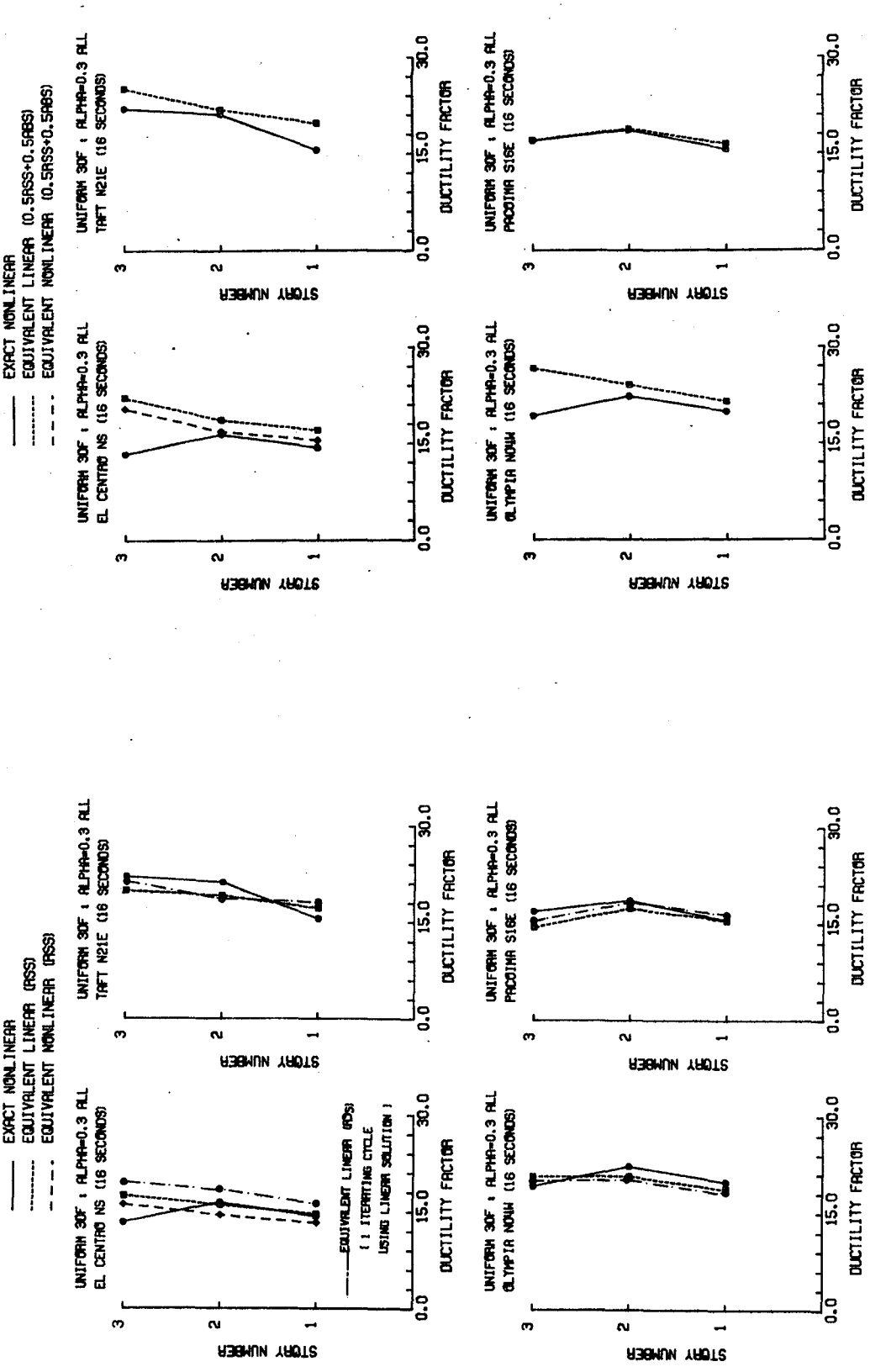

FIGURE 5.14 COMPARISON OF EXACT AND APPROXIMATE STORY DUCTILITIES (UNDAMPED UNIFORM BILINEAR 3DF SYSTEMS, α_e = 0.3, YIELD LEVEL 3)

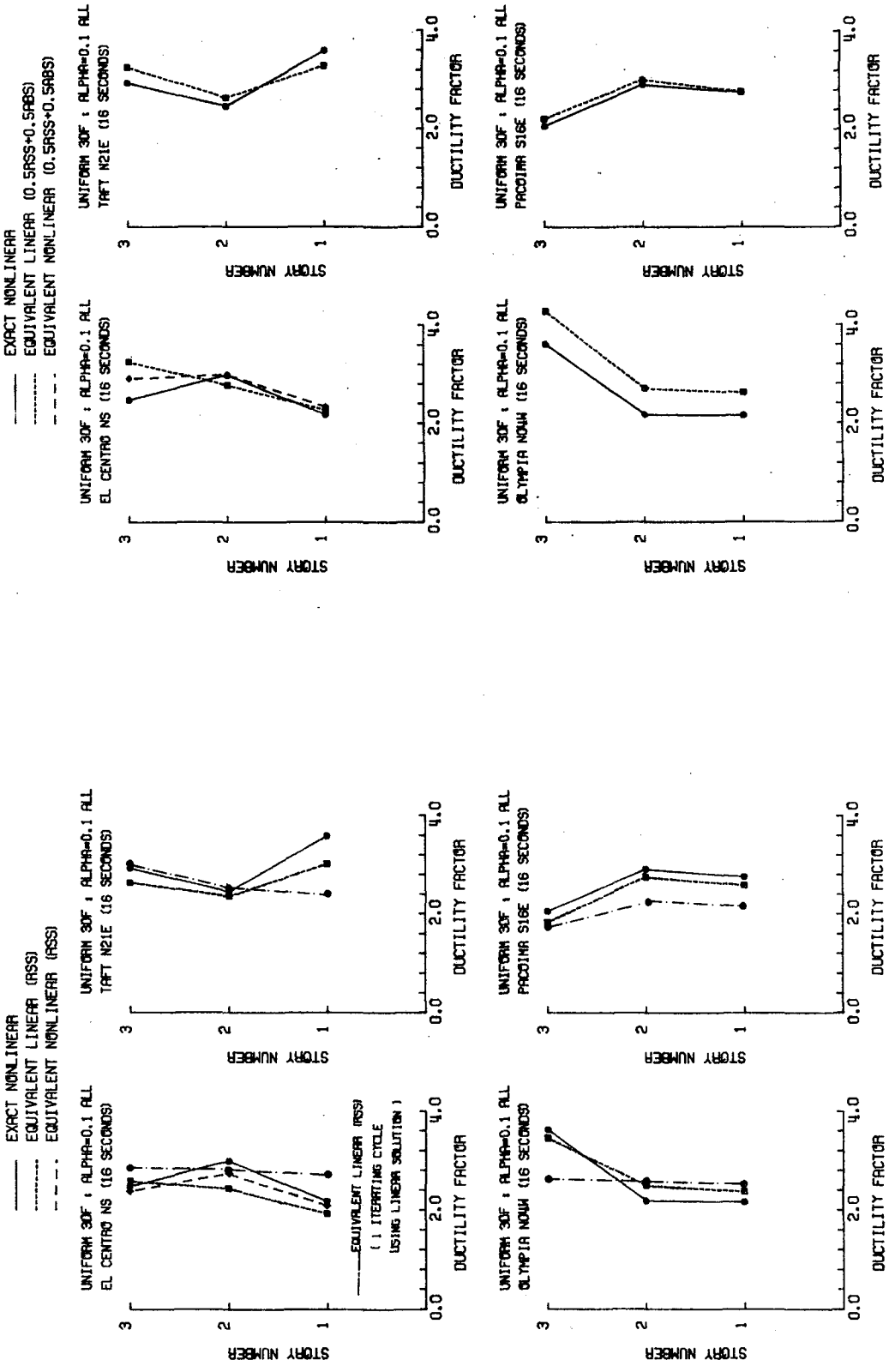

FIGURE 5.15 COMPARISON OF EXACT AND APPROXIMATE STORY DUCTILITIES (UNDAMPED UNIFORM BILINEAR 3DF SYSTEMS, α_e = 0.1, YIELD LEVEL 1)

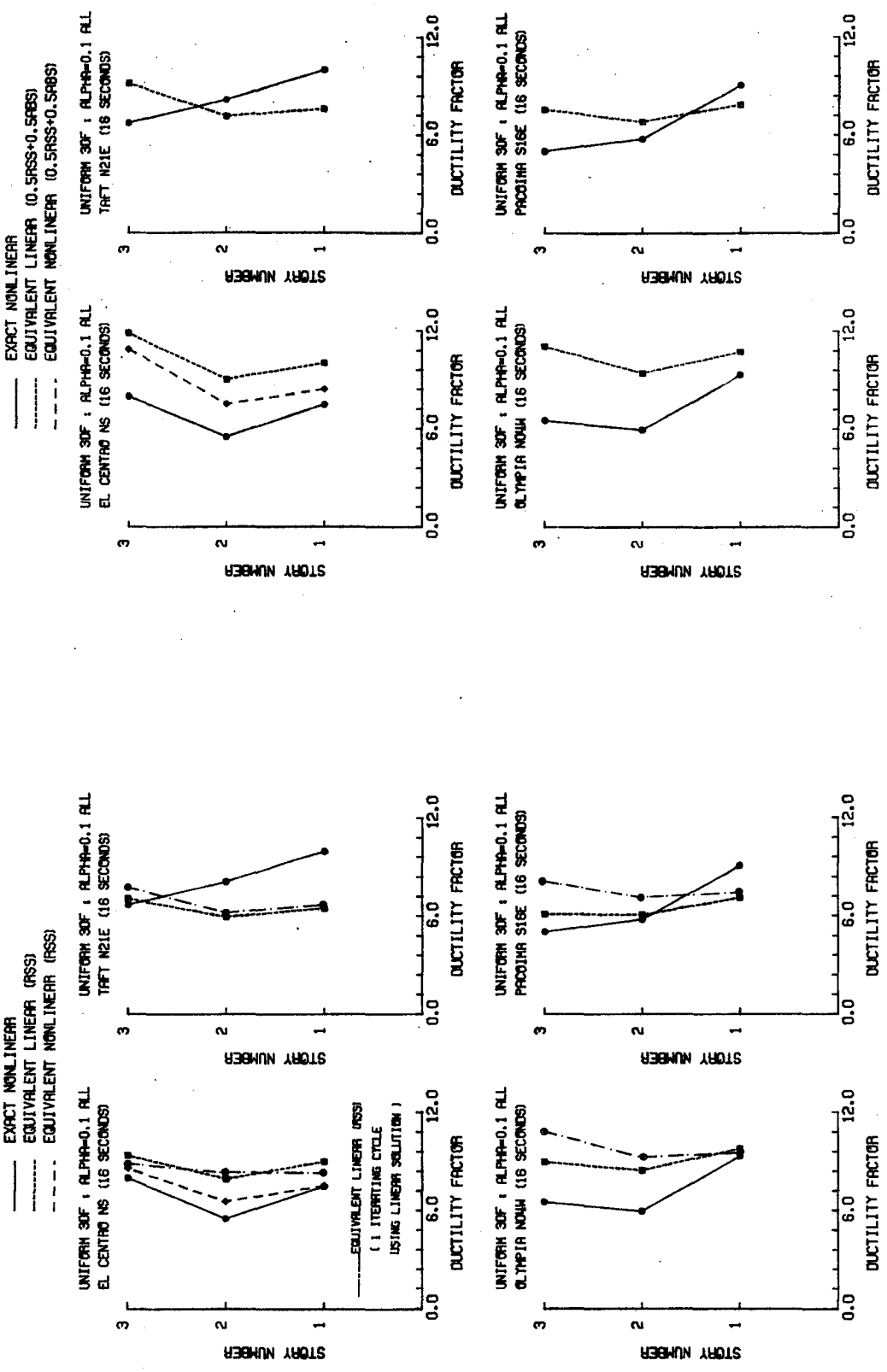

FIGURE 5.16 COMPARISON OF EXACT AND APPROXIMATE STORY DUCTILITIES (UNDAMPED UNIFORM BILINEAR 3DF SYSTEMS, α_e = 0.1, YIELD LEVEL 2)

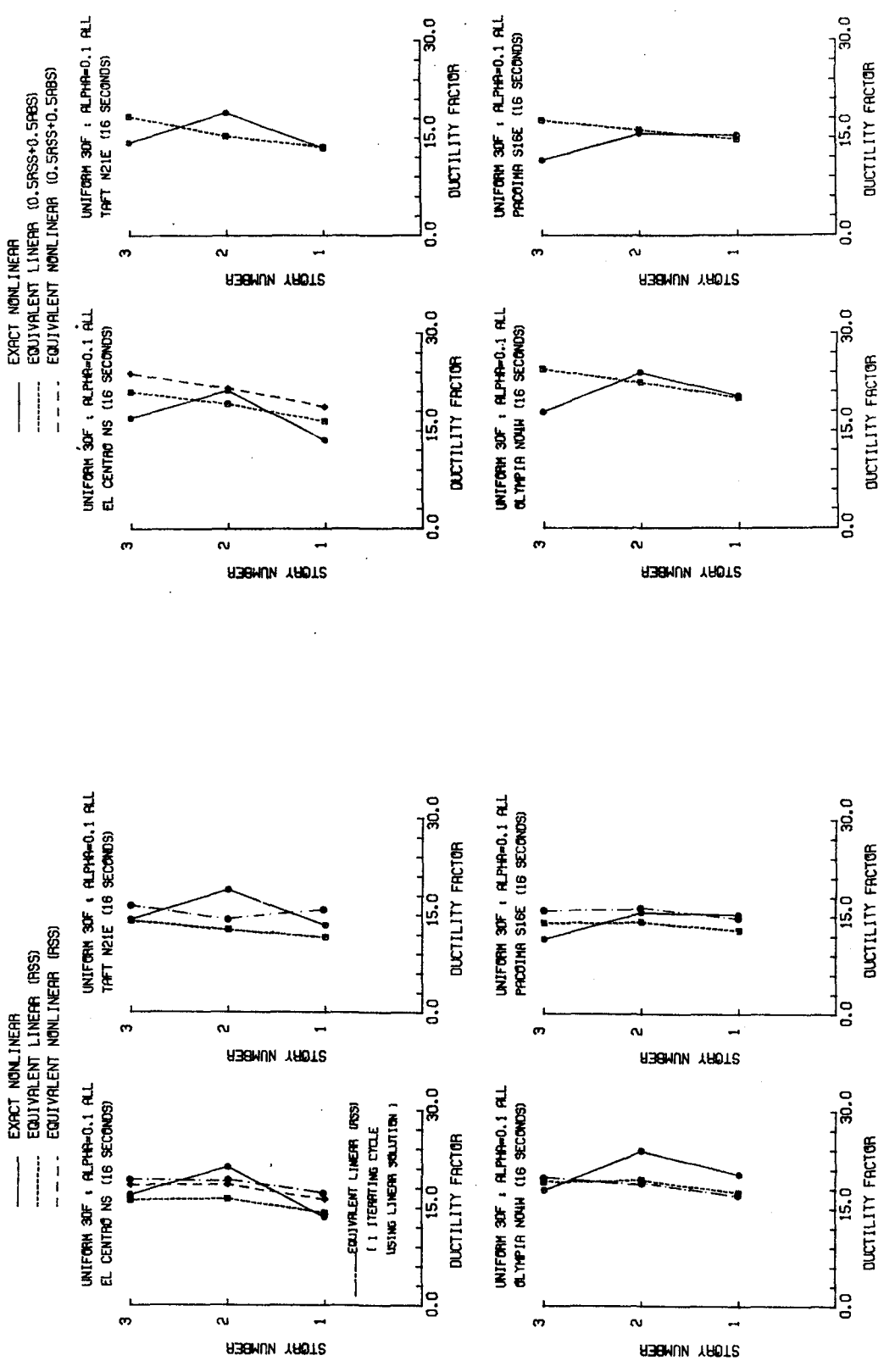

FIGURE 5.17 COMPARISON OF EXACT AND APPROXIMATE STORY DUCTILITIES (UNDAMPED UNIFORM BILINEAR 3DF SYSTEMS, α_e = 0.1, YIELD LEVEL 3)

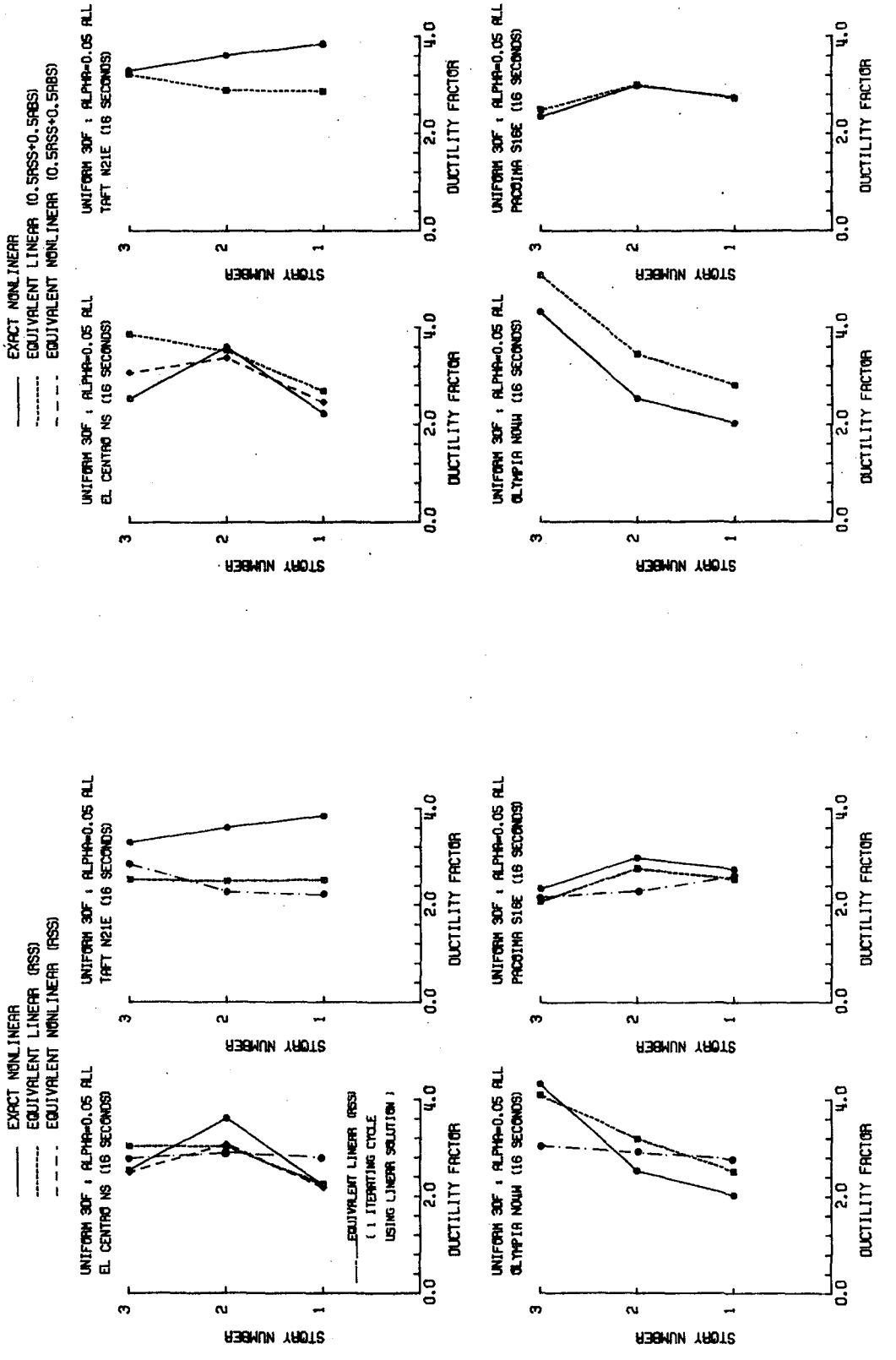

FIGURE 5.18 COMPARISON OF EXACT AND APPROXIMATE STORY DUCTILITIES (UNDAMPED UNIFORM BILINEAR 3DF SYSTEMS, α_e = 0.05, YIELD LEVEL 1)

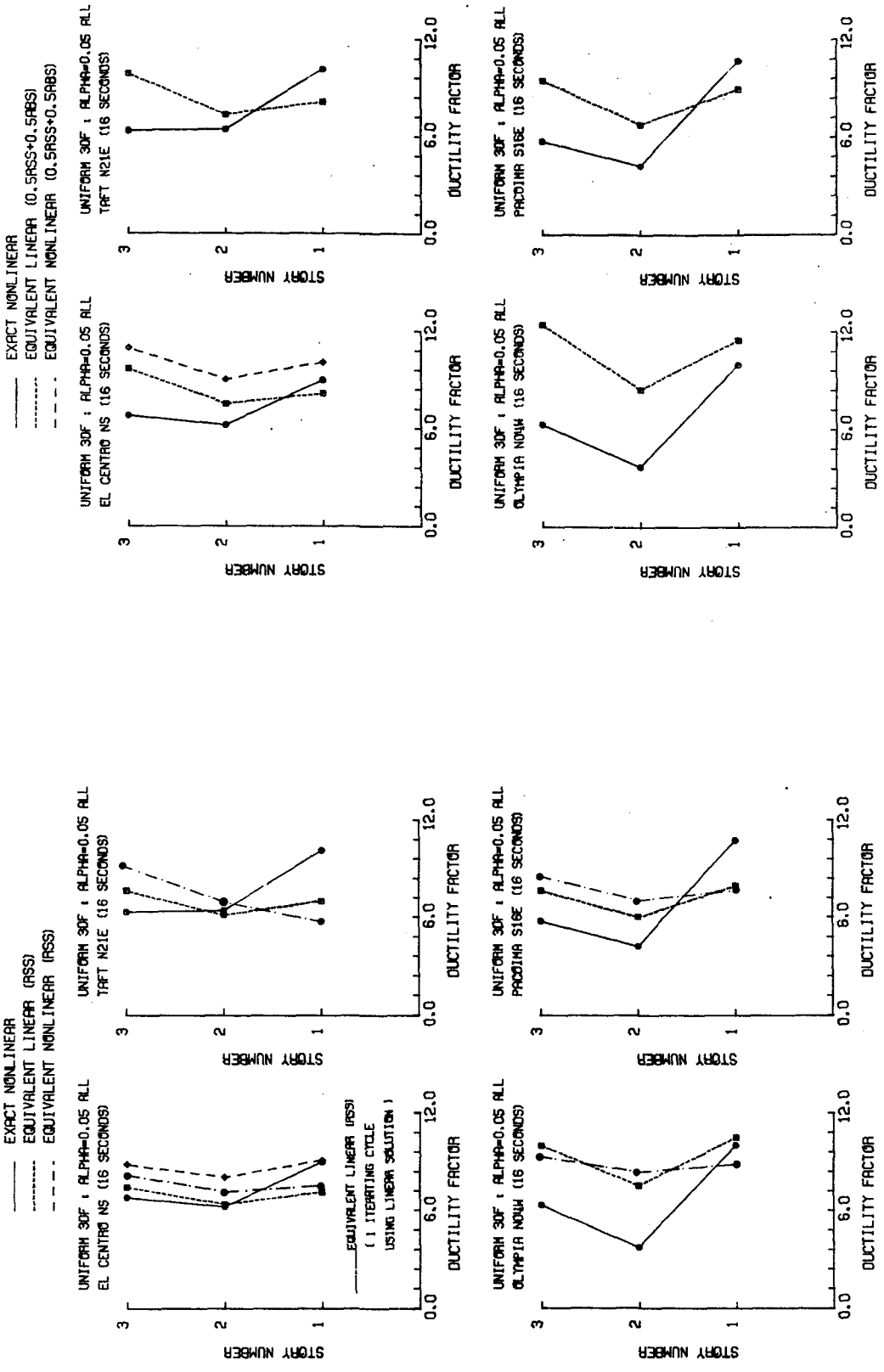

FIGURE 5.19 COMPARISON OF EXACT AND APPROXIMATE STORY DUCTILITIES (UNDAMPED UNIFORM BILINEAR 3DF SYSTEMS, α_e = 0.05, YIELD LEVEL 2)

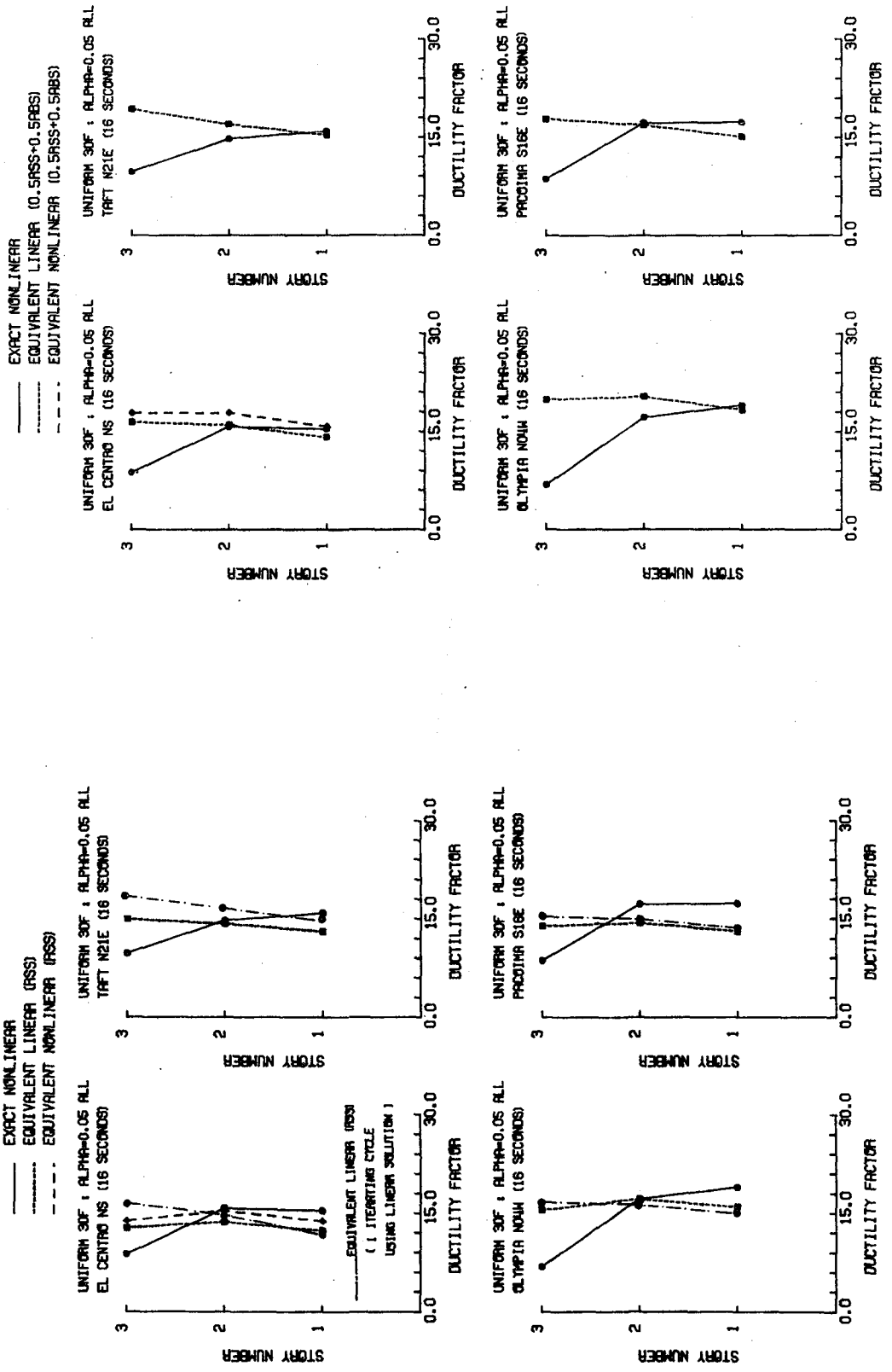

FIGURE 5.20 COMPARISON OF EXACT AND APPROXIMATE STORY DUCTILITIES (UNDAMPED UNIFORM BILINEAR 3DF SYSTEMS, α_e = 0.05, YIELD LEVEL 3)

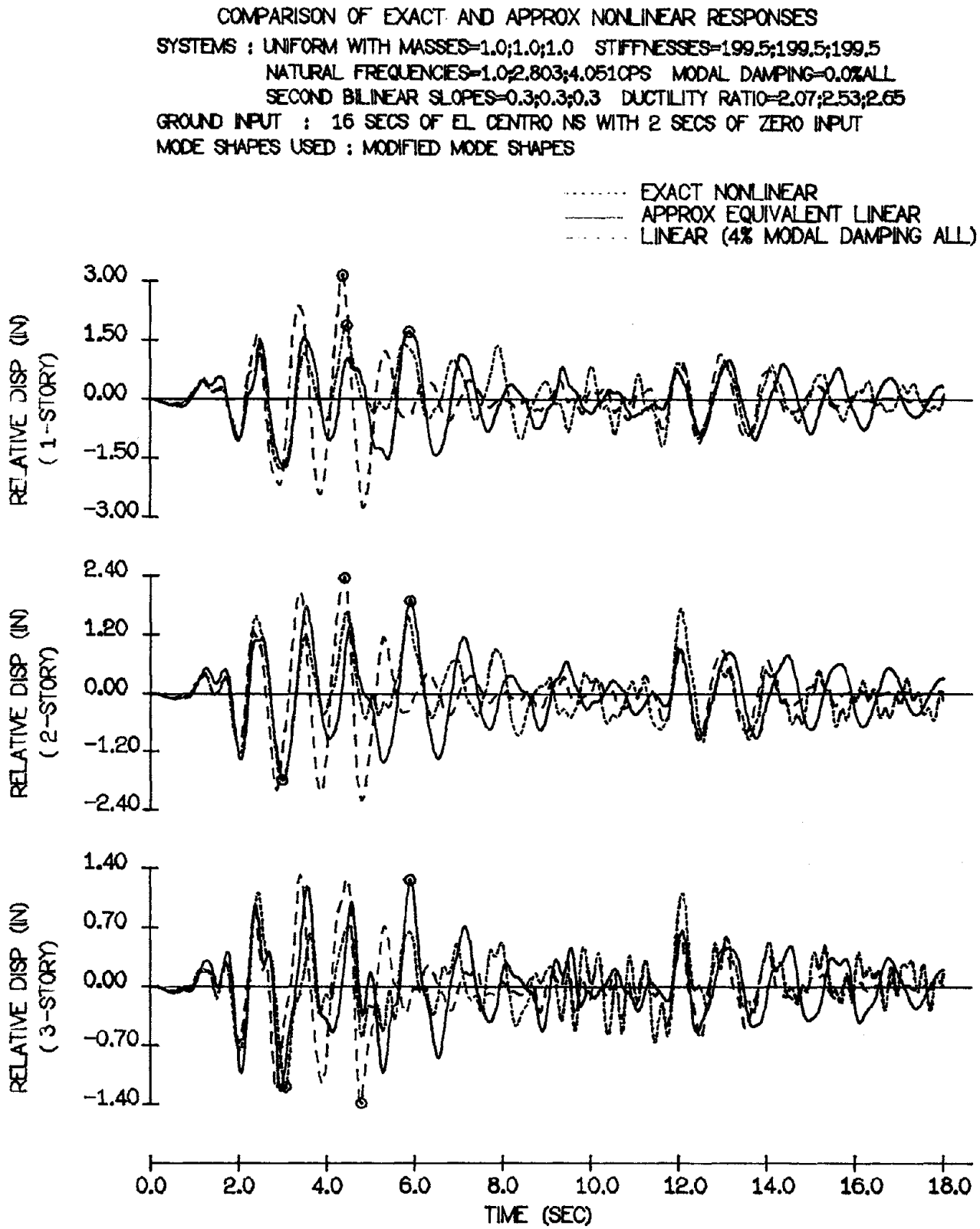

FIGURE 5.21 COMPARISON OF EXACT AND EQUIVALENT LINEAR DISPLACEMENT TIME HISTORIES (UNDAMPED UNIFORM BILINEAR 3DF SYSTEM, α_e = 0.3, EL CENTRO 1940-NS, YIELD LEVEL 1)

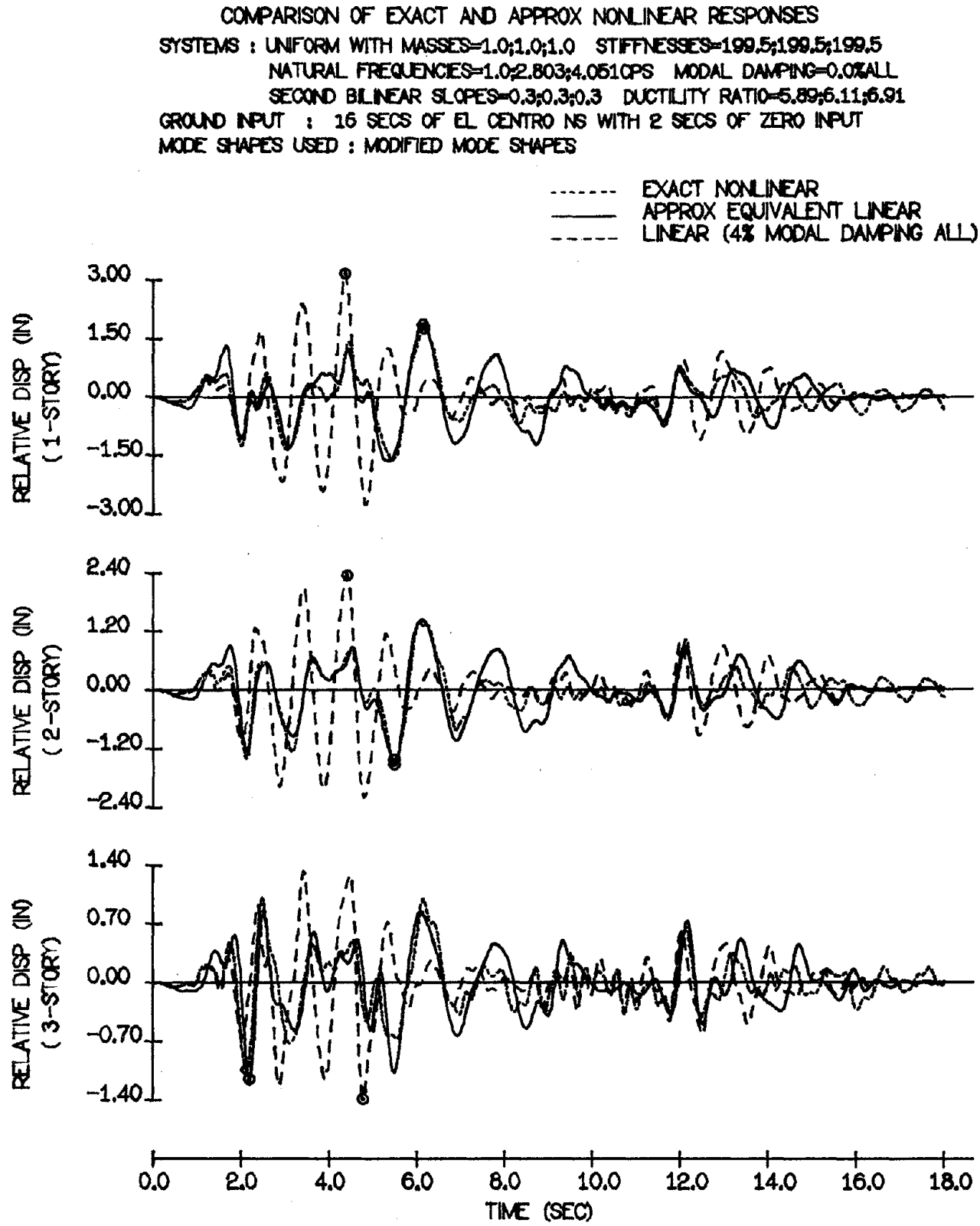

FIGURE 5.22 COMPARISON OF EXACT AND EQUIVALENT LINEAR DISPLACEMENT TIME HISTORIES (UNDAMPED UNIFORM BILINEAR 3DF SYSTEM, α_e = 0.3, EL CENTRO 1940-NS, YIELD LEVEL 2)

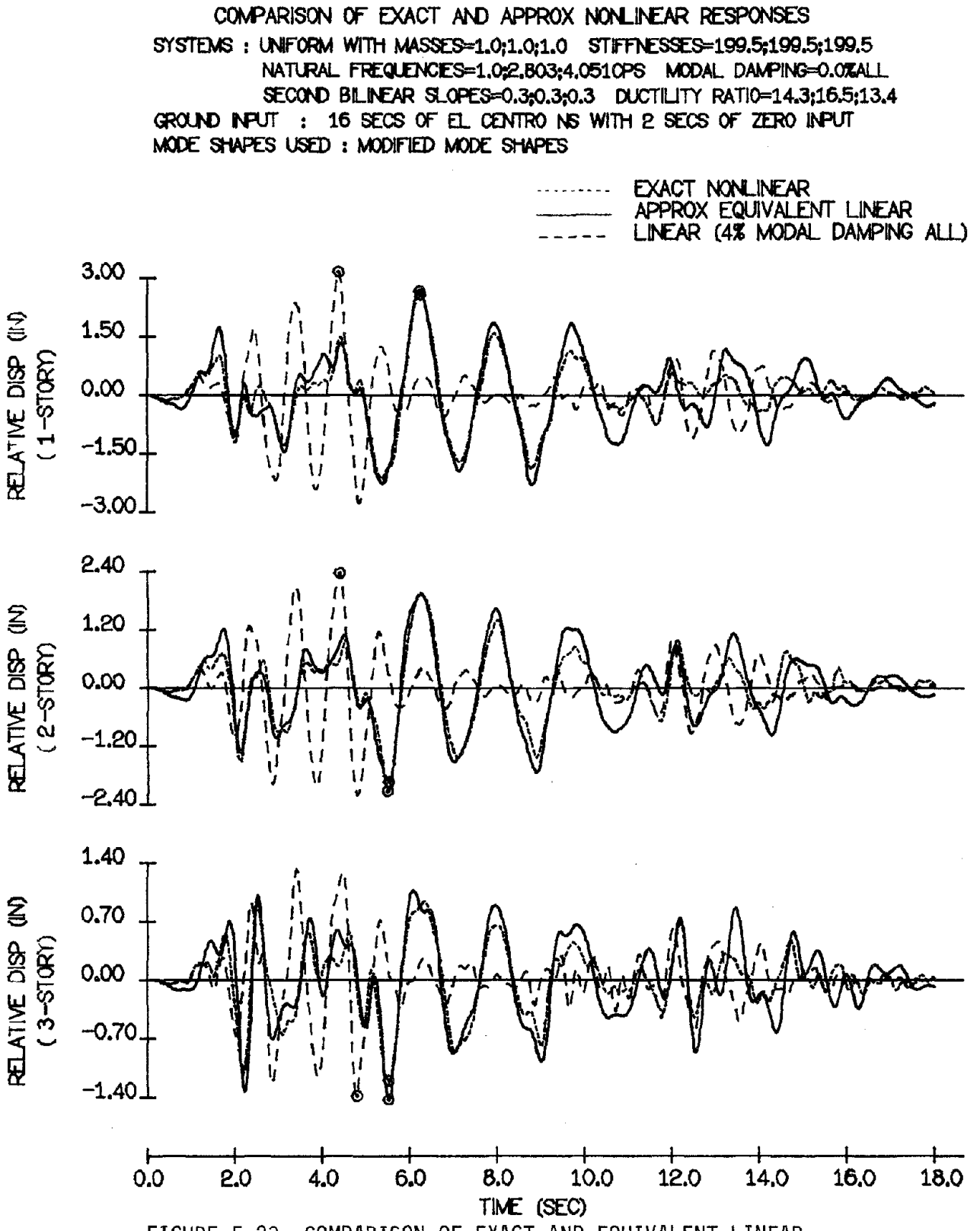

FIGURE 5.23 COMPARISON OF EXACT AND EQUIVALENT LINEAR DISPLACEMENT TIME HISTORIES (UNDAMPED UNIFORM BILINEAR 3DF SYSTEM, α_e = 0.3, EL CENTRO 1940-NS, YIELD LEVEL 3)

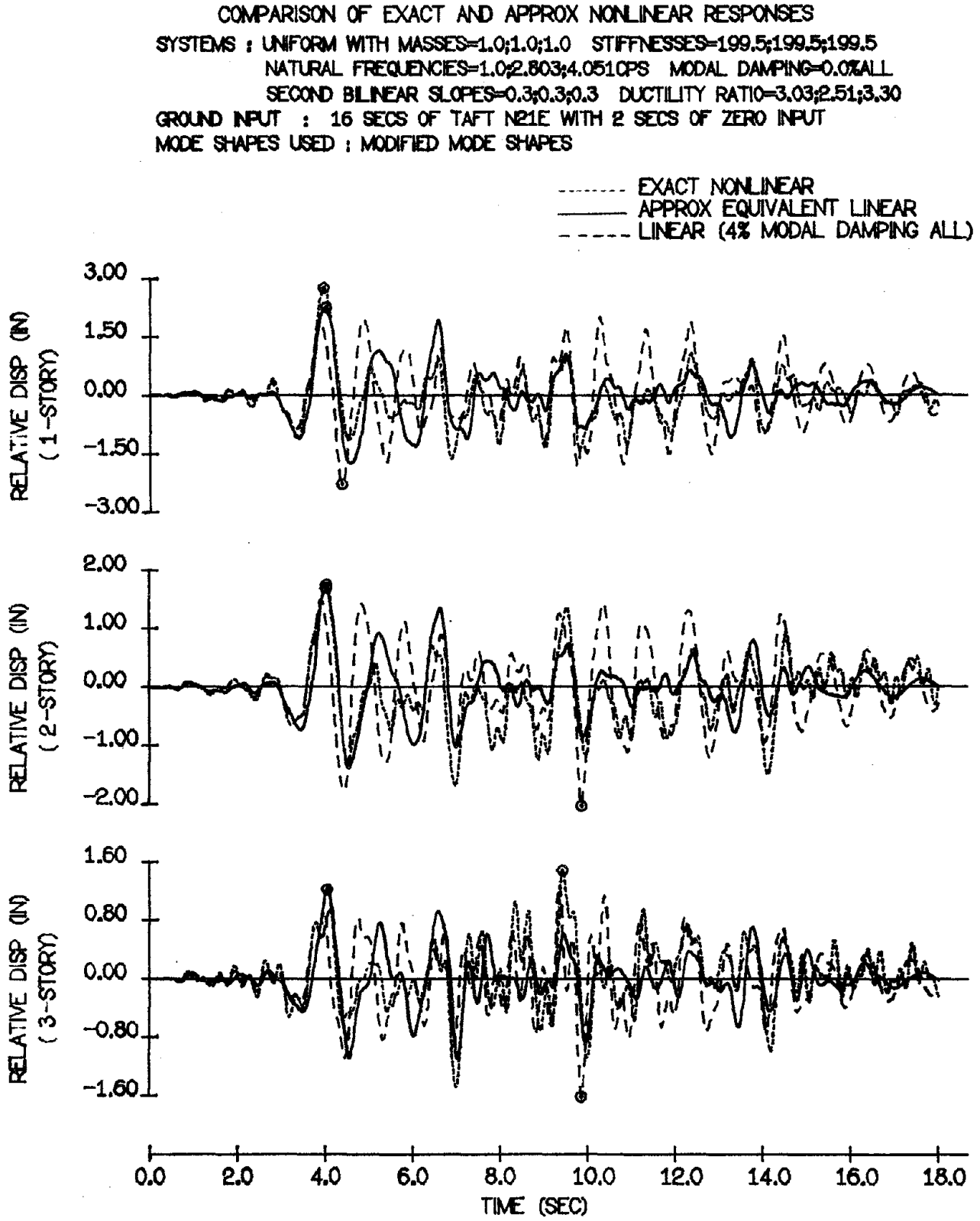

FIGURE 5.24 COMPARISON OF EXACT AND EQUIVALENT LINEAR DISPLACEMENT TIME HISTORIES (UNDAMPED UNIFORM BILINEAR 3DF SYSTEM, α_e = 0.3, TAFT 1952-N21E, YIELD LEVEL 1)

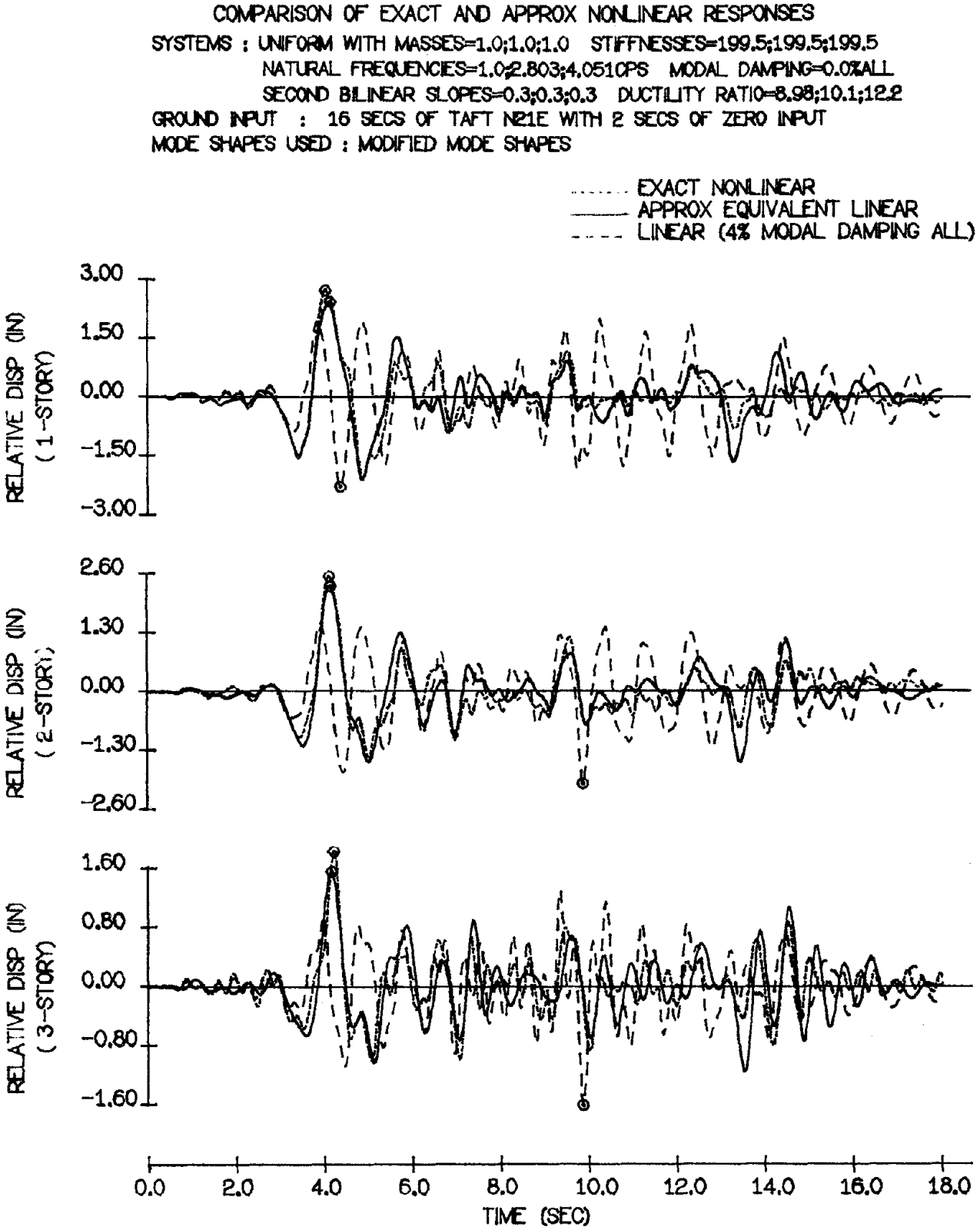

FIGURE 5.25 COMPARISON OF EXACT AND EQUIVALENT LINEAR DISPLACEMENT TIME HISTORIES (UNDAMPED UNIFORM BILINEAR 3DF SYSTEM, α_e = 0.3, TAFT 1952-N21E, YIELD LEVEL 2)

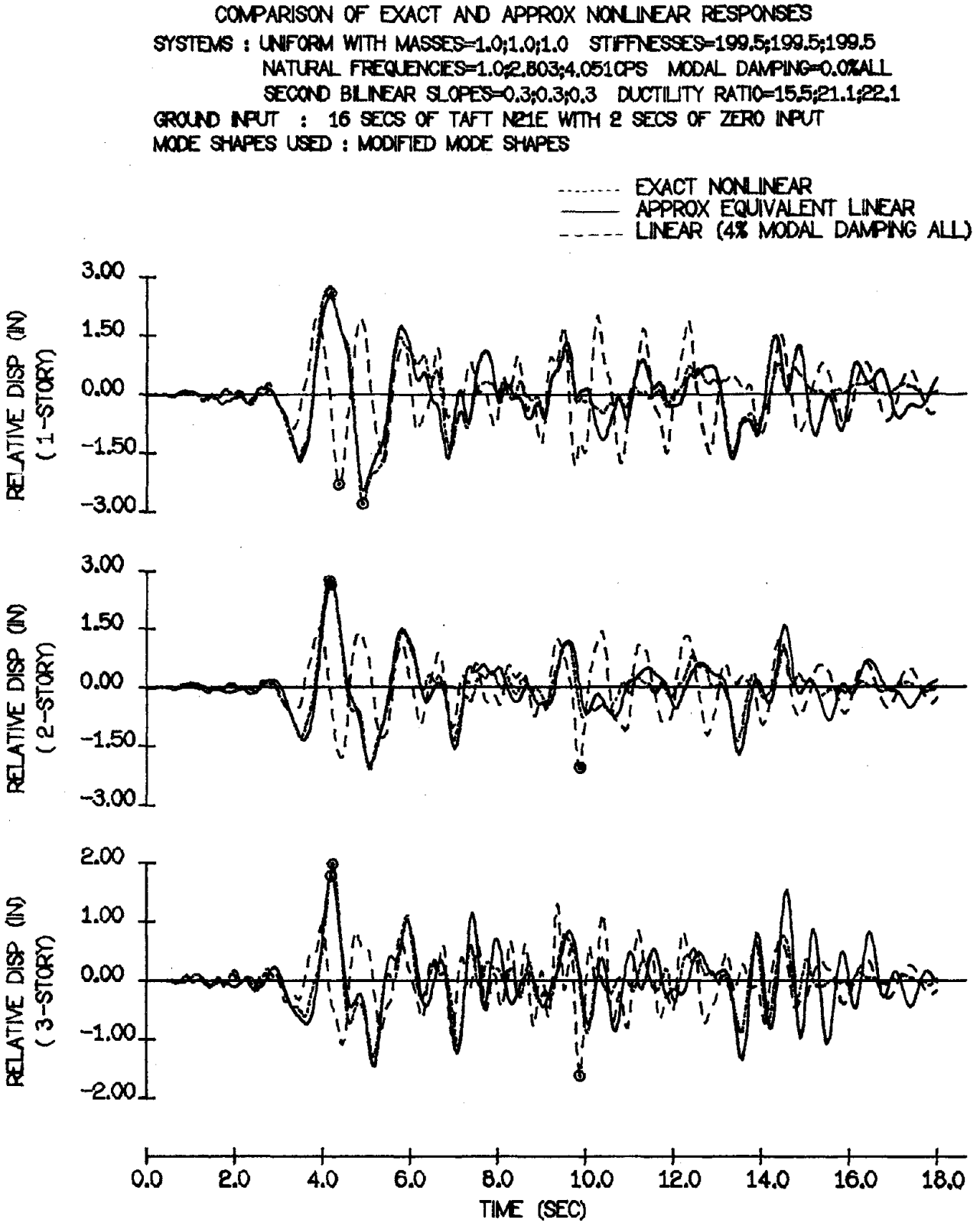

FIGURE 5.26 COMPARISON OF EXACT AND EQUIVALENT LINEAR DISPLACEMENT TIME HISTORIES (UNDAMPED UNIFORM BILINEAR 3DF SYSTEM, α_e = 0.3, TAFT 1952-N21E, YIELD LEVEL 3)

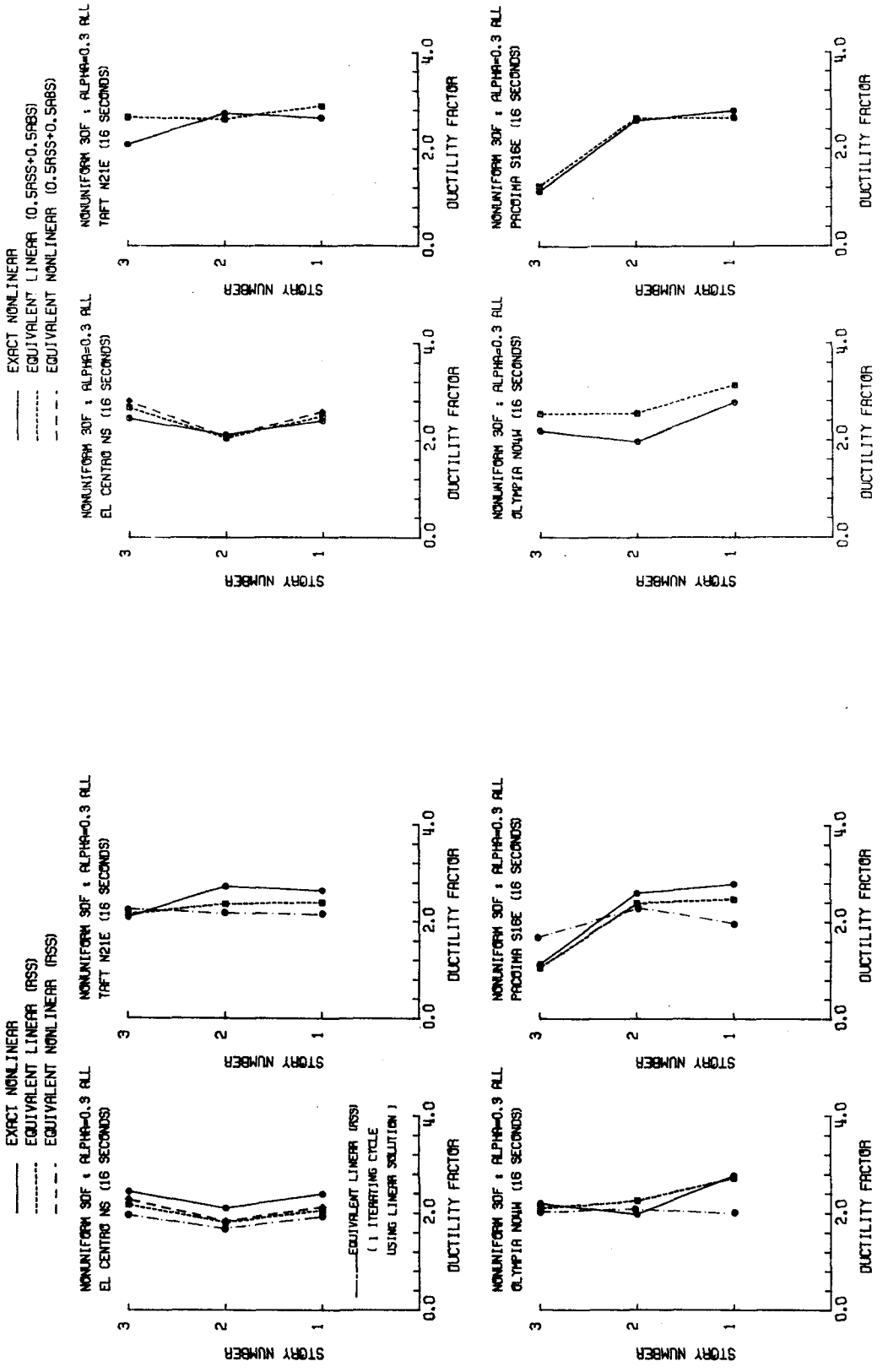

FIGURE 5.27 COMPARISON OF EXACT AND APPROXIMATE STORY DUCTILITIES (UNDAMPED NONUNIFORM BILINEAR 3DF SYSTEMS, α_e = 0.3, YIELD LEVEL 1)

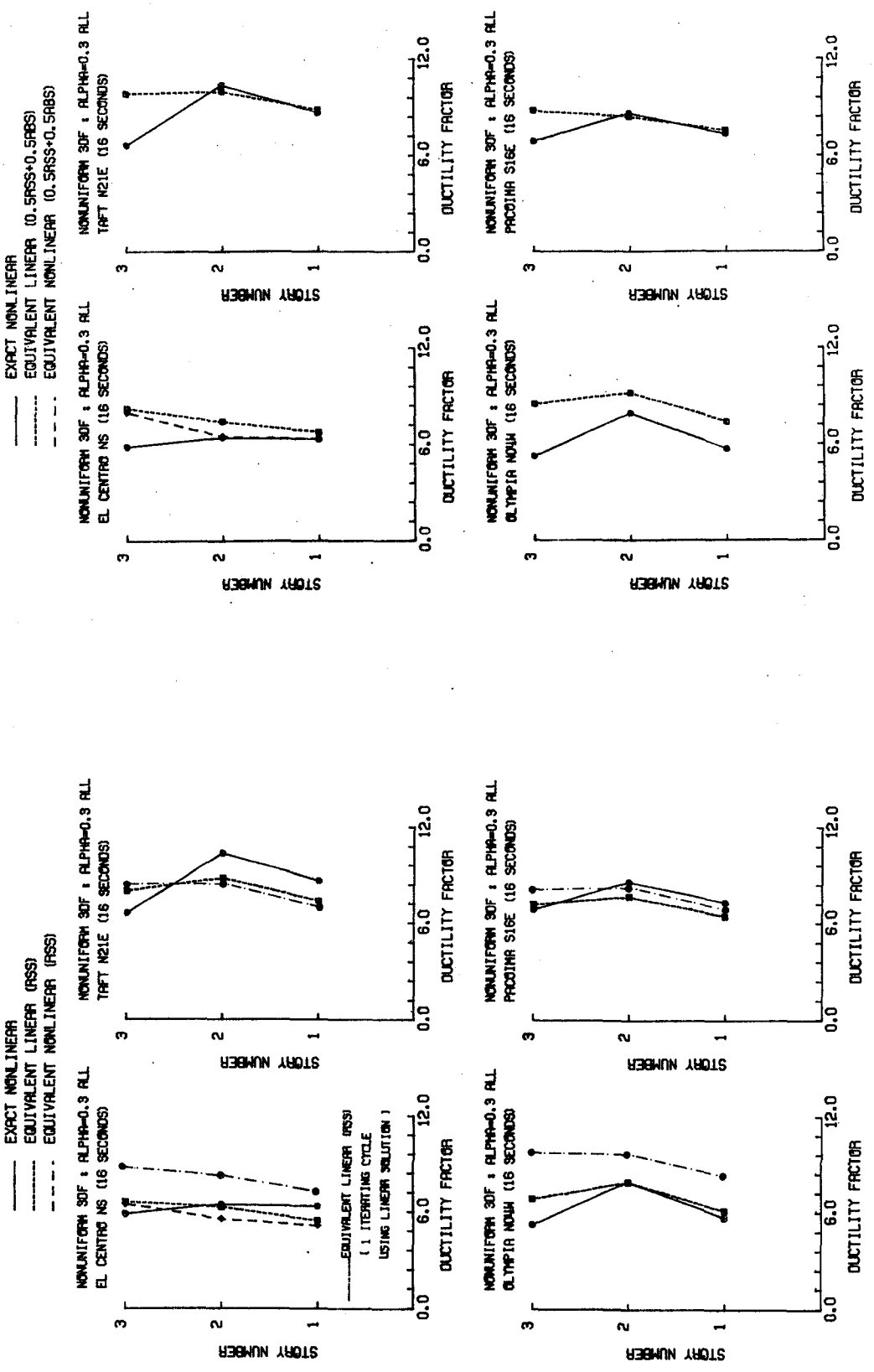

FIGURE 5.28 COMPARISON OF EXACT AND APPROXIMATE STORY DUCTILITIES (UNDAMPED NONUNIFORM BILINEAR 3DF SYSTEMS, α_e = 0.3, YIELD LEVEL 2)

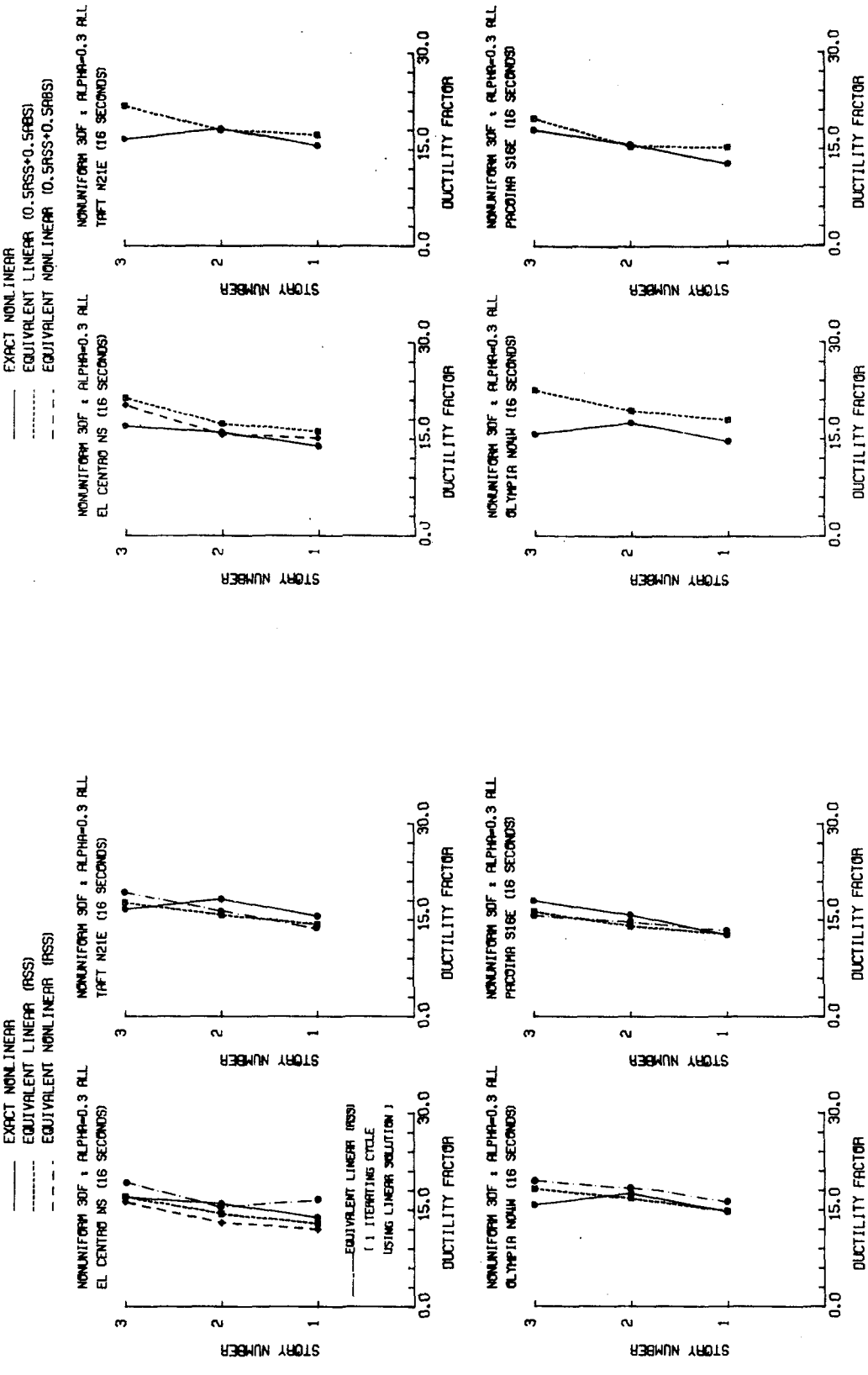

FIGURE 5.29 COMPARISON OF EXACT AND APPROXIMATE STORY DUCTILITIES (UNDAMPED NONUNIFORM BILINEAR 3DF SYSTEMS, α_e = 0.3, YIELD LEVEL 3)

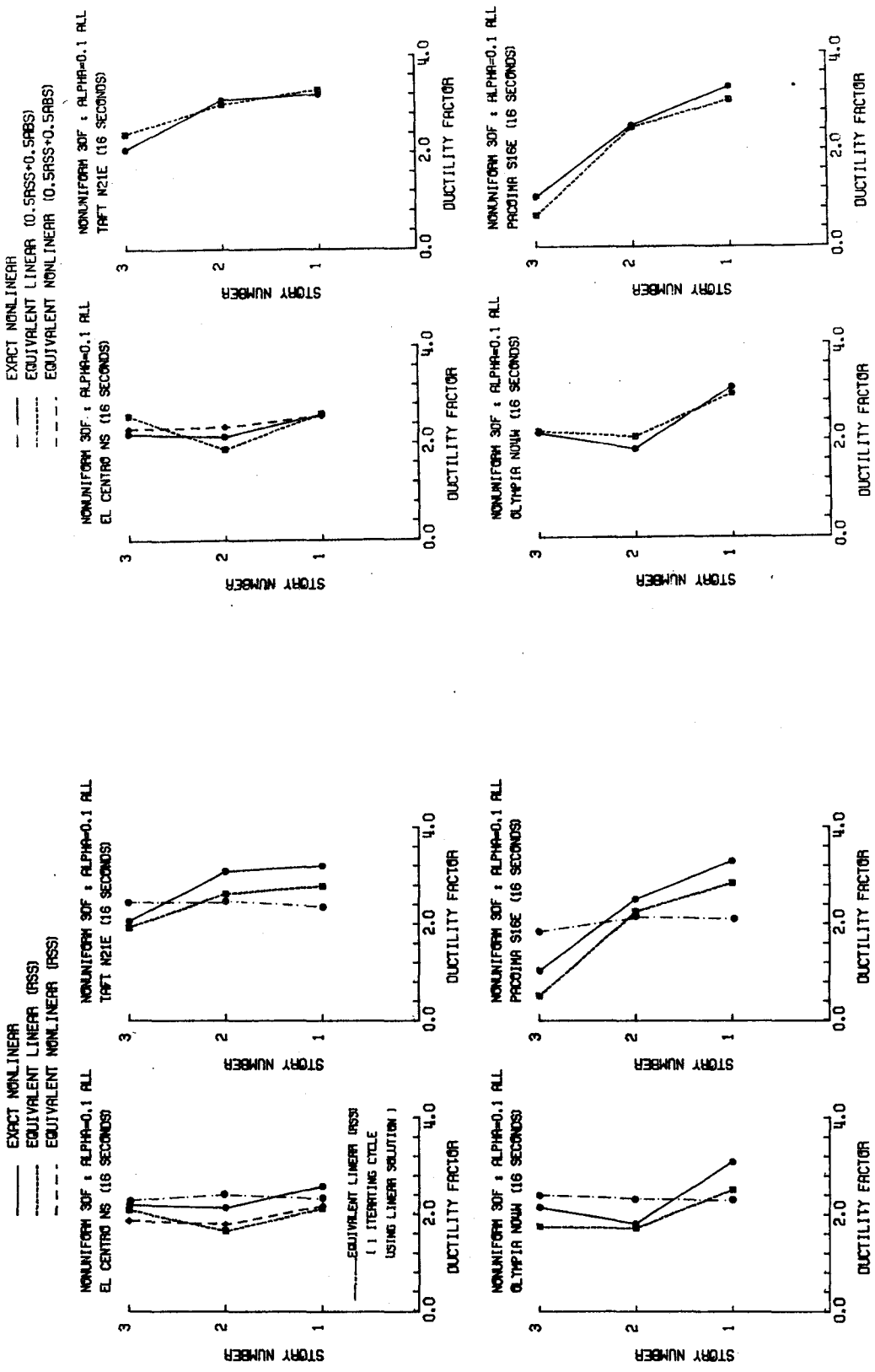

FIGURE 5.30 COMPARISON OF EXACT AND APPROXIMATE STORY DUCTILITIES (UNDAMPED NONUNIFORM BILINEAR 3DF SYSTEMS, α_e = 0.1, YIELD LEVEL 1)

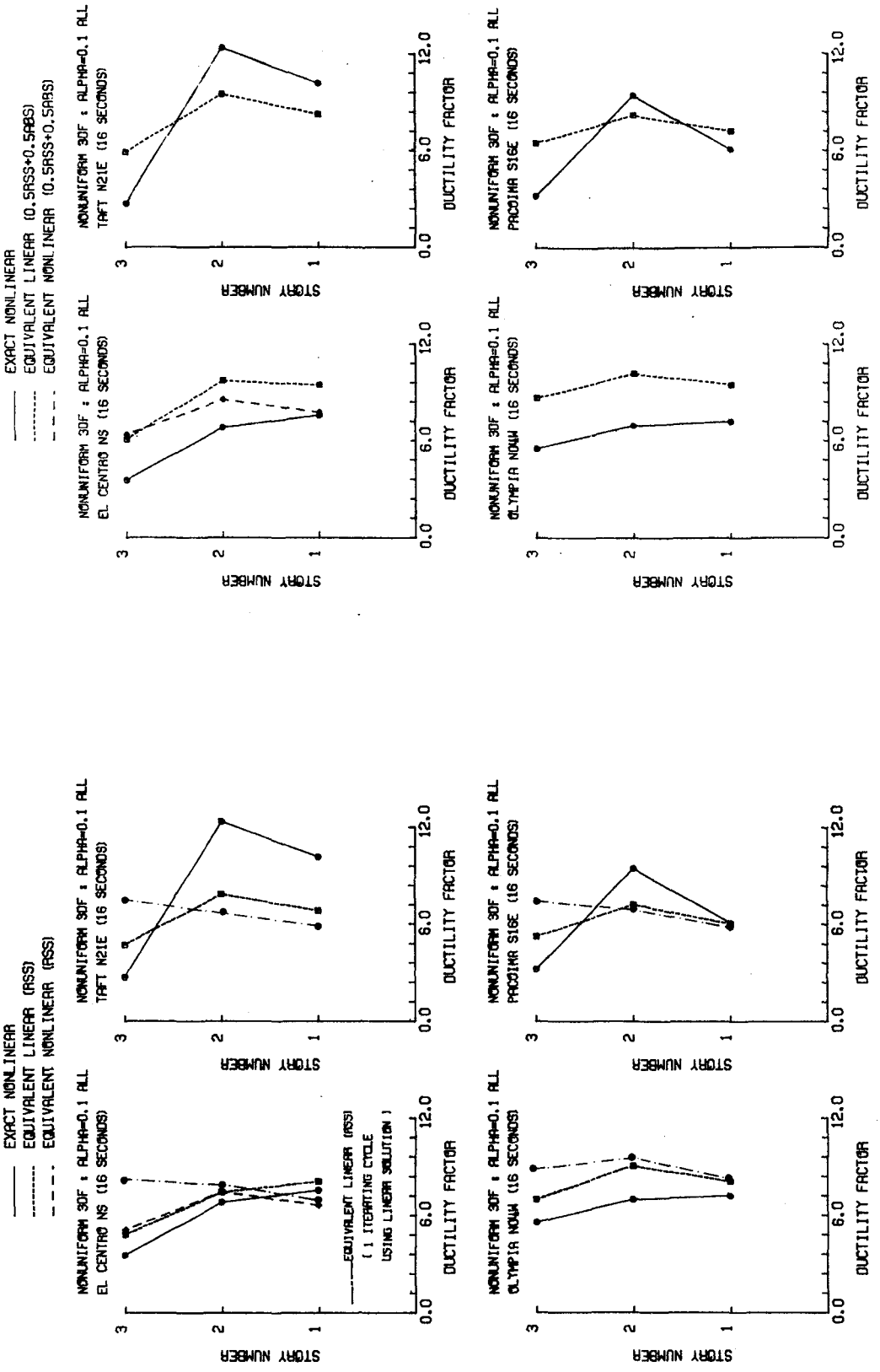

FIGURE 5.31 COMPARISON OF EXACT AND APPROXIMATE STORY DUCTILITIES (UNDAMPED NONUNIFORM BILINEAR 3DF SYSTEMS, α_e = 0.1, YIELD LEVEL 2)

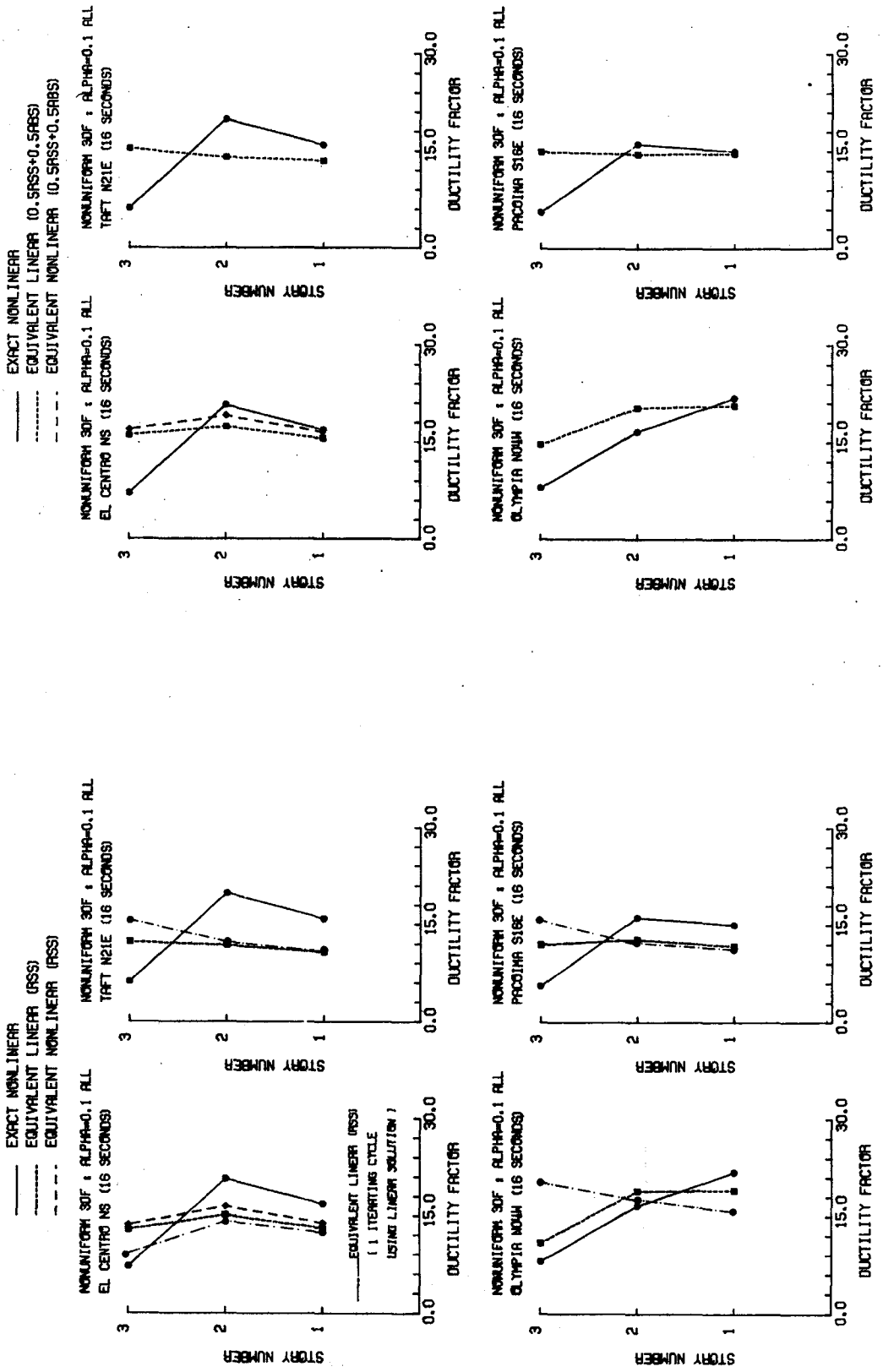

FIGURE 5.32 COMPARISON OF EXACT AND APPROXIMATE STORY DUCTILITIES (UNDAMPED NONUNIFORM BILINEAR 3DF SYSTEMS, α_e = 0.1, YIELD LEVEL 3)

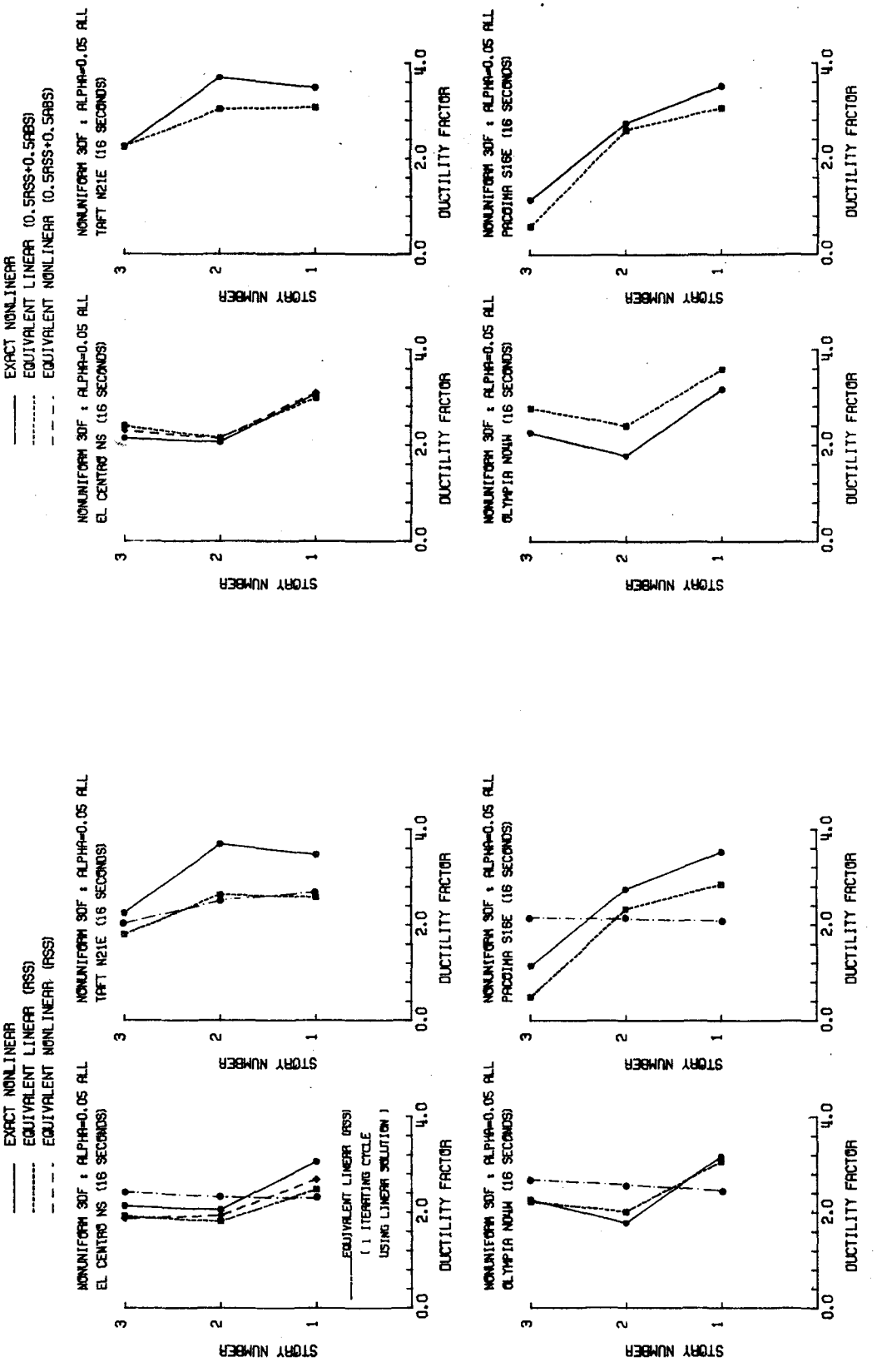

FIGURE 5.33 COMPARISON OF EXACT AND APPROXIMATE STORY DUCTILITIES (UNDAMPED NONUNIFORM BILINEAR 3DF SYSTEMS, α_e = 0.05, YIELD LEVEL 1)

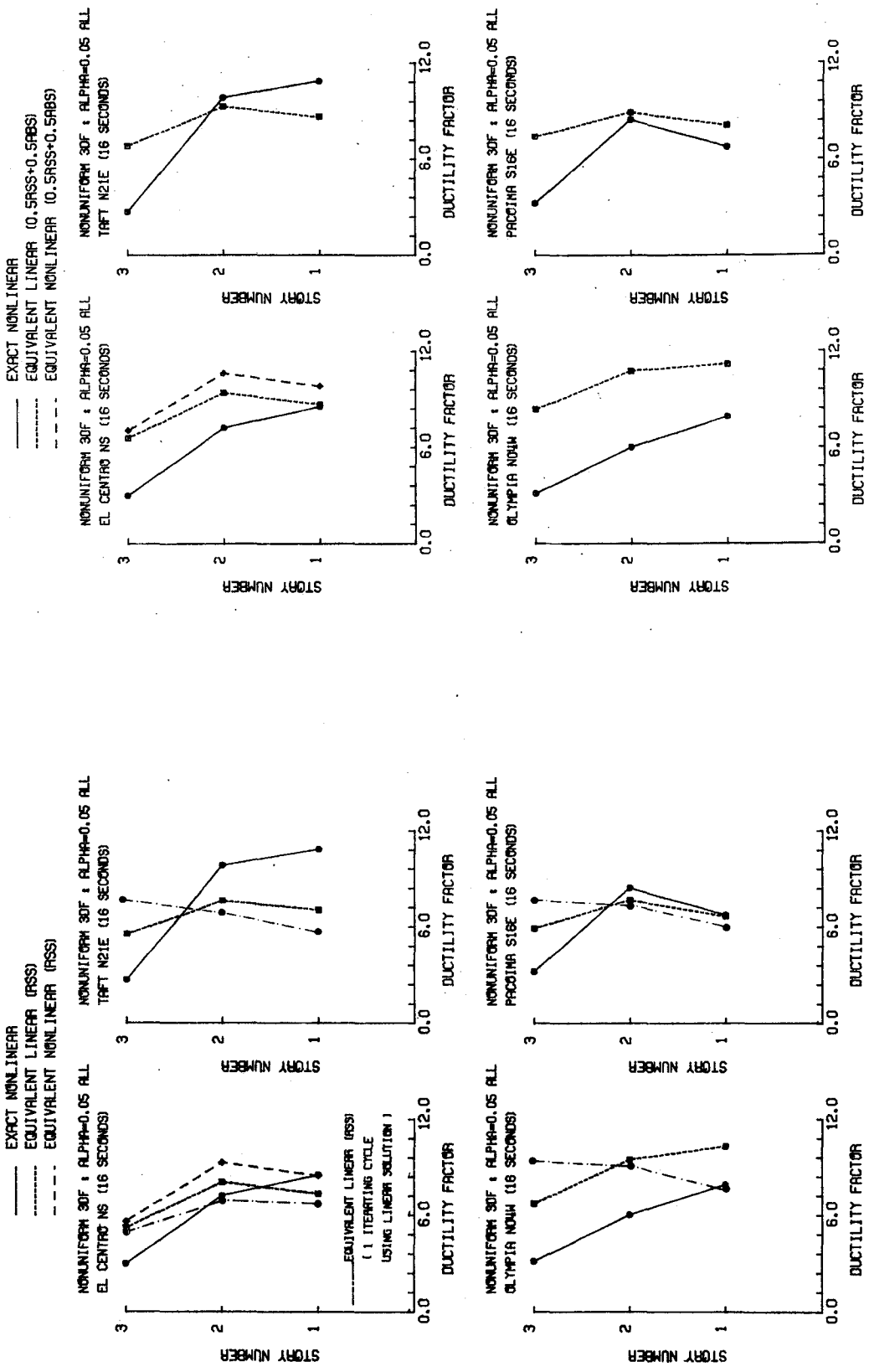

FIGURE 5.34 COMPARISON OF EXACT AND APPROXIMATE STORY DUCTILITIES (UNDAMPED NONUNIFORM BILINEAR 3DF SYSTEMS, α_e = 0.05, YIELD LEVEL 2)

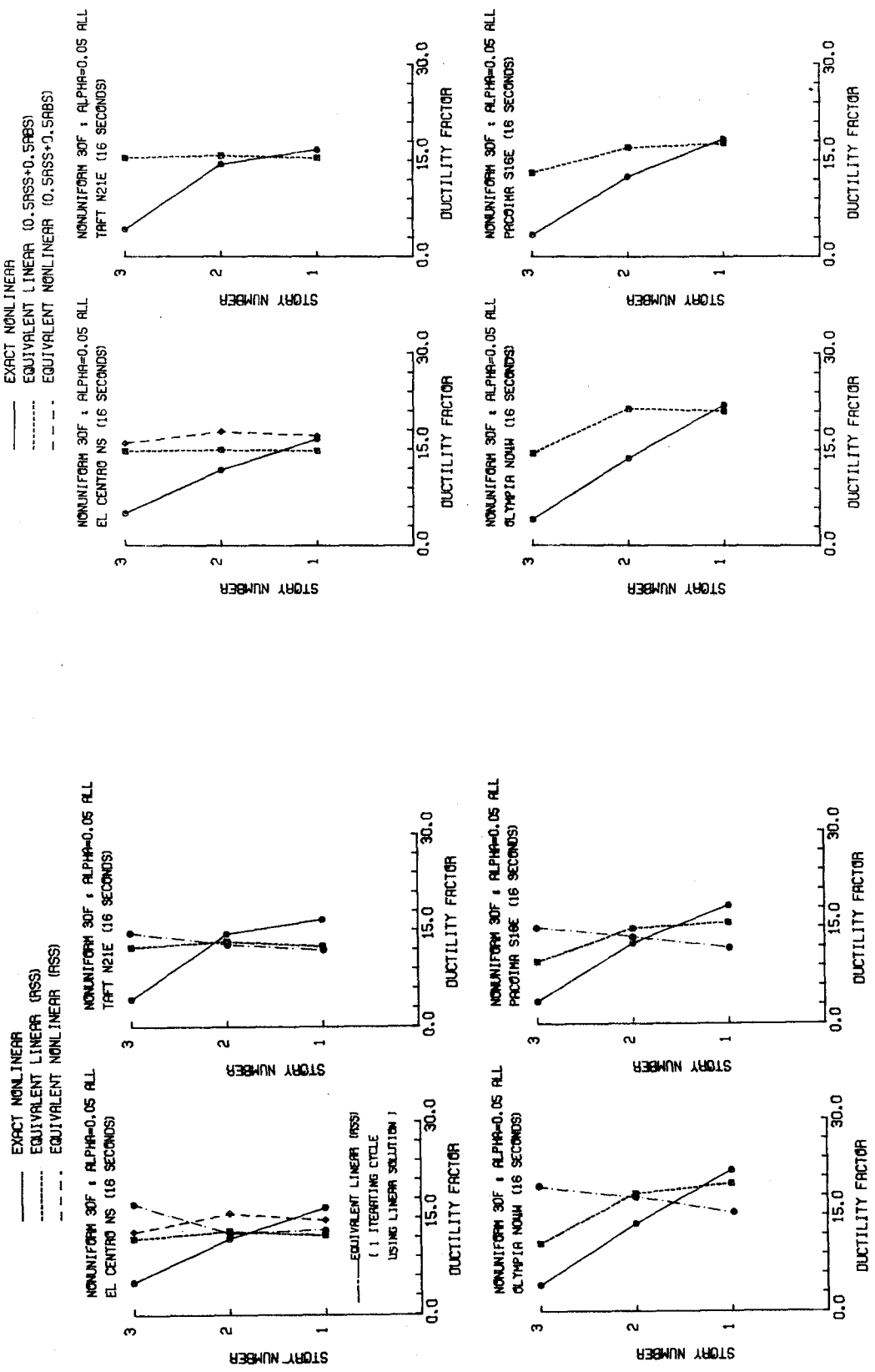

FIGURE 5.35 COMPARISON OF EXACT AND APPROXIMATE STORY DUCTILITIES (UNDAMPED NONUNIFORM BILINEAR 3DF SYSTEMS, α_e = 0.05, YIELD LEVEL 3)

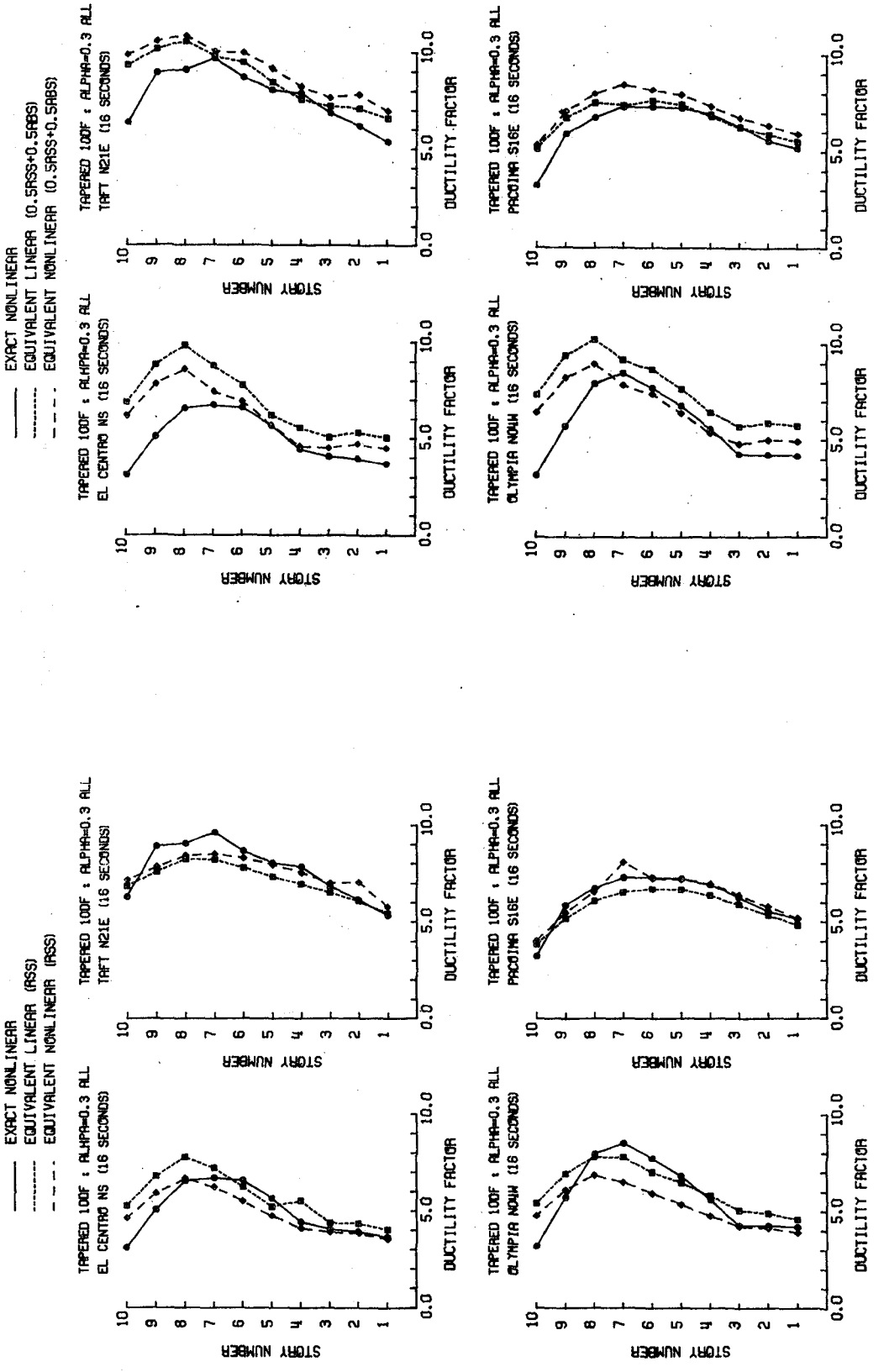

FIGURE 5.36 COMPARISON OF EXACT AND APPROXIMATE STORY DUCTILITIES (UNDAMPED TAPERED BILINEAR 10DF SYSTEMS, α_e = 0.3, YIELD LEVEL 2)

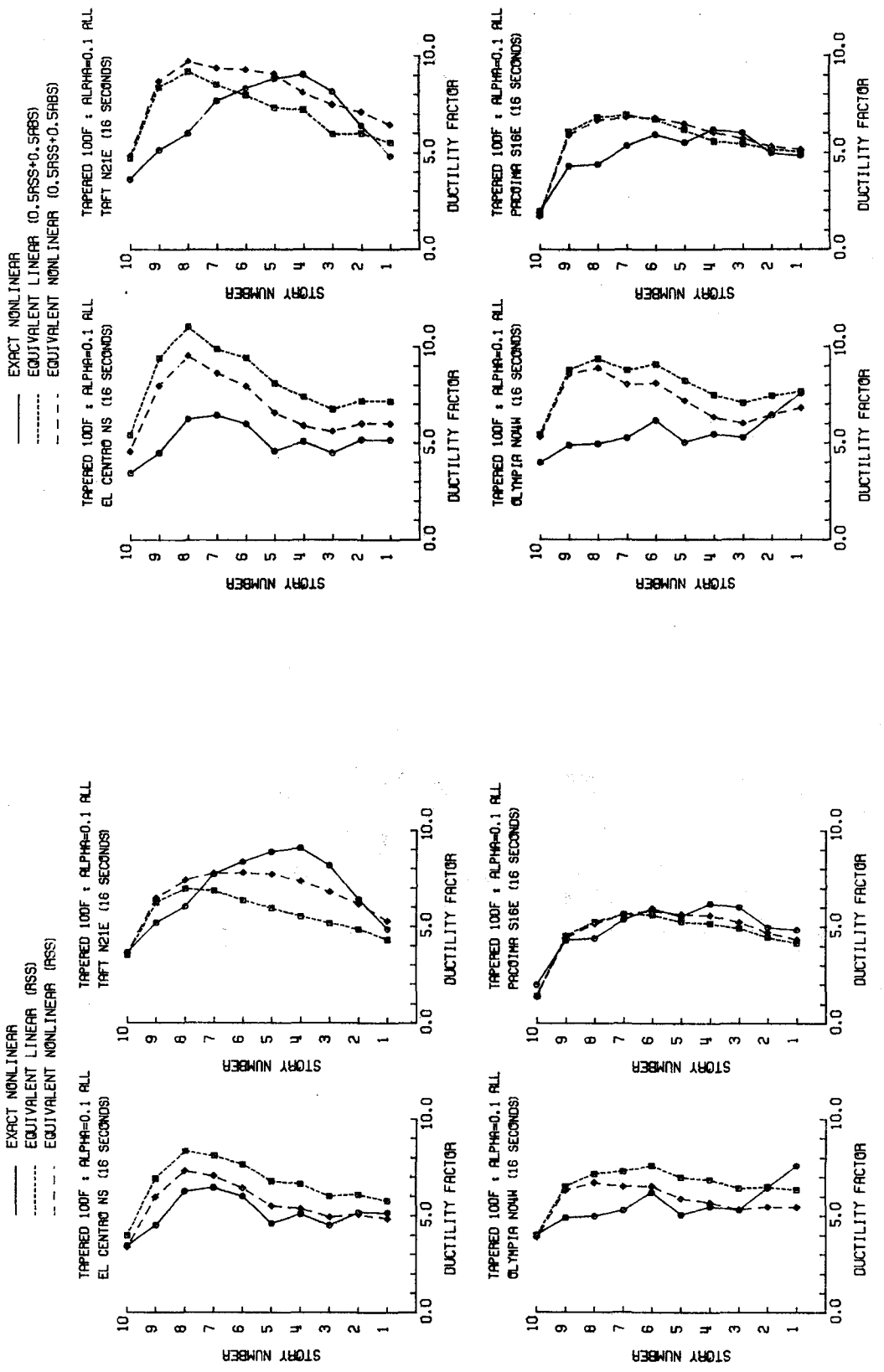

FIGURE 5.37 COMPARISON OF EXACT AND APPROXIMATE STORY DUCTILITIES (UNDAMPED TAPERED BILINEAR 10DF SYSTEMS, α_e = 0.1, YIELD LEVEL 2)

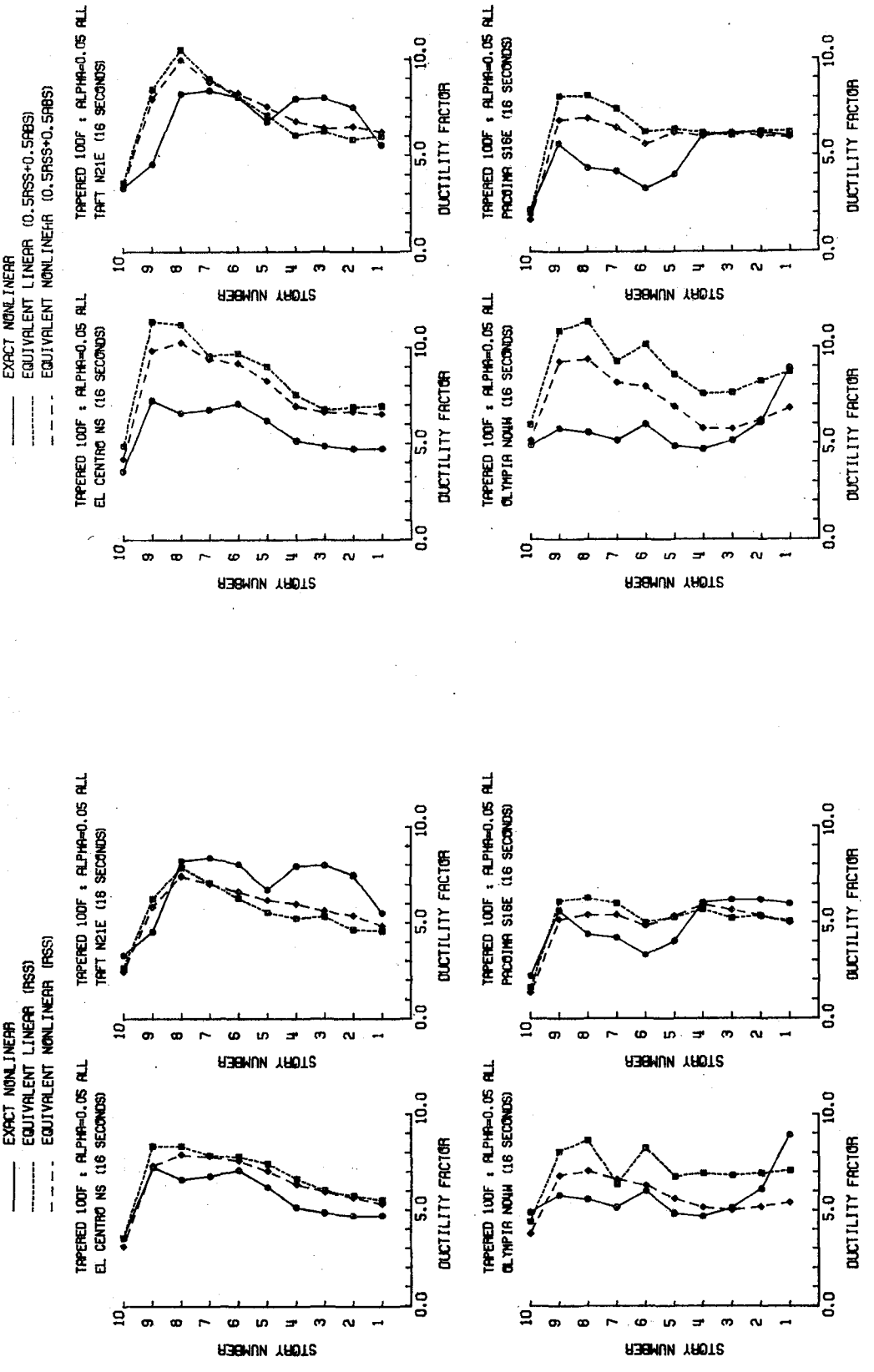

FIGURE 5.38 COMPARISON OF EXACT AND APPROXIMATE STORY DUCTILITIES (UNDAMPED TAPERED BILINEAR 10DF SYSTEMS, α_e = 0.05, YIELD LEVEL 2)

APPENDIX A

NOTATION

The following symbols are used in this study:

A = response amplitude

A_n = modal response amplitude

A_{n_0} = modal response amplitude in elastic mode shape coordinates

$[B]_e$ = element strain-displacement relation matrix of order (SXM)

c = system damping coefficient

c_{eq} = equivalent linear damping coefficient

$\overline{C}_e$ = element equivalent linear stiffness defined in Eq. (2.38c) or (2.41b)

$\overline{C}_n$ = modal equivalent linear stiffness defined in Eq. (2.48a)

$\overline{C}(A)$ = equivalent linear stiffness defined in Eq. (2.24e) or (2.27a)

$[C]$ = system damping coefficient matrix of order (NXN)

$[C]_{eq}$ = equivalent linear damping coefficient matrix of order (NXN)

e = element index

E_e = element strain amplitude

E_{en} = element strain amplitude in mode n

f = frequency in cps

f_n = modal nonlinear force

f_0 = elastic natural frequency in cps

$\{f\}_e$ = element hysteretic restoring force vector of order (MX1)

$\{F\}$ = hysteretic restoring force vector of order (NX1)

k_e = element stiffness

k_{eq} = equivalent linear stiffness

k_n = modal elastic stiffness

k_{neq} = modal equivalent linear stiffness

k_0 = system elastic stiffness

$\overline{k}_n$ = elastic stiffness of the nonlinear modal SDF system

$[K]$ = system stiffness matrix of order (NXN)

$[K]_e$ = element stiffness matrix of order (MXM)

$[K]_{eq}$ = equivalent linear stiffness matrix of order (NXN)

$[\tilde{K}]_e$ = element stress-strain matrix of order (SXS)

$[L]_e$ = element localizing matrix of order (MXN)

m = system mass

m_n = modal mass

m_{n_0} = modal mass defined in Eq. (2.47b)

M = number of degrees-of-freedom in element e

$[M]$ = system mass matrix of order (NXN)

n = modal index

N = number of degrees-of-freedom

$\{r\}$ = vector of order (NX1) representing the displacements resulting from a unit base displacement

R = harmonic base exciting intensity

RF = equivalent linear damping reduction factor

S = number of strain components in element e

S_0 = power spectral density of the stationary Gaussian white noise

$\overline{S}_e$ = element hysteresis parameter defined in Eq. (2.32d) or (2.41a)

$\overline{S}_n$ = modal hysteresis parameters defined in Eqs. (2.48b)

$\overline{S}(A)$ = hysteresis parameters defined in Eq. (2.24f) or (2.27b)

t = time

T_d = base excitation duration

$\{u\}$ = displacement vector relative to the base of order (NX1)

$\{\dot{u}\}$ = velocity vector relative to the base of order (NX1)

$\{\ddot{u}\}$ = acceleration vector relative to the base of order (NX1)

$\{U\}$ = displacement amplitude vector of order (NX1)

x = spring displacement

$\dot{x}$ = spring velocity

$\ddot{x}$ = spring acceleration

x_y = yield displacement

x_{y_e} = element yield displacement

$X(f)$ = complex function in frequency domain

α = bilinear hardening coefficient

α_e = element bilinear hardening coefficient

α_n = model bilinear hardening coefficient

β_{eq} = equivalent linear fraction of critical damping

β_{neq} = modal equivalent linear fraction of critical damping

ψ_e = element strain phase angle

ϕ = phase angle

ϕ_n = modal phase angle

ϕ_{n_0} = modal phase angle in elastic mode shape coordinates

ε_e = element strain

ε_{en} = element strain in mode n

$\varepsilon(x,\dot{x},t)$ = equation deficiency

$\varepsilon_n(\eta_n,\dot{\eta}_n)$ = modal equation deficiency

$\{\varepsilon\}_e$ = element strain vector of order (SX1)

η_n = normal mode displacement

$\dot{\eta}_n$ = normal mode velocity

ω = exciting circular frequency in radian/sec

ω_0 = system elastic natural circular frequency in radian/sec

ω_{eq} = equivalent linear natural circular frequency in radian/sec

ω_n = modal natural circular frequency in radian/sec

ω_{neq} = modal equivalent linear natural circular frequency in radian/sec

μ = ductility defined as the ratio of maximum displacement to yield displacement

μ_A = steady state maximum ductility

μ_A^* = pseudo-steady state maximum ductility

$\mu_{A_F}^*$ = pseudo-steady state maximum ductility for equivalent linear frequency

$\mu_{A_D}^*$ = pseudo-steady state maximum ductility for equivalent linear damping

μ_s = stationary rms peak ductility

μ_z = maximum ductility; zero-start

μ_{σ_A} = steady state rms ductility

μ_{σ_s} = stationary rms ductility

$\theta_n = \omega t + \phi_n$

σ_x^2 = mean squared displacement

$\sigma_{\dot{x}}^2$ = mean squared velocity

$\{\sigma_{en}\}$ = element stress vector in mode n of order (SX1)

$\{\sigma\}_e$ = element stress vector of order (SX1)

ξ = system fraction of the critical damping

ξ_n = fraction of the modal critical damping

$\{\gamma\}$ = displacement phase angle vector of order (NX1)

$\{\Phi_n\}$ = effective mode shape

$\{\Phi_{n_0}\}$ = elastic mode shape

$[\Phi]$ = effective mode shape matrix

Γ_n = modal participation factor

Γ_{neq} = modal equivalent linear participation factor

$[\ ]^T$ = transpose of a matrix

Δ = change in quantity

APPENDIX B

FOURIER TRANSFORMATION

B.1 Introduction

This appendix briefly describes the Fourier transformation techniques used in this study. Details may be found in Ref. [3].

B.2 Fourier Transforms

The Fourier integral of a complex signal x(t) (or real signal if the imaginary terms vanish) can be formed as

$$X(f) = \int_{-\infty}^{\infty} x(t)\, e^{-i2\pi ft}\, dt \qquad (B.1)$$

where X(f) is a complex function in the frequency domain, f is frequency, t is time, and $i = \sqrt{-1}$.

The function X(f) is the Fourier transform of x(t) if the integral in Eq. (B.1) exists for every real value of f. The function x(t) can be obtained from X(f) by the inversion formula

$$x(t) = \int_{-\infty}^{\infty} X(f)\, e^{i2\pi ft}\, df \qquad (B.2)$$

The function x(t) and X(f) in Eqs. (B.1) and (B.2) are known as a Fourier transform pair because the frequency function can be derived from the time function or vice versa by equivalent processes. A necessary condition for the existence of the Fourier transforms is that

$$\int_{-\infty}^{\infty} |x(t)|\, dt \qquad (B.3)$$

be finite. Equation (B.2) gives x(t) every point at which it is continuous. If x(t) is discontinuous at $t = t_0$, Eq. (B.2) gives a value equal to the average of $x(t=t_0^-)$ and $x(t=t_0^+)$.

The time domain responses, x(t), as used in Chapter 3 are real. Then the real part of X(f) is an even function of frequency and the imaginary part of X(f) is an odd function of frequency. The even part of x(t) and the real part of X(f) are cosine transforms of each other while the odd part of x(t) and the imaginary part of X(f) are negative sine transforms of each other. X(-f) is the complex conjugate of X(f).

More details regarding the theory of Fourier transforms can be found in mathematical texts; for example, Ref. [29].

C.3 Discrete Fourier Transforms

In many practical situations such as the earthquake engineering problem, the time domain response, x(t), is only nonzero over a finite interval.

$$\begin{aligned} x(t) &= x(t) && 0 \leq t \leq T \\ &= 0 && \text{elsewhere} \end{aligned} \tag{B.4}$$

Equation (B.1) then becomes

$$X(f) = \int_0^T x(t)^{-i2\pi ft}\, dt \tag{B.5}$$

where T is the maximum time duration used in x(t).

If the duration (0, T) is discretized into N equal intervals, the time interval, Δt, becomes

$$\Delta t = \frac{T}{N} \tag{B.6}$$

Equation (B.5), in discrete form, becomes

$$X_K \equiv X(k\Delta f) = \Delta t \sum_{j=0}^{N-1} x(j\Delta t)\, \exp(-i\ell\pi\, jk/N); \quad k = 0,1,2,\ldots, N-1 \qquad (B.7)$$

where Δf is the frequency interval

$$\Delta f = \frac{1}{N\Delta t} \qquad (B.8)$$

and $x(j\Delta t)$, $j = 0,1,\ldots, N-1$ are sampled values of the signal $x(t)$.

The maximum frequency is

$$f_{max} = N\Delta f = \frac{1}{\Delta t} \qquad (B.9)$$

The frequency interval $(0, \frac{1}{2\Delta t})$ contains all the information about the discrete Fourier transform X_k since X_k is the complex conjugate of X_{N-k}. The frequency $\frac{1}{2\Delta t}$ is known as the Nyquist frequency, f_{max}.

The inverse of the Fourier transform in Eq. (B.2) may also be assumed that

$$\begin{aligned} X(f) &= X(f) && 0 \leq f \leq f_{max} \\ &= 0 && \text{elsewhere} \end{aligned} \qquad (B.10)$$

Equation (B.2) becomes

$$x(t) = \int_0^{f_{max}} X(f)\, e^{i2\pi ft}\, df \qquad (B.11)$$

Equation (B.11) may be written as a discrete Fourier transform as follows.

$$x(k\Delta t) = \Delta f \sum_{j=0}^{N-1} X(j\Delta t)\, \exp(i2\pi jk/N); \; k = 0,1,2,\ldots, N-1 \qquad (B.12)$$

B.4 Fast Fourier Transform Analysis

The discrete Fourier transforms in Eqs. (B.7) or (B.12) can be effectively calculated by the Fast Fourier Transformation algorithms (FFT). The algorithms significantly reduce the time in computation of the Fourier transforms if the number of data points, $N = 2M$, where M is an integer. The details of the FFT algorithms are beyond the scope of this brief summary and may be found in Ref. [3].

B.5 Accuracy of the Discrete Fast Fourier Transform Analysis

Some of the important factors influencing the accuracy of the FFT procedure are briefly discussed in this section.

B.5.1 Aliasing -- Aliasing occurs when high frequency components in the signal cannot be distinguished from lower frequency components because the sampling interval Δt is too large. It can be shown that frequencies $\frac{m}{\Delta t} \pm f_0$ where $m = 1,2,\ldots$ cannot be distinguished from frequencies f_0, when the signal is sampled at intervals Δt.

The problem can be avoided by selecting a time interval Δt such that the frequency range $(0, f^*_{max})$ contains the significant frequency content of the signal.

B.5.2 Insignificant Low Frequency Content -- Extremely low frequency content in a time response, $x(t)$, can be detected only if the time duration is very long. The lowest significant frequency in the discrete Fourier transform is $\frac{1}{T}$ where T is the time duration. The frequency interval at which the transform is calculated is also $1/T$, so that adequate determination of the shape of the transform in the frequency domain places some

constraints on the minimum duration of signal required.

B.5.3 Interval Selection -- The time and frequency intervals are related to the number of points used in the discrete Fourier transforms as shown by Eq. (B.8). For a fixed number of points, it is impossible to obtain a fine interval for both time and frequency. Since the number of data points N is limited by computational cost, a compromise must be made between the conflicting objectives of obtaining both small time and frequency intervals.

B.5.4 Leakage -- The discrete Fourier transforms use a finite time duration, T. This is equivalent to multiplying an actual time function, x(t), with a finite length rectangular "boxcar function" which is unity within the time duration used and is zero elsewhere. This creates an undesirable spreading effect in the frequency domain called "leakage". To minimize the leakage effect, the time function, x(t), is multipled by a bell-shaped window. A simple window introduced by Hanning is used. The window has a form in the time domain as follows.

$$\begin{aligned} d_c(t) &= 0 && \text{for } t < 0 \\ &= \frac{1}{2}\left[1 - \cos\frac{2\pi t}{T}\right] && \text{for } 0 \leq t \leq T \\ &= 0 && \text{for } t > T \end{aligned} \qquad \text{(B.13)}$$

which is equivalent to smoothing the Fourier modulus spectrum (called Hanning Smoothing) in the frequency domain as follows.

$$|X_i(f)|_{\text{smoothed}} = \frac{1}{4}|X_{i-1}(f)| + \frac{1}{2}|X_i(f)| + \frac{1}{4}|X_{i+1}(f)| \qquad \text{(B.14)}$$

B.5.5 Periodic Effect -- The Fourier transforms computed by the FFT technique are the Fourier transforms of the periodically extended time function rather than the true time function. To minimize the errors due to the period effect in a damped system, the input time function may be extended by inclusion of a significant interval of zeros at the end. This is to let the periodic effect damp away and not interfere with the next cycle.

B.6 Computed Nonlinear Transfer Functions by Discrete FFT

The nonlinear transfer functions computed by the discrete FFT technique in Chapter 3 used the methods mentioned in the previous sections. The discrete Fourier transforms in Eq. (B.7) were done using the FFT2 and FFRDR2 library subroutines provided by the IMSLIB.

For the pulse-like input shown in Fig. D.5, the time increment used was 0.01 second with 10 seconds of response. A band of zeros were added at the end so that the total number of points, $N = 2^{12}$. In this case, the Nyquist frequency, f^*_{max}, was 50 cps which is high enough to minimize the effects of aliasing and periodicity. The frequency interval was 0.0244 cps which was small enough for accurate determination of the transfer functions in the frequency domain. Five cycles of Hanning smoothing were performed. This smoothed the nonlinear transfer functions but also resulted in more spreading out.

For the earthquakes as shown in Figs. D.1 to D.4, the time increment used was 0.02 seconds with 18 seconds of response. A band of zeros was added at the end so that the total number of points, $N = 2^{12}$. The Nyquist frequency, f^*_{max}, was 50 cps. The frequency interval was 0.0122 cps, and 5 cycles of Hanning smoothing were performed.

APPENDIX C

PERTURBATION METHOD FOR APPROXIMATE DETERMINATION OF EQUIVALENT LINEAR MODE SHAPES

C.1 Introduction

Both approximate modal analysis procedures summarized in Chapter 4 use the "equivalent linear mode shapes" of the MDF system to decompose the response history.

These equivalent linear mode shapes are the mode shapes of a linear MDF system which has element stiffnesses equal to the equivalent linear stiffnesses $\overline{C}_e$ determined in Chapter 3.

In the iterative procedure, the equivalent linear stiffnesses change at every cycle of iteration. To avoid solving a new eigenvalue problem during every iteration cycle, a perturbation method is used which approximately determines the equivalent linear mode shapes as functions of the element stiffness change, $\Delta k_e = k_e - C_e$. The mode shapes determined by the perturbation method are termed "modified mode shapes". since they are determined by modifying the elastic mode shapes. Details of the perturbation method may be found in Ref. [24].

The procedure is straightforward and is briefly outlined in the following paragraphs.

C.2 Perturbation Method

Consider the eigenvalue problem for the elastic MDF system as given by Eq. (2.4) as follows

$$\left[[K]^{(0)} - \omega_n^{2\,(0)}\,[M]\right]\,\{\Phi_n\}^{(0)} = \{0\} \qquad (C.1)$$

where $\{\Phi_n\}$ and ω_n are the orthonormal elastic mode shapes and modal natural circular frequency, respectively. The superscript (0) denotes the elastic values. It is assumed in the following development that the elastic frequencies are distinct from each other.

The stiffness matrix of the equivalent linear system, assembled from the element equivalent linear stiffnesses, $\bar{C}_e$, is denoted by $[K]_{EL}$.

The equivalent linear stiffness matrix can be expressed as

$$[K]_{EL} = \sum_e [L]_e^T [B]_e^T \tilde{[K]}_e [B]_e [L]_e \tag{C.2a}$$

in which

$$\tilde{[K]}_e = \bar{C}_e \tag{C.2b}$$

for a single strain component. The summation over the elements represents a standard stiffness assembly. The notation in Chapter 2 is used.

Let the stiffness change from the elastic system to the equivalent linear system be denoted by $\varepsilon[K]^{(1)}$. Then the equivalent linear stiffness matrix becomes

$$[K]_{EL} = [K]^{(0)} + \varepsilon[K]^{(1)} \tag{C.3}$$

The eigenvalue problem for the equivalent linear MDF system becomes

$$\left[[K]^{(0)} + \varepsilon[K]^{(1)} - \omega_{n_{EL}}^2 [M]\right]\{\Phi_n\}_{EL} = \{0\} \tag{C.4}$$

Rather than solve the eigenvalue problem given by Eq. (C.4) directly, the solution is expanded as a power series in ε, in which the first terms (for $\varepsilon = 0$) are the elastic values.

$$\{\Phi_n\}_{EL} = \{\Phi_n\}^{(0)} + \varepsilon\{\Phi_n\}^{(1)} + \varepsilon^2\{\phi_n\}^{(2)} + \ldots \tag{C.5}$$

$$\omega_{n_{EL}}^2 = \omega_n^{2(0)} + \varepsilon\omega_n^{2(1)} + \varepsilon^2\omega_n^{2(2)} + \ldots \tag{C.6}$$

Equations (C.5) and (C.6) are substituted into Eq. (C.4) and the coefficients of each power of ε are grouped and set equal to zero. This procedure yields the following system of equations.

$$\left[[K]^{(0)} - \omega_n^{2(0)}[M]\right]\{\Phi_n\}^{(0)} = \{0\} \tag{C.7}$$

$$\left[[K]^{(1)} - \omega_n^{2(1)}[M]\right]\{\Phi_n\}^{(0)} + \left[[K]^{(0)} - \omega_n^{2(0)}[M]\right]\{\Phi_n\}^{(1)} = \{0\} \tag{C.8}$$

$$-\omega_n^{2(2)}[M]\{\Phi_n\}^{(0)} + \left[[K]^{(1)} - \omega_n^{2(1)}[M]\right]\{\Phi_n\}^{(1)} + \left[[K]^{(0)} - \omega_n^{2(0)}[M]\right]\{\Phi_n\}^{(2)} = \{0\} \tag{C.9}$$

The mode shape changes $\{\Phi_n\}^{(1)}$, $\{\Phi_n\}^{(2)}$,... are now expressed as linear combinations of the elastic mode shapes, with constants $A_{kn}^{(1)}$, $A_{kn}^{(2)}$,... which are to be determined. Thus

$$\{\Phi_n\}^{(i)} = \sum_{k=1}^{N} A_{kn}^{(i)} \{\Phi_k\}^{(0)} \quad ; \; i = 1,2,\ldots \tag{C.10}$$

To determine the first order frequency changes, Eq. (C.8) is premultiplied by $\{\Phi_n\}^{T(0)}$. Using Eq. (C.10), and the orthogonality conditions for elastic mode shapes, Eq. (C.8) becomes

$$\omega_n^{2(1)} = \{\phi_n\}^{T(0)}[K]^{(1)}\{\phi_n\}^{(0)} \tag{C.11}$$

When combined with Eqs. (C.3) and (C.8), Eq. (C.11) gives the first order expression for equivalent linear frequency.

$$\omega_{n_{EL}}^2 \approx \omega_n^{2(0)} + \varepsilon\omega_n^{2(1)}$$

$$= \{\Phi_n\}^{T(0)}[K]_{EL}\{\Phi_n\}^{(0)} \quad \text{(first-order)} \tag{C.12}$$

Equation (C.12) is just the Rayleigh quotient expression for frequency using the elastic mode shapes and the equivalent linear stiffness matrix.

To determine the first-order changes in mode shapes, Eq. (C.8) is premultiplied by $\{\Phi_k\}^{T(0)}$ where $k \neq n$. Equation (C.10) and the orthogonality conditions for the elastic mode shapes yields

$$A_{kn}^{(1)} = \frac{\{\Phi_k\}^{T(0)}[K]^{(1)}\{\Phi_n\}^{(0)}}{\omega_n^{2(0)} - \omega_k^{2(0)}} \quad ; \; k \neq n \tag{C.13}$$

The coefficient $A_{nn}^{(1)}$ is arbitrary and is taken as zero, since $\{\Phi_n\}^{(0)}$ is already present in $\{\Phi_n\}_{EL}$. Thus

$$A_{nn}^{(1)} = 0 \tag{C.14}$$

It is convenient to relate the changes in mode shapes and frequencies directly to the changes in element stiffnesses. The stiffness matrix change $\varepsilon[K]^{(1)}$ can be expressed in terms of element stiffness changes as

$$\varepsilon[K]^{(1)} = -\sum_e [L]_e^T[B]_e^T[\tilde{K}_e - \bar{C}_e][B]_e[L]_e \tag{C.15}$$

Thus, the numerator of the expression for $A_{kn}^{(1)}$ in Eq. (C.13) can be written as

$$\varepsilon\{\Phi_k\}^{T(0)}[K]^{(1)}\{\Phi_n\}^{(0)} = -\sum_e \varepsilon_{ek}^{(0)} (k_e - \bar{C}_e) \varepsilon_{en}^{(0)} \tag{C.16}$$

where ε_{ek} is the element strain in mode k, and k_e is the element elastic stiffness. Let the strain energy change given by Eq. (C.16) be denoted by

$$\Delta E_{kn} = -\sum_e \varepsilon_{ek}^{(0)} (k_e - \bar{C}_e) \varepsilon_{en}^{(0)} \tag{C.17}$$

$$= \sum_e \varepsilon_{ek}^{(0)} \bar{C}_e \varepsilon_{en}^{(0)} \quad \text{when} \quad k \neq n$$

Note that $\Delta E_{kn} = \Delta E_{nk}$

Combining Eqs. (C.5), (C.13), (C.16) and (C.17), the first-order approximations for the equivalent linear mode shapes are

$$\{\Phi_n\}_{EL} \simeq \{\Phi_n\}^{(0)} + \varepsilon\{\Phi_n\}^{(1)}$$

$$\simeq \{\Phi_n\}^{(0)} + \sum_{\substack{k=1 \\ k\neq n}}^{M} \frac{\Delta E_{nk}}{\omega_n^{2(0)} - \omega_k^{2(0)}} \{\Phi_k\}^{(0)} \qquad \text{(first-order)} \qquad \text{(C.18)}$$

where ΔE_{nk} is given by Eq. (C.17) and M is the number of modes considered.

Equation (C-12) for the first-order frequency change becomes

$$\omega_{n_{EL}}^2 \simeq \sum_e \varepsilon_{en}^{2(0)} \bar{C}_e \qquad \text{(first-order)} \qquad \text{(C.19)}$$

A more accurate expression for equivalent linear frequency can be obtained by using the mode shapes given by Eq. (C.18) in a Rayleigh quotient expression

$$\omega_{n_{EL}}^2 \simeq \sum_e \varepsilon_{en}^2 \bar{C}_e \qquad \text{(C.20)}$$

which is consistent with development in Chapter 2.

Equations (C.18) and (C.20) are the first-order modified mode shapes and frequencies in terms of element equivalent linear stiffnesses. These expressions are sufficiently accurate for most cases, especially when the yielding in the structure is relatively uniform.

If more accuracy is required because of large localized ductilities in the structure, the second-order perturbation expansions can be used. The second-order expressions are determined by using the same procedure as defined above with Eq. (C.9).

The resulting second-order expressions for the equivalent linear mode shapes are

$$\{\Phi_n\}_{EL} \simeq \{\Phi_n\}^{(0)} + \sum_{\substack{k=1 \\ k\neq n}}^{N} \frac{\Delta E_{kn}}{\omega_n^{2(0)} - \omega_k^{2(0)}} \left[1 - \frac{\Delta E_{nn}}{(\omega_n^{2(0)} - \omega_k^{2(0)})}\right] \{\Phi_k\}^{(0)}$$

$$+ \sum_{\substack{k=1 \\ k\neq n}}^{N} \sum_{\substack{m=1 \\ m\neq n}}^{N} \frac{\Delta E_{mn}\, \Delta E_{mk}}{(\omega_n^{2(0)} - \omega_m^{2(0)})(\omega_n^{2(0)} - \omega_k^{2(0)})} \{\Phi_k\}^{(0)} \qquad (C.21)$$

and the equivalent linear frequencies are again determined from the Rayleigh quotient, now using the modal strains from the second-order approximation,

$$\omega_{n_{EL}}^2 \simeq \sum_e \varepsilon_{en}^2\, \bar{C}_e \qquad (C.22)$$

C.3 Accuracy of the Perturbation Procedure

A number of 3DF systems with uniform mass and elastic stiffness distributions were analyzed to study the accuracy of the modified mode shapes and frequencies calculated by the perturbation method. The stiffnesses of the systems were reduced in several combinations as shown in Table C.1.

For each system, the mode shapes and frequencies are shown for the unaltered stiffnesses, and for the altered stiffnesses using (1) the first-order approximation, Eqs. (C.18) and (C.20), (2) the second-order approximation, Eqs. (C.21) and (C.22), and (3) an exact eigenvalue solution.

It is noted that the first-order approximation gives good estimates of the exact equivalent linear mode shapes and frequencies even when there

are rather severe stiffness changes. In all numerical calculations reported in this study, the first-order approximation was used.

TABLE C.1 MODIFIED MODE SHAPES AND FREQUENCIES

Uniform System with 70% Reduction in the First Story Stiffness

	Mode No.	Frequency (cps) Orig	Exact	Approx	1st Mode Shape Orig	Exact	Approx	2nd Mode Shape Orig	Exact	Approx	3rd Mode Shape Orig	Exact	Approx
1st order	1	.071	.046	.047	.3280	.4857	.4423	.7370	.7459	.7840	.5910	.4558	.4362
	2	.198	.171	.171	.5910	.5902	.5939	.3280	.1049	.1187	-.7370	-.8004	-.8086
	3	.287	.278	.278	.7370	.6448	.6720	-.5910	-.6578	-.6094	.3280	.3893	.3949
2nd order	1	.071	.046	.046	.3280	.4857	.4818	.7370	.7459	.7854	.5910	.4558	.4763
	2	.198	.171	.171	.5910	.5902	.5921	.3280	.1049	.1011	-.7370	-.8004	-.7933
	3	.287	.278	.278	.7370	.6448	.6453	-.5910	-.6578	-.6107	.3280	.3893	.3793

Uniform System with 70% Reduction in the Second Story Stiffness

	Mode No.	Frequency (cps) Orig	Exact	Approx	1st Mode Shape Orig	Exact	Approx	2nd Mode Shape Orig	Exact	Approx	3rd Mode Shape Orig	Exact	Approx
1st order	1	.071	.052	.054	.3280	.1652	.2386	.7370	.9554	.8651	.5910	.2448	.4394
	2	.198	.180	.182	.5910	.6573	.6289	.3280	.0784	.1902	-.7370	-.7495	-.7424
	3	.287	.237	.234	.7370	.7353	.7400	-.5910	-.2847	-.4642	.3280	.6151	.5057
2nd order	1	.071	.052	.052	.3280	.1652	.1940	.7370	.9554	.9234	.5910	.2448	.4540
	2	.198	.180	.180	.5910	.6573	.6449	.3280	.0784	.0989	.7370	-.7495	-.7433
	3	.287	.237	.234	.7370	.7353	.7392	-.5910	-.2847	-.3710	.3280	.6151	.4912

TABLE C.1 (continued)

Uniform System with 70% Reduction in the Third Story Stiffness

	Mode No.	Frequency (cps) Orig	Exact	Approx	1st Mode Shape Orig	Exact	Approx	2nd Mode Shape Orig	Exact	Approx	3rd Mode Shape Orig	Exact	Approx
1st order	1	.071	.062	.065	.3280	.2331	.2972	.7370	.5402	.4814	.5910	.8086	.8131
	2	.198	.136	.134	.5910	.4308	.5404	.3280	.6881	.6172	-.7370	-.5839	-.5793
	3	.287	.263	.263	.7370	.8718	.7872	-.5910	-.4844	-.6223	.3280	.0723	.0578
2nd order	1	.071	.062	.063	.3280	.2331	.2742	.7370	.5402	.3651	.5910	.8086	.7502
	2.	.198	.136	.139	.5910	.4308	.5032	.3280	.6881	.7042	-.7370	-.5839	-.6435
	3	.287	.263	.261	.7370	.8718	.8195	-.5910	-.4844	-.6090	.3280	.0723	.1518

Uniform System with 70%, 75%, 65% Reduction in Story Stiffnesses

	Mode No.	Frequency (cps) Orig	Exact	Approx	1st Mode Shape Orig	Exact	Approx	2nd Mode Shape Orig	Exact	Approx	3rd Mode Shape Orig	Exact	Approx
1st order	1	.071	.038	.038	.3280	.3095	.3238	.7370	.8264	.7625	.5910	.4705	.5600
	2	.198	.111	.112	.5910	.6112	.5974	.3280	.2061	.2940	-.7370	-.7641	-.7461
	3	.287	.156	.155	.7370	.7284	.7337	-.5910	-.5241	-.5764	.3280	.4413	.3603
2nd order	1	.071	.038	.038	.3280	.3095	.3203	.7370	.8264	.7947	.5910	.4705	.5810
	2	.198	.111	.111	.5910	.6112	.6020	.3280	.2061	.2492	-.7370	-.7641	-.7378
	3	.287	.156	.155	.7370	.7284	.7314	-.5910	-.5241	-.5535	.3280	.4413	.3438

APPENDIX D

CHARACTERISTICS OF GROUND EXCITATIONS

This appendix contains acceleration versus time plots and the corresponding Fourier amplitude spectra for the ground excitations used in this study. The ground motion excitations are

1. El Centro 1940-NS in Fig. D.1.
2. Taft 1952-N21E in Fig. D.2.
3. Olympia 1949-NO4W in Fig. D.3.
4. Pacoima 1971-S16E in Fig. D.4.
5. Simple pulse-like excitation in Fig. D.5.

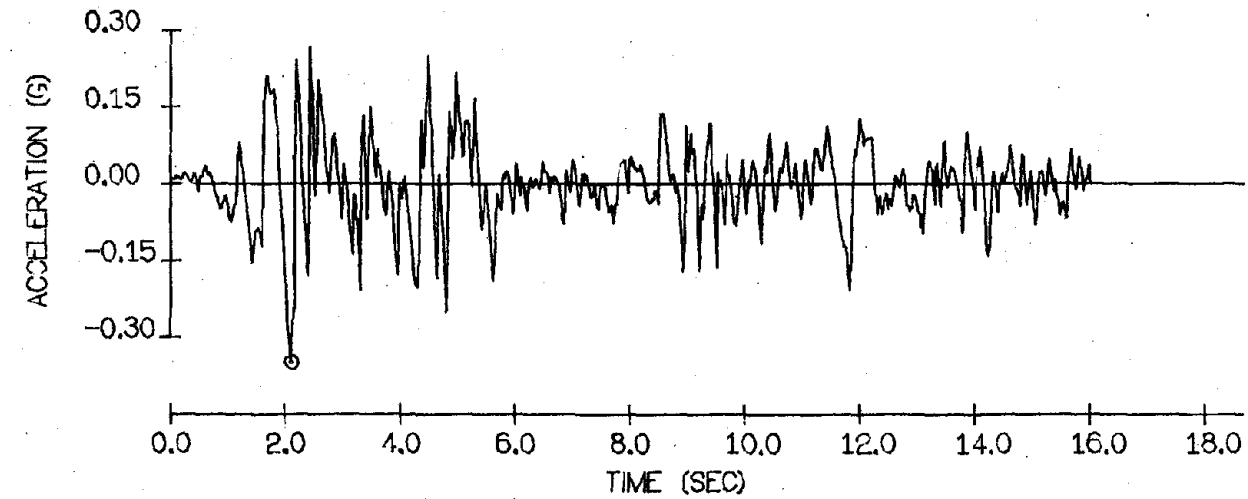

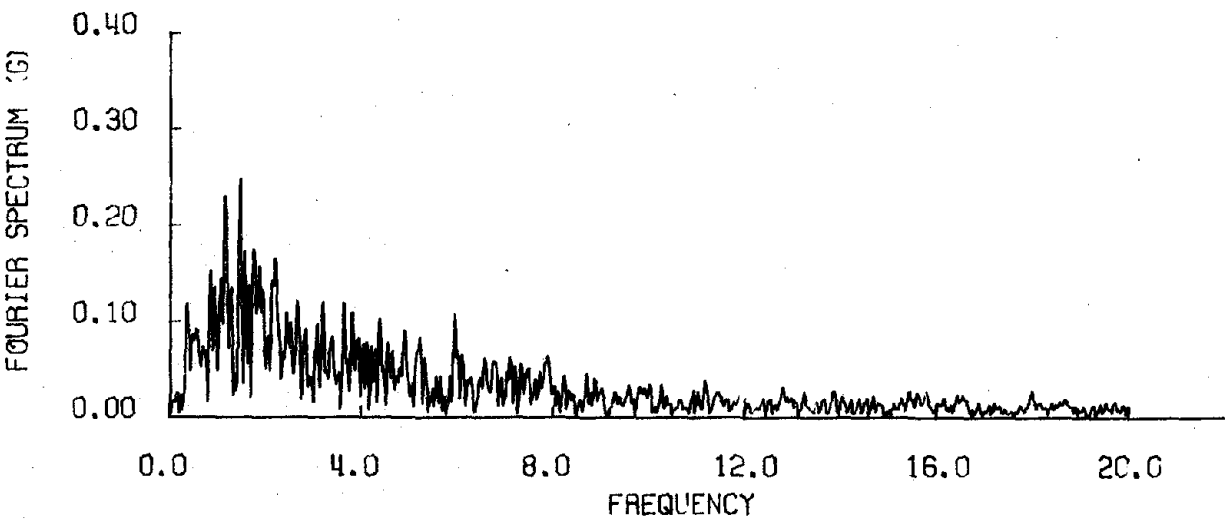

FIGURE D.1 TIME HISTORY AND FOURIER AMPLITUDE SPECTRUM
(EL CENTRO 1940-NS)

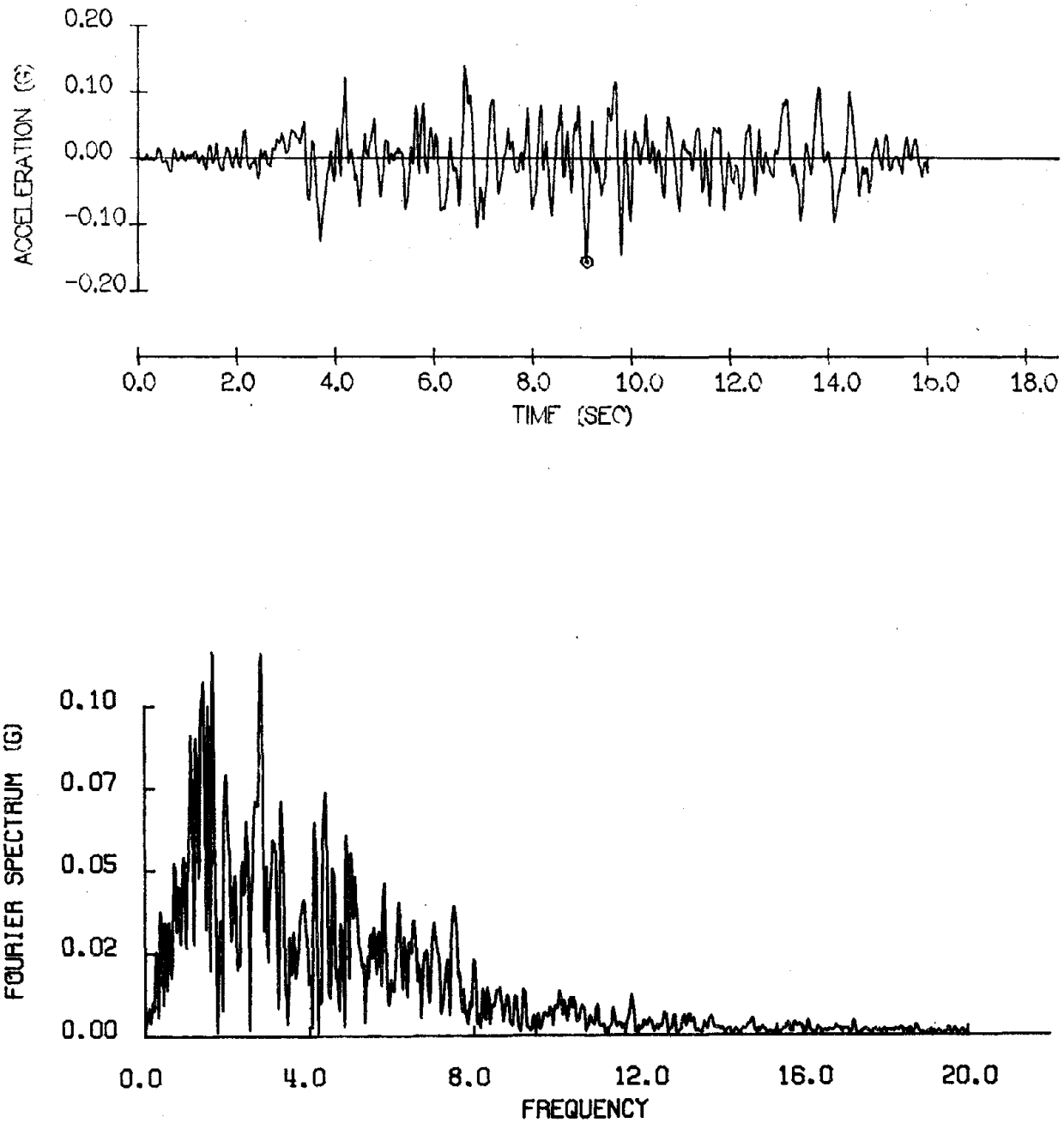

FIGURE D.2 TIME HISTORY AND FOURIER AMPLITUDE SPECTRUM
(TAFT 1952-N21E)

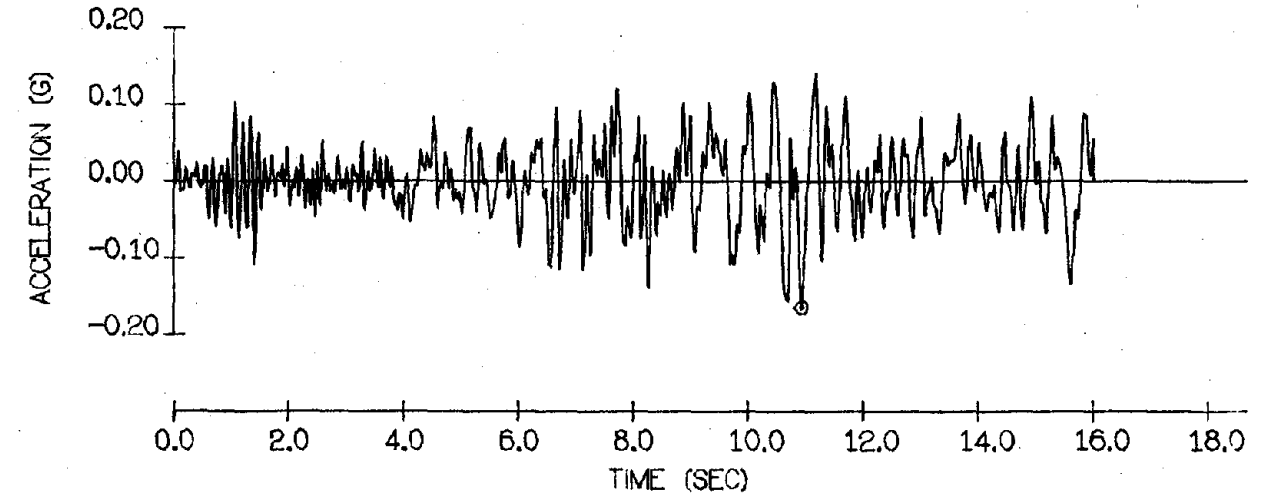

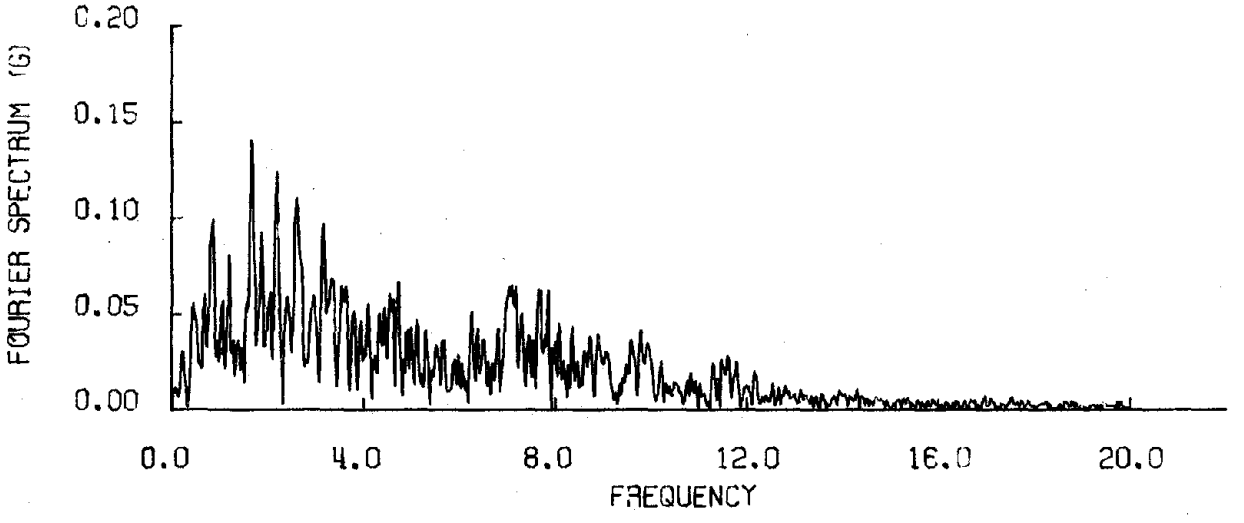

FIGURE D.3 TIME HISTORY AND FOURIER AMPLITUDE SPECTRUM
(OLYMPIA 1949-NO4W)

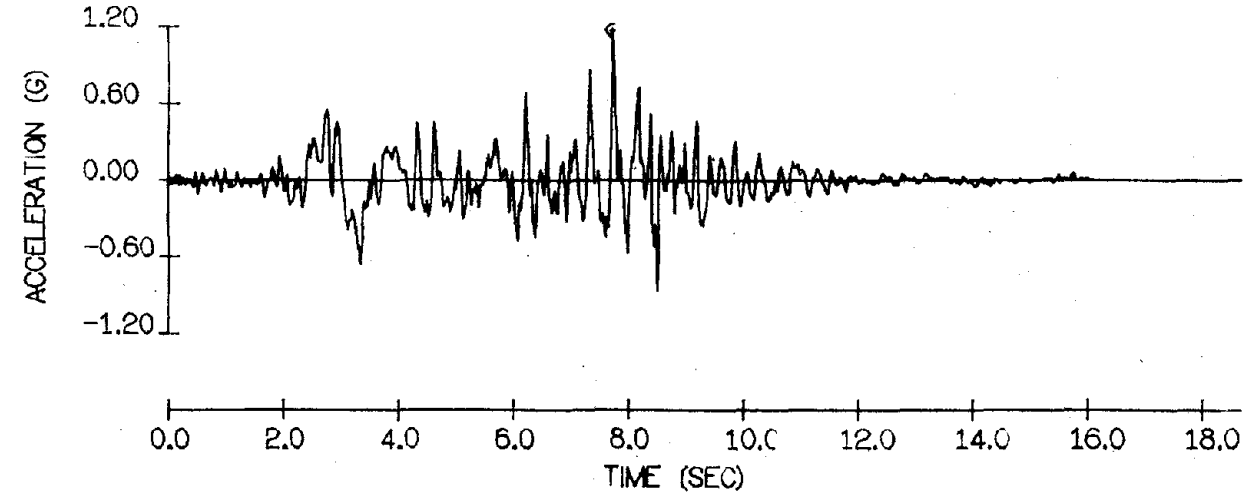

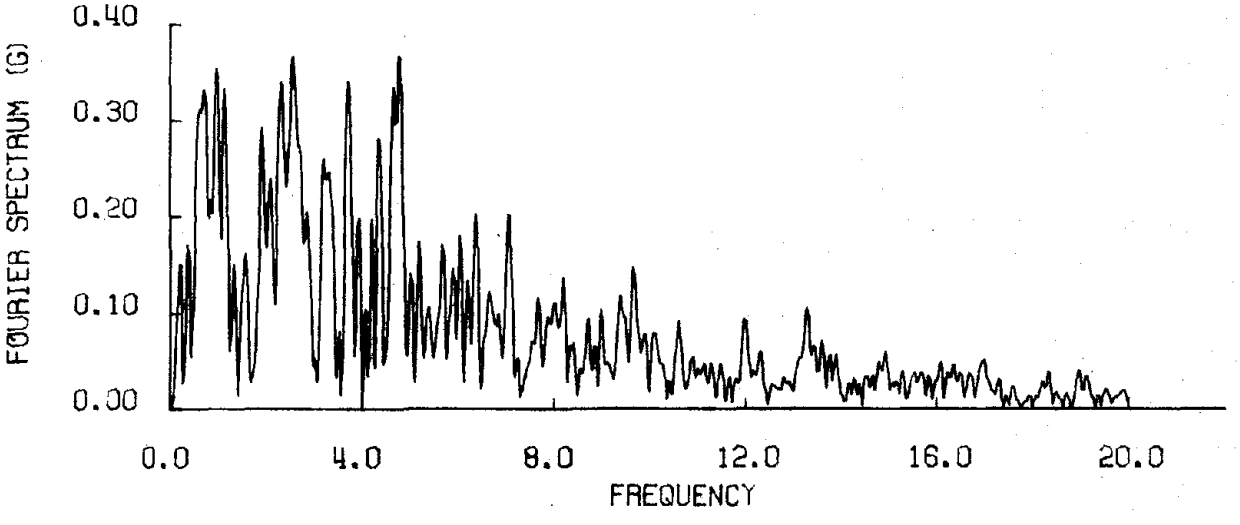

FIGURE D.4 TIME HISTORY AND FOURIER AMPLITUDE SPECTRUM
(PACOIMA 1971-S16E)

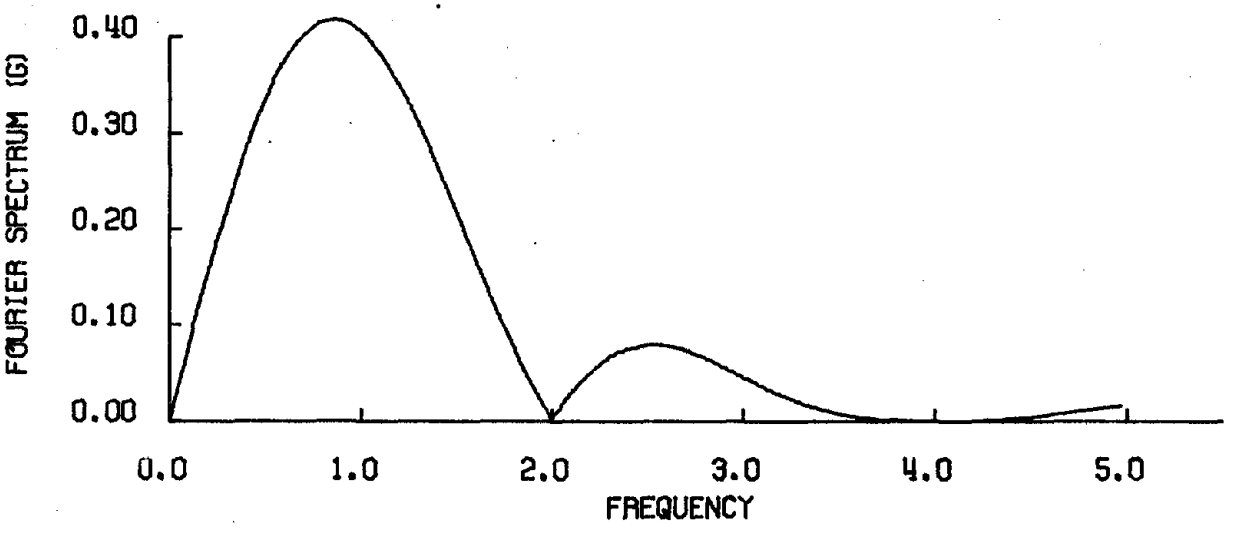

FIGURE D.5 TIME HISTORY AND FOURIER AMPLITUDE SPECTRUM
(SIMPLE PULSE-LIKE EXCITATION)

APPENDIX E

COMPARISON OF EXACT AND EQUIVALENT LINEAR RESPONSES FOR SDF AND 3DF SHEAR BEAM SYSTEMS

This appendix contains:

1. The complete results of the study on bilinear SDF systems by the equivalent linear system approach described in Section 5.2. The earthquakes and system parameters used are described in Section 5.2.1 and tabulated in Table 5.1. The approximate solutions are obtained with one cycle of iteration starting from the exact solutions. The equivalent linear system maximum relative displacements and velocities are compared with the exact solutions calculated by step-by-step numerical integration and are shown in Figs. E.1a to E.9a. Each figure shows a series of systems with the natural frequency ranging from 0.25 to 11 cps and with one value of viscous damping, ξ, and bilinear hardening, α, subjected to one earthquake excitation. Yield strengths are varied corresponding to the design yield strength spectrum in Fig. 5.1 to yield four different ductility ranges. Figures E.1a, E.2a, ..., E.9a show the maximum relative displacement response spectra while Figs. E.1b, E.2b, ..., E.9b show the corresponding maximum relative velocity response spectra.

2. The relative velocity and spring force histories corresponding to the relative displacement response histories in Figs. 5.21 to 5.26 are shown in Figs. E.10 to E.15.

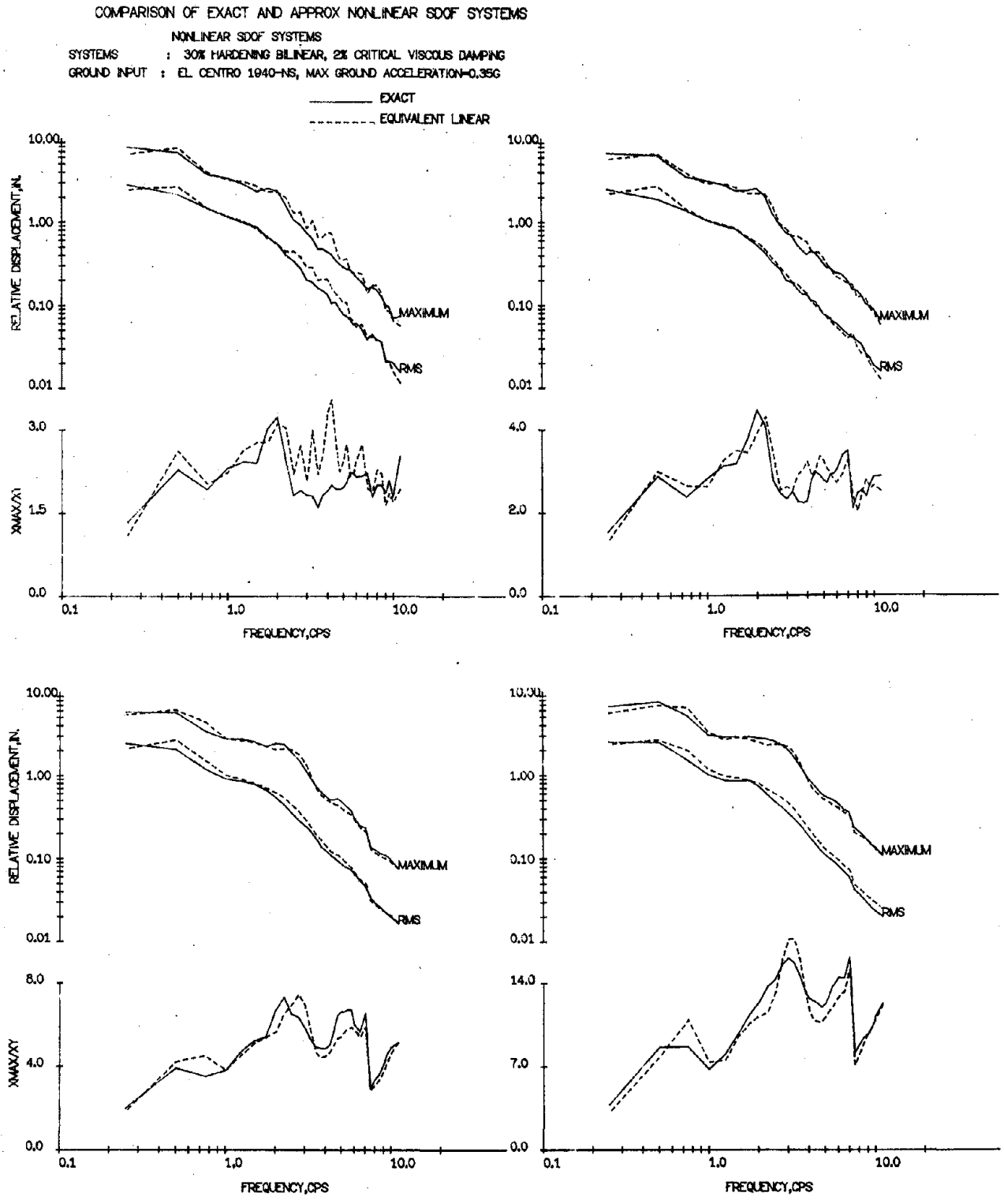

FIGURE E.1a DISPLACEMENT RESPONSE SPECTRA
(α = 0.3, ξ = 0.02, EL CENTRO 1940-NS)

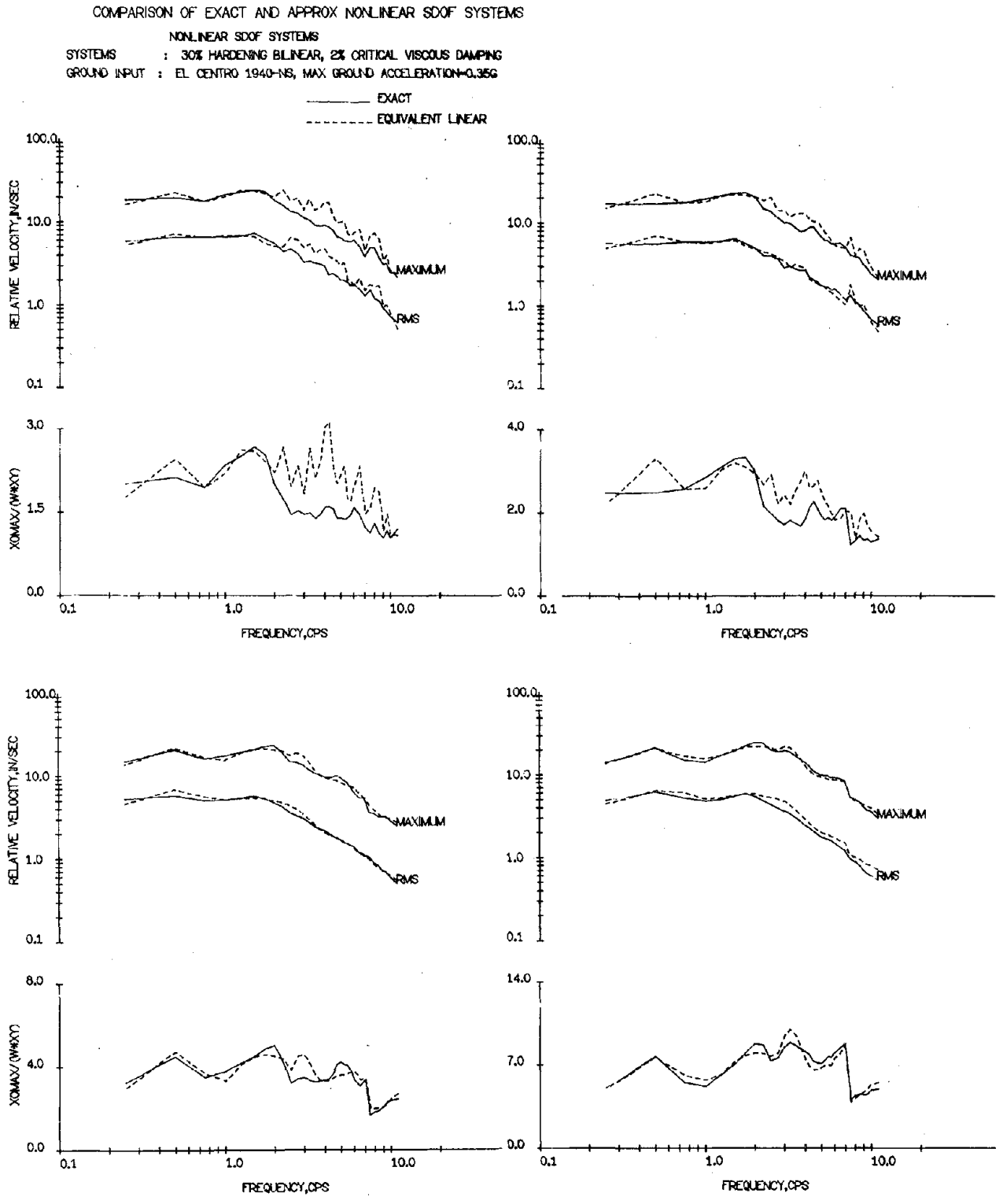

FIGURE E.1b VELOCITY RESPONSE SPECTRA
(α = 0.3, ξ = 0.02, EL CENTRO 1940-NS)

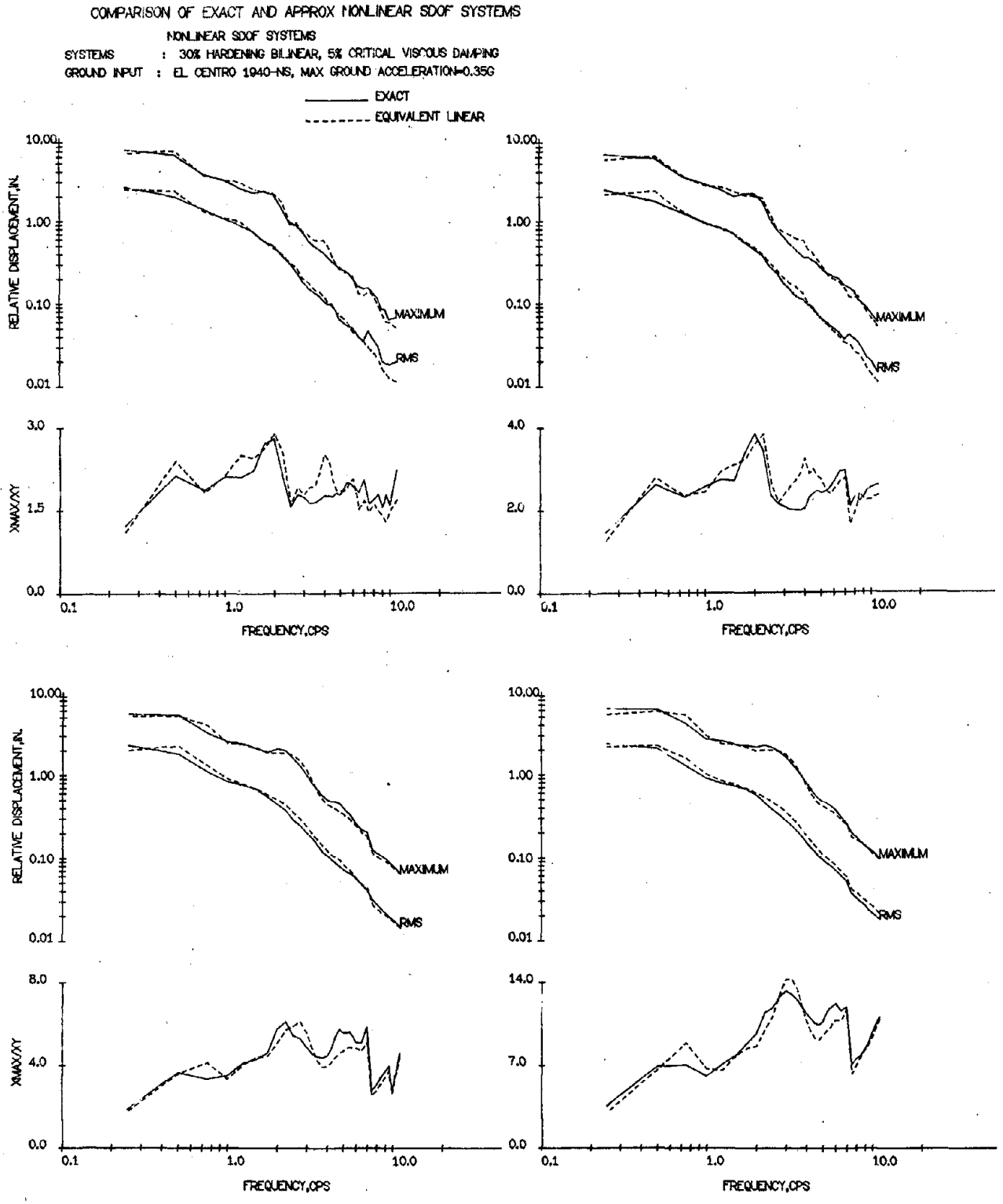

FIGURE E.2a DISPLACEMENT RESPONSE SPECTRA
(α = 0.3, ξ = 0.05, EL CENTRO 1940-NS)

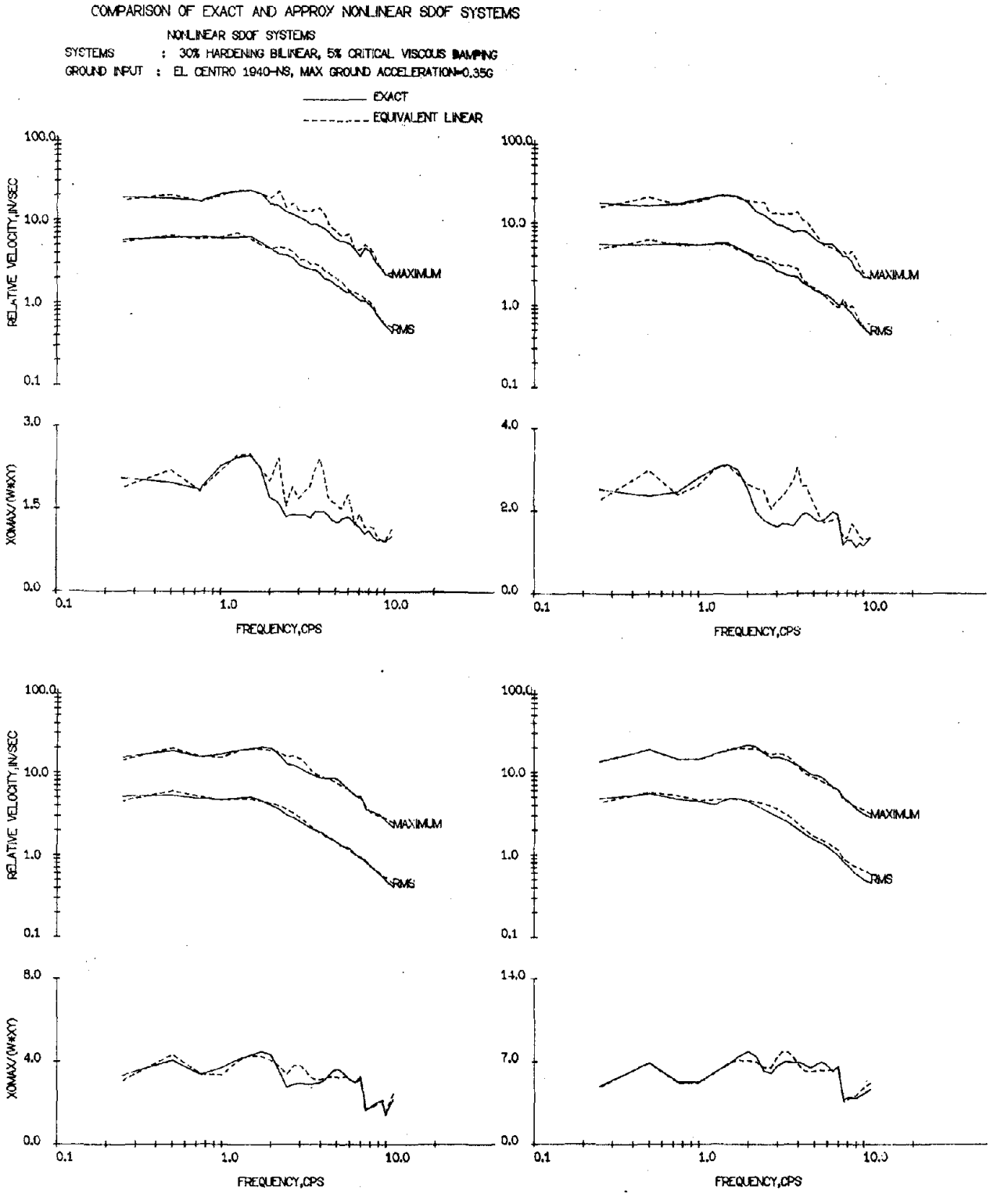

FIGURE E.2b VELOCITY RESPONSE SPECTRA
(α = 0.3, ξ = 0.05, EL CENTRO 1940-NS)

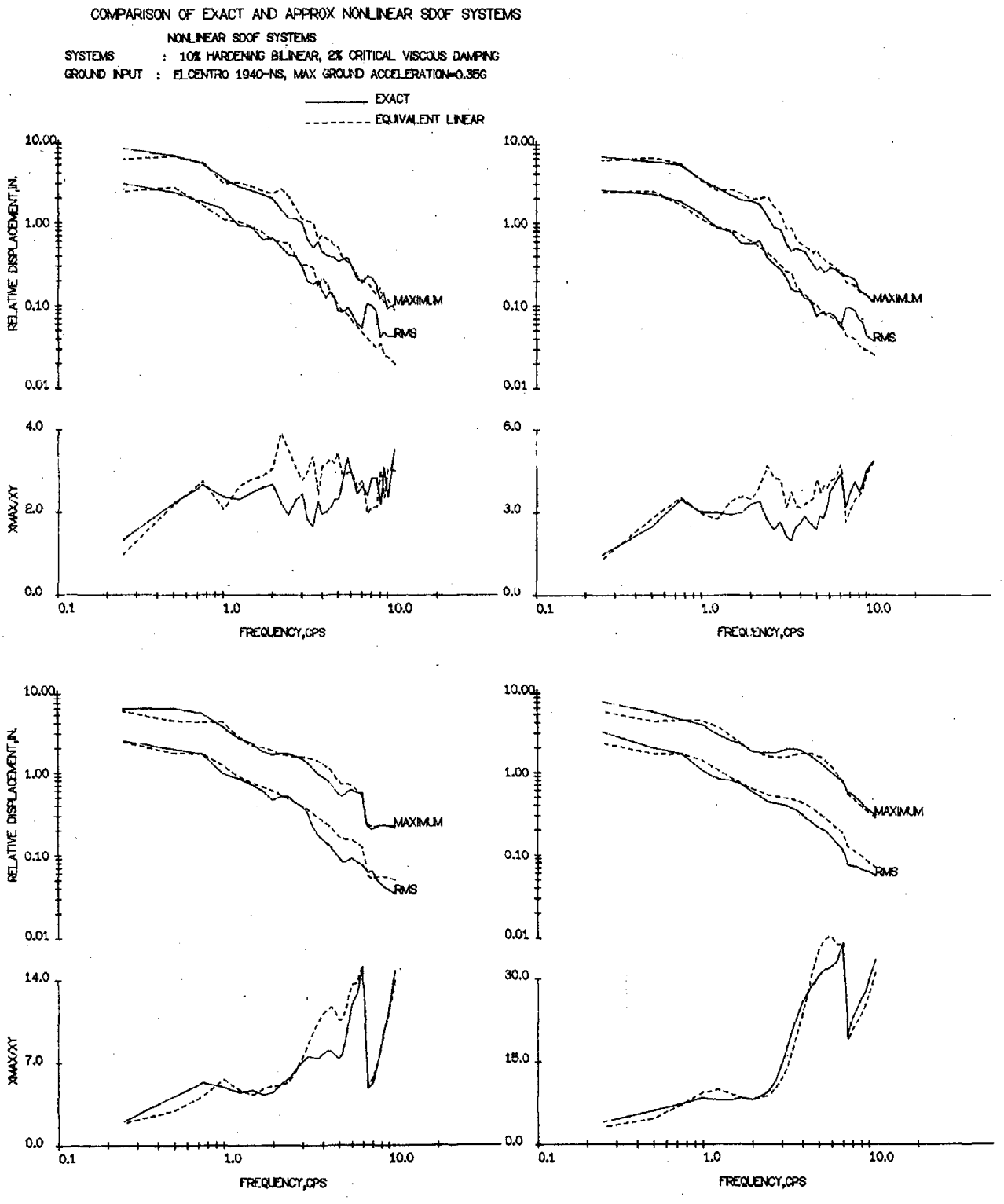

FIGURE E.3a DISPLACEMENT RESPONSE SPECTRA
(α = 0.1, ξ = 0.02, EL CENTRO 1940-NS)

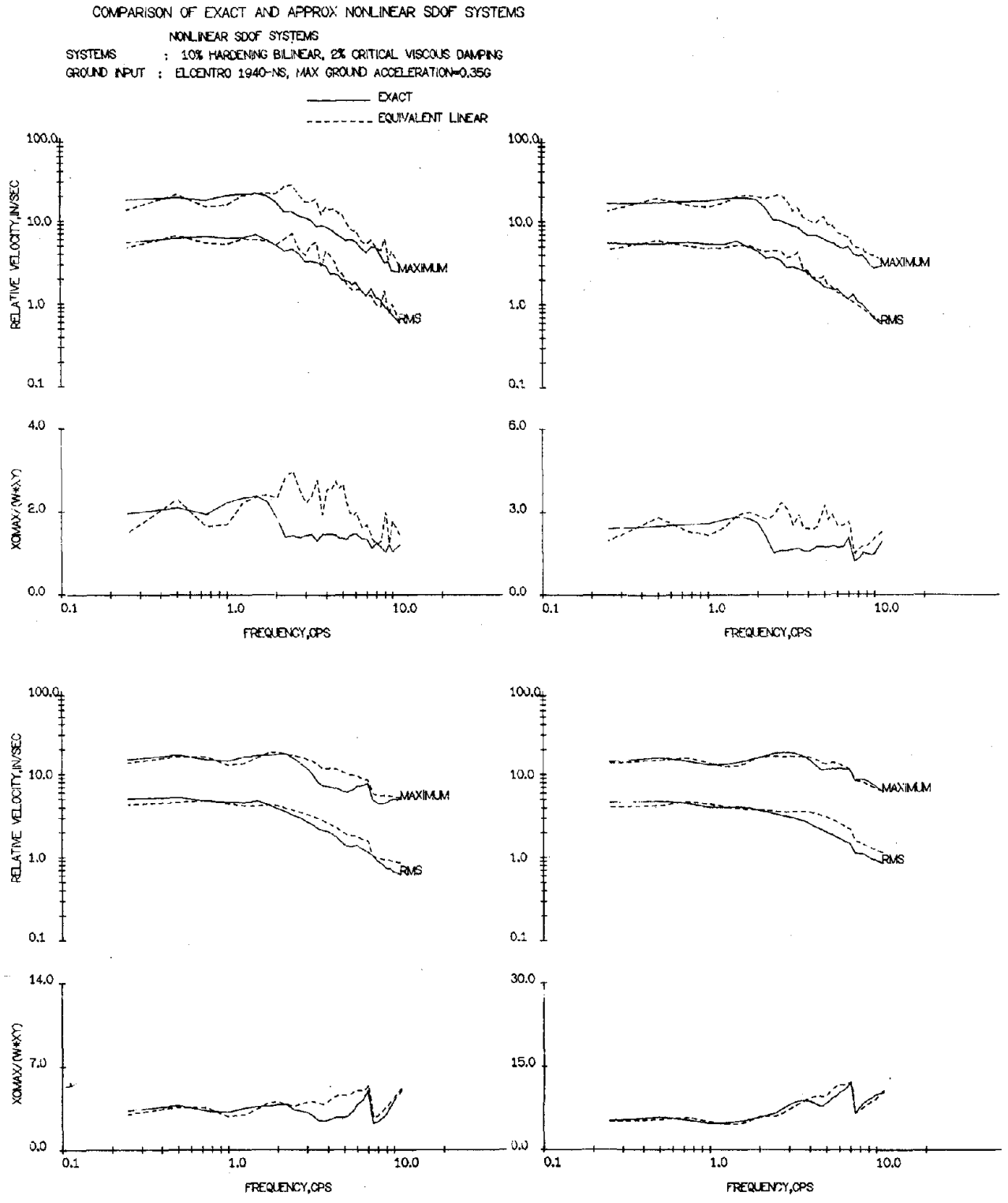

FIGURE E.3b VELOCITY RESPONSE SPECTRA
(α = 0.1, ξ = 0.02, EL CENTRO 1940-NS)

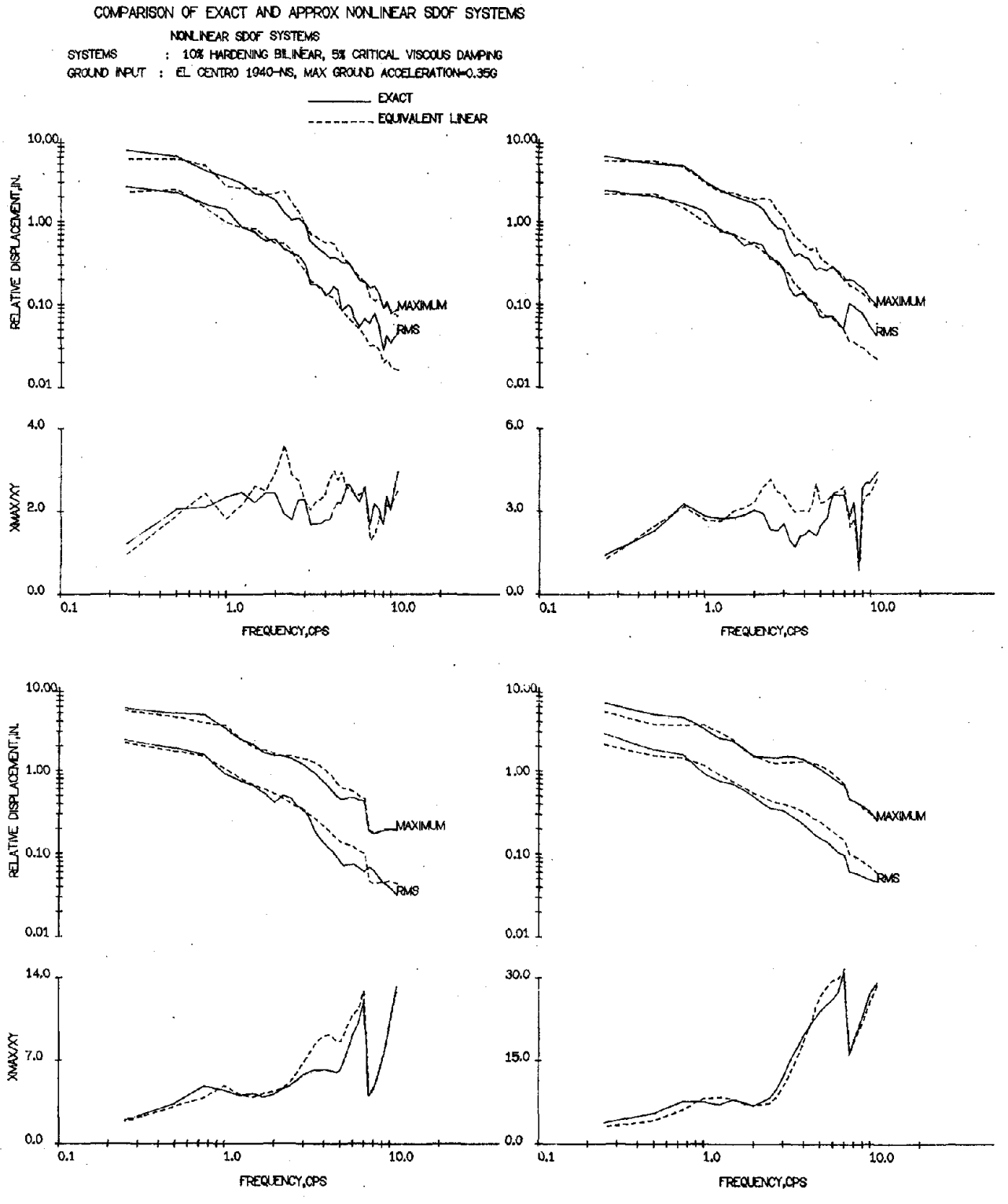

FIGURE E.4a DISPLACEMENT RESPONSE SPECTRA
(α = 0.1, ξ = 0.05, EL CENTRO 1940-NS)

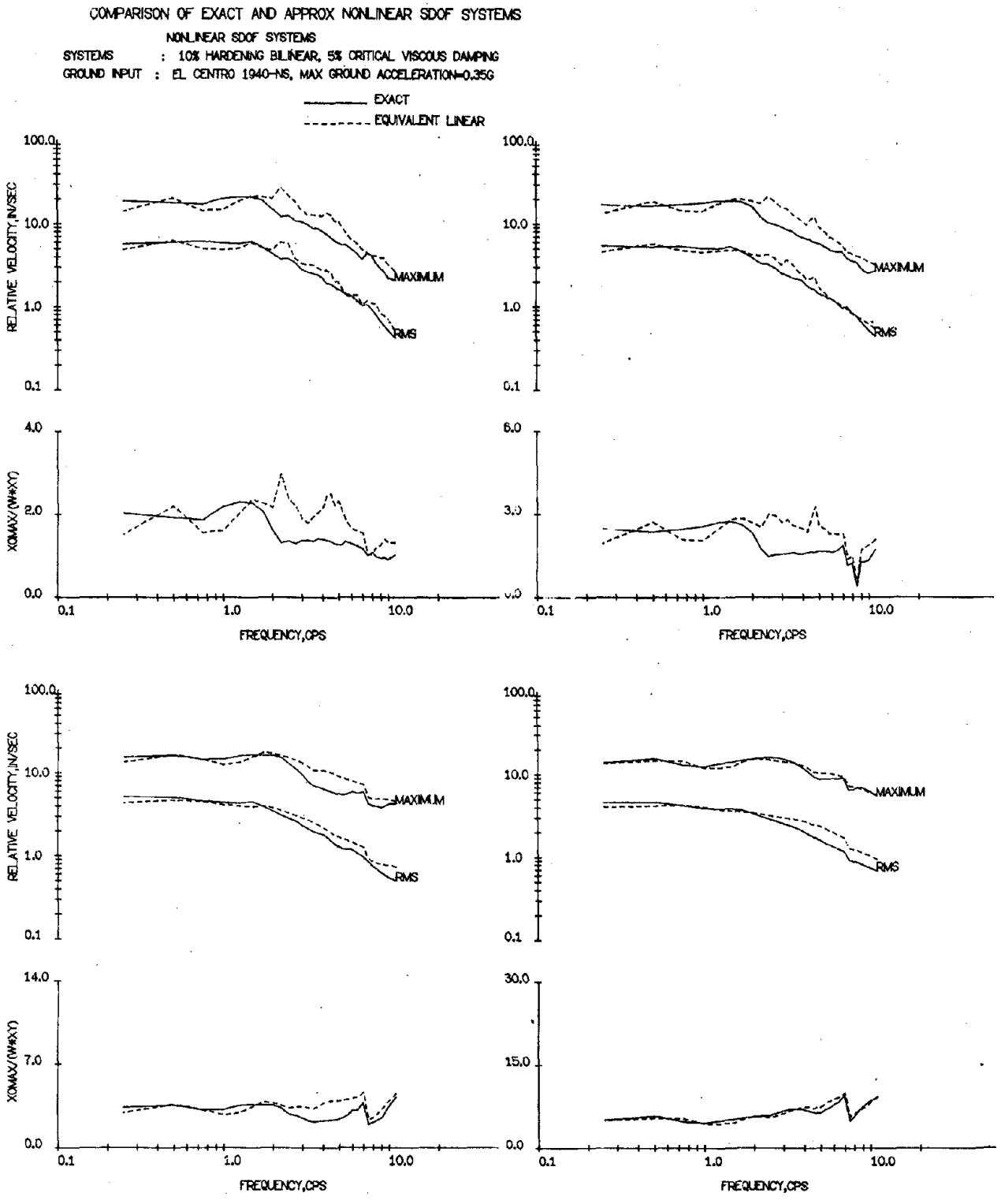

FIGURE E.4b VELOCITY RESPONSE SPECTRA
(α = 0.1 ξ = 0.05, EL CENTRO 1940-NS)

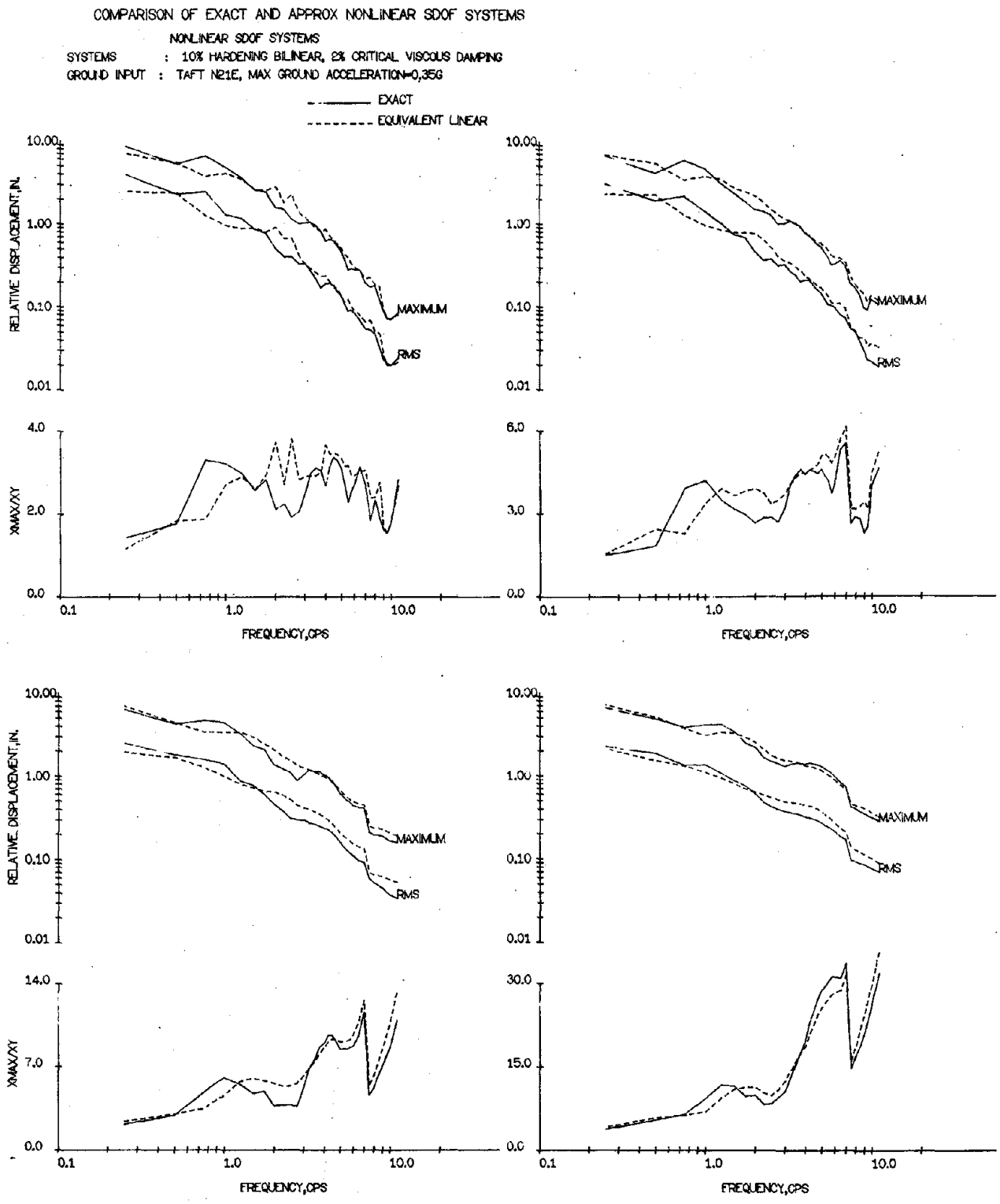

FIGURE E.5a DISPLACEMENT RESPONSE SPECTRA
(α = 0.1, ξ = 0.02, TAFT 1952-N21E)

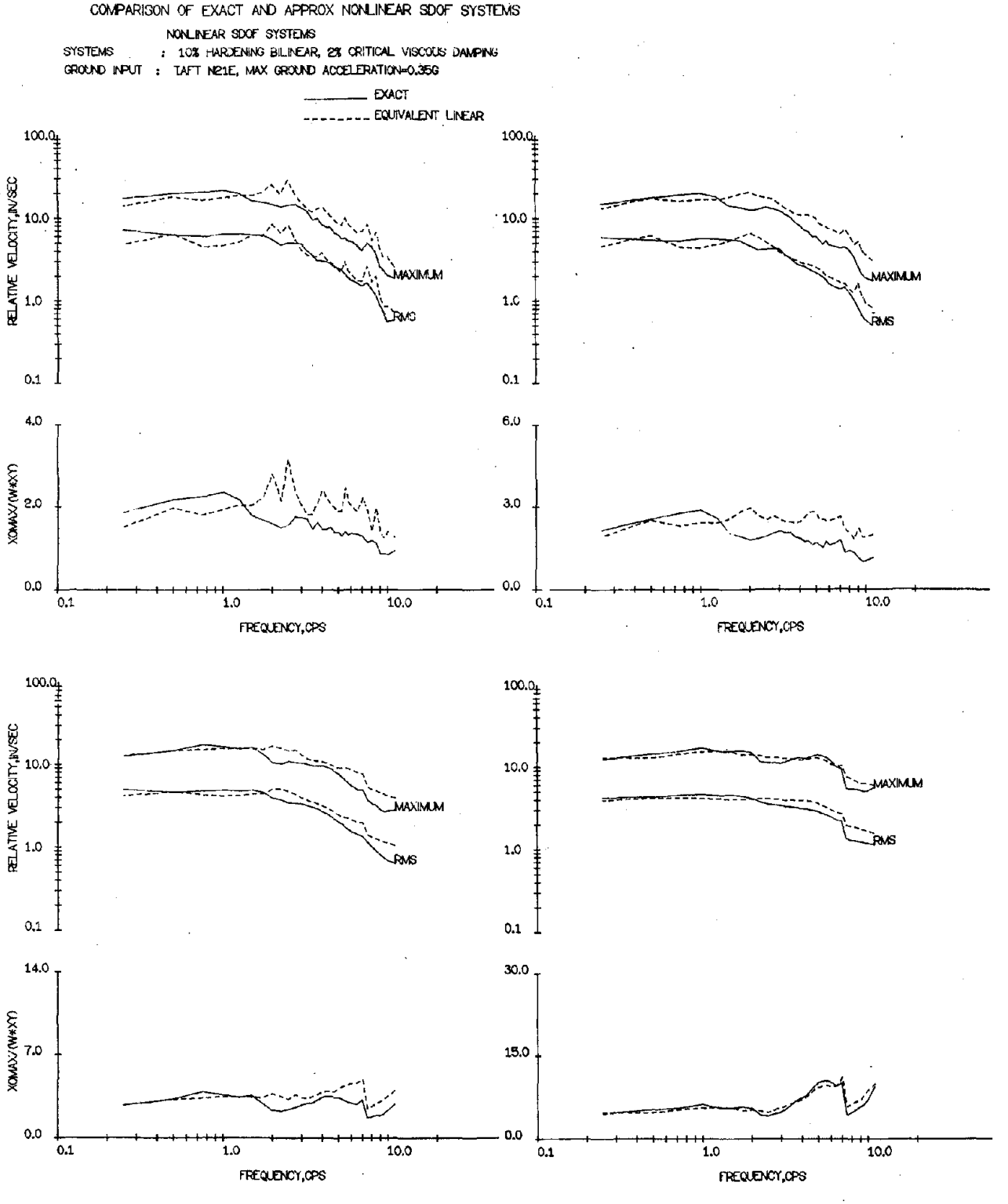

FIGURE E.5b VELOCITY RESPONSE SPECTRA
(α = 0.1, ξ = 0.02, TAFT 1952-N21E)

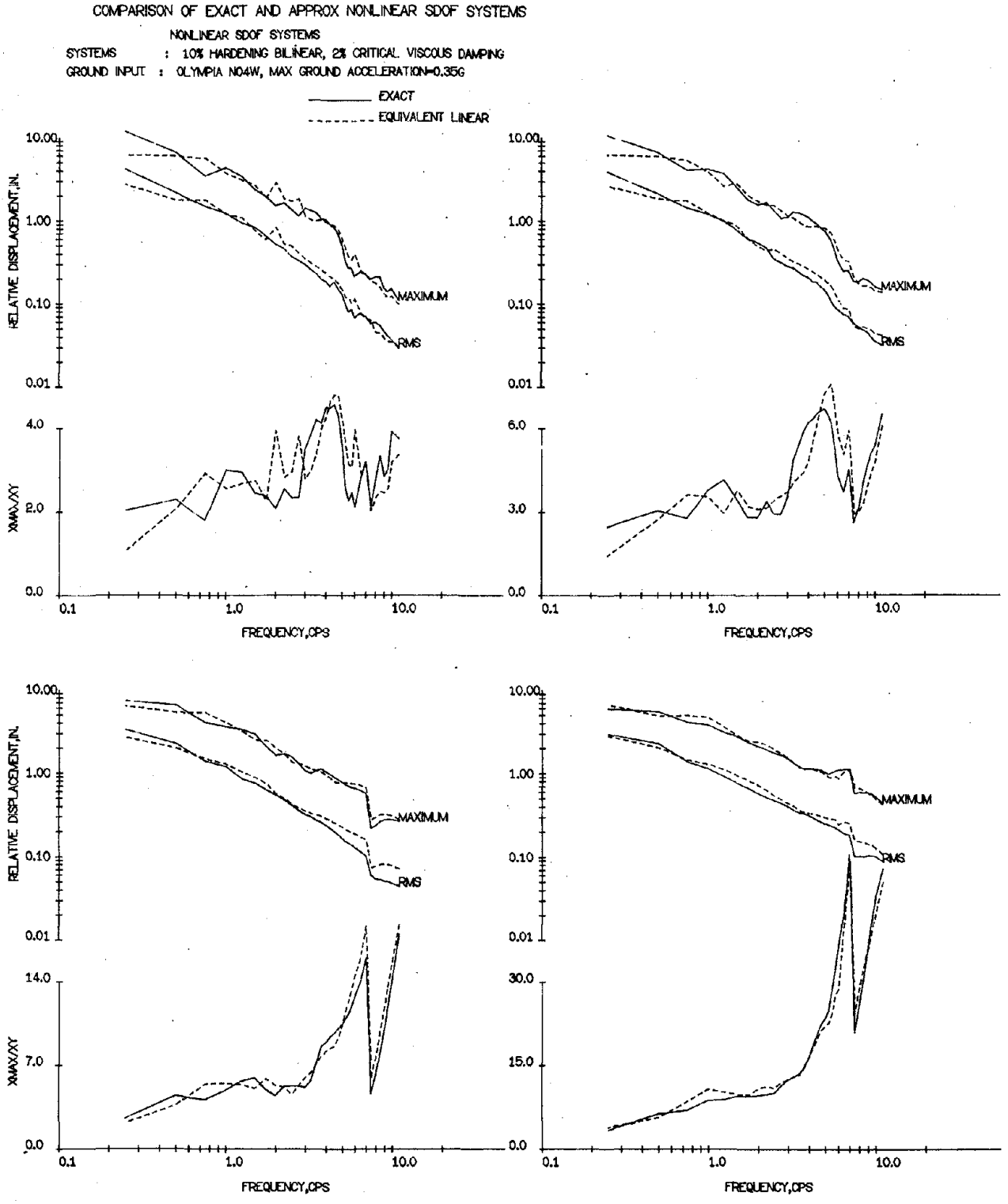

FIGURE E.6a DISPLACEMENT RESPONSE SPECTRA
(α = 0.1, ξ = 0.02, OLYMPIA 1949-N04W)

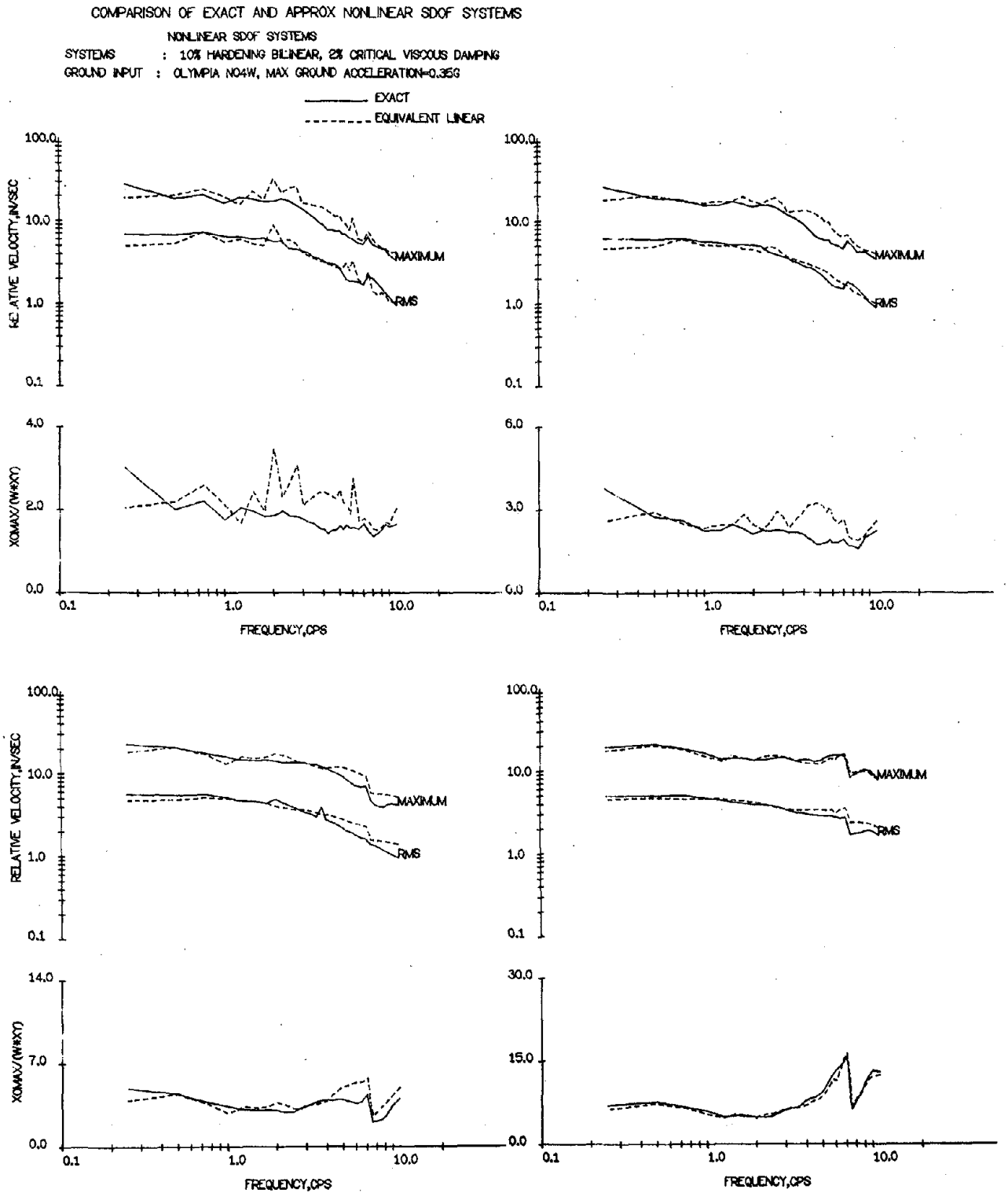

FIGURE E.6b VELOCITY RESPONSE SPECTRA
(α = 0.1, ξ = 0.02, OLYMPIA 1949-NO4W)

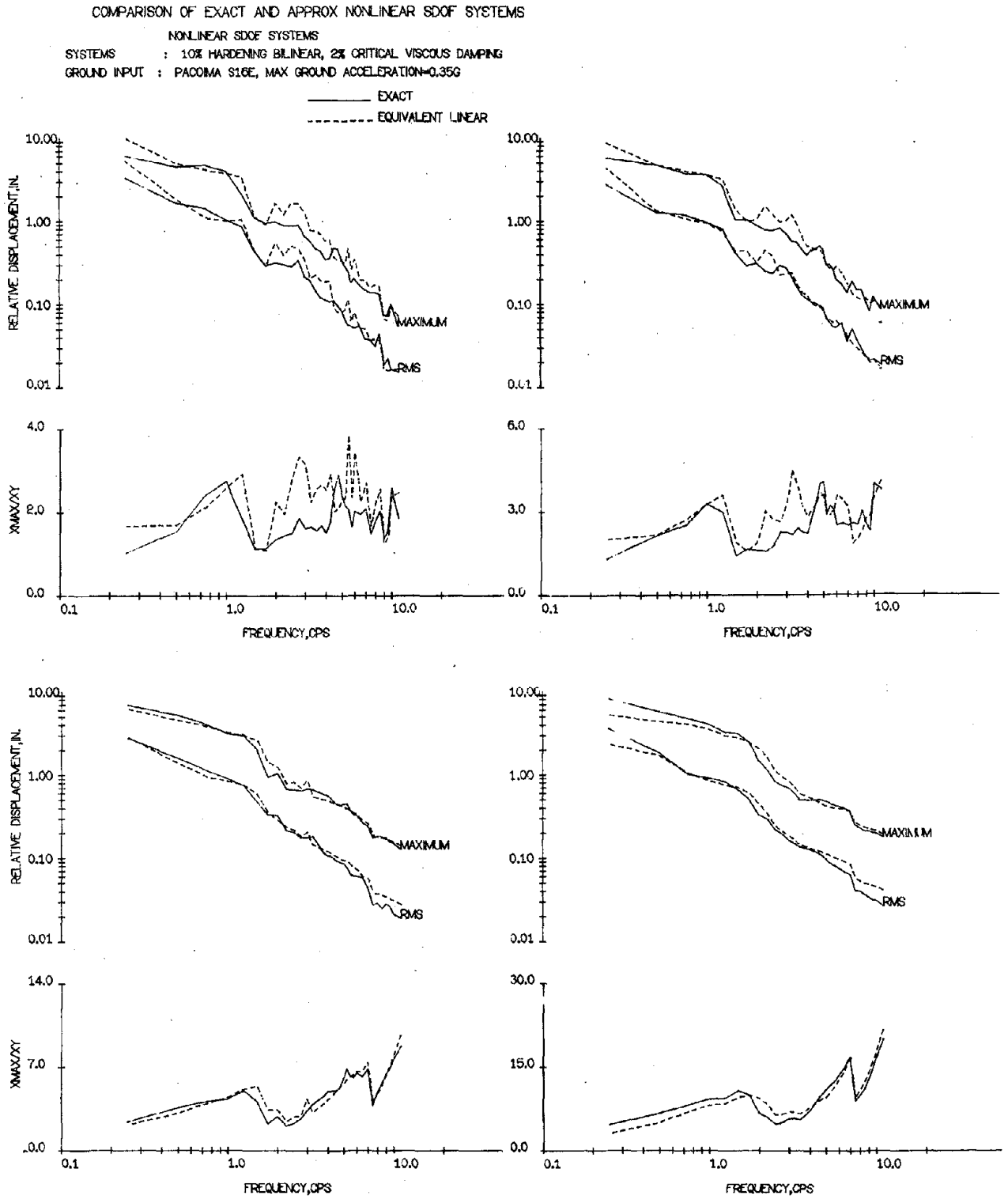

FIGURE E.7a DISPLACEMENT RESPONSE SPECTRA
(α = 0.1, ξ = 0.02, PACOIMA 1971-S16E)

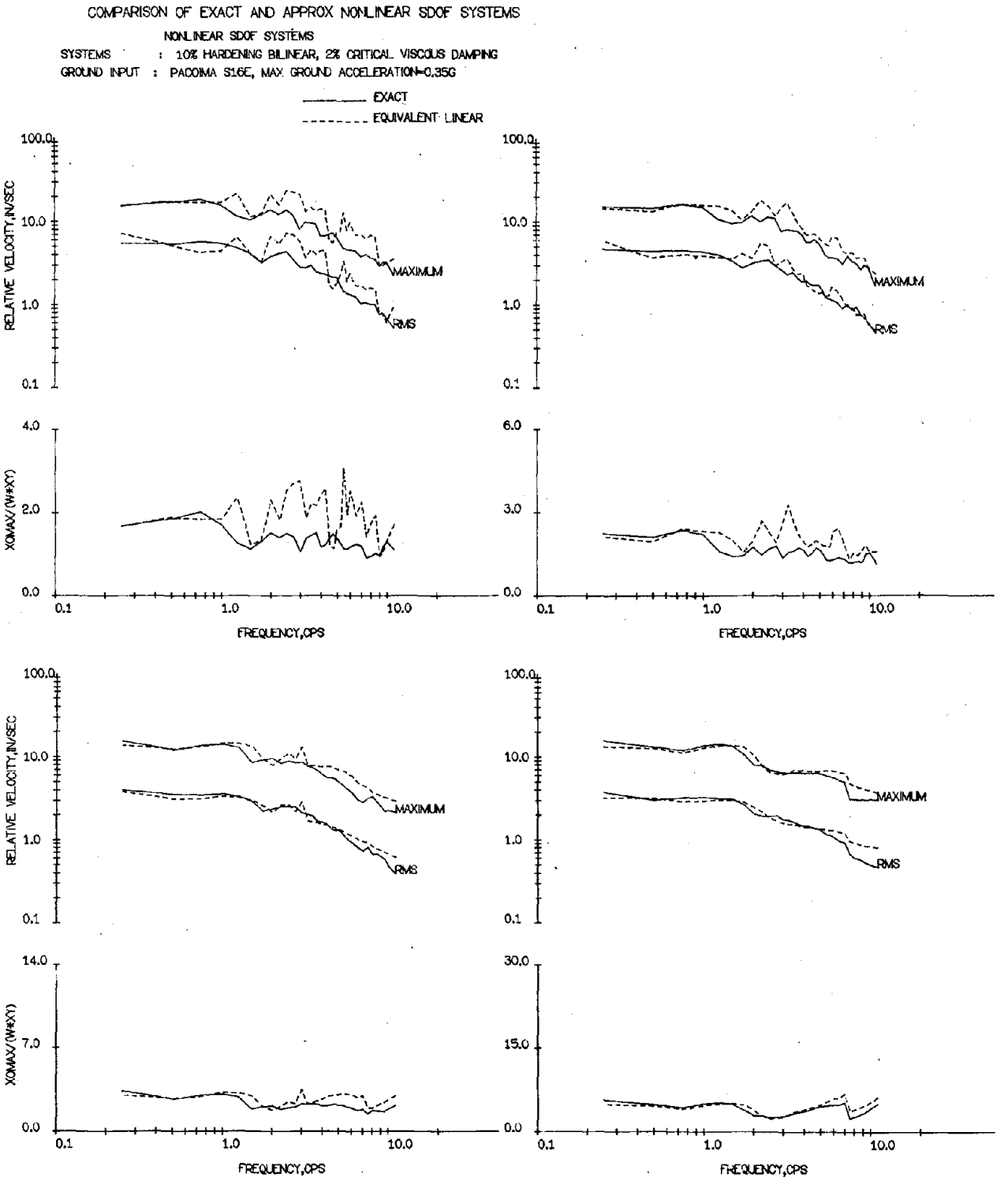

FIGURE E.7b VELOCITY RESPONSE SPECTRA
(α = 0.1, ξ = 0.02, PACOIMA 1971-S16E)

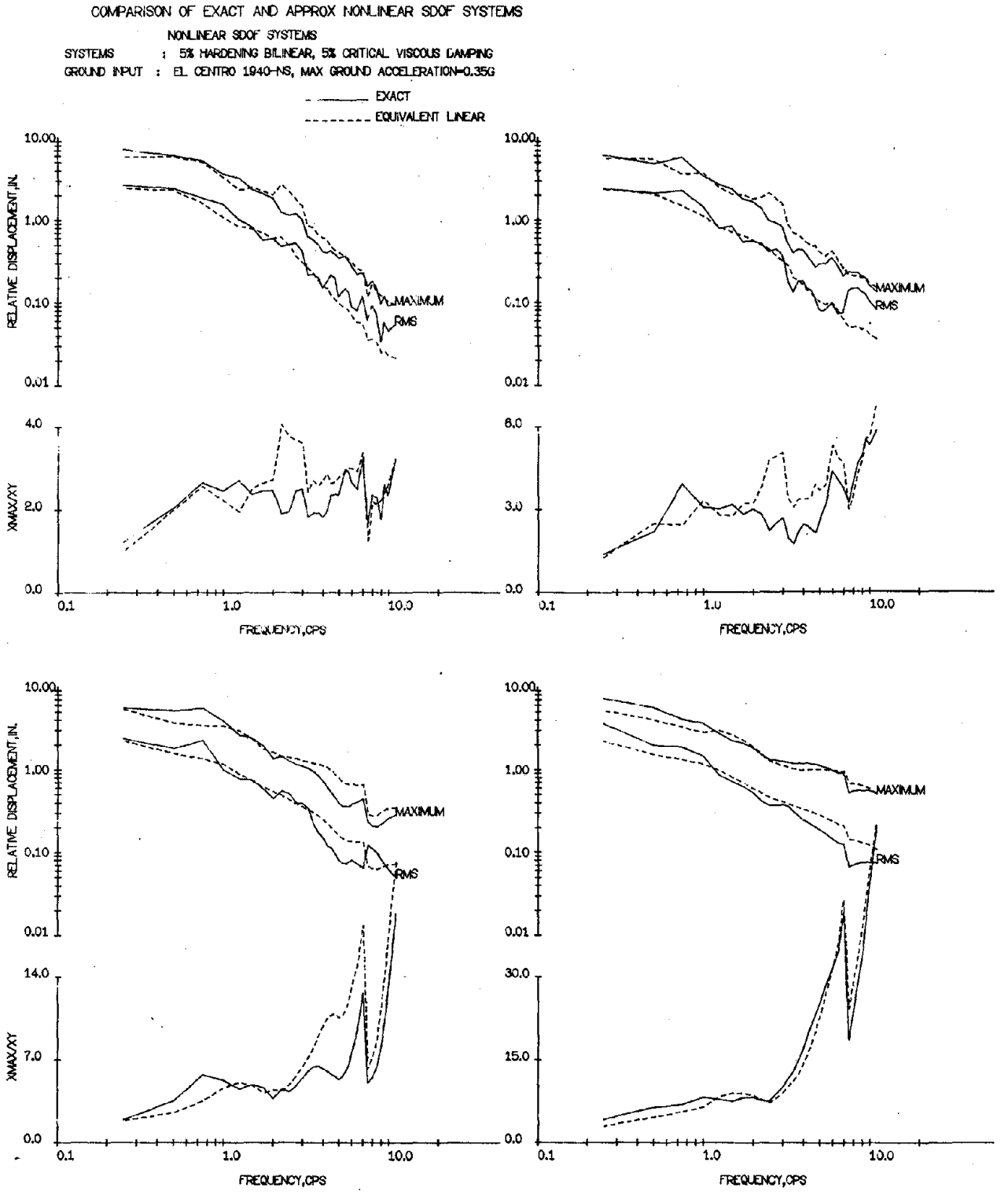

FIGURE E.8a DISPLACEMENT RESPONSE SPECTRA
(α = 0.05, ξ = 0.05, EL CENTRO 1940-NS)

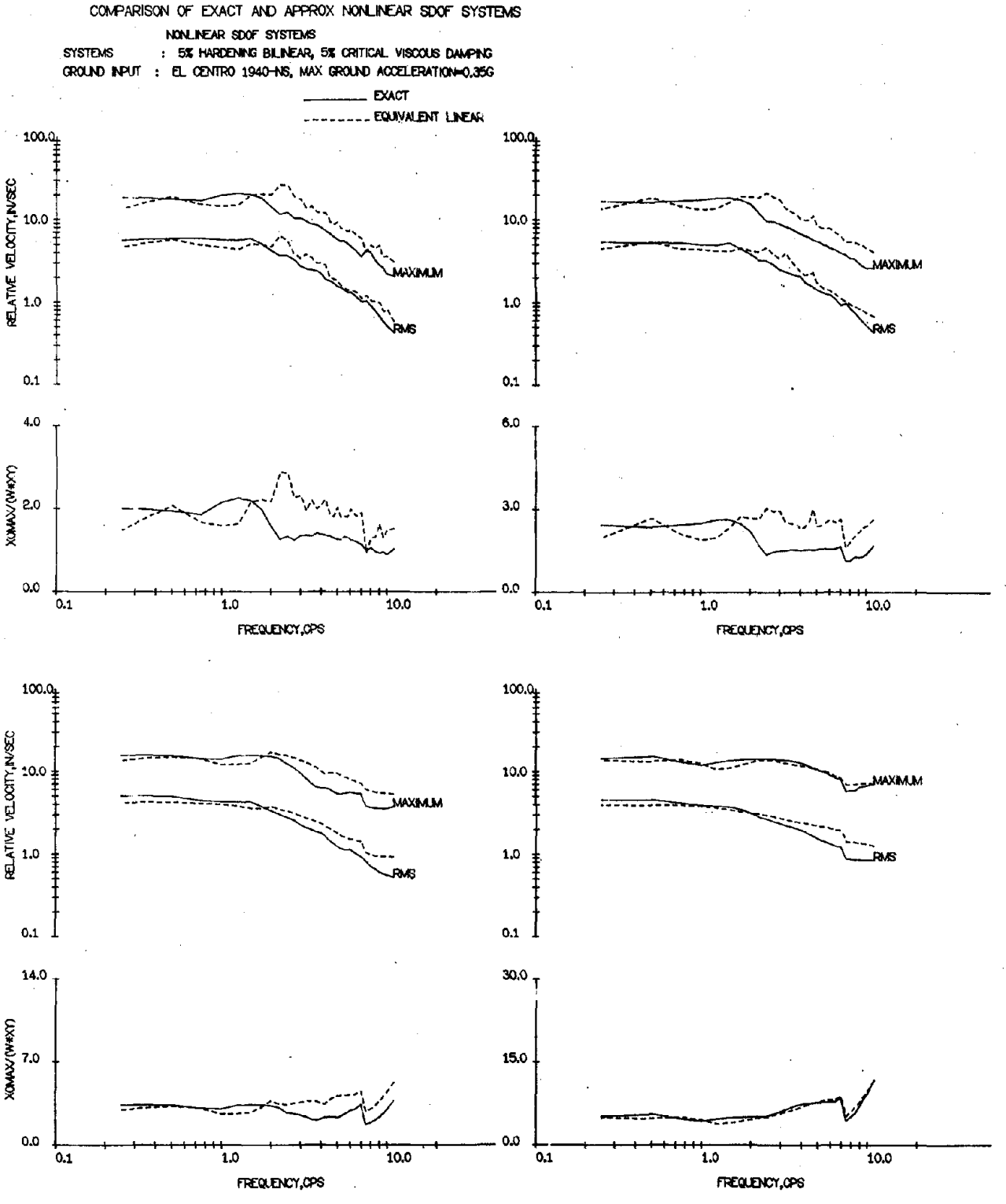

FIGURE E.8b VELOCITY RESPONSE SPECTRA
(α = 0.05, ξ = 0.05, EL CENTRO 1940-NS)

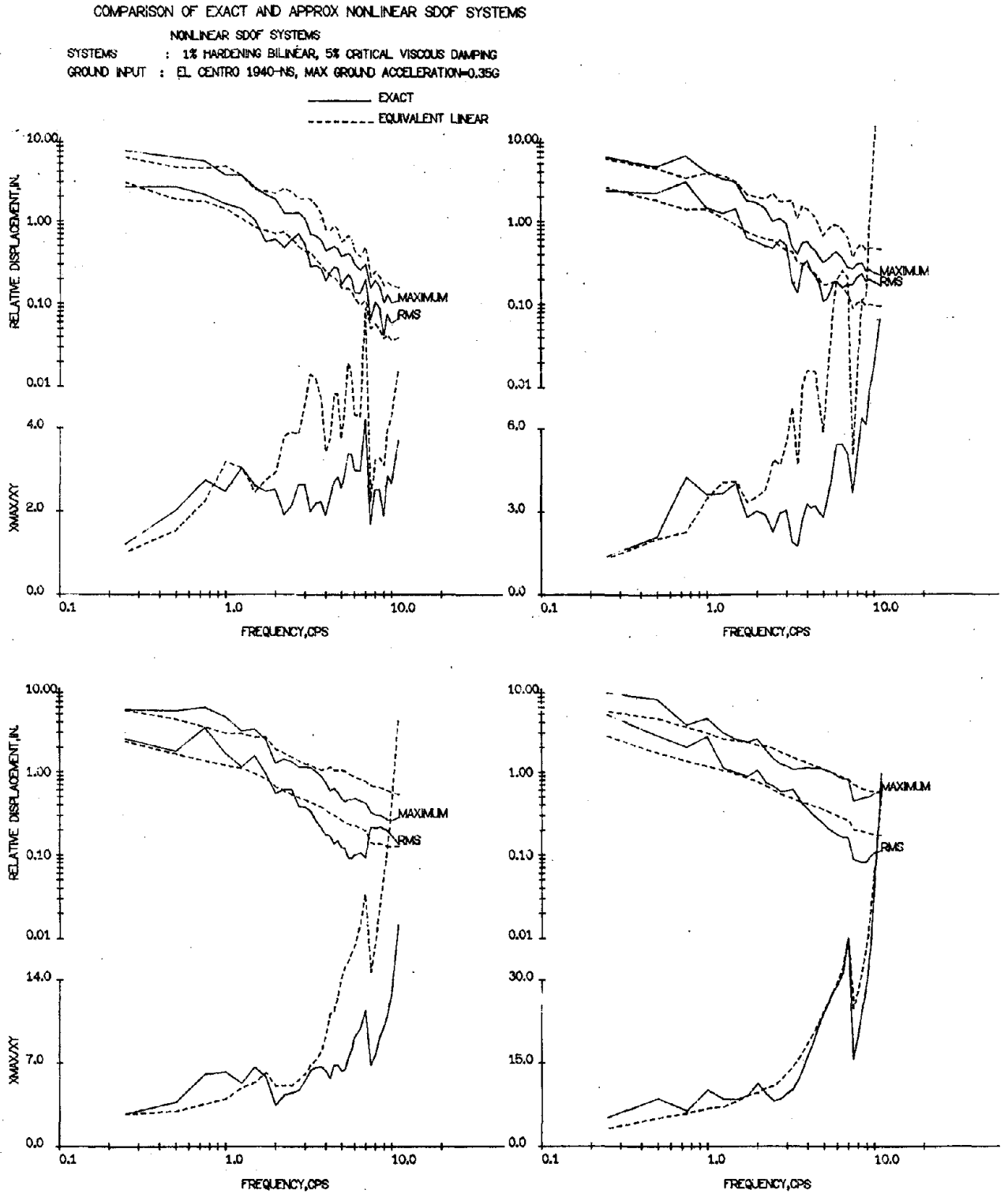

FIGURE E.9a DISPLACEMENT RESPONSE SPECTRA
(α = 0.01, ξ = 0.05, EL CENTRO 1940-NS)

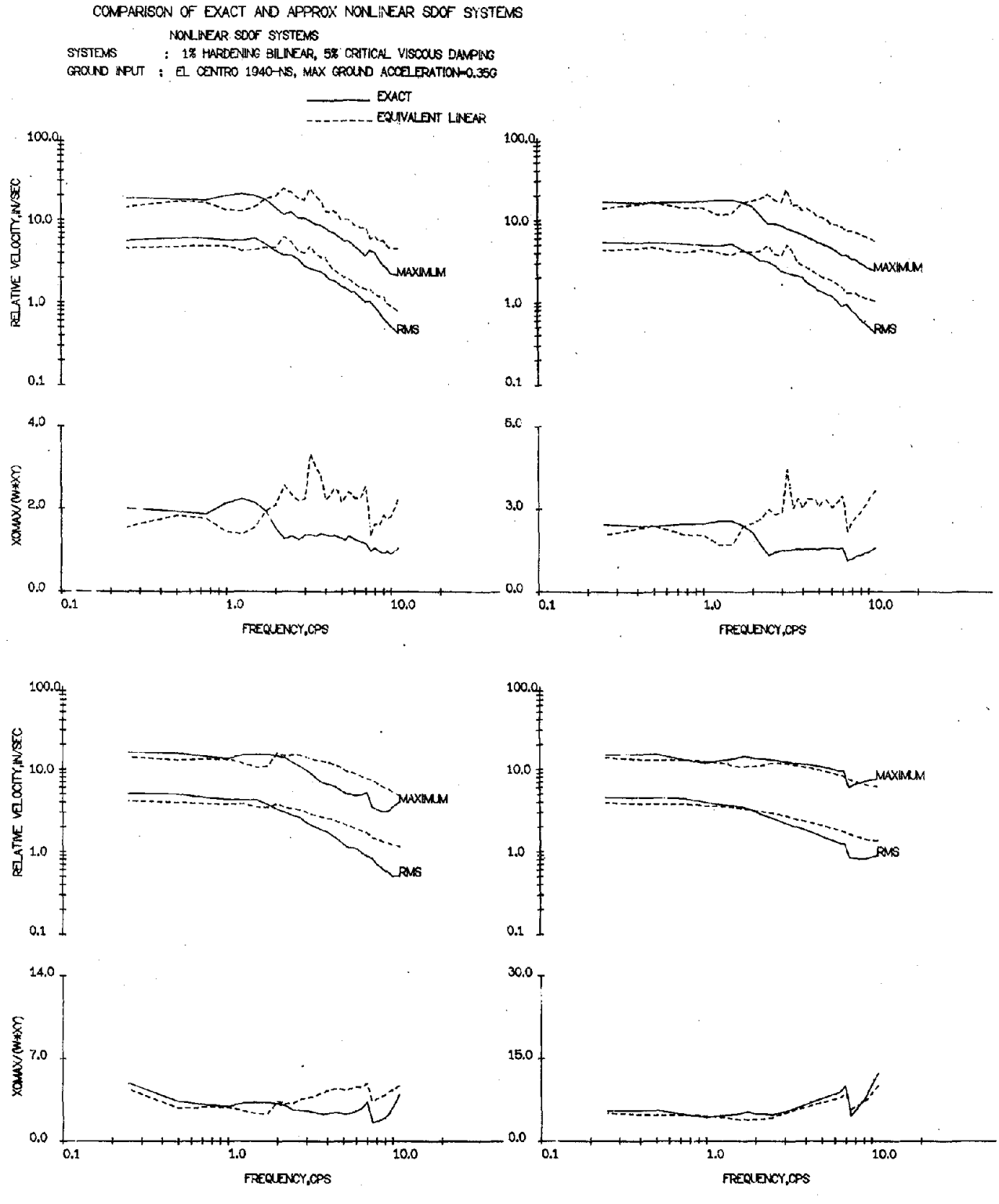

FIGURE E.9b VELOCITY RESPONSE SPECTRA
(α = 0.01, ξ = 0.05, EL CENTRO 1940-NS)

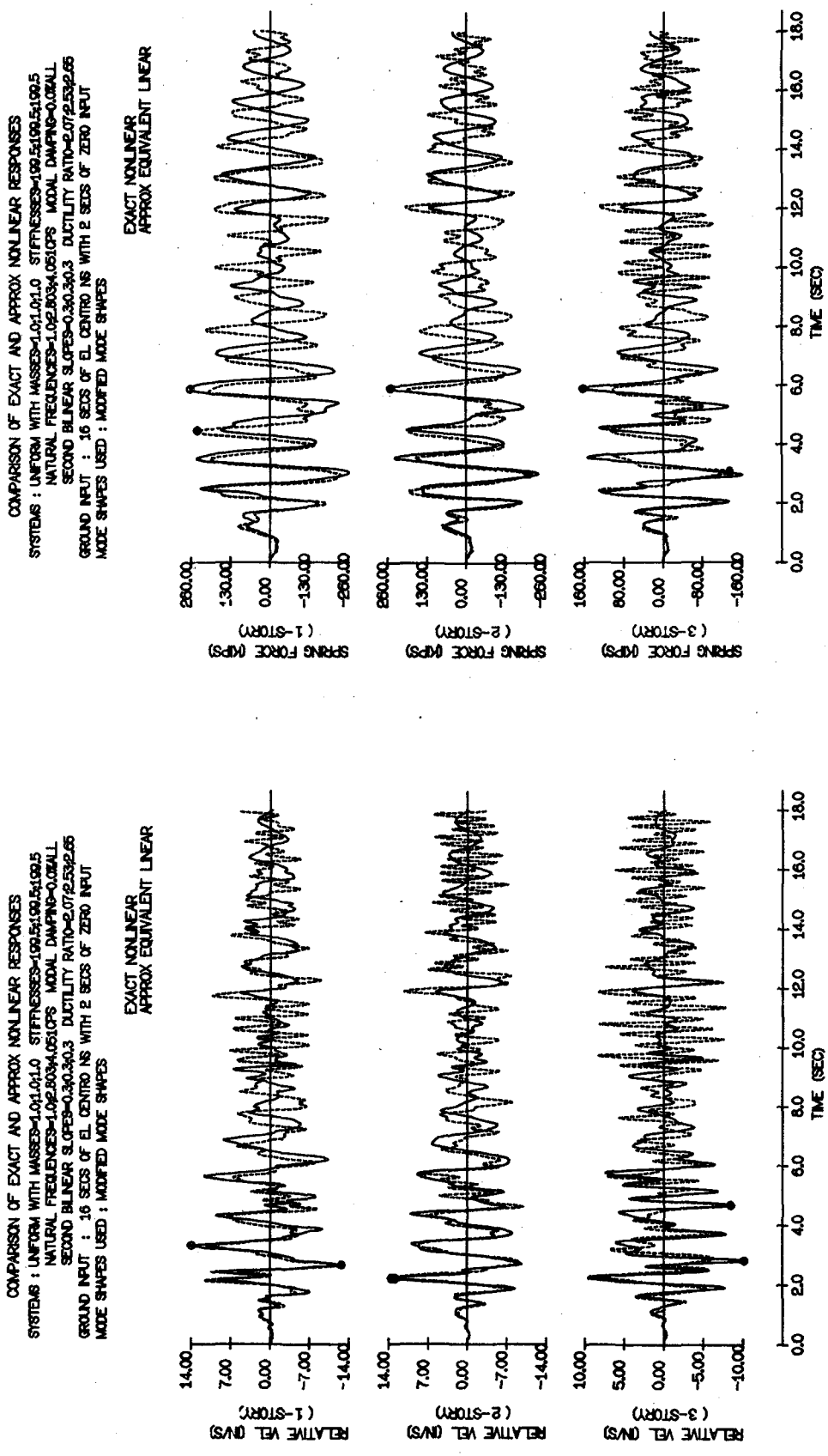

FIGURE E.10 COMPARISON OF EXACT AND EQUIVALENT LINEAR VELOCITY AND SPRING FORCE TIME HISTORIES (UNDAMPED UNIFORM BILINEAR 3DF SYSTEM, α = 0.3, EL CENTRO 1940-NS, YIELD LEVEL 1)

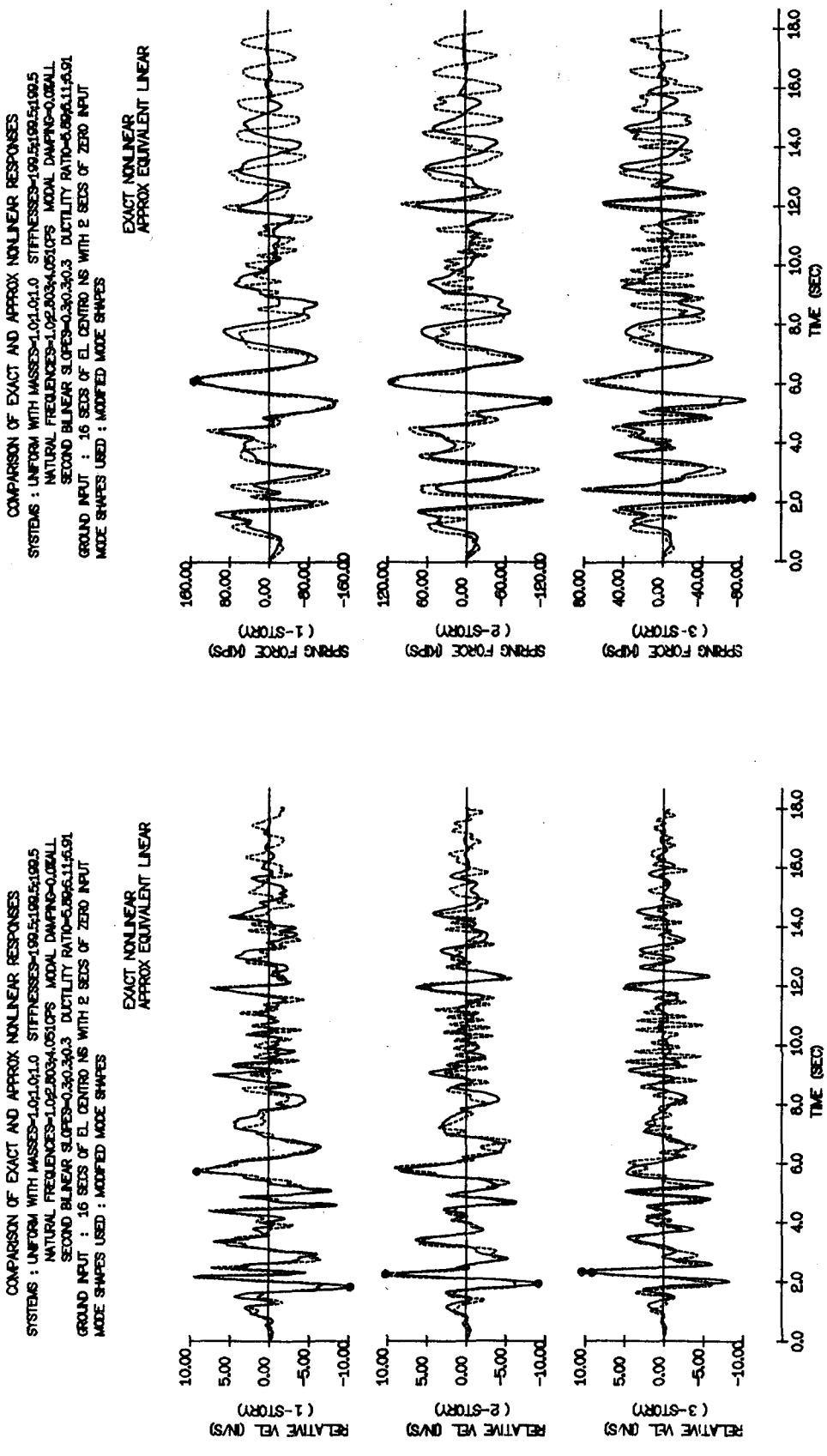

FIGURE E.11 COMPARISON OF EXACT AND EQUIVALENT LINEAR VELOCITY AND SPRING FORCE TIME HISTORIES (UNDAMPED UNIFORM BILINEAR 3DF SYSTEM, α = 0.3, EL CENTRO 1940-NS, YIELD LEVEL 2)

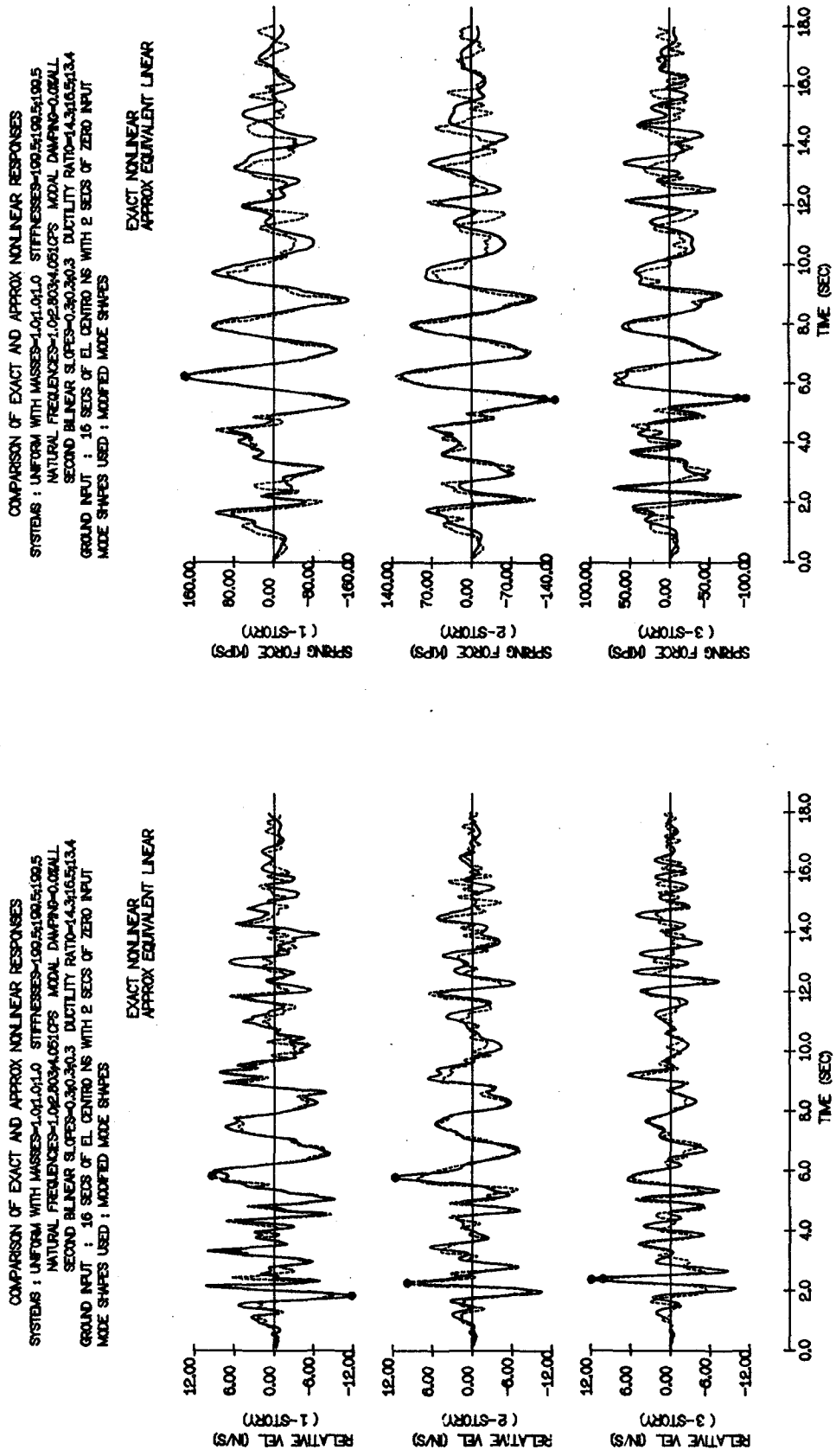

FIGURE E.12 COMPARISON OF EXACT AND EQUIVALENT LINEAR VELOCITY AND SPRING FORCE TIME HISTORIES (UNDAMPED UNIFORM BILINEAR 3DF SYSTEM, α = 0.3, EL CENTRO 1940-NS, YIELD LEVEL 3)

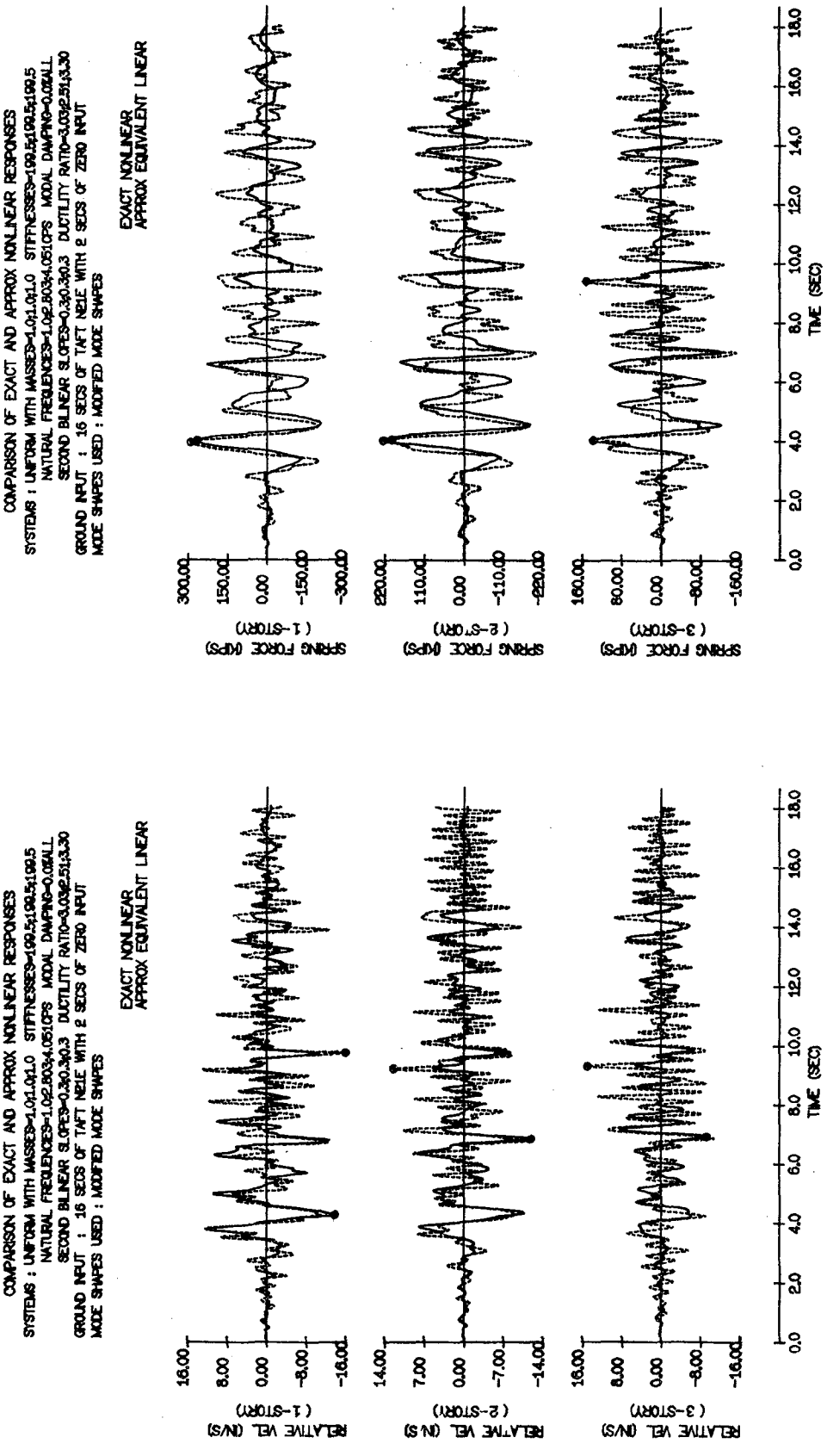

FIGURE E.13 COMPARISON OF EXACT AND EQUIVALENT LINEAR VELOCITY AND SPRING FORCE TIME HISTORIES (UNDAMPED UNIFORM BILINEAR 3DF SYSTEM, α = 0.3, TAFT 1952-N21E, YIELD LEVEL 1)

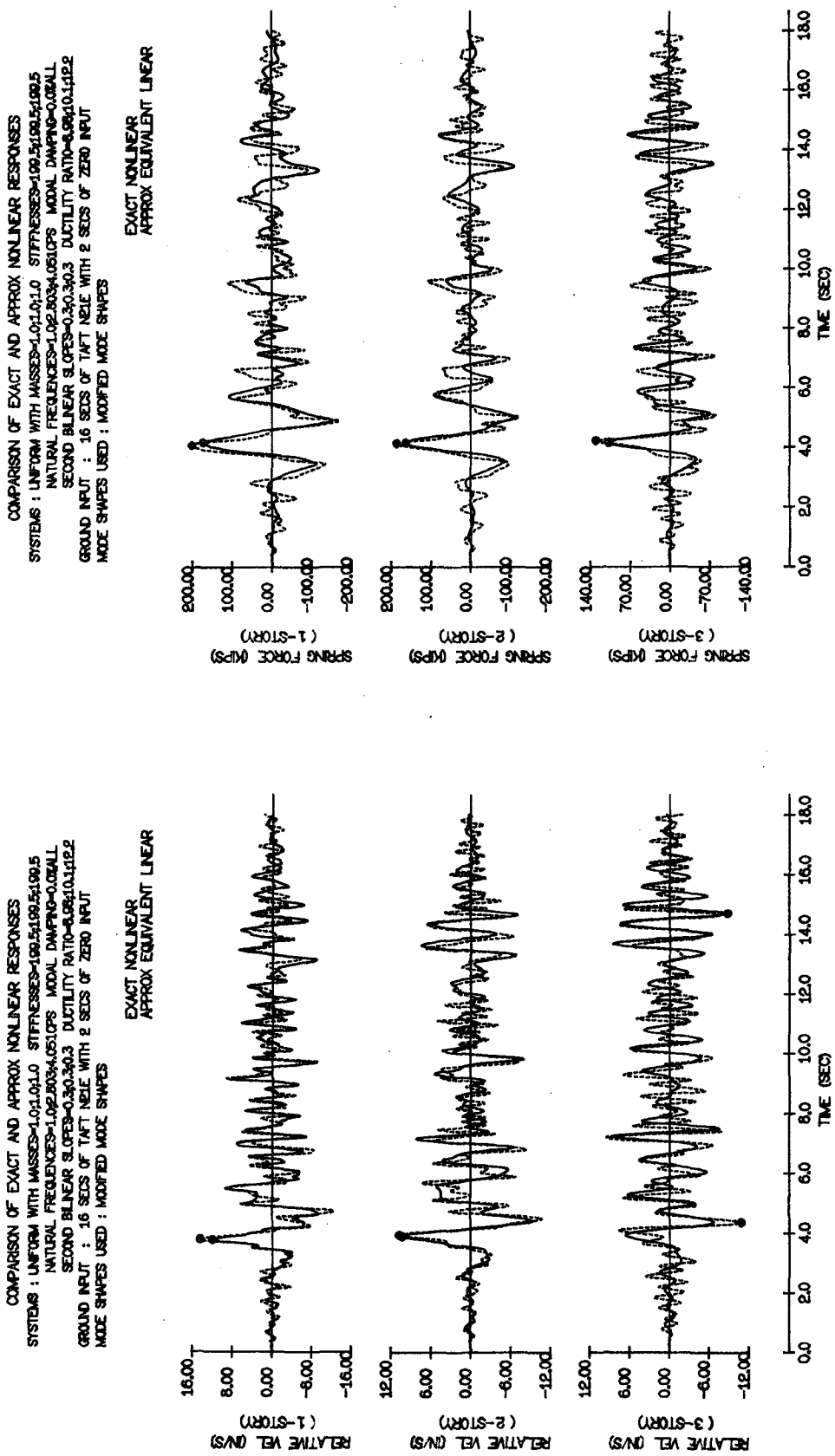

FIGURE E.14 COMPARISON OF EXACT AND EQUIVALENT LINEAR VELOCITY AND SPRING FORCE TIME HISTORIES (UNDAMPED UNIFORM BILINEAR 3DF SYSTEM, α = 0.3, TAFT 1952-N21E, YIELD LEVEL 2)

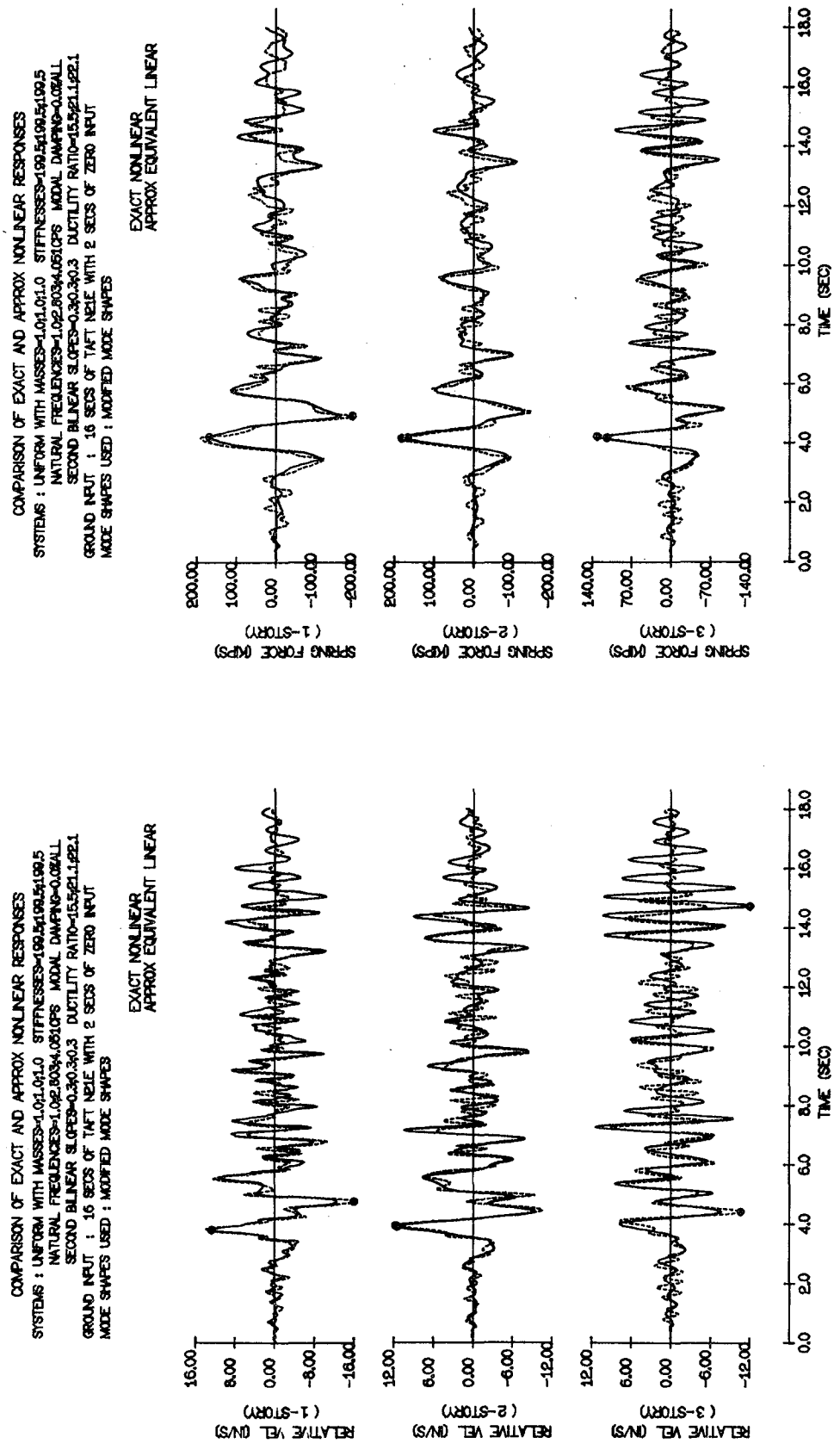

FIGURE E.15 COMPARISON OF EXACT AND EQUIVALENT LINEAR VELOCITY AND SPRING FORCE TIME HISTORIES (UNDAMPED UNIFORM BILINEAR 3DF SYSTEM, α = 0.3, TAFT 1952-N21E, YIELD LEVEL 3)